

The Realisation of Fragment- Oriented Synthesis

Emily Louise Faulkner

Submitted in accordance with the
requirements for the degree of
Doctor of Philosophy

University of Leeds
School of Chemistry

August 2021

The candidate confirms that the work submitted is her own, except where work which has formed part of jointly-authored publications has been included. The contribution of the candidate and the other authors to this work has been explicitly indicated below. The candidate confirms that appropriate credit has been given within the thesis where reference has been made to the work of others.

Fragment-oriented synthesis: β -elaboration of cyclic amine fragments using enecarbamates as platform intermediates' A. F. Trindade, E. L. Faulkner, A. G. Leach, A. Nelson, S. P. Marsden, *Chem. Commun.* 2020, **56**, 8802–8805

- Synthesis of enecarbamate intermediates for the above publication

This copy has been supplied on the understanding that it is copyright material and that no quotation from the thesis may be published without proper acknowledgement.

The right of Emily Faulkner to be identified as Author of this work has been asserted by her in accordance with the Copyright, Designs and Patents Act 1988.

Acknowledgements

I would like to thank a number of people, without whom this thesis would not have been possible. Firstly, I would like to thank Adam and Steve for giving me the opportunity to work within their groups on an incredibly varied project. For their support and guidance through my past four years of study on both science and my career, I could not be more grateful.

A large thank you to the technical and administration staff in the school of Chemistry. I would like to give special thanks to Mark and Jeanine for their invaluable help with NMR and analytical services. I would also like to extend my recognition to those who have been involved in this project, Chris and Syed for teaching assay skills and molecular biology and to Martin for his help with docking. Thanks to EPSRC and Astex for funding my project.

I would like to thank all the Marsden and Nelson group members over my time in Leeds. Alex FT, thank you for teaching me a huge amount about synthesis and giving the best advice. Tanya, without you my time in Leeds would have been a lot less enjoyable, thank you for always making me laugh and bringing bucks fizz! Thanks to previous PhDs Matthew and Bobby for always keeping things interesting and all the best for your PhDs to Alex, Harrison and Scott.

Outside of the lab, I would like to thank my friends and family for their continued love and support. Katherine and Becca, for their support and some brilliant memories over the past four years. Katy and Sophie for their support throughout my entire time at university, giving the best pep talks and the much-needed positivity. To my Mum and Nick for their unwavering support throughout my entire university experience, without which none of this would have been possible. Finally, to my partner James, we got through PhDs and writing together. Thank you for listening to my endless presentation practices, proof-reading, coffees, and most importantly, believing in me.

Abstract

Fragment-based ligand discovery (FBLD) has been transformed over the last 20 years into a mainstream approach for the discovery of drugs. FBLD relies on the initial identification of small molecule “fragments” (MW < 250 g mol⁻¹) that bind weakly and efficiently to a target protein. Binding fragments are then elaborated to yield more potent and selective ligands. FBLD has thus far yielded four FDA-approved drugs and around 50 candidates that are currently in clinical trials.

Despite the rise of FBLD, significant chemical challenges remain for the field. Fragment elaboration is dominated by a limited reaction toolkit which is heavily focused on heteroatom functionalisation, enabling direct fragment “growth” along specific vectors. Here we develop and apply synthetic methods for the elaboration of cyclic amines on the carbon skeleton, which may help address the chemical challenges for the field and could be deployed within FBLD projects.

A procedure is developed for the regioselective formation of endocyclic enecarbamates from *N*-Cbz amines employing electrochemical oxidation and elimination, enabling access to twenty endocyclic enecarbamates.⁹ These enecarbamates afford a platform for the elaboration of cyclic amines from the β -position. To realise the full impact of this synthetic methodology, a library of hinge-binding fragments was designed, synthesised and screened for their activity against Aurora-A, yielding 30-active fragments. Fragment hits were elaborated using the described methodology and screened, yielding 9-active compounds. Finally, we investigate the selectivity of our fragment libraries against a panel of 100-kinases, to explore the applicability of synthetic elaboration for the development of selective kinase inhibitors from common fragments.

Our results demonstrate that the underpinning synthetic methods developed during the project enable efficient exploration of synthetic vectors on cyclic amines. We show these strategies can be applied to FBLD and furthermore, show that chemical elaboration of ATP-binding fragments can tune kinase-selectivity.

Abbreviations

μ W	Microwaves
$^{\circ}$ C	Degrees Celsius
δ	Chemical shift
3D	Three dimensional
A	Alanine
ABL	Abelson kinase
Ac	Acetyl
ADP	Adenosine diphosphate
AE	Antibacterial efficiency
ADME	Absorption, distribution, metabolism and excretion
ADMET	Absorption, distribution, metabolism, excretion and toxicity
Ala	Alanine
APC	Anaphase promoting complex
APE	Alanine-proline-glutamic
Ar	Aryl
ATAD2	ATPase family AAA domain-containing protein 2
ATP	Adenosine triphosphate
AURKBA	Aurora-B kinase
Ax	Axial
BET	Bromo- and Extra-Terminal domain
BCR	Breakpoint cluster region
BMX	Bone marrow kinase on chromosome X
Bn	Benzyl
Boc	<i>tert</i> -butyloxycarbonyl
<i>t</i> -BPA	<i>tert</i> -butyl peracetate
<i>t</i> -Bu	<i>tert</i> -butyl
BRD1	Bromodomain Containing 1
Br	Broad
BRAFA	B-raf kinase
Bz	Benzoyl
C	Cysteine
Cbz	Carboxybenzyl
CDC	Cyclin-dependent kinase
Cdh1	Epithelial cadherin
CDK	Cyclin dependent kinase
CDKN2A	Cyclin-dependent kinase inhibitor 2A
CLK3A	CDC Like Kinase 3
CNS	Central nervous system
CoA	Co-enzyme A

Conc	Concentrated
COMT	Catechol <i>O</i> -methyltransferase (COMT)
COSY	Correlation spectroscopy
CV	Cyclic voltammetry
CWC	Chemical weapons convention
CYP	Cytochrome
d	Doublet
DCM	Dichloromethane
DEPT	Distortionless enhancement by polarization transfer
DFG	Asp-Phe-Gly
DFT	Density functional theory
DIBAL-H	Diisobutylaluminium hydride
DIPEA	Diisopropylethylamine
DMac	Dimethylacetamide
DMF	Dimethylformamide
DMSO	Dimethylsulfoxide
DSF	Differential scanning fluorimetry
E	Glutamic acid
EDC	1-Ethyl-3-(3-dimethylaminopropyl)carbodiimide
eq	Equatorial
Eq.	Equivalents
ESI	Electrospray ionisation
F	Phenylalanine
FBDD	Fragment-based drug discovery
FBLD	Fragment-based ligand discovery
FDA	Food and Drugs Administration
Fsp ³	Fraction of sp ³ carbons
FRET	Fluorescence resonance energy transfer
FT-IR	Fourier transform infrared
G1	Gap phase 1
G2	Gap phase 2
GE	Group efficiency
Glu	Glutamic acid
GSK	GlaxoSmithKline
H	histidine
HA	Heavy atom
HAC	Heavy atom count
HAT	Hydrogen atom transfer
HATU	(1-[Bis(dimethylamino)methylene]-1H-1,2,3-triazolo[4,5-b]pyridinium 3-oxide hexafluorophosphate

HOBT	Hydroxybenzotriazole
HMG	3-hydroxy-3-methylglutaryl
HPV	Human papillomavirus
HRD	His-Arg-Asp
HRMS	High resolution mass spectrometry
HSQC	Heteronuclear single quantum coherence
HTS	High throughput screening
I	Isoleucine
IPA	Isopropyl alcohol
IR	Infrared spectroscopy
IC ₅₀	Concentration of an inhibitor where the response is reduced by 50%
ITC	Isothermal titration calorimetry
j	Coupling constant
JAK-2	Janus kinase 2
JMJD2	Jumonji domain 2
K _M	Michaelis constant
K _D	equilibrium dissociation constant
L	Leucine
LLAMA	Lead-Likeness and Molecular Analysis
LC-MS	Liquid chromatography- mass spectrometry
LE	Ligand efficiency
LED	Light-emitting diode
LLE	Lipophilic ligand efficiency
M	Methionine
M	Mitosis
M	Molar
M	Multiplet
MAP	Mitogen activated protein kinase
MAPKAPK2A	MAP kinase-activated protein kinase 2
Me	Methyl
MeCN	Acetonitrile
MeOH	Methanol
MDAP	Mass-directed auto purification
Mmol	Millimole
m.p	Melting point
MHz	Megahertz
Mps1	Monopolar spindle-1
Ms	Mesyl
MS	Mass spectrometry

N	Asparagine
NADP	Nicotinamide adenine dinucleotide phosphate
NBS	<i>N</i> -bromosuccinimide
NCS	<i>N</i> -Chlorosuccinimide
<i>n</i> -Bu	<i>n</i> -butyl
NME	New molecular entities
NMR	Nuclear Magnetic Resonance
OPLS-AA	All-atom optimised potentials for liquid simulations
p53	Tumour protein p53
PAIN	Pan-assay interference
pIC ₅₀	log ₁₀ (IC ₅₀)
Ph	Phenyl
PHKG2A	Phosphorylase Kinase Catalytic Subunit Gamma 2
PD	Pharmacodynamics
PK	Pharmacokinetics
PMI	Principle moment of inertia
Ppm	Parts per million
PSA	Polar surface area
PTM	Post-translational modification
q	Quartet
R	Arginine
R&D	Research and development
RET	Rearranged during transfection
RO3	Rule of three
RO5	Rule of five
ROCS	Rapid overlay of chemical structures
ROK	Rho-kinase
RNA	Ribonucleic acid
rt	Room temperature
S	Serine
s	Singlet
SAM	<i>S</i> -adenosyl-L-methionine
SAR	Structural activity relationship
SCE	Saturated calomel electrode
Ser	Serine
S _N 2	Nucleophilic substitution bimolecular
S _N Ar	Nucleophilic aromatic substitution
SPR	Surface plasmon resonance
STAB	Sodium triacetoxy borohydride
t	Triplet

T	Threonine
T _M	Denaturation midpoint
TBAB	Tetrabutylammonium bromide
TEA	Triethylamine
Tf	Triflate
TFA	Trifluoroacetic acid
TLC	Thin layer chromatography
TMS	Trimethylsilyl
THF	Tetrahydrofuran
TRK-4	Tropomyosin receptor kinase-4
TS	Transition state
TTKA	Mps1, Monopolar spindle-1
UV	Ultraviolet
V	Valine
V _{Max}	Reaction rate when the enzyme is fully saturated by substrate
W	Tryptophan
wt	Weight
WT	Wild-type
Y	Tyrosine

Table of Contents

1 Chapter 1: Introduction	- 14 -
1.1 An Overview of the Drug Discovery Process	- 14 -
1.2 Challenges Facing the Pharmaceutical Industry	- 15 -
1.3 Rates of Attrition and their Underlying Causes	- 16 -
1.4 The Approach to Drug Discovery: High Throughput Screening	- 16 -
1.5 Fragment-based drug discovery: An Alternative Approach for Lead Discovery	- 19 -
1.6 A Matter of Chemical Space	- 24 -
1.7 Fragment Elaboration	- 25 -
1.8 Applications of Fragment Based Drug discovery	- 27 -
1.9 Thesis Aims and Objectives:	- 34 -
2 Chapter 2: Evaluation and Development of Methodology For use in Fragment Elaboration in Fragment Based Ligand Discovery	- 38 -
2.1 Part 1: Evaluation of Existing Methodology for the Elaboration of Cyclic Amine Fragments	- 38 -
2.2 Introduction	- 38 -
2.3 Results and Discussion	- 39 -
2.4 Conclusion	- 48 -
2.5 Part 2: Synthesis of Enecarbamates and Enamides as Precursors for Fragment Elaboration	- 49 -
2.6 Introduction	- 49 -
2.7 Results and Discussion	- 55 -
2.8 Conclusion	- 77 -
2.9 Future work	- 77 -

3 Chapter 3: Synthesis, Biological Evaluation and Elaboration of Fragments Targeting Aurora-A Kinase	- 79 -
3.1 Introduction	- 79 -
3.2 Results and Discussion	- 95 -
3.3 Conclusion	- 158 -
3.4 Future Work	- 159 -
4 Chapter 4: Investigating the Selectivity of ATP-binding Site-Targeting Fragments with a Diverse Range of Kinases	- 162 -
4.1 Introduction	- 162 -
4.2 Results and Discussion	- 165 -
4.3 Conclusion	- 178 -
4.4 Future Work	- 179 -
5 Chapter 5: Thesis Conclusion	- 181 -
6 Experimental	- 184 -
6.1 General Information	- 184 -
6.2 General Procedures	- 186 -
6.3 Characterisation of Compounds	- 189 -
6.4 Biochemical Experimental	- 317 -
8 References	- 320 -
Appendix 1: Synthesised Fragments and Their Potency Against Aurora-A from Chapter 3	- 335 -
Appendix 2: IC ₅₀ Curves of the Fragments Screened in Chapter 3	- 337 -
Appendix 3: Elaborated Fragments Screened in Chapter 3	- 342 -
Appendix 4: IC ₅₀ Curves of the Elaborated Fragments Screened in Chapter 3	- 343 -

1 Chapter 1: Introduction

1.1 An Overview of the Drug Discovery Process

Developing an efficacious drug molecule which both produces the desired effect in patients while being safe is a well-documented challenge.^{1, 2}

The drug discovery process begins with the identification of a target. Characteristics of a suitable target are that it is safe, meets both clinical and commercial demand and importantly is “druggable”.³ A druggable target is a protein, peptide or nucleic acid which can have its activity modulated by a drug, eliciting a biological response which can be measured both *in vitro* and *in vivo*.^{4, 5}

The target is validated through chemical, biological and biophysical techniques.⁶ Target identification and validation increases confidence in the relationship between the target and the disease state, enabling understanding of mechanism-based side effects on target modulation.⁴ High-throughput screening (HTS) can then be utilised to screen large compound libraries in order to identify compounds which interact with a target, known as “hit” compounds.⁷ In addition to this approach, hit compounds can also be identified through biophysical screening, literature searching or *in silico* modelling.⁸

Confirmed hit compounds which demonstrate specific and concentration-dependent activity against the target are analysed, clustered and prioritised.⁹ A highly ranked hit compound is then subjected to exploratory synthesis and further screening to generate a “lead” compound, in a process known as hit-to-lead optimisation.⁸ The objective of hit-to lead optimisation is to identify “lead” compounds suitable for full scale lead optimisation.⁹ The aim of lead optimisation is to generate a clinical candidate with the desired mix of affinity, efficacy, ADME and physicochemical properties. Lead molecules are

screened in cell-based assays and animal models predictive of the disease-state to characterise efficacy and toxicology.^{4, 10}

Once a lead compound has passed through the pre-clinical stages of development, the drug candidate progresses into clinical trials. Phase I is concerned with examining safety and dosage regimes of the drug candidate within a small number of healthy volunteers. Phase II assesses drug efficacy and side effects within several hundreds of patients with the relevant disease/condition. Phase III provides the greatest amount of information on safety, efficacy and dosage compared to the current leading treatment for a disease in thousands of patients. Efficacy can also be tested at varying stages of a disease. Drug candidates that pass these trials can be approved and consequently be used clinically, with only one in nine drugs in clinical development making it to market.¹¹ Following approval, further trials can take place (phase IV) to assess long term effects of a drug.^{12, 13} Figure 1 displays an overview of the drug discovery process.

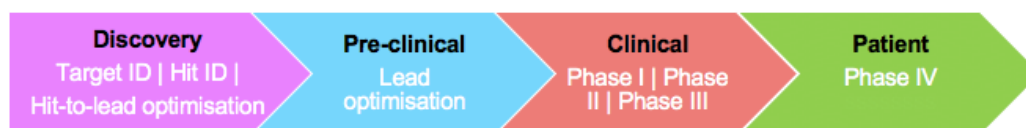


Figure 1: The typical drug discovery approach starts with the identification of a target. After hit identification and hit to lead optimisation, the compound enters pre-clinical development and then enters three phases of clinical trials. The entire process requires 10-years on average.

1.2 Challenges Facing the Pharmaceutical Industry

The post-genomic era has led to a significant increase in the number of potential targets with no known modulators.⁷ The pharmaceutical industry is under increasing pressure to produce new molecular entities (NME), made more challenging by poor late stage pipelines, patent expiration and increasingly rigorous safety requirements from regulatory authorities.^{2, 14} The price of drug discovery is expensive, (valued at \$2.6 US billion per launched drug) and time-consuming (a typical time to market of 13 years).¹⁵ Furthermore, a clinical success rate of 11%, which drops to 8% for central

nervous system (CNS) targets and 5% for oncology targets, highlights the importance of timely and efficient choices for pharmaceutical development.^{16,17} Improving the efficiency of drug discovery will not only benefit pharmaceutical research and development, but ultimately the patient.

1.3 Rates of Attrition and their Underlying Causes

In 1991, pharmacokinetic (PK) and bioavailability was the most significant cause of attrition, accounting for ~40% of all attrition. With the high cost of development, this represented a major economic loss for pharmaceutical corporations. By 2000, there had been a dramatic reduction in these factors, showing PK and bioavailability to now contribute to ~10% of all attrition.² This was remedied by the introduction of early stage ADME (absorption, distribution, metabolism, excretion) testing. The failures of drug candidates due to poor PK profiles diminished significantly, but this was accompanied by a shift towards failures as a result of efficacy and safety.⁶ This swung the temporal attrition profiles of drug candidates to the later stages of clinical trials, as PK complications would be realised in phase I, dramatically increasing the cost of failure.

1.4 The Approach to Drug Discovery: High Throughput Screening

Over the past two decades, HTS has been the principal tool implemented by the pharmaceutical industry to identify new lead compounds. It was thought that the low accuracy of the results obtained would be overcome by the efficiency of the technique. However, a high incidence of false positives and false negatives has hindered its success.^{5, 18} There is also the suggestion that HTS has stifled the creativity of medicinal chemists, leading to a general pattern of synthetic reactions, bioisosteres or existing drugs being repositioned.^{19, 20} Molecules identified by HTS tend to be large, hydrophobic and sample a minute fraction of chemical space.² Hence, there has been increased pressure to develop new lead discovery methods in order to discover more suitable chemical starting points.

1.4.1 Characteristics of Drug-Like Molecules

Medicinal Chemists have highlighted the importance of physiochemical properties on the success of drug candidates in drug discovery.² Pharmacodynamics considers the direct interaction between a ligand and the biological target, a recognition that is determined by how well the compound interacts in the target site. Pharmacokinetics refers to the journey of the drug from its point of entry to the site of action and subsequent elimination from the body. This process can be defined by the following phases: absorption, distribution, metabolism, and excretion (ADME).^{21, 22} In drug discovery, the first chemical step is the physical creation of ligands with high affinity for a given target, fulfilling the pharmacodynamic condition. Drug-like properties ideally should be taken into consideration as early as possible, in order to fulfil the pharmacokinetic condition.²³⁻²⁵

Lipinski raised awareness of the importance of physiochemical properties on the success of orally bioavailable drug candidates through identifying properties associated with poor absorption or permeability of a compound.²⁵⁻²⁷ Pharmacokinetic properties can be predicted from the *in vitro* ADME profile, which can be guided by Lipinski's rule of five. Some of the guidelines are summarised in Table 1.

Entry	Physiochemical property	Ideal Value
1	Molecular weight	≤500
2	LogP	≤5
3	Hydrogen bond acceptors	≤10
4	Hydrogen bond donors	≤5

Table 1: Lipinski's Rule of 5 (RO5) provides an empirical guide for determining if a compound will be orally bioavailable. The Lipinski criteria are widely used to predict not only absorption of compounds but overall drug like-ness.²³ LogP is defined as the 1-octanol-water partition coefficient.

The criteria are utilised as a guide and compliance does not necessarily make a compound drug-like.²⁸ It is noted that for drugs targeting the CNS²⁹ and protein-protein interactions,³⁰ violation of the Lipinski RO5 is more prevalent.

$\text{Log}P$ is an important parameter to control in drug discovery due to its composite nature.^{31,32} The $\text{Log}P$ of a compound encompasses molecular shape, polarity, hydrogen bonding capacity and describes how lipophilic a molecule will be. Lipophilicity reflects molecular desolvation on moving from the aqueous phase to cell membranes and protein binding sites, which are mainly hydrophobic.³³ As lipophilicity increases ($\text{cLog}P > 3$) binding affinity increases, but this leads to poor solubility, metabolic clearance and increased promiscuity.^{31,34,35}

Statistical analysis by Leeson *et al.* displayed that mean molecular mass and thus lipophilicity of a drug candidate increased on progression through pre-clinical and clinical development.^{17,33} This encouraged the suggestion that when the size of a compound approaches that of a phospholipid molecule, passive absorption is reduced.³⁶ Drug candidates of larger molecular weight are also more likely to contain toxic pharmacophores or rapidly metabolised motifs.

Lovering and co-workers determined a positive correlation between the number of sp^3 -hybridised carbons and aqueous solubility, which consequently led to increased success in clinical development.³⁷ Wang *et al.* showed that a decrease in saturation led to increased structural planarity and improved crystal-stacking capability leading to a poorer value of solubility.³⁸ Additionally, it is postulated that a larger number of aromatic moieties in a drug molecule (≥ 3), increase the likelihood of failure as a drug molecule.³⁹

1.5 Fragment-based drug discovery: An Alternative Approach for Lead Discovery

Fragment-based drug discovery involves the elaboration of weak binding molecules of low molecular mass, for the generation of lead compounds in drug discovery (Figure 2). Fragment screening was initially developed to generate hit compounds against targets for which HTS had been unsuccessful.⁴⁰ This approach varies from HTS in almost every aspect; library size, screening method, hit value and dependence on structural methods.

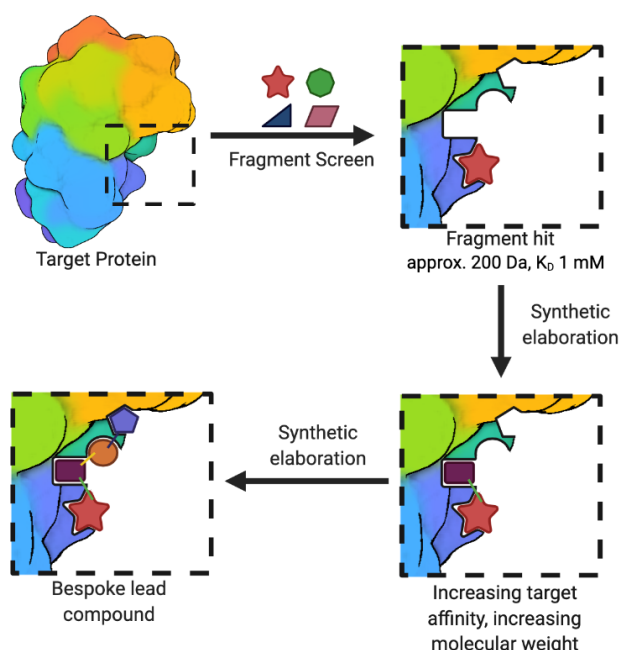


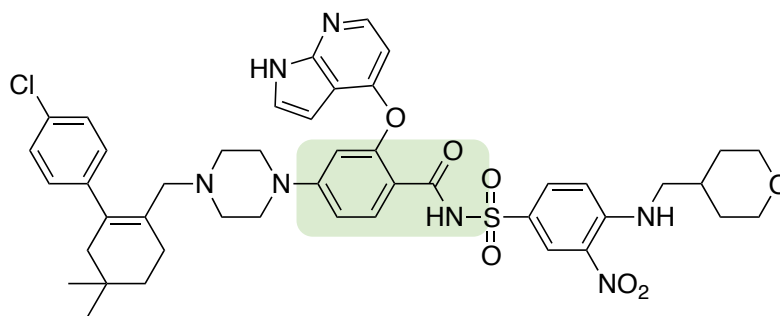
Figure 2: Fragment based drug discovery approach. Fragments <250-300 Da are elaborated into high affinity lead compounds.⁴¹ Image created with Biorender.com.

The origin of FBDD can be traced back to seminal publications by Page and Jencks who postulated that the expected binding affinity of joined molecule would exceed that of two weakly binding chemical entities (fragments).⁴²⁻⁴⁴ This idea was developed by Andrews *et al.*⁴⁵ who reported the contribution of individual functional groups to binding energies. Abeles provided experimental support for these hypotheses in 1985 by dividing a known inhibitor of HMG-CoA reductase into smaller structural components and

observing weak binding of each.⁴⁶ Another notable contribution was from Verlinde who designed and merged fragments complementary to specific sub-regions of a protein binding pocket, to generate highly potent lead compounds against *Trypanosoma brucei*.⁴⁷ Pioneering screening studies by Abbott⁴⁸ utilising SAR by NMR (structural activity relationships by nuclear magnetic resonance) and Astex^{49,50} employing high-throughput X-ray crystallography, renewed interest in the field. The techniques enabled identification of discrete molecular components (fragments) that displayed binding at a given target. The fragment hits can then be developed into high affinity drug molecules through chemical elaboration, merging or linking with other fragments to build a more complex lead series.

FBDD has been successfully utilised against varied drug target classes such as kinases,⁵¹ protein-protein interactions,^{52,53} transcription factors,⁵⁴ protein chaperones^{55,56} and RNA.⁵⁷ Subsequently, it has become clear that this approach is generic and can be applied successfully to proteins which have structural information readily available. In addition to dealing with a range of targets, FBDD has shown promise in improving the screening and chemical optimisation approach for conventional drug targets as well as enabling prioritisation of screening compounds for HTS, showing that the two approaches could be used in tandem.⁵⁸

The first FDA approved drug developed by FBDD was Zelboraf in 2011,⁵⁹ and a second, Venetoclax, in 2016. The development of Venetoclax illustrates the power of fragments to tackle a difficult target by accessing unusual chemical space. Venetoclax is noted to violate the Lipinski rule of five, highlighting that this 'rule' should be used only as a guide (Figure 3).



1

Figure 3: The structure of Venetoclax, an orally administered drug targeting Bcl-2, discovered by fragment-based drug discovery, with the original fragment starting point highlighted in green. MW 868 Da and LogP 10.4.

In FBDD, the ideal optimisation process begins with fragments of small size and efficient binding, ideally with each atom of the fragment participating in the desired binding interaction. The size, complexity and physical properties of a molecule can potentially be more precisely controlled when starting with a high affinity fragment (a molecular weight of 150-300 Da can give a binding affinity of the order of mM) than starting from a HTS hit which likely contains functionality unessential to binding (a molecular weight of 500 Da gives a maximum binding affinity of nM).⁶⁰ As a result of the low affinity, to detect the binding of fragments, sensitive biophysical screening methods must be used rather than activity-based assays, a summary is shown in Table 2. Higher concentrations are required for fragment screening compared to those used in HTS bioactivity assays.

Technique	Description	Example
Differential Screening Fluorimetry (DSF)	Fragments are detected that increase the unfolding temperature of the target protein (ΔT_m) by binding to and stabilising the proteins folded state in the presence of a fluorescent dye. ^{61,62}	p53 ⁵⁴
Surface Plasmon Resonance (SPR)	The target protein is covalently linked to a gold surface on a biosensor chip, and solutions of the single fragments are sequentially flowed through the chip. Binding affinity and kinetics can be obtained through a time- dependent fragment association-dissociation response. ⁶³	BACE-1, ⁶⁴ MMP-12, ⁶⁵ thrombin, ⁶⁶ chymase ⁶⁷
Electrospray Ionisation Mass Spectroscopy (ESI-MS)	The fragment/protein mixture is ionised by ESI, with fragment binding observed by an increase in the mass of the protein ion corresponding to that of the bound fragment. ⁶⁸ Native mass spectroscopy is utilised as complementary fragment screening approach.	PMT, ⁶⁹ CA-II ⁷⁰
X-Ray Crystallography	Crystals of the target protein are soaked with high concentration solutions of fragments or cocktails of fragments. Protein crystals are exposed to an X-ray source and a diffraction pattern recorded. The diffraction pattern is used to generate an electron density map, subsequently used to solve the structure of the protein. Identification of fragments bound to the protein can be done by inspection of the electron density maps of the complex and the protein alone. ⁷¹	CDK2, ⁷¹ ATAD2 ⁷²
Nuclear Magnetic Resonance (NMR)	Different experimental formats have been employed. ⁷³⁻⁷⁵ The foundation of fragment screening by NMR is that binding equilibria modulate both frequency and width of NMR spectral lines in response to the rate of “chemical exchange” between the free and unbound state of the fragment and target protein.	HSP90 ⁷⁶

Table 2: Common biophysical techniques utilised in fragment-based drug discovery.

1.5.1 Characteristics of Fragments: Building a fragment library

Zartler and Shapiro stated that in FBDD “ontogeny recapitulates phylogeny” (i.e. the physical properties of the fragments remain largely the same in the final drug candidate).⁷⁷ One of the first approaches to describe the chemical properties of fragments was the rule of three, shown in Table 3.⁷⁸

Entry	Physiochemical property	Ideal Value
1	Molecular weight	≤ 300
2	Log P	≤ 3
3	Hydrogen bond acceptors	≤ 3
4	Hydrogen bond donors	≤ 3

Table 3: The rule of three, as proposed by Jhoti and colleagues.⁷⁸

Hubbard *et al.* defined the rule of three as the upper limit of desirable fragment properties, but observed that it gave no information on the lower limit or distribution.⁷⁹ The same publication highlighted the importance of polar surface area (PSA), due to its role in human intestinal permeability and states that fragments should be limited to a PSA of no more than 60 Å. Pfizer designed a fragment library which imposed more stringent rules on chemical properties; a molecular weight of no more than 250 Da and a cLog $P \leq 2$, to promote high aqueous solubility and to allow for a broad target application. Pfizer placed restrictions on molecular complexity, in accordance with the Hann model.⁶⁰ According to this model, the probability of finding a fragment hit increases when small, less complex fragments with fewer interactions are screened with high sensitivity, an approach validated by Novartis.⁸⁰ Gibbs *et al.*⁸¹ reported exclusion of more than 45 functional groups and substructures as part of a primary library filter. The RO3 has attracted some criticism; for example Koster *et al.* assembled a fragment library without emphasis on conforming to the RO3 and screened the fragments against endothiapepsin.⁸² They discovered eleven hit fragments, with only four obeying the RO3, illustrating their use should be as a guide.

In 2016 Astex updated their list of desirable properties in line with some of the findings of other groups and their own research (Table 4).⁸³ They highlighted the importance of a variety of three-dimensional shapes for fragment libraries, as additional sp³-hybridised carbon atoms act as growth points for fragment hits, but cautioned against its prioritisation, since fragments without stereocentres may adopt 3D or chiral conformations on binding with a target.⁸⁴ These updated guidelines place emphasis on a fragment's physical properties and their potential for chemical evolution.⁸⁵

Entry	Physiochemical property	Ideal range
1	Molecular weight	140-230 Da
2	Lipophilicity	0 < cLogP < 2
3	Heavy atom count	10 – 16
4	Solubility	Aqueous solubility (preferably ³ 5 mM in 5% DMSO, or other screening co-solvents)
5	Substructures	Remove moieties associated with high reactivity, aggregation in solution or false positives.

Table 4: The updated aspirational properties in fragment design, proposed by Murray and Rees.⁸³

1.6 A Matter of Chemical Space

Fragment-based drug discovery (FBDD) and HTS are important approaches to find chemical starting points for drug discovery programs. HTS libraries often derive from earlier medicinal chemistry projects and combinatorial chemistry which are often already drug-like according to Lipinski's RO5, leaving little room for lead optimisation. For drug-like compounds in the size of 30 heavy atoms (C, N, O and S), the chemical space is estimated to comprise of 10³⁰-10⁶⁰ molecules and so a library of 1000 molecules would cover a very small fraction of chemical space.⁸⁶ However, screening small molecules of approximately 12 heavy atoms in size to screen, gives a total of 160 million possible compounds. Therefore, 1000 compounds would

represent 0.001% of the whole subset of chemical space. To put this simply, an increase of 19 orders of magnitude of chemical space coverage is possible with a library of smaller molecules (12 heavy atoms) than of large molecules (36 heavy atoms).

Hann *et al.*⁶⁰ stated that the probability of a compound being a hit molecule is determined by its complexity. A complex molecule is more likely to have a single defined binding mode than smaller, less decorated fragments. This idea was supported by computational modelling which suggested there is optimum complexity; molecules should be simple enough to bind to several different target proteins, while being complex enough to still bind in a single defined orientation. Flaws arise in the theory when it is applied to real molecules and size is used to measure complexity. This is because highly functionalised molecules with ornate 3-dimensional shapes are more complex than equivalently sized molecules which are planar and less decorated. A second consideration is that as molecular size increases, so often does lipophilicity and thus promiscuity; promiscuity could mask the expected correlation.

Overall, useful starting points for lead identification can be identified from relatively small libraries of low molecular weight compounds (120-300 Da range).

1.7 Fragment Elaboration

Fragment hits are structurally elaborated to increase their potency through an iterative process of rational design and synthesis, usually relying on structural information to guide optimisation. There are three main methods of increasing potency from fragment hits: fragment merging, linking and growth. Fragment merging uses attributes of two overlapping motifs to produce a single molecule, while linking utilises two non-overlapping fragment hits and attempts to link them.^{40,41,87}

The most common strategy implemented is fragment growth, which employs chemical synthesis to elaborate a fragment to explore further interactions. Prior to fragment growth, the potency of the initial fragment will be optimised through examining analogues or fragments with minor elaboration, to probe the protein ligand interaction and confirm that the optimum fragment has been found. The choice of fragment for growth will be influenced by potency, synthetic tractability and ligand efficiency.^{41,56,83} Ligand efficiency (LE) was first described by scientists at Pfizer⁸⁸ to describe the average free energy binding per heavy atom. Monitoring of ligand efficiency throughout fragment elaboration enables assessment of whether the additional molecular mass added in the growth process has been added efficiently. An LE value of approximately 0.3 kcal mol⁻¹ should lead to a rule-of-five compliant 10 nM inhibitor.⁸⁷ An advancement on LE is group efficiency (GE) which accounts for the contributions from each chemical group incorporated.⁸⁹ At each stage of fragment growth, LE can be utilised to describe efficient binding to a target.

1.7.1 Fragment Elaboration: The Trouble with Fragments

Drug discovery using fragments poses difficulties due to their small size, lipophilicity and need for synthetic vectors to allow growth of the fragment in three dimensions. Leading practitioners have cited two areas requiring research within fragment-based drug discovery; methodology for the elaboration of small low affinity fragments into high affinity lead molecules and inclusion of precisely controlled synthetic vectors to allow for fragment growth.⁸³ FBDD programs are frequently challenged and subsequently delayed by the requirement to develop methodology to access growth vectors in 3D space.⁹⁰ Other issues encountered in fragment growth are the lack of synthetic methodologies compatible with the presence of multiple heteroatoms and polar functional groups, and the synthesis of molecules with high aqueous solubility, which is required for fragment screening.

Robust methods for the elaboration of fragment libraries into diverse lead-like compounds libraries are beginning to emerge, but such studies remain under-represented in the literature. As such there is still a substantial demand to increase the arsenal of methods to elaborate fragments.

1.8 Applications of Fragment Based Drug discovery

This section details successful application of fragment-based drug discovery approaches, illustrating the steps taken in the development of lead compounds against varied targets.

1.8.1 ATAD2

Researchers at GSK conducted a fragment screen using X-ray crystallography against ATAD2 (ATPase Family AAA Domain Containing 2), with a hit rate of 0.25% (Figure 4). Their initial aim was to inhibit ATAD2 with μM activity, while maintaining selectivity over BET bromodomains.⁹¹ X-ray crystallography led to the identification of **2** as the binding fragment. The binding mode was characterised, elucidating that **2** acted as a mimic of the native acetyl-lysine ligand for the bromodomain, forming hydrogen-bonding interactions with N1064 and Y1021 in the binding site. Modelling suggested introduction of an ether linkage could direct hydrophobic groups towards the lipophilic RVF shelf in ATAD2 and ultimately, through an iterative process of computational docking and synthesis led to **5**, a 130 nM inhibitor of ATAD2, which displayed selectivity over BRD4 and maintained LE of 0.3 kcal mol⁻¹.⁷² The researchers demonstrated through growth of the original fragment that both nM potency and selectivity against a target previously thought to be undruggable was achievable.

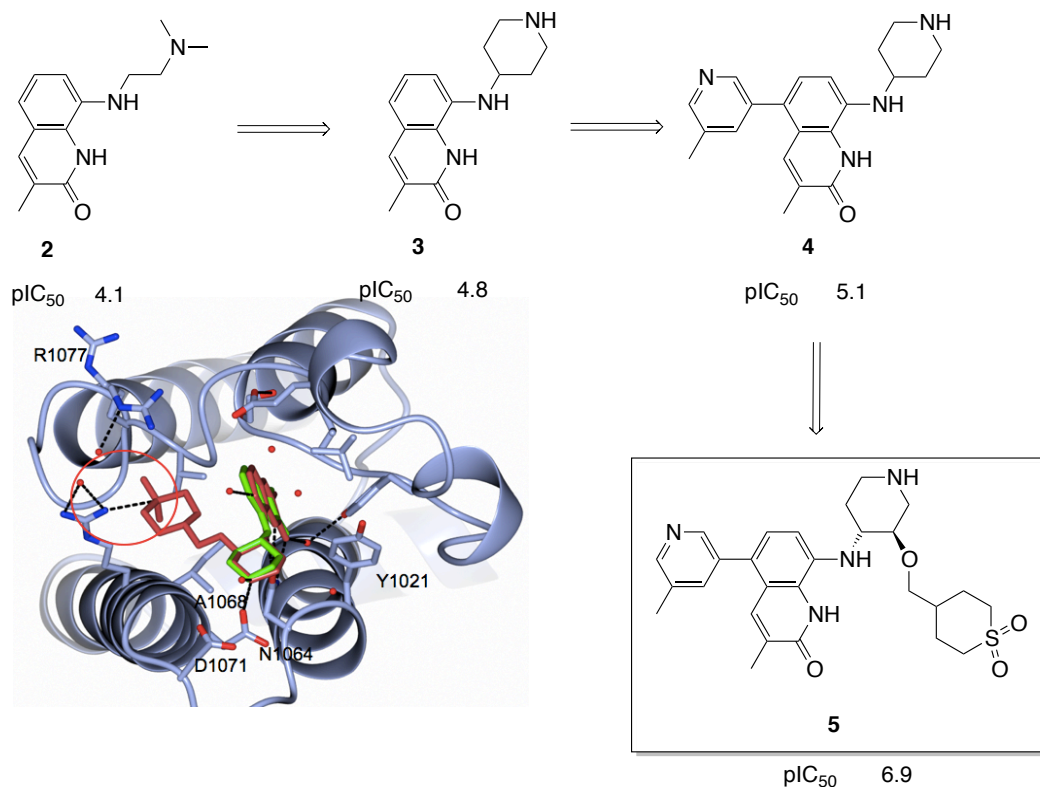


Figure 4: X-ray structure of ATAD2 bound to **5** (Crimson, PDB: 5a82) superimposed on **3** (green, PDB 5a5q). Right details the interactions within the binding site, with the RVF shelf circled in red. Left shows the electrostatic charge coloured protein surface, with **8** in the binding site.^{72,91}

1.8.2 Aurora-A Kinase

Kinases are a class of proteins with well-defined and druggable active sites and are, in general, structurally tractable.⁹² Aurora enzymes are serine/threonine kinases that are known to be important regulators of mitosis.⁹³ Aurora A is of considerable interest in cancer drug discovery due to its elevated expression in solid tumours and leukaemia. Howard *et al.*⁷¹ reported the discovery of a selective Aurora A inhibitor based on a fragment previously discovered in a CDK2 program (Figure 5, structure **6**). Examination of the binding mode of the pyrazole-benzimidazole fragment showed that it bound in the ATP-binding pocket and potentially allowed room for growth at the 4-position of the pyrazole or the 6-position of the benzimidazole. Addition of a *p*-fluorobenzamide at the 4-position of the pyrazole and introduction of an *N*-methylene morpholine motif in the 6-position of the benzimidazole gave

excellent affinity for Aurora A, but poor PK properties. Keeping the solubilising *N*-methylene-morpholine motif in place, while optimising the *p*-fluorobenzamide to a urea linked-cyclopropyl moiety gave compound **8** with an improved *in vitro* affinity, ADME properties, PK mouse profile and anti-HCT116 carcinoma cell activity. It is noted that **8** (AT9238) hits more than 20 other kinases with a similar potency, raising questions about selectivity and potential off-target effects. AT9238 (**8**) progressed into phase I clinical trials, demonstrating Aurora kinase inhibition tolerance and disease stabilisation in a variety of childhood tumours. The trial closed prematurely in phase II due to no evidence of clinical efficacy being observed.⁹⁴

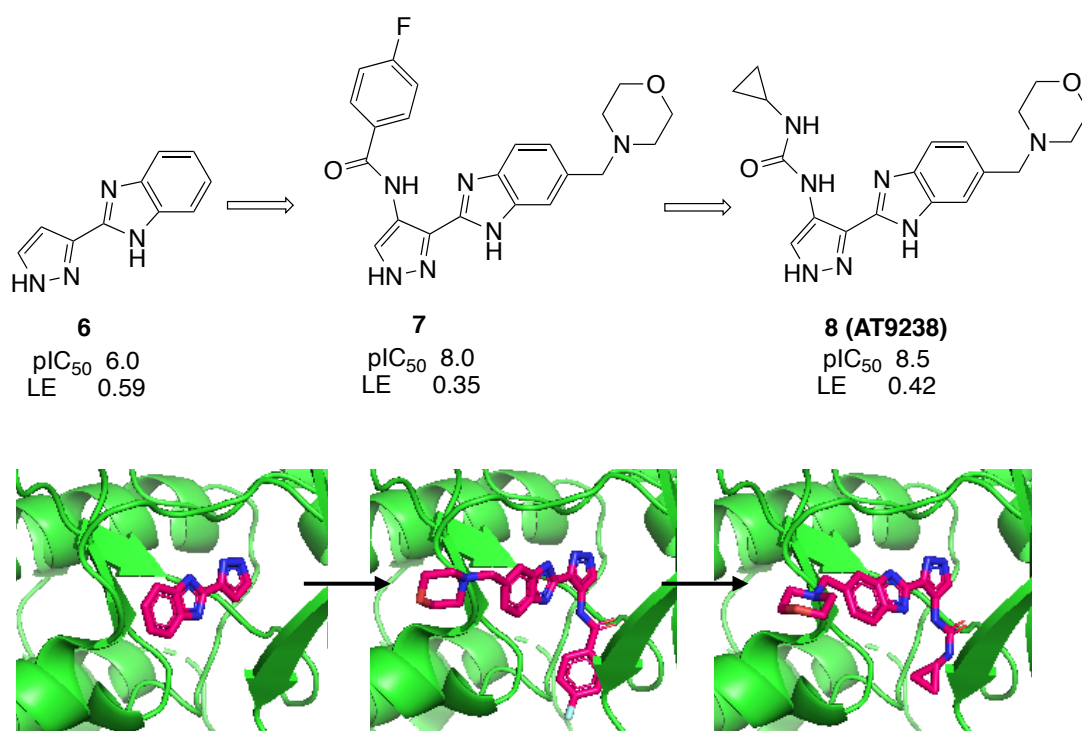


Figure 5: Fragment growth leading to development of **8**, AT9283, an ATP binding site inhibitor of Aurora A (PDB: 2W1D, 2W1C, and 2W1G).⁷¹

1.8.3 Catechol *O*-methyltransferase

Catechol *O*-methyltransferase (COMT) catalyses the Mg^{2+} dependent methyl transfer from SAM (S-adenosyl-L-methionine) to a hydroxyl group of endogenous catechols and neurotransmitters such as dopamine, terminating their biological activity. COMT is a validated target against Parkinson's disease and has applications in disease-states characterised by low dopamine levels.⁹⁵ Roche identified a pyrazole class of inhibitors targeting the SAM pocket, as opposed to the catechol and hydroxypyridine inhibitors previously reported which chelate the Mg^{2+} site.⁹⁶ They screened 6000 RO3 compliant fragments using SPR, obtaining 600 fragment hits. Follow-up involved a SPR dose-response measurements, confirming 200 fragments, which were examined using ligand-detected NMR and ($^1H/^{15}N$ HSQC) NMR. It was found that 3 of the 4 fragment inhibitors that surpassed these filters were pyrazoles, almost identical to the starting structures reported by Takeda.⁹⁶ This could mean that COMT requires a very specific ligand or that fragment screening libraries may not be as diverse as once thought.

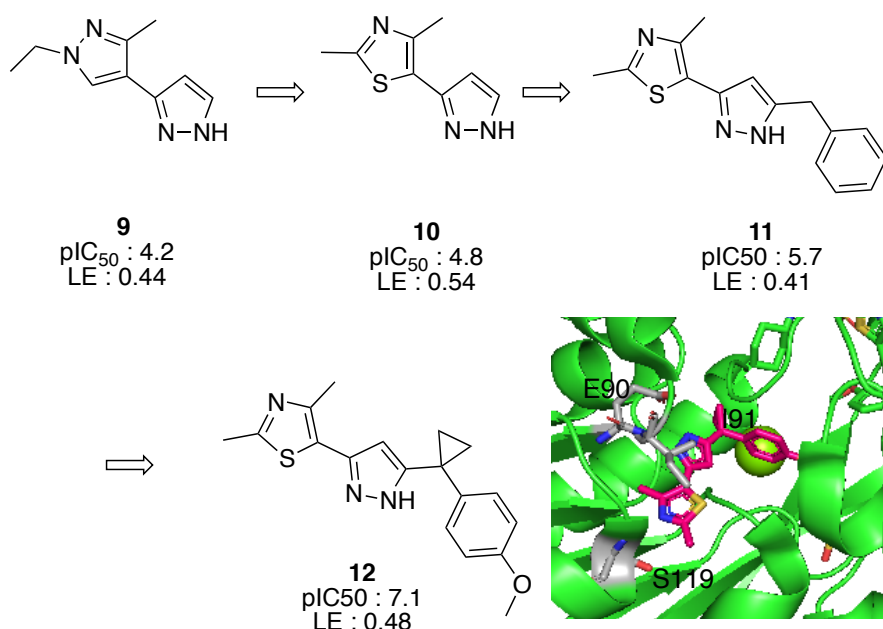


Figure 6: Fragment growth to develop a potent inhibitor of COMT. PDB: 5k01.

Roche utilised iterative structure-guided fragment growth to improve the potency of compound **9** (Figure 6). It was found that exchange of the substituted pyrazole for a thiazole led to a 3-fold improvement in potency, shown in compound **10**. The crystal structure shows that the nitrogen atom of the thiazole ring is involved in hydrogen bonding to the backbone NH of Ser119. The pyrazole occupies the ribose-binding region and both nitrogen atoms form hydrogen bond interaction to E90 and I91. Sterically demanding functionality was found not to be tolerated at the 2- and 4-positions of the thiazole. Examining the 3' position of the pyrazole displayed that direct attachment of a phenyl ring was not tolerated but addition of a small linking chain between the pyrazole and the phenyl led to an improvement in potency. Addition of a cyclopropyl group in the benzylic position led to a further gain in potency. It was found binding affinity tended to increase when the electron density of the phenyl ring was increased, and in particular a *para*-substituted alkoxy group gave the biggest increase in potency leading to compound **12**.

96

1.8.4 FtsZ

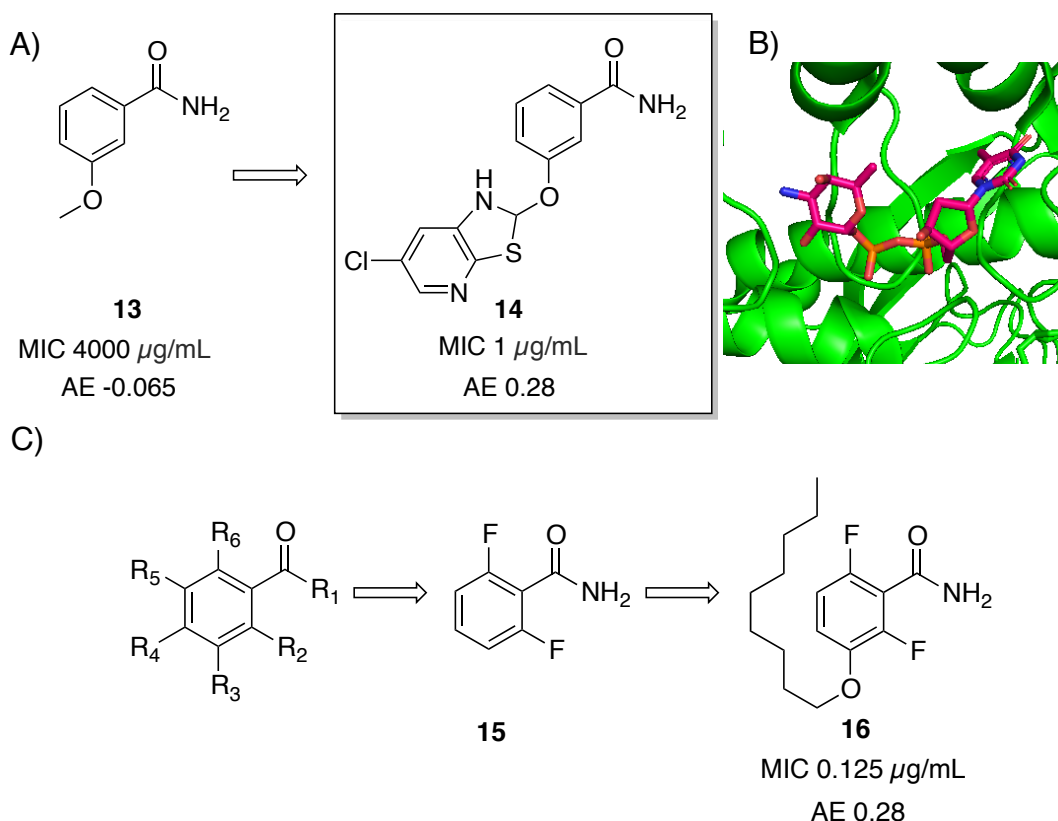


Figure 7: A) FtsZ inhibitor 3-methoxybenzamide (**13**) was the starting point for optimisation into lead compound (**14**) B) which was shown to bind in a hydrophobic cleft (PDB code 4DXD). MIC is the minimal inhibitory concentration measured mg/mL and AE is the antibacterial efficiency, a variation on ligand efficiency C) Displays evolution towards **14** via **15** and **16**.

In eukaryotic cells, targeting the proteins involved in cytokinesis has been a successful approach for anticancer activity.⁹⁷ Prokaryotic cells contain a tubulin homologue, FtsZ, which is the most abundant protein involved in prokaryotic cell division, and is highly conserved in both Gram-positive and Gram-negative bacteria.⁹⁸ On binding GTP (guanosine 5'-triphosphate) it polymerises to form the Z-ring at the site of cell division and slows the recruitment and assembly of cell division machinery.⁹⁹ Inhibition of FtsZ does not directly stop cell growth but leads to formation of long filaments that eventually cause lysis of the cell. The majority of inhibitors act by preventing FtsZ polymerisation, destabilising or stabilising polymers.⁹⁹ Following the discovery of the function of FtsZ, 3-methoxybenzamide (3-MBA) was reported

as a starting point for a fragment-based drug discovery program (Figure 7). Czaplewski *et al.* optimised 3-MBA to a potent lead compound.^{100,101} Optimisation efforts utilised minimum inhibitory concentration (IC) against *Bacillus subtilis*. SAR displayed that any substitutions in positions other than R₃ greater than a single atom eliminated growth inhibition and filamentation *in vivo*. Introduction of a lipophilic nonyl group in position R₃ increased potency by 8000 times (**16**). They evaluated progress using anti-bacterial efficiency, defined as a logarithmic function of MIC in mg/mL per non-hydrogen atom.

Further optimisation gave **14** which displayed dose-dependent efficacy against *B. subtilis* and *S. aureus* but no other Gram-positive or Gram-negative bacteria. By use of a resistance mutation profile, an apo structure of FtsZ and subsequent crystallography, compound **14** is thought to bind to an allosteric site adjacent to a nucleotide binding site, analogous to the mode of action of Taxol on tubulin. This mode of action was confirmed to promote FtsZ polymerisation and stabilise FtsZ polymers.¹⁰²

1.8.5 Summary

FBDD is now an established technique for lead discovery and there are an increasing number of very encouraging applications in the literature. The approval of the first drug to be discovered by FBDD, Zelboraf, was an important milestone in this methodology. As more fragment leads are progressed into clinical trials it will be possible to assess the impact of FBDD upon attrition rates in the pharmaceutical industry.

1.9 Thesis Aims and Objectives:

The overall aim for this project is to identify and develop methodology to aid fragment growth and to apply this methodology in FBLD. The aim can be broken down into five main objectives:

- (1) To identify and evaluate literature methodology applicable to the elaboration of cyclic amine-containing fragments
- (2) To develop synthetic methodology which can be applied to elaboration of cyclic amine-containing fragments
- (3) To design, synthesise and biochemically screen a fragment library against Aurora-A
- (4) To elaborate fragments hits arising from objective (3) using methodology from objectives (1) and (2) where applicable
- (5) To investigate the selectivity of the fragments produced in (2) and elaborated fragments (4) against a panel of 100-kinases towards the development of selective kinase inhibitors

Project Aim 1: To identify and evaluate existing methodology and develop methodology for the elaboration of cyclic amine fragments

The project will involve the evaluation of literature synthetic methodology as well as the development of new synthetic methodology for use in the elaboration of cyclic amine containing fragments. This methodology could be used in elaboration of the fragments synthesised in Chapter 3 of the thesis.

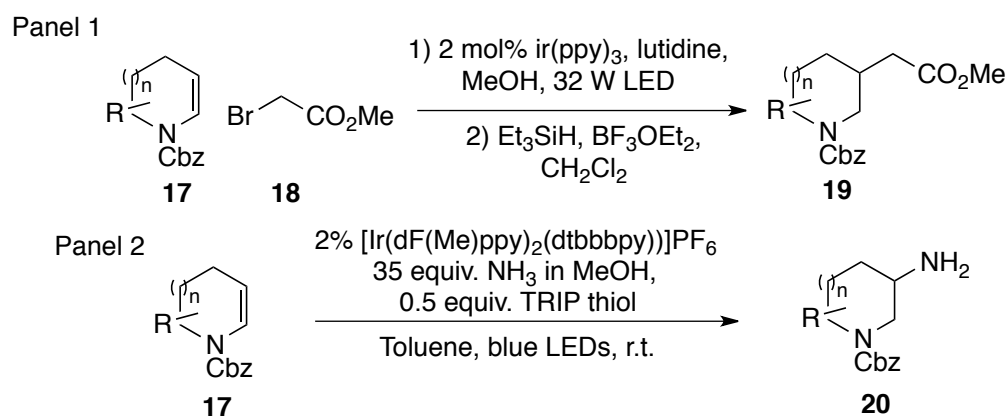
Objective 1: Evaluation and Development of Methodology For use in Fragment Elaboration in Fragment Based Ligand Discovery

The first objective within aim 1 is to evaluate existing synthetic methodology reported in the literature that could be used to elaborate cyclic amine containing fragments. From our own analysis of fragment-to-lead publications in 2019, it was shown that 59% of campaigns utilised a fragment growth approach.¹⁰³ Of all fragment-to-lead publications in 2019, 37% required a

bespoke synthetic strategy in order to access chemical analogues, conveying the huge synthetic effort that fragment growth can require. This part of the project will enable a diverse toolkit of reactions applicable to the elaboration of cyclic amines to be built, with the aim of reducing the requirement for *de novo* synthesis in fragment growth.

Objective 2: Synthesis of Enecarbamates and Enamides: Precursors for Fragment Elaboration

As previously described, leading-practitioners have called for methodology for the elaboration of small low affinity fragments into high affinity lead molecules to be developed.⁸³ The second objective is to develop synthetic methodology applicable to the elaboration of cyclic amine containing fragments. Within the Nelson and Marsden groups, elaboration methods have been described for unsaturated amine derivatives (enecarbamates and enamides) at the β -position to nitrogen, using a photoredox-mediated alkylation employing bromoacetic esters (Scheme 1, panel 1).¹⁰⁴ This methodology has been extended to introduce acetamide derivatives, facilitated by use of activated bromoacetic esters which undergo subsequent amidation in a single pot. A second transformation reported within the groups is a procedure to diversify cyclic amine fragments at the β -position (Scheme 9, panel 2), by use of photoredox-mediated hydroamination amenable to the use of ammonia and both alkyl and (hetero)aryl amines.¹⁰⁵ To demonstrate the value and utility of these synthetic methodologies, access to a variety of endocyclic enecarbamates starting materials is required.



Scheme 1: Panel 1: A photoredox mediated alkylation of enecarbamates using bromoacetic esters. Panel 2: A photoredox mediated hydroamination of enecarbamates using primary and secondary amines.

Specifically, the objective for this part of the project is to develop an efficient route towards the regioselective generation of endocyclic enecarbamates, which can then be used in the β -functionalisation chemistries previously developed within the group.

Project Aim 2: Synthesis, biochemical screening and elaboration of a kinase-directed fragment library targeting Aurora-A

Objective 1: Design and Synthesis of a Kinase-targeting fragment library

The project will involve the design and synthesis of fragments, for the use in kinase fragment-based drug discovery. The fragments will be designed through literature searching to identify heteroaromatic warheads, to target kinases. These fragments will aim to obey the following guidelines as described by literature, summarised below⁸³ using molecular properties predicted by the open access computational tool, LLAMA.¹⁰⁶

- Physicochemical properties: Molecular weight of 130-230 Da with no more than 19 heavy atoms, $-1 < \text{cLogP} < 3$ and high aqueous solubility, to enable biophysical screening at high concentrations. An upper limit for polar surface area is set at 60 Å. LLAMA will be utilised to predict

A_{LogP} and polar surface area and well as removal of any toxic functionality.

- Synthetic Tractability: Synthesis from readily available starting materials and able to readily produce 50-100 mg.

Objective 2: Biochemical Screening

Screening of the fragment library from **Aim 2 Objective 2** against our chosen kinase target, Aurora-A. This will enable identification of potential hits that target Aurora-A which can then be elaborated by methodology discussed in **Aim (1)**.

Objective 3: Fragment Elaboration and Subsequent Screening

Fragments hits identified from **Aim (2), Objective (2)** will be elaborated using methodology either identified in **Aim (1), Objective 1** or developed from **Aim (1), Objective 2** to generate elaborated fragments which can then be screened against Aurora-A. The outcome of this work will inform on how chemical elaboration affects the potency and ligand efficiency of fragment hits against Aurora-A.

Project Aim 4: Profiling of Fragments against a panel of 100 Protein-Kinases

The human genome encodes 518 protein kinases, most of which have some genetic link with disease.¹⁰⁷ The availability of selective kinase inhibitors has demonstrated potential to address the uneven exploration of kinase biology, with potential to unlock new therapeutics opportunities.

Fragments and elaborated fragments synthesised from **Aim (2), Objective 1** and **Aim (2), Objective 4**, plus additional supplementary fragments, will be profiled against a representative panel of 100 kinases. This work is carried out in collaboration with Prof. Stefan Knapp's Laboratory, at the SGC Frankfurt.

The outcome of this work will enable investigation of the selectivity of ATP-binding sites in 100 protein kinases, and to elucidate whether fragments synthesised in this project show selectivity between different kinases and how chemical elaboration of hit fragments can affect their binding selectivity.

2 Chapter 2: Evaluation and Development of Methodology For use in Fragment Elaboration in Fragment Based Ligand Discovery

2.1 Part 1: Evaluation of Existing Methodology for the Elaboration of Cyclic Amine Fragments

2.2 Introduction

Fragment-based ligand discovery (FBLD) has been transformed over the last 20 years into a mainstream approach for the discovery of drugs in industrial and academic settings. FBLD relies on the initial identification of small fragments (typically with MW < 250 Da) that bind weakly, yet efficiently, to a target protein. Binding fragments can then be elaborated, usually in the light of structural information, to yield more potent and/or selective ligands.

Despite the remarkable rise in the use of FBLD, significant chemical challenges remain for the field. Medicinal chemistry continues to be underpinned by a remarkably narrow toolkit of reliable reactions that enable direct fragment “growth” along specific vectors.^{108,109} Often the positions within fragments which are easiest to functionalise (typically heteroatoms) are also those that are required for productive interaction with the target protein. As a result, bespoke syntheses of elaborated fragments is often demanded when direct fragment growth would be desirable.

This section will explore potential methods for the fragment elaboration of cyclic amines. Emerging transformations in the literature applicable to the functionalisation of cyclic amines are trialled; these transformations may have applications in Chapter 3 of the project.

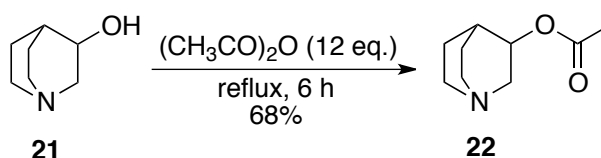
2.3 Results and Discussion

2.3.1 α -Functionalisation of Cyclic Amines

2.3.1.1 C-H Arylation of Cyclic Amines

Shaw *et al.* reported a general and selective strategy for the functionalisation of C-H bonds under photoredox catalysis by use of a hydrogen atom transfer (HAT) co-catalyst, 3-acetoxyquinuclidine (**22**).¹¹⁰ The HAT catalyst undergoes oxidation by the excited photocatalyst, to give the corresponding tertiary amine radical. Hydrogen abstraction by the tertiary amine radical is selective for the most hydridic site on *N*-Boc pyrrolidine, to give the α -amino carbon-centred radical. The combination of the HAT activation mode with metallaphotoredox catalysis enabled selective arylation of the α -position of pyrrolidine.¹¹¹ This transformation would be useful in fragment growth, since it enables activation of an array of C-H bonds as handles for cross-coupling reactions.

The HAT catalyst, 3-acetoxyquinuclidine (**22**) was prepared by acetylation of 3-hydroxyquinuclidine (**21**) through heating in an excess of acetic anhydride for six hours. The product was successfully isolated following distillation in good yield.



Scheme 2: Synthesis of the HAT catalyst.

Attention turned to using the catalyst in C-H arylation.¹¹⁰ Exploration of this reaction enabled scoping of medicinally relevant aryl groups, which could be used in fragment growth. The aryl bromide scope examined is listed in Table 5. A lower yield was obtained with 2-bromo-1,4-dichlorobenzene (**26**, Table 5, entry 3) thought to be due to increased steric hindrance of the aryl bromide. Entry 5 utilised 4-bromo-1-methyl-1H-pyrazole (**28**), which was unsuccessful, with only starting material isolated.

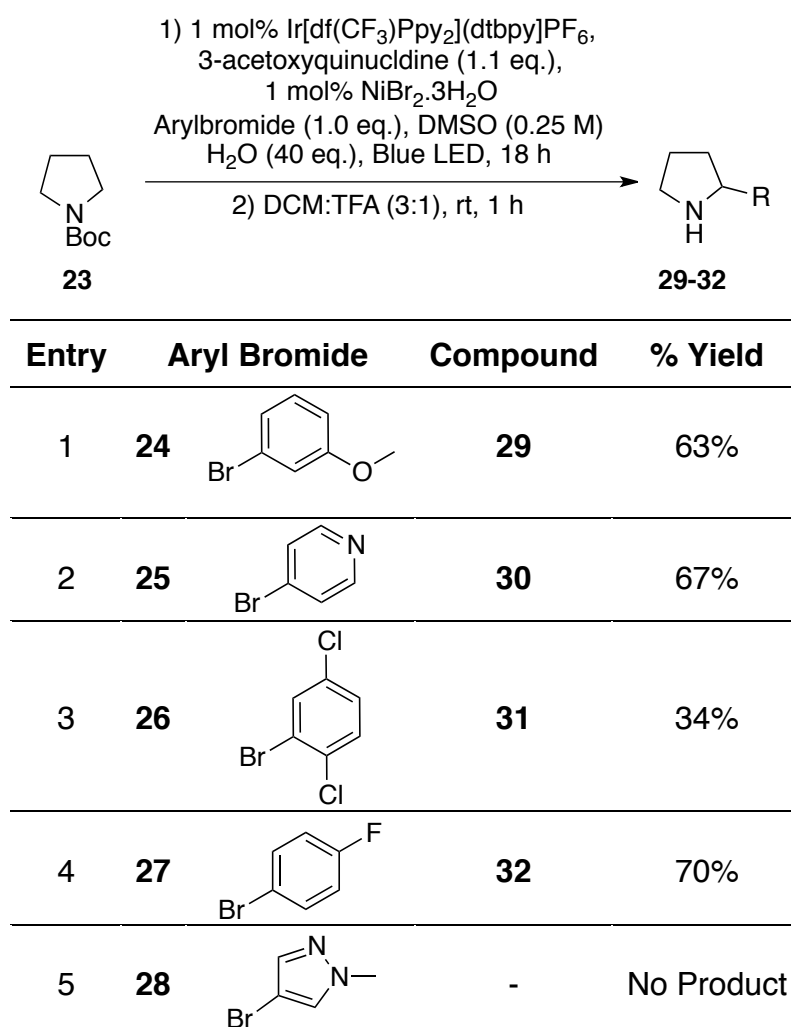
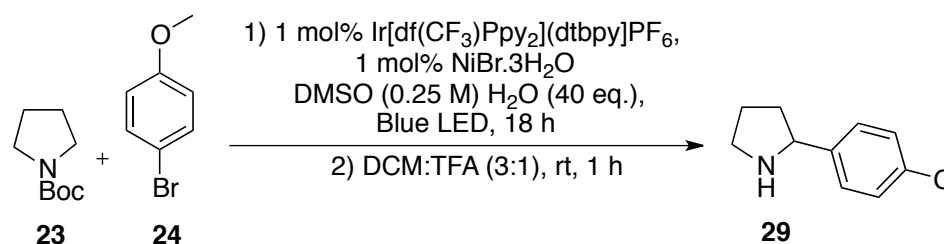


Table 5: Aryl bromide scope of photoredox C-H arylation.

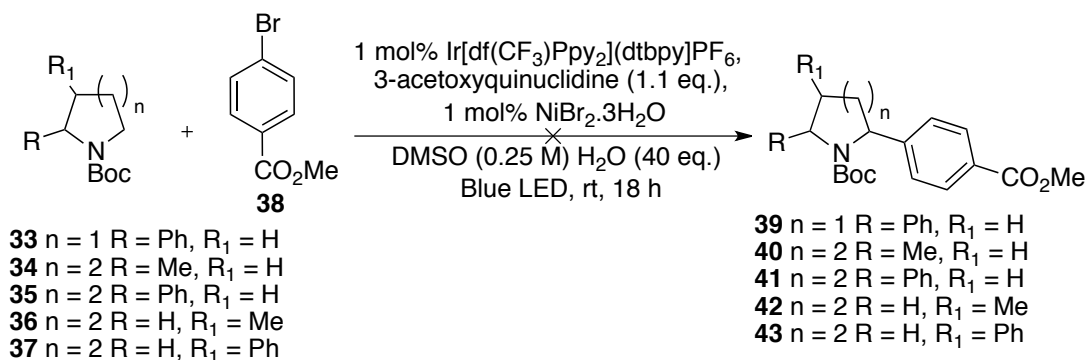
Due to the restricted access to the precursor **22** of the HAT catalyst, because of its inclusion in the Chemical Weapons Convention (CWC), we attempted to source an alternative HAT catalyst.¹¹² A series of alternatives were trialed in the reaction using **24** and *N*-Boc pyrrolidine without success (Table 6).



Entry	HAT Catalyst	Outcome
1	3-acetoxyquinuclidine	64% isolated
2	Quinuclidol	No product
3	Quinuclidone	No product
4	Quinuclidine	No product

Table 6: Variation in HAT catalyst.

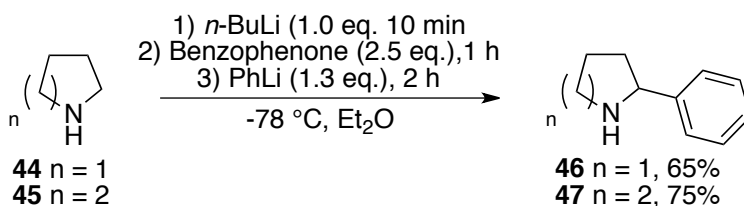
Attention turned to the synthesis of difunctionalised cyclic amines, which introduces the element of regiocontrol into the reaction. MacMillan and coworkers reported that when unsymmetrical amine substrates were exposed to this HAT protocol, preferential coupling of methylene C-H bonds over methine C-H bonds was observed.¹¹⁰ In order to appreciate the utility of this transformation in fragment growth, we applied this methodology to pre-functionalised *N*-Boc cyclic amines (Scheme 3). These experiments examined previously unreported α - and β - functionalised 5- and 6- membered cyclic amines, using the conditions reported by MacMillan.¹¹⁰ Regrettably, these reactions did not yield the difunctionalised product and protected pyrrolidines **33-37** were recovered. The original study did not explore substrates bearing phenyl substituents or functionalised piperidines. Therefore, use of this reaction in the fragment growth of pre-functionalised cyclic amines would be deprioritised.



Scheme 3: Experiments to analyse the regioselectivity of the transformation.¹¹⁰

Given the difficulty in accessing the HAT catalyst and the lack of reactivity with pre-functionalised heterocycles, we examined an alternative method of α -C-H functionalisation.

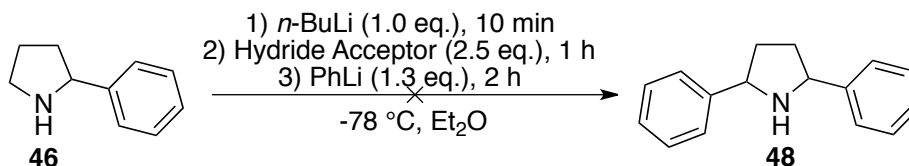
Seidel *et al.* developed a procedure for the α -C-H bond functionalisation of a broad range of unprotected cyclic N-H amines *via* nucleophilic addition to imines generated *in situ*.¹¹³ This procedure required anhydrous conditions and was unlikely to be functional group tolerant, but had advantages over using photoredox/nickel catalysed C-H acylation; it is more step-economic, with amine protection not required and therefore was an amenable approach for the growth of cyclic amine containing fragments (Scheme 4).



Scheme 4: Seidel and co-workers method for α -arylation of cyclic amines.¹¹³

Treatment of pyrrolidine (**44**) and piperidine (**45**) with *n*-BuLi resulted in *in situ* deprotonation to the lithium amide. The lithiated heterocycle engages with benzophenone, a sacrificial hydride acceptor, to provide the corresponding cyclic imine. Capture of the imine with commercially available phenyllithium furnished the functionalised amines in improved yield (**46** and **47**). compared to literature.¹¹³

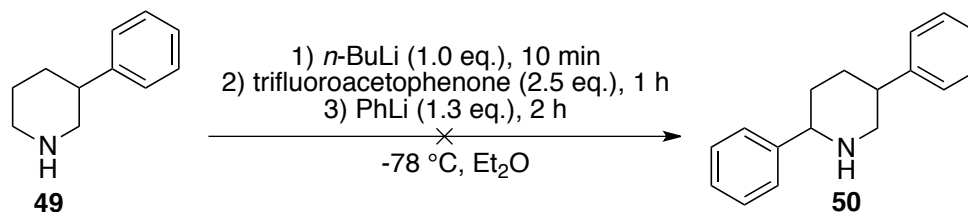
Once the synthesis of fragments **46** and **47** was complete, we examined the regioselectivity of the transformation. Seidel reported that when unsymmetrical substrates are utilised, replacement of the sterically more accessible C-H bond occurs.¹¹³ Repetition of literature substrate using 2-phenylpyrrolidine, employing benzophenone as the hydride acceptor displayed the product $[M+H]^+$ by LC-MS, but analysis by crude ^1H NMR and ^{13}C NMR did not show product and isolation of **48** was unsuccessful.



Scheme 5: Experiments to analyse the regioselectivity of the transformation

To try to understand this failure, the formation of the intermediate imine was examined as a separate step by stopping the reaction prior to the addition of the phenyllithium and the crude mixture analysed by ^{13}C NMR. Overwhelmingly, analysis displayed the presence of starting fragment **46** and benzophenone, without the occurrence of any other species. Variation of the sacrificial hydride acceptor was explored, but use of phenyl-*tert*-butyl ketone, trifluoroacetophenone and L-fenchone gave no product.

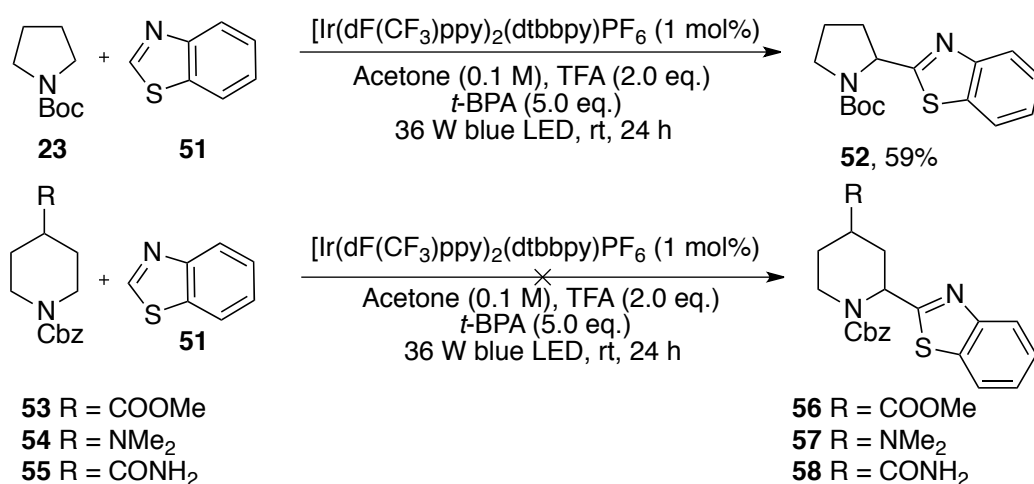
In parallel, attempts were made to repeat the reaction using the non-literature substrate 3-phenylpiperidine, employing trifluoroacetophenone as the hydride acceptor. These attempts were unsuccessful and the reaction was deprioritised as a method to elaborate pre-functionalised fragments.



Scheme 6: Applying Seidel's method to 3-phenylpiperidine employing trifluoroacetophenone as the hydride acceptor.

The Minisci reaction is a powerful methodology for combining electron deficient heteroarenes with nucleophilic radicals. The formation of nucleophilic α -amino radicals has been utilised for Minisci reactions in recent work. Dong and coworkers¹¹⁴ demonstrated conditions to couple protected saturated nitrogen heterocycles with benzothiazole. Application of *tert*-butyl peracetate (*t*-BPA) as a HAT reagent, was shown to be crucial for the reaction. Grainger *et al.*¹¹⁵ developed conditions for the high-throughput coupling of an array Boc-protected amines with nitrogen containing heteroaromatics. Bosset *et al.*¹¹⁶ reported the functionalisation of *N*-Boc azetidine with a range of heteroarenes using photoredox mediated Minisci conditions. We envisaged that by utilising the cross-dehydrogenative conditions reported by Dong *et al.*¹¹⁴ we would be able to α -functionalise fragments with varying heteroarene motifs.

Previous work within the group completed by Dr. Andrew Gomm, focused on the adaptation and optimisation of Dong's procedure to the construction of bio-active molecules in an array format on 96-well plates.¹¹⁷ Using the results of this work as a guide, we sought preparative synthesis of α -functionalised cyclic amines. We commenced by repeating the reaction of *N*-Boc pyrrolidine as the substrate hydrogen donor and benzo[*d*]thiazole (**51**) as the heteroarene using the conditions reported within the group to give pyrrolidine **52**, in a comparable yield.



Scheme 7: Synthesis of fragments using the Minisci-type heteroarylation.

In order to examine the reactions applicability to fragment elaboration, we utilised 4-functionalised piperidines **53-55** containing an ester (**53**), tertiary amine (**54**) and a primary carboxamide (**55**). These reactions were unsuccessful, giving a complex mixture of unidentifiable products. Although the work within the group did not explore Cbz-protected amines, they are reported in work by Wang *et al.* so would be expected to be tolerated. Equally, work within the group displayed variations in ring size to be tolerated. From the results we obtained with pre-functionalised amines, this method was deprioritised as a method to elaborate fragments.

2.3.1.2 C-H Alkylation through Cross-Coupling of Carboxylic Acids with Alkyl Halides

MacMillan *et al.* reported a dual catalytic system which employs photoredox and nickel-catalysed substitution reactions of alkyl halides with cyclic amines through decarboxylative generation of α -aminoalkyl radicals.¹¹⁸ The synthesis of an array of alkyl halides was attempted using this procedure, entries 3 and 4 are not previously reported substrates of this reaction (Table 7).

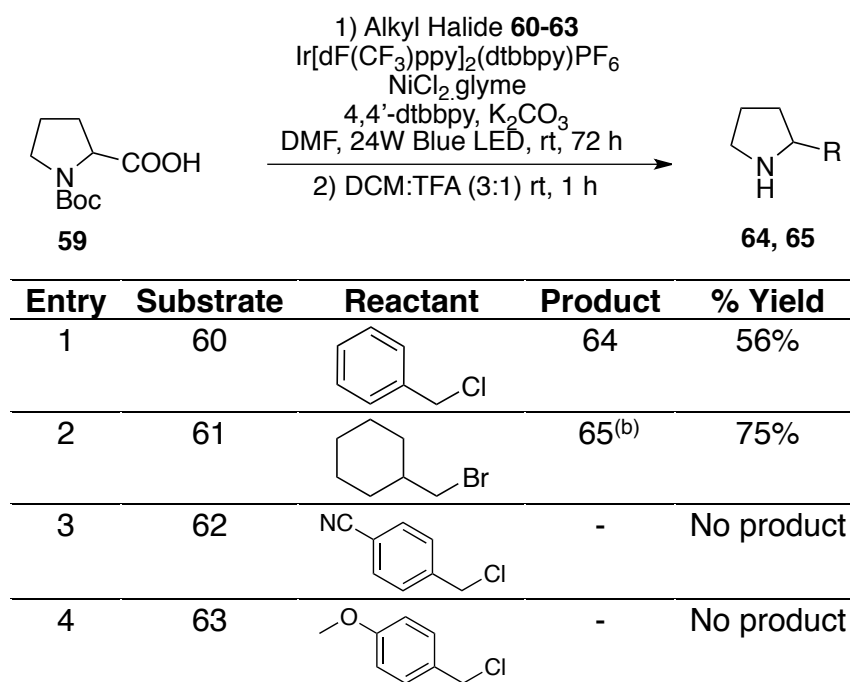
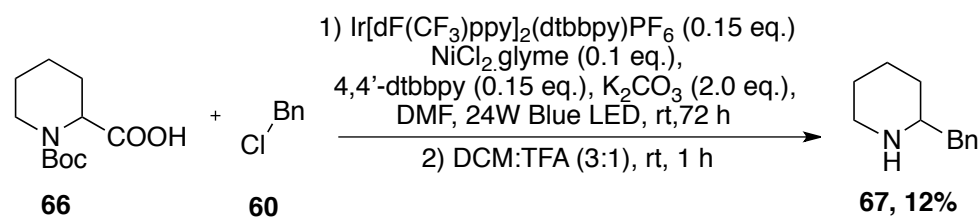


Table 7: Synthesis of α -C-H functionalised pyrrolidines through sp^3 - sp^3 bond formation. (b) entry 2 was left as the protected amine.

Entries 1 and 2 were repetitions of exact literature procedures and afforded modest yields, for entry 1 a lower yield was observed when compared to literature. Functionalisation of the aromatic ring was investigated by use of +M (positive mesomeric effect) and -M (negative mesomeric effect) functional groups in the *para*-position of the aromatic ring (entries 6-7) and were unsuccessful. The protocol was repeated using a non-literature substrate, *N*-Boc pipercolic acid **66** (Scheme 8), with benzyl chloride (**60**) as the alkyl halide giving a 12% yield.

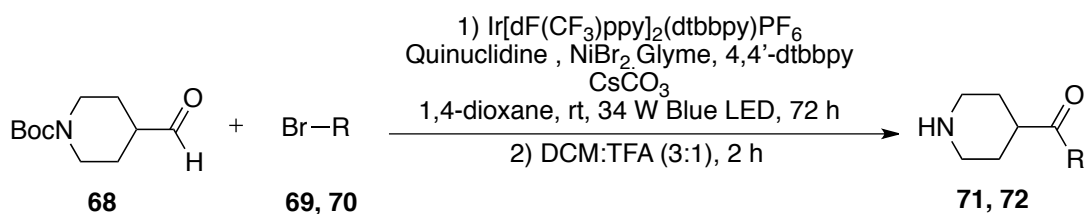


Scheme 8: Synthesis of α -C-H functionalised piperazines through sp^3 - sp^3 bond formation

2.3.2 Functionalisation of Appended Substituents

2.3.2.1 Direct Aldehyde C-H Arylation Employing Nickel, Hydrogen Atom Transfer and Photoredox Catalysis

Aldehyde C-H functionalisation was achieved by Zhang and MacMillan under mild conditions via a synergistic merger of photoredox, nickel, and HAT catalysis.¹¹⁹ Known aldehyde (**68**) and previously unreported aryl bromides were subjected to the reported conditions to afford ketone fragments **71** and **72** in moderate yields. Although 1-Bromo-4-fluorobenzene **70** (Table 8, entry 1) was not previously reported as a substrate in this reaction, success is unsurprising as a range of *para*-substituted activated aromatic electrophiles are reported to be tolerated in this transformation.

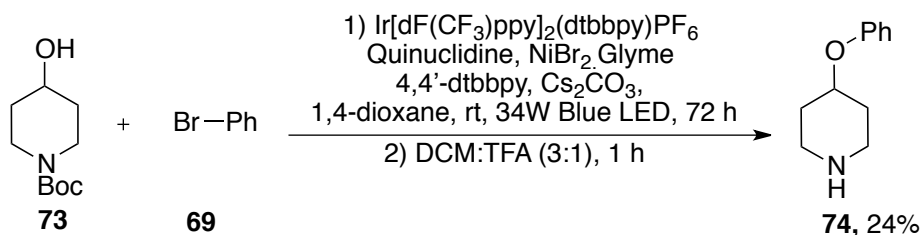


Entry	Substrate	Aryl Bromide	Product	% Yield
1	69		71	54%
2	70		72	84%

Table 8: Scope of the aryl bromides utilised in C-H aldehyde functionalisation.

2.3.2.2 Direct Alcohol Functionalisation Employing Photoredox Catalysis

MacMillan and co-workers reported a strategy for arylation of aliphatic alcohols via transient Ni(III) complexes, through the use of visible-light-mediated photoredox catalysis.¹²⁰ This reaction has had applications in various challenging carbon-oxygen cross-coupling reactions.¹²⁰ This protocol was applied to alcohol **73**, which was previously unreported as a substrate in this reaction. Subsequent removal of the Boc protecting group gave the secondary amine fragment **74** in 24% yield.



Scheme 24: Alcohol functionalisation in the synthesis of **74**.

This compound synthesis could also have been completed through use of a Mitsunobu¹²¹, although S_N2 reactions are known to be difficult for cyclic substrates. An alternate method could be by Chan-Lam cross-coupling, but alkyl halide availability often exceeds that of boronic acids.¹²² This

transformation was de-prioritised as a method to elaborate fragments, due to the expensive nature of the catalyst and the ability to generate analogues of this type by other means. However, it could be used when other methods are unsuccessful or starting materials are unavailable.

2.4 Conclusion

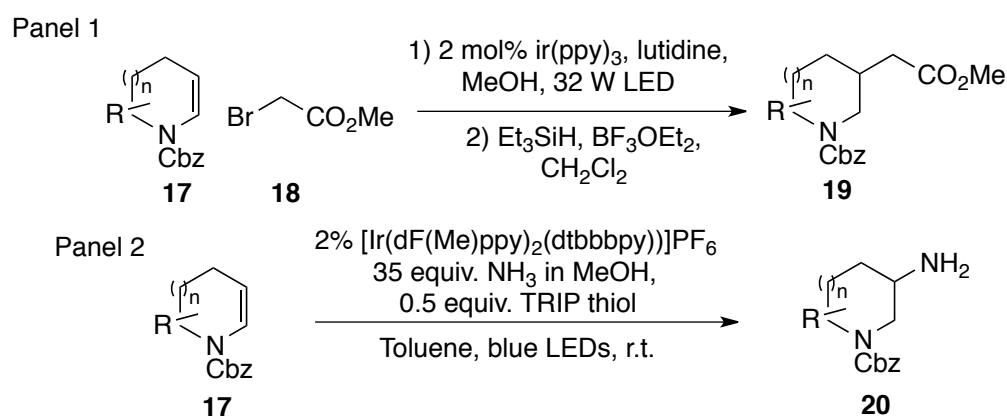
Six emerging chemical transformations have been tested against protected functionalised cyclic amines, generating a range of amine fragments functionalised in the α -position and at appended substituents (e.g. aldehydes and alcohols). These transformations have applications in Chapter 3, to enable the growth of a fragment hit, towards generating a lead compound.

2.5 Part 2: Synthesis of Enecarbamates and Enamides as Precursors for Fragment Elaboration

2.6 Introduction

Endocyclic enecarbamates are heterocyclic compounds which are useful building blocks in the preparation of functionalised nitrogen heterocycles. Within the Marsden and Nelson groups, two fragment diversification transformations have been described which require enecarbamate precursors (Scheme 9).

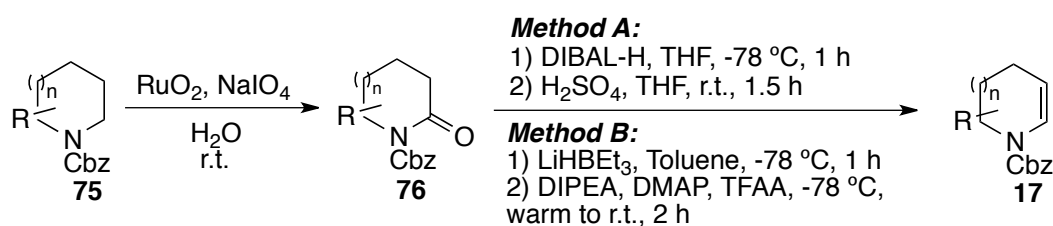
Trindade *et al.* (Scheme 9, panel 1) described a method of elaboration of unsaturated amines at the β -position using a photoredox-mediated alkylation employing bromoacetic esters.¹⁰⁴ This methodology was extended to introduce acetamide derivatives, facilitated by use of activated bromoacetic esters which undergo subsequent amidation in a single pot. Francis *et al.* (Scheme 9, panel 2) developed a procedure to diversify cyclic amine fragments at the β -position by use of photoredox-mediated hydroamination amenable with ammonia and both alkyl and (hetero)aryl amines.¹⁰⁵



Scheme 9: Panel 1: A photoredox mediated alkylation of enecarbamates using bromoacetic esters. Panel 2: A photoredox mediated hydroamination of enecarbamates using primary and secondary amines.

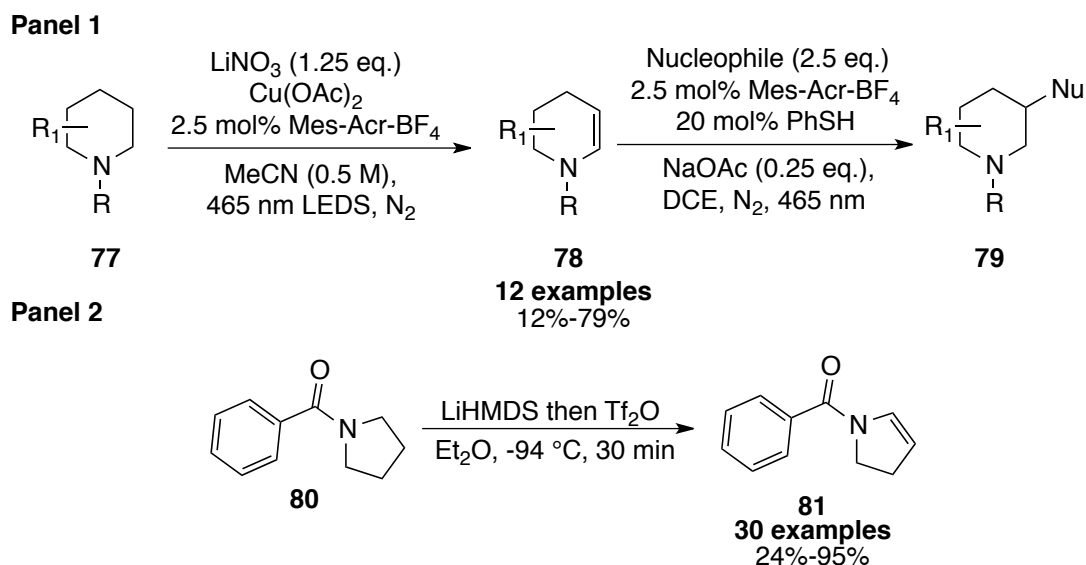
Previous methodology used to generate enecarbamates from their saturated derivatives employed the α -oxidation of *N*-acyl amines to generate *N*-acyl

lactams, using catalytic ruthenium tetroxide produced *in situ* (Scheme 2).¹²³ The endocyclic enecarbamate is then constructed through reduction of *N*-acyl lactam to the corresponding α -hydroxycarbamates using DIBAL-H or SuperHydride.¹²⁴ Subsequently, β -elimination promoted by sulfuric acid or trifluoroacetic anhydride in the presence of hindered nitrogen bases such as diisopropylethylamine (Scheme 10) provides a pathway into the enecarbamate.^{125,126}



Scheme 10: Oxidation of *N*-acyl amines to *N*-acyl lactams followed by reduction to the corresponding α -hydroxycarbamates and β -elimination to yield enecarbamates.

More recently, and subsequent to our own work, Nicewicz *et al.* have reported a photoredox-catalysed copper-mediated dehydrogenation of protected saturated cyclic amines to their enecarbamates.¹²⁷ These enecarbamates then underwent an anti-Markovnikov hydrofunctionalisation, with heteroatom containing nucleophiles to generate β -functionalised cyclic amines bearing C-C, C-N and C-O bonds in the β -position (Scheme 11, panel 1). Maulide and co-workers have demonstrated a one pot *N*-dehydrogenation of amides to yield enamides, employing LiHMDS and triflic anhydride as an electrophilic activator and oxidant in the reaction.¹²⁸ The enamides generated could then be used successfully in cycloadditions, ring functionalisation and ring deconstruction reactions (Scheme 11, Panel 2).



Scheme 11: Reported methods for enecarbamates and enamide synthesis. Panel A displays a procedure reported by Nicewicz.¹²⁷ Panel B illustrates a procedure by N. Maulide for the synthesis of enamides.¹²⁸

The literature synthesis of enecarbamates from their saturated derivatives is therefore limited, with only a few reported methodologies applicable to the construction of more complex endocyclic enecarbamates.^{124,127–130} The shortage of literature on their synthesis is assumed to be a limiting factor for more extensive use of these *N*-acyl enamines in organic synthesis and we sought a milder and general method for their synthesis.

2.6.1 Introduction to Synthetic Electrochemistry

Electrochemical experiments are carried out in an electrochemical cell, a reactor that is comprised of an electroactive species, electrolyte, solvent and at least two electrodes (an anode and cathode).¹³¹ The anode is connected to the positive pole of the power source and is oxidative, whereas the cathode is connected to the negative pole and is reductive.

Electrochemical cells can be constructed according to two approaches; undivided and divided cells. In an undivided cell, the anode and cathode are not separated, whereas the anode and cathode are separated in a divided cell. The undivided cell set up is preferred for preparative electrochemistry due

to ease of construction, allowing both reduction and oxidation to occur in the same vessel. Employment of this set-up, however, requires understanding of species produced at the auxiliary electrode i.e. the electrode other than where the reaction of interest is carried out.

Electron transfer events occurring at the anode or cathode are respectively classified as oxidations or reductions. Electrochemical reactions occur on the surface of electrodes and therefore are heterogenous processes. The resulting species generated following the initial electron transfer event between the electrode and an organic substrate subsequently diffuses into solution and can subsequently undergo a secondary reaction of the initial radical species.^{132,133} The potential of the electrode (E), is the difference between the potential at the electrode of interest and the selected reference electrode, such as the saturated calomel electrode (SCE), and will determine whether an electron transfer process is thermodynamically feasible and is denoted by Equation 1

$$\Delta G = -nFE$$

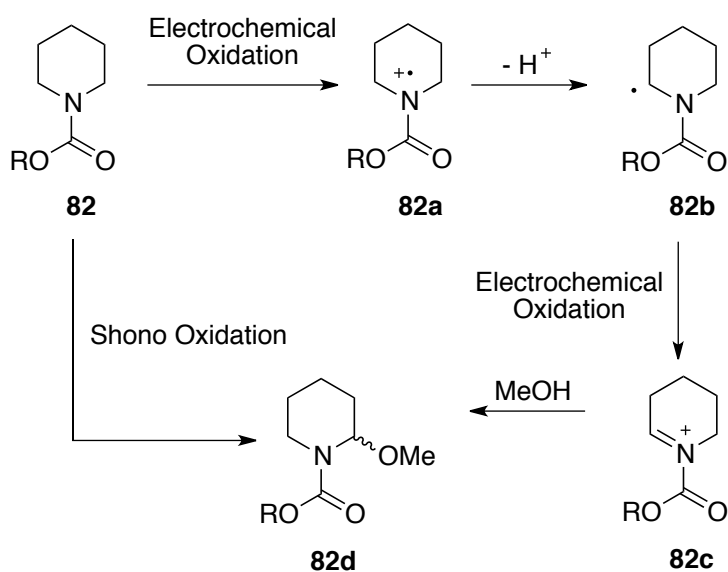
Equation 1: Free energy and cell potential. Where ΔG is the free energy change, F is Faraday's constant, 96485 Coulombs mol^{-1} , and n is the number of electrons involved in the overall reaction.

Electrochemical experiments can be conducted in either current-controlled or controlled-potential mode. Controlled-potential experiments use a three-cell electrode setup, where the voltage is fixed and cyclic voltammetry (CV) of the compound is necessary to determine its oxidation potential prior to reaction. It is noted that although the potential can be controlled, the current will fluctuate as the resistance of the cell changes. Current-controlled experiments use a two-electrode setup where the current is held constant while the voltage gradually increases until the potential is reached for an electroactive species. Once depleted, the potential will continue to rise until a second electroactive species or solvent molecules is oxidised or reduced. It is therefore imperative to consider the redox potentials of the substrate, as well as other species in the system to ensure that the initial redox reaction does not involve participation of the solvent or other additives. Although the current-controlled

method is operationally simpler, it can lead to over oxidation of the compound if the optimal parameters are not chosen, as the voltage will fluctuate during the reaction.

2.6.2 Shono Oxidation

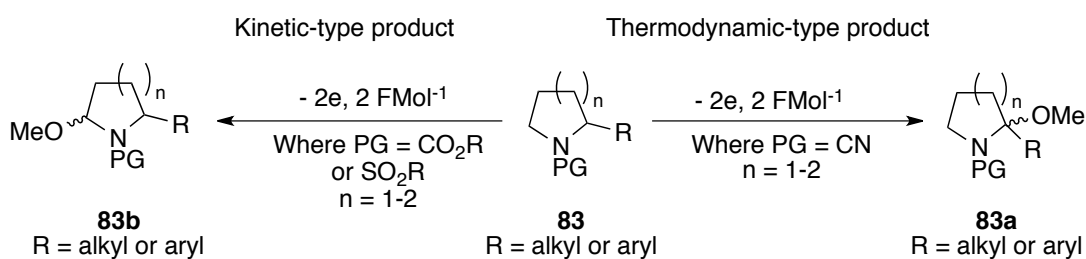
In 1975 Shono and co-workers reported the first direct electrochemical oxidation of an α -methylene group of an amide (or carbamate) to generate a new carbon-oxygen bond using an anodic methoxylation step.^{134–136} The Shono oxidation is a well-documented and operationally straightforward synthetic transformation and can be completed in a single electrochemical system, using carbon-based electrodes.¹³⁷ The reaction mechanism is thought to proceed through a single electron oxidation to form a nitrogen centred radical cation (Scheme 10).¹³⁵ The radical cation then undergoes proton loss, leading to α -amino radicals. A subsequent one-electron oxidation generates the iminium ion (**82c**), which can then be trapped by nucleophilic solvent (methanol), to give the isolable α -methoxycarbamate (**82d**). This species can then be treated with Lewis or Bronsted acid, regenerating the *N*-acyliminium ion to allow for further functionalisation.



Scheme 12: The proposed mechanism for the Shono oxidation.

Although the original report examined the products of the anodic oxidation of acyclic *N,N*-dialkylcarbamates in methanol, the method was soon expanded to cover simple cyclic amines.¹³⁸ The Shono oxidation enables direct functionalisation of the α -position adjacent to the nitrogen atom in heterocycles as well as indirect functionalisation of the β - and γ -carbons through conversion to the corresponding enecarbamates.

When an unsymmetrical secondary amide or carbamate is used in the Shono oxidation, the oxidation occurs preferentially at the less substituted position, as shown in Scheme 13. However, studies by Onomura¹³⁹ and co-workers have revealed that the regiochemical outcome may be reversed using cyanoamines wherein the methoxylation at the more substituted position is favoured. Computational studies suggested that when using a cyano protecting group (Scheme 13) the more-substituted iminium ion is stabilised and so favours methoxylation at this position. Contrariwise, for carbamates the iminium intermediates were shown to be of similar stability, where steric effects are thought to predominate. However, these calculations examined only the stability of the intermediates and did not offer an explanation for the kinetic selectivity in their formation, or how the equilibrium may be established for thermodynamic considerations to dominate.



Scheme 13: Variation in amine protecting group and its influence on regioselectivity in the Shono oxidation.

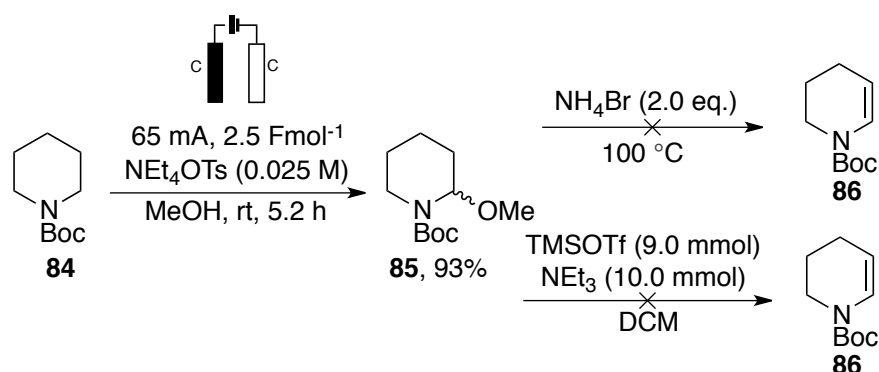
As a result of the limited literature precedent on the synthesis of complex enecarbamates, we elected to examine whether the Shono oxidation could be used to deliver functionalised and substituted enecarbamates from their saturated derivatives in a selective manner.

2.7 Results and Discussion

2.7.1 Method Development

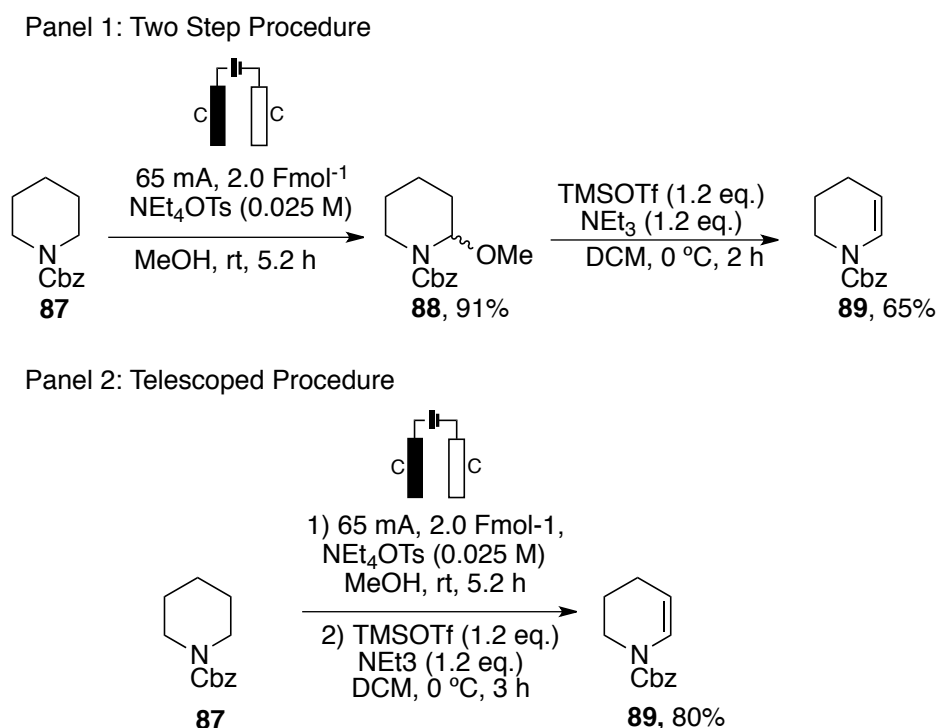
In our first experiments, using conditions reported by Shono¹³⁴ employing graphite electrodes with a supporting electrolyte of tetraethylammonium tosylate, *N*-Boc piperidine **84** gave excellent conversion to the α -methoxycarbamate **85**, which was isolated in 93% yield (Scheme 14).¹⁴⁰ The presence of the α -methoxycarbamate product was confirmed by ¹H NMR, with the spectrum of the methoxylated product (**85**) being complicated by relatively slow rotation of the carbamate function.¹⁴⁰

Repetition of Shono's conditions to eliminate methanol from α -methoxycarbamate **85** utilising ammonium bromide were unsuccessful, with only decomposition of the starting material observed, a result echoed by Oliveira.^{5,18} It is well documented in the literature that trimethylsilyl triflate when combined with a non-nucleophilic base enables elimination of methanol from **85** via the *N*-alkoxycarbonyl iminium ion.¹²⁵ Attempts to form the *N*-alkoxycarbonyl iminium ion of **85** under these conditions were unsuccessful and led to decomposition, possibly due to deprotection of the Boc-amine.



Scheme 14: Initial studies towards the synthesis of endocyclic enecarbamates using *N*-Boc piperidine

To circumvent issues associated with use of an acid-labile protecting group, it was decided to investigate *N*-Cbz piperidine as a substrate. *N*-Cbz piperidine gave excellent conversion in the Shono oxidation to give the corresponding α -methoxycarbamate **88**, which was isolated in 91% yield (Scheme 15). Treatment of α -methoxycarbamate **88** with ammonium bromide again did not induce elimination and so the combination of trimethylsilyl triflate and triethylamine was employed. Satisfyingly, enecarbamate **89** was isolated in a 65% yield, which was increased to 87% on implementation of a telescoped procedure (Scheme 15). An explanation for the improvement in yield is the potential instability of the α -methoxycarbamate to silica, leading to decomposition.¹²⁵ Enecarbamate **89** could be purified using flash column chromatography to yield analytically pure compound.

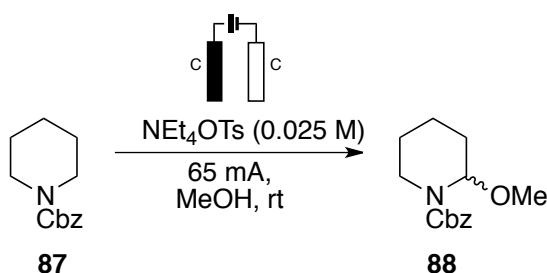


Scheme 15: Comparison of a two-step procedure and a telescoped to access enecarbamates

With a procedure to access enecarbamates in place, attention turned to optimisation of the anodic oxidation and the successive elimination reaction step.

2.7.1.1 Optimisation of the Synthetic Route to Enecarbamates

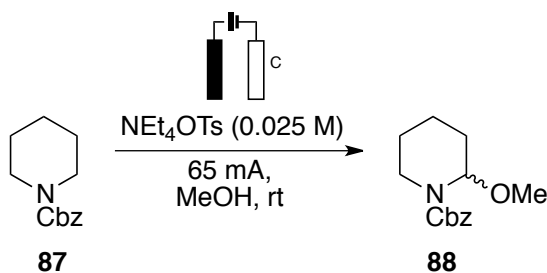
Initially, optimisation studies considered the optimal electric charge per mole. The Shono oxidation is a two-electron process and so should only necessitate the use of 2 Fmol⁻¹, however often an excess of 4 Fmol⁻¹ is employed.¹⁴² Table 9 displays that employing 2.5 – 4 Fmol⁻¹ produced the α -methoxycarbamate **88** in excellent yield. Unsurprisingly 1 Fmol⁻¹ produced **88** in poor yield (Table 9, entry 1). A modest improvement in yield was observed using 4 Fmol⁻¹, which could be attributed to concurrent oxidation of methanol or adventitious water introduced through use of a hygroscopic supporting electrolyte. It is important to note that on implementation of conditions using 5 and 6 Fmol⁻¹, decomposition began to be observed in the crude ¹H NMR. In the case of entry 6, a complex mixture of enecarbamate and unidentifiable products were obtained. Use of 2.5 Fmol⁻¹ gave high yield with a shorter reaction time.



Entry	Fmol ⁻¹	Reaction Time (mins)	Yield
1	1	54	37%
2	2.5	107	93% (91%)
3	4	215	98%
4	5	269	67% ^a
5	6	323	9% ^a

Table 9: The effect of varying Fmol⁻¹ in the Shono oxidation of **87**. The current was held at 65 mA. The NMR yield is determined with respect to an internal standard, 1,3,5-trimethoxybenzene. ^a decomposition was observed in the ¹H NMR spectrum, indicative of over reaction. Entry 5, 15% enecarbamate observed. Bracketed yields are isolated yields.

Next, we surveyed the anode material, with graphite giving the greatest yield overall, while glassy carbon gave the lowest yield.

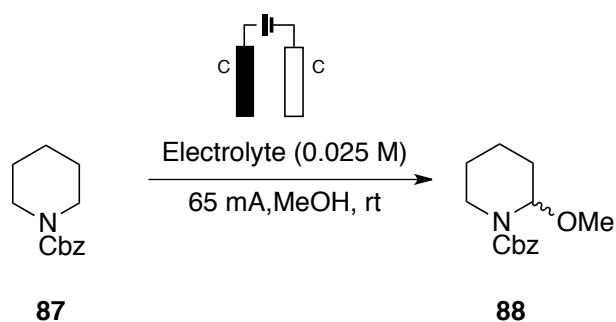


Entry	Electrodes	Yield
1	Graphite	93% (91%)
2	Platinum	65%
3	Stainless Steel	66%
4	Glassy carbon	42%

*Table 10: The effect of anode material on the electrochemical oxidation of model substrate **87**. Yields were determined from ¹H NMR. The NMR yield is determined with respect to an internal standard, 1,3,5-trimethoxybenzene. Bracketed yields are isolated yields.*

It was found that stainless steel and platinum electrodes performed similarly but led to a reduction in yield when compared with graphite. Interestingly, Ley and co-workers describe a Shono oxidation of **87** using an electrochemical flow cell, where the use of steel or platinum electrodes resulted in no conversion to product.¹⁴³ They accredit this result to *N*-Cbz protected cyclic amines and methanol having very close redox potentials and so methanol may be participating in the redox process. This could account for the reduction in yield seen.

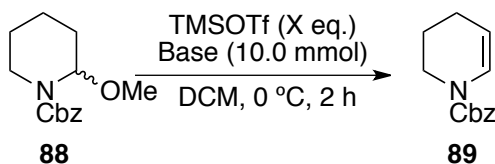
The choice of supporting electrolyte was considered, with our original choice of tetraethylammonium tosylate affording the greatest yield by ¹H NMR. All electrolytes were prepared according to literature procedures prior to use.¹⁴⁴ Use of NBu₄OAc gave excellent yield, but separation of the electrolyte from the product proved difficult using column chromatography and therefore was not pursued (Table 11, entry 3). During this study we observed poor conversion using NaCl as the supporting electrolyte (Table 11, entry 5).



Entry	Electrolyte	Yield
1	NEt ₄ OTs	93% (91%)
2	NEt ₄ BF ₄	88%
3	NBu ₄ OAc	96% ^a
4	NaBF ₄	n.d. ^b
5	NaCl	15%

Table 11: The effect of modifying the electrolyte on the Shono oxidation of **87**. Electrolyte concentration at 0.25 M.¹⁴⁴ Yields were determined from ¹H NMR. The NMR yield is determined with respect to an internal standard, 1,3,5-trimethoxybenzene. Bracketed yields are isolated yields. ^aIssues with separation from enecarbamate observed. ^b low solubility of the electrolyte in methanol at 0.025 M.

With optimised reaction conditions for the anodic oxidation in hand, a brief survey of the elimination procedure was conducted (Table 12). Initially, formation of **89** utilised conditions reported by Bach for similar substrates.¹⁴⁵ It was found that increasing the excess of trimethylsilyl triflate from 2 – 2.2 equivalents improved the yield modestly. The experiment was found to produce excellent yields when conducted at 0 °C. Substitution of triethylamine with *N,N*-diisopropylethylamine led to an improvement in yield from 79% to 84%. On variation of the base to 2,6-lutidine, a reduction in yield was observed. An explanation for this could be the formation of a more acidic lutidinium triflate salt, leading to decomposition of the product. Once the reaction had concluded, the crude reaction mixture was diluted with hexane and filtered through celite.

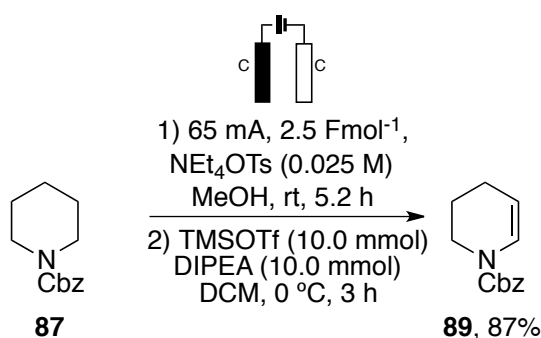


Entry	TMSOTf (eq.)	Base	Temperature / °C	Yield
1	2	NEt ₃	0	79
2	1	NEt ₃	0	22
3	4	NEt ₃	0	51
4	2.2	NEt ₃	0	80
5	2.2	NEt ₃	rt	65
6	2	DIPEA	0	84
7	2.2	DIPEA	0	87
8	2.2	DIPEA	rt	81
9	2	2,6-Lutidine	0	40
10	2.2	2,6-Lutidine	0	42

Table 12: Optimisation of parameters of the trimethylsilane elimination on **12**. Yields were determined from ¹H NMR. The NMR yield is determined with respect to an internal standard, 1,3,5-trimethoxybenzene.

2.7.1.2 Summary of Optimised Conditions

Following optimisation, a set of conditions were defined for efficient synthesis of endocyclic enecarbamate **89** (Scheme 16). With these optimised conditions for the formation of a simple enecarbamate in hand, we investigated the substrate tolerance of the transformation.

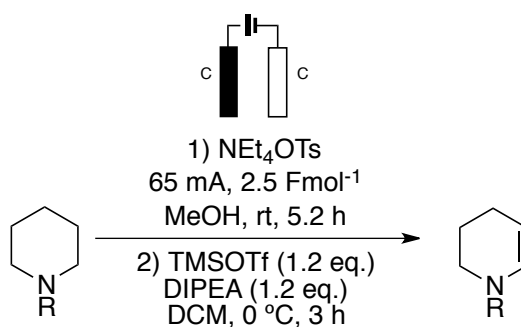


Scheme 16: Optimised conditions for the synthesis of endocyclic enecarbamates.

2.7.2 Preparation of Endocyclic Enecarbamates

2.7.2.1 Variation of protecting group

With optimised conditions in hand, a series of *N*-protecting groups for piperidine were screened. This was a useful study as a future application of the protocol would be in direct fragment elaboration, where installation of a Cbz protecting group may not be amenable.



Entry	Substrate	R	Product	Yield
1	84	Boc	86	n.d.
2	87	Cbz	89	87%
3	90	Ac	93	75%
4	91	Bz	94	72%
5	92	Ms	-	No reaction

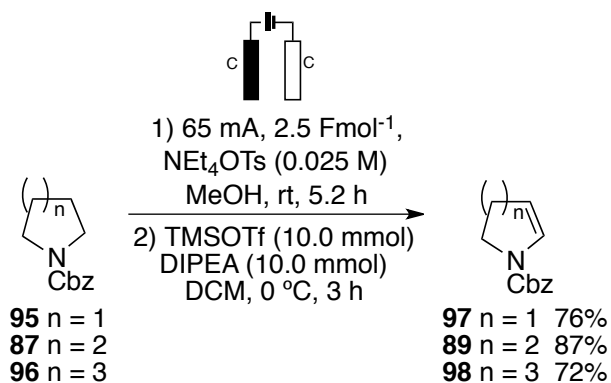
Table 13: Variation of the protecting group of piperidine. Yields denote isolated yield, n.d. not determined.

It was established previously that *N*-Boc moieties were not stable under the chosen elimination conditions (Table 13, entry 1). Acetyl and benzoyl groups were tolerated, proceeding with clean conversion to the enamides in excellent yields of 75% and 72% respectively (Table 13, entries 3 and 4). However, for mesyl protected piperidine (Table 13, entry 5) the anodic oxidation did not take place under our conditions, mirroring observations in the literature, suggesting that the oxidation of sulfonamides is more difficult than the oxidation of carbamates.^{146,147}

2.7.2.2 Variation of Ring Size

From our studies, the formation of the endocyclic enecarbamates using *N*-Cbz piperidine proceeded in excellent yield. The procedure was extended to encompass pyrrolidine and azepane as substrates, which are common motifs within fragments and drug candidates.¹⁴⁸

Commercially available *N*-Cbz pyrrolidine and *N*-Cbz azepane underwent the Shono oxidation, under the optimised conditions, with complete consumption of the starting material observed by TLC and crude ¹H NMR. The elimination protocol was then applied to yield enecarbamates **97** and **98** in good yield, without recourse to modifying our original procedure (Scheme 17).



Scheme 17: Variation of ring size in the one pot procedure to access enecarbamates.

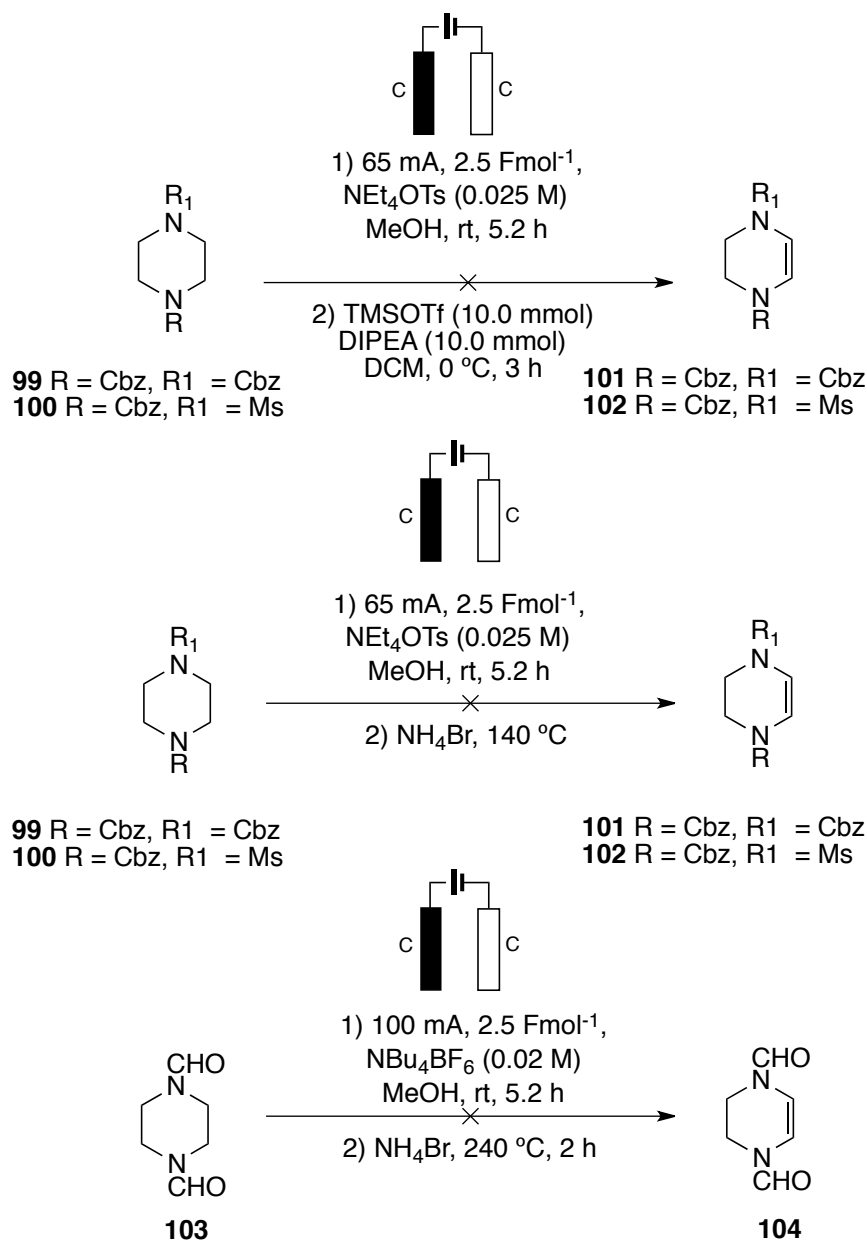
2.7.2.3 Inclusion of β -heteroatoms

As our one-pot procedure had proved robust across variations in ring size, our attention turned to the exploration of substrates containing β -heteroatoms. Firstly, we considered piperazines, a common ring system in FDA approved drugs.^{149, 148} Nyberg reported conversion of piperazine-1,4-dicarbaldehyde to the enecarbamate in a 46% yield by Shono oxidation and dehydration of the *N,O*-acetal with ammonium bromide.^{132,137} We envisaged use of dibenzyl piperazine-1,4-dicarboxylate (**99**) in our procedure would yield the desired enecarbamate (**101**). However, disappointingly, the reaction resulted in no isolated product. Analysis of the crude ¹H NMR following oxidation indicated presence of the α -hydroxycarbamate alongside decomposition of the starting

material. Since the α -hydroxycarbamate was present in the crude ^1H NMR, this suggested issues with the elimination step and so an alternative method was attempted. In this case, neat ammonium bromide was utilised at $140\text{ }^\circ\text{C}$ but led to decomposition and no product was isolated.

Subsequently, we considered differentially protected piperazine **100**. We had found that *N*-Ms protected piperidine was redox inactive under our optimised reaction conditions. It was thought therefore that use of a mesylate protecting group in piperazine, could prevent multiple oxidation products forming, producing a cleaner crude ^1H NMR. Nonetheless, no product was observed following the oxidation and decomposition of the starting material had occurred, which was confirmed by crude ^1H NMR (Scheme 18).

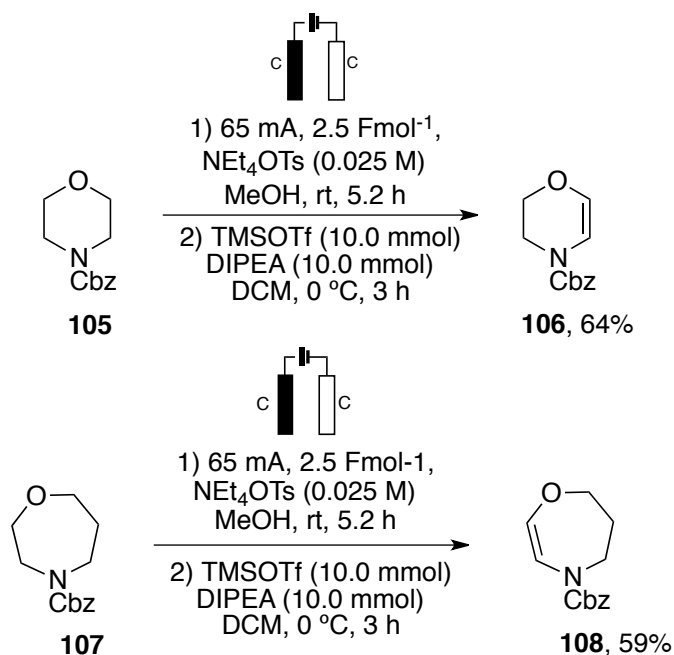
Finally, we conducted a repeat of the experimental procedure reported by Nyberg, using bis-amide **103** and ammonium bromide as the dehydrating agent to generate the corresponding enecarbamate.¹³² Unfortunately, this result was unable to be repeated and product **104** was not isolated (Scheme 18). Following these results, piperazines were deprioritised as substrates in this protocol.



Scheme 18: Methods used towards the synthesis of *N*-protected piperazine enecarbamates.¹³²

From our experience with employing piperazines as substrates, we envisaged similar difficulties when employing morpholines as substrates. To our delight, **105** underwent oxidation and subsequent telescoping of the α -methylamino acetal gave the corresponding enecarbamate in 64% yield, following purification by column chromatography (Scheme 19). We believe the oxidation occurred adjacent to nitrogen on amine **105** rather than the adjacent to oxygen of *N*-Cbz morpholine. This was deduced from the chemical shift

value from the ^{13}C NMR of the crude reaction mixture, which was in accordance with reported literature values.¹⁴⁰

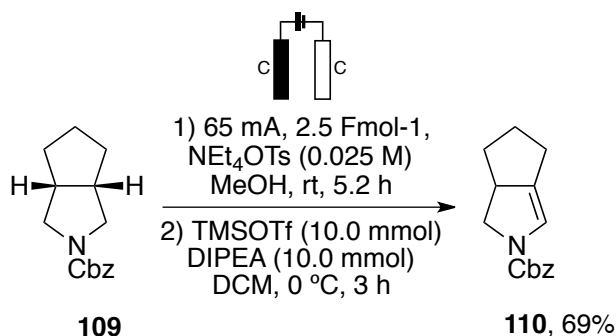


Scheme 19: Application of N-Cbz morpholine and N-Cbz oxazepane in the telescoped method to access the enecarbamates.

With the morpholine enecarbamate in hand, we applied the procedure to oxazepane **107**. Analysis by crude ^1H NMR displayed a single regioisomeric enecarbamates product, which was subsequently isolated using column chromatography. Analysis of ^1H and 2D NMR confirmed the isolated product as the doubly-heteroatom substituted alkene regioisomer.

2.7.2.4 Bicyclic Amine

Our optimised procedure was applied to fused bicyclic N-Cbz amine **109**. Synthesis of the α -methoxycarbamate was followed by TLC, with full conversion of starting material observed. Conversion to enecarbamate **110** proceeded in a 69% yield over the two steps and was confirmed by 2D NMR and HRMS.

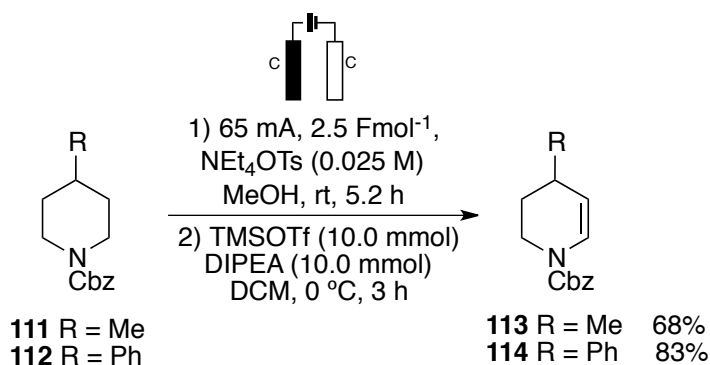


Scheme 20: Synthesis of fused bicyclic enecarbamate 110.

2.7.2.5 Functionalised Piperidines

Our attention turned to the exploration of appended substituents on symmetrical piperidine analogues. These experiments enabled appreciation of the functional group tolerance of the transformation, without introducing the challenge of regiocontrol.

To our delight, a range of appended substituents were tolerated in this transformation, proceeding in good yield (Scheme 21). In particular, compound **112** smoothly underwent oxidation, showing clean conversion of starting material by TLC; following elimination and purification by column chromatography, enecarbamate **114** was obtained in excellent yield. Although a slight decrease in yield was observed with all analogues examined when compared to model substrate **87**, the yields obtained still make this approach amenable for use in fragment elaboration strategies.



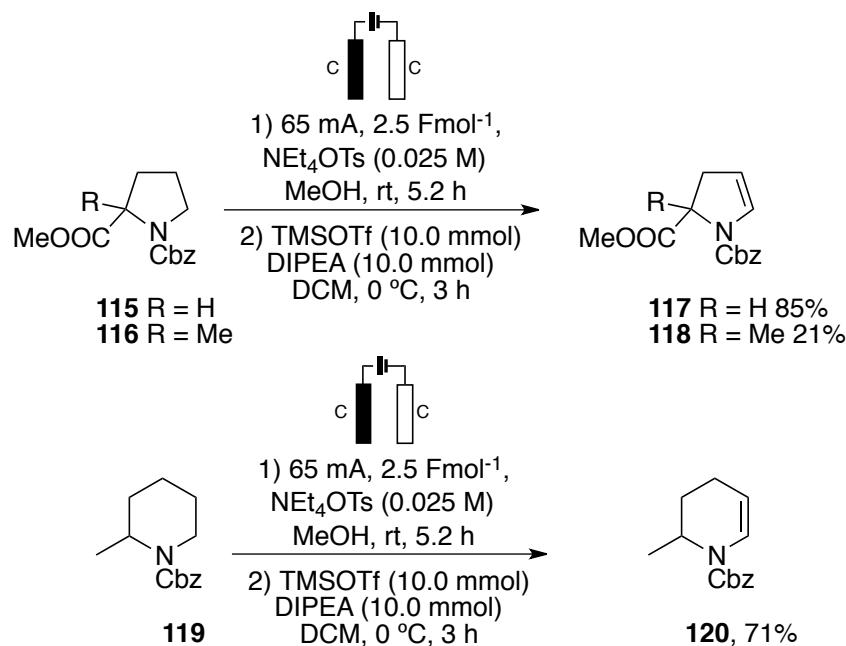
Scheme 21: Application of 4-substituted N-Cbz piperidine analogues in the telescoped method to access the enecarbamates.

2.7.3 Preparation of Unsymmetrical Endocyclic Enecarbamates

2.7.3.1 α -Functionalised Cyclic Amines

The oxidation of unsymmetrical substrates introduces the challenge of regiocontrol. For 2-substituted carbamate-protected amines methoxylation at the less substituted site has been observed, although the mechanism for the high regioselectivity is unclear.^{139,150} We sought to replicate the high regioselectivity seen in the literature for the anodic oxidation of 2-substituted *N*-Cbz cyclic amines and pair this step with the elimination of methanol to synthesise the enecarbamates.

Initially we considered **115**, a protected proline derivative. Subjecting **115** to our optimised conditions gave the less-substituted enecarbamate in good yield (Scheme 22). In parallel, we made efforts towards the synthesis of **116**, a quaternary centre-containing derivative. Following the reaction by TLC, the anodic oxidation of **116** did not show complete consumption of the starting material. An increase in electric charge per mol from 2.5 Fmol⁻¹ to 4 Fmol⁻¹ was investigated but resulted in decomposition of the α -methoxycarbamate product, as seen by ¹H NMR. Comparison of **117** to the quaternary centre-containing analogue **118** saw a reduction in yield from 85% to 21%. It was believed the sterically encumbered quaternary centre of **116** potentially hindered the anodic oxidation step occurring on the surface of the graphite electrode, resulting in the low yield obtained.



Scheme 22: Shono oxidation and elimination to access enecarbamates of 2-substituted substrates.

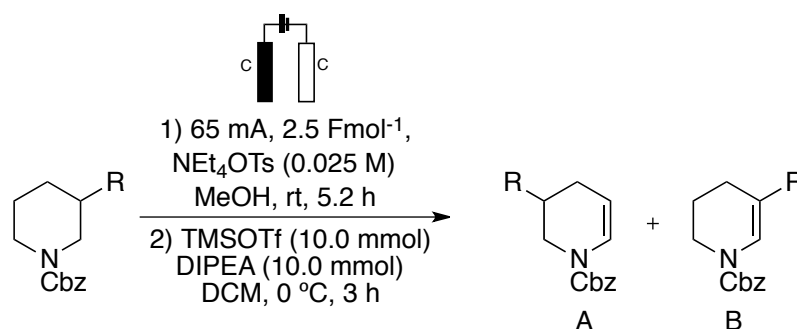
Next, anodic oxidation of **119** proceeded cleanly by TLC and subsequently elimination of methanol gave the less-substituted enecarbamate in a good 71% yield over the two steps (Scheme 22).

2.7.3.2 Distally Substituted Piperidines

The prospects for observing regiocontrol with more distal substituents seemed less encouraging. Nevertheless, since high levels of regioselectivity were observed in the formation of α -substituted cyclic enecarbamates we envisaged some selectivity may be seen, and so our initial investigation explored β -substituted piperidines.

We considered five β -substituted piperidines, with varying functionality in the β -position. To our delight, it was found that the reactions of β -substituted carbamates were also highly selective. Of the five substrates investigated, four were isolated as single enecarbamate regioisomers (Table 14). In the case of **126**, where the smallest β -substituent (methyl) was considered, the less-substituted alkene regioisomer was predominant in an inseparable 2:1

(**126A**, **126B**) mixture. These experiments exhibited the broad substrate scope of the Shono oxidation, showing tolerance to secondary carbamates (**125**), ethers and heteroarenes (**129**).



Entry	Substrate	R	Ratio of a:b	Product a, b	Yield
1	121	Me	2:1	126A, 126B	40% ^a
2	122	Ph	N/A	127A	67%
3	123	COOEt	N/A	128A	72%
4	124		N/A	129A	41%
5	125		N/A	130A	63%

Table 14: Formation of enecarbamates of distally substituted piperidines. ^a enecarbamates had formed in a 2:1 ratio of the least substituted: most substituted enecarbamates, with the presence of both α -methoxycarbamates in a 3:1 ratio.

For substrate **121**, it was found that the elimination reaction did not run to completion, with residual α -methoxycarbamate remaining. For this, an additional 1.0 equivalent of trimethylsilyl triflate and 1.0 equivalent of diisopropylethylamine were added after 3 hours and the reaction followed by TLC. After an additional 6 hours, analysis of the TLC displayed presence of α -methoxycarbamate and the reaction was ended. It was confirmed by crude ¹H NMR and 2D NMR that both enecarbamates had formed in a 2:1 ratio of the less-substituted:more-substituted alkene regioisomers, as well as the presence of both α -methoxycarbamates in a 3:1 ratio. On attempted purification using flash column chromatography, the mixture of enecarbamates and residual α -methoxycarbamate were found to be

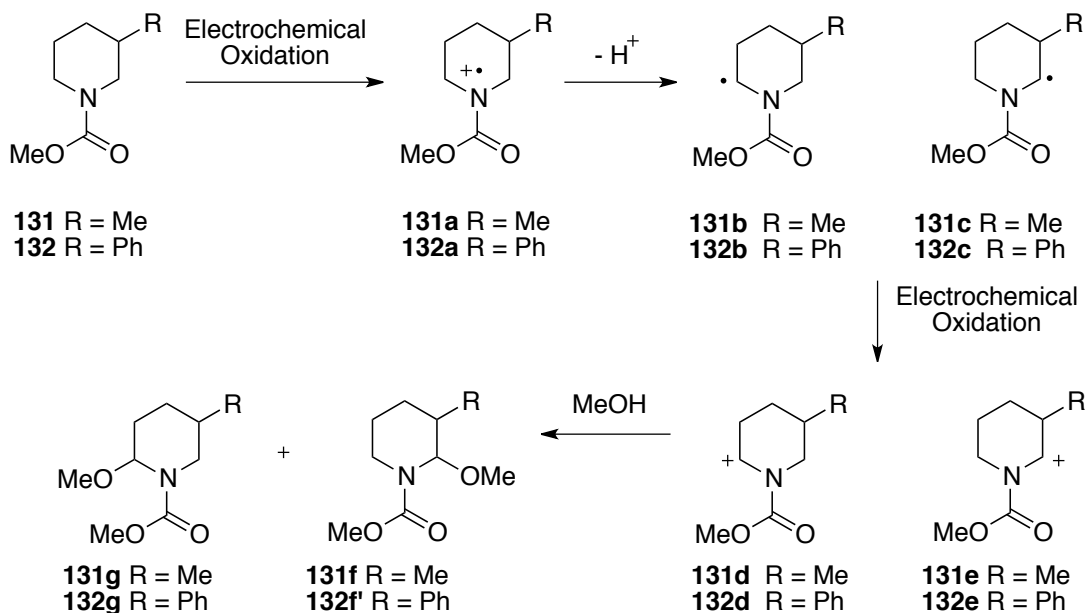
inseparable. Efforts were made to assign the structures of the residual α -methoxycarbamates, but this was not possible due to overlapping signals within the ^1H NMR and 2D NMR.

The origin of the high levels of regioselectivity seen was puzzling, and so was probed by Dr. Andrew Leach at the University of Manchester using DFT calculations (M06-2X/6-31+G** level of theory)^{151–153} focusing on the β -methyl (**121**) and β -phenyl (**122**) variants.¹⁵⁴ Solvation energies were computed as single points on the optimized geometries and employed the same level of theory and the IEFPCM formalism.¹⁵⁴ The gas phase and water solvation were used to delimit the extremes of solvent effects. Continuum solvation in methanol was used to check quantitative agreement with experiment. All calculations were performed in Gaussian09.¹⁵⁵ Free energies were computed using the GoodVibes program.¹⁵⁶ A range of conformations were studied for each species, where relevant, and the relative energies of each was used to compute a Boltzmann factor in order to assign its contribution to the overall population.

The two systems chosen to probe the reaction mixture were **121** (Me) and **122** (Ph), which gave contrasting experimental outcomes. **121** (Me) gave a mixture of **126A** and **126B** in a 2:1 ratio, whereas **122** (Ph) gave **127** in a >9:1 ratio. Within these experimental studies, cyclic amines are protected with benzyl carbamate, but for the purpose of these studies it was abbreviated to a methyl carbamate for computational simplicity.

As previously described (Scheme 23), the mechanism of the reaction is postulated to proceed following loss of an electron from each substrate (**131**, **132**), generating an (alkoxycarbonyl)amino radical cation (**131a**, **132a**). The radical cation can then undergo proton loss leading to isomeric α -amino radicals, where subsequent one electron oxidation generates iminium ions

(**131d**, **132d** and **131e**, **132e**), which can then be trapped by methanol, giving the observed products.



Scheme 23: The proposed mechanism of the Shono oxidation of **131/132**.

Initial investigations focused on the energies of the two radicals arising from deprotonation of the radical cation. This indicated that for **131a** (Me), the two radicals, **131b** and **131c** are close in energy, which would represent an equilibrium mixture observed in the gas phase (47:53) and in water (48:52), indicating there is little preference regardless on the polarity of the medium. In contrast for **132a**, the radical **132c** is computed to be the preferred isomer (**132b**) and to be dominant in both the gas phase (17:83) and water (also 17:83). This preference is opposite to the experimental outcome (Figure 8), and hence the stability of the α -amino radicals cannot be the determinant of the regiochemical outcome.

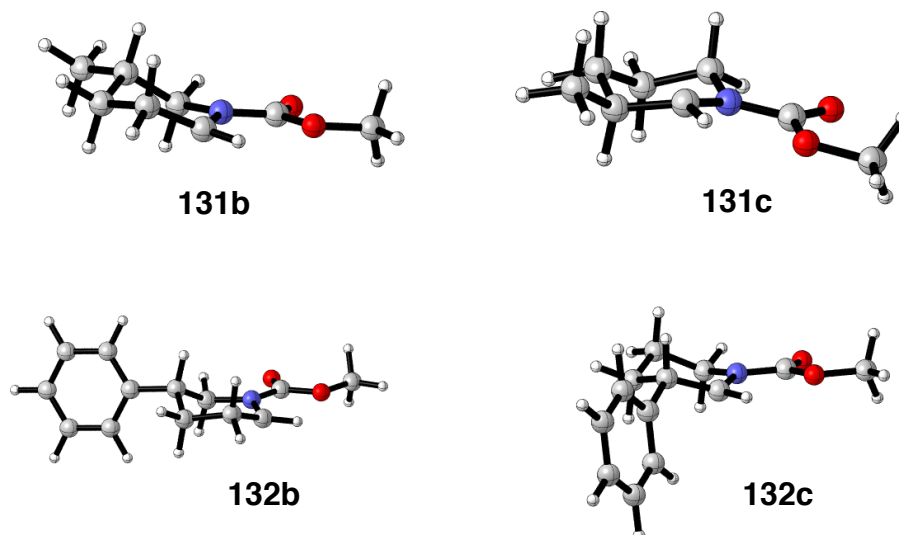


Figure 8: The lowest free energy conformations of each of the radicals.

Following this, the iminium cations **131d/132d** and **131e/132e** were studied (Figure 9), with an effect of solvent computed. A preference for cation **131d** was found, as 65:35 in the gas phase and 84:16 in water; however, a preference for **132e** in the gas phase (66:34) becomes a preference for **131e** (92:8) in aqueous conditions. Under aqueous conditions, the experimentally observed dominant isomer is preferred but there is little effect of changing R = Me to R = Ph predicted, and hence it is felt unlikely that iminium stability is the origin of the selectivity. It should be noted that the error intrinsic to the calculations mean that it cannot be precluded that this is in agreement with the experiment.

An alternative mechanism, in which regioselective formation of the radicals takes place was considered, where the two isomers cannot be rapidly equilibrated.

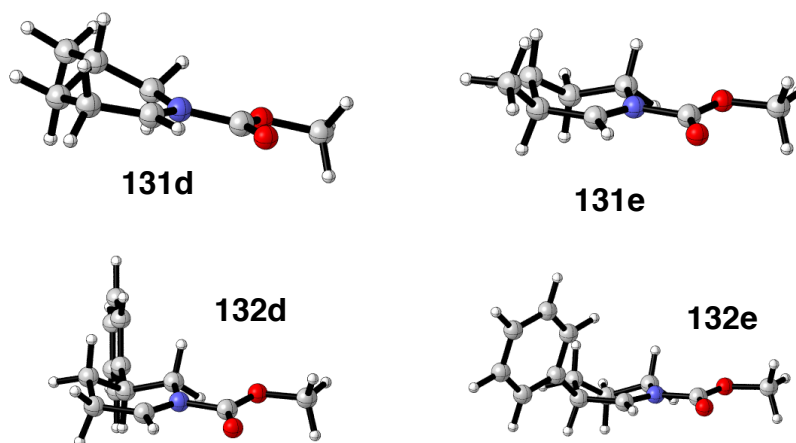


Figure 9: The lowest energy conformations of each of the cations.

The transition states for the proton transfer from the radical cation to the solvent (methanol) were obtained and structural variations were considered; including whether the departing proton was axial or equatorial (in addition to the methyl or phenyl substituent being axial or equatorial). In the transition state, it was assumed that the OH of methanol orients towards the carbamate (to form a hydrogen bond with either carbonyl or ester oxygen). The methyl of the methanol could either be placed over the piperidine ring or away from it. Up to five attempts were made to obtain each of the transition states, but some were not found.

In the gas phase, a kinetic preference of 30:70 in favour of formation of **131c** was computed. In solvent this changed modestly, becoming 15:85 in methanol. By contrast, a 98:2 preference for **132b** becomes 92:8 in methanol. The latter is in near perfect agreement with experimental observation, while the preference for **131c** is within the intrinsic error in the calculations. This provides a plausible explanation for the observed preference.

In order to understand the origin of selectivity, the transition states for the selective reaction (R=Ph) were examined visually (Figure 10). The lowest energy transition state **TS1(132b)** (leading to **132b**) features the phenyl group in an equatorial position, during removal of an axial proton. The methanol forms a hydrogen bond with the carbonyl oxygen and the methyl group of

methanol is placed away from the piperidine ring. The same features are present in the lowest energy transition state leading to **132c**, **TS1(132c)**, with the exception of the orientation of the methyl of methanol which is placed over the piperidine ring. This suggests that the preference has a steric influence, given that orienting the methyl away from the piperidine would cause it to clash with the phenyl group; a transition state with such a configuration could not be obtained. This steric model provides a consistent rationale for the preference for reaction, regardless of the origin of the selectivity the calculation seems to suggest that kinetic deprotonation is the regioselectivity determining factor.

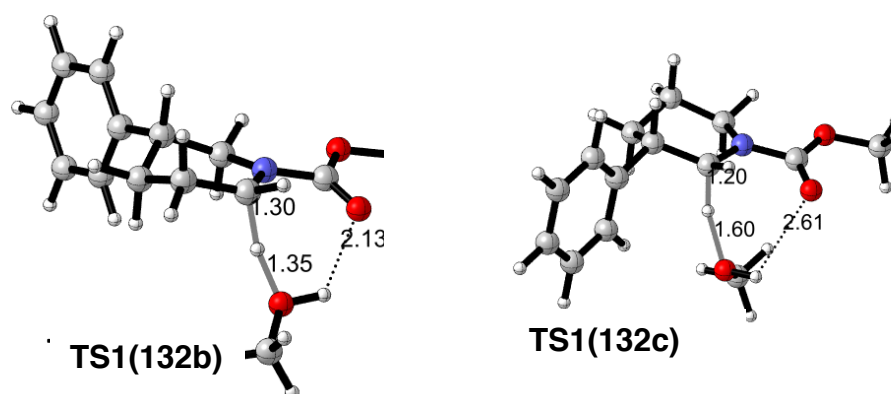


Figure 10: The lowest energy conformations of the transition states for formation of **132b** and **132c**

2.7.3.3 Applications to Fragments and Late-Stage Functionalisation

With our optimised procedure developed, we next wished to demonstrate the application of enecarbamate/enamide formation to aid the growth of chemical fragments. Piperonyl azepane **133** has been found by high-throughput X-ray crystallography to be a fragment hit for the m7GpppN-mRNA hydrolase DCP2B.¹⁵⁷ It was identified that elaboration of this fragment in the β -position of the nitrogen was a potential vector for fragment growth, which could be completed by use of previously developed methodologies within the group. For the elaboration to be possible, synthesis of the enamide precursor of **133** would need to be accomplished.

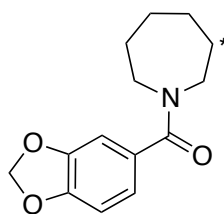
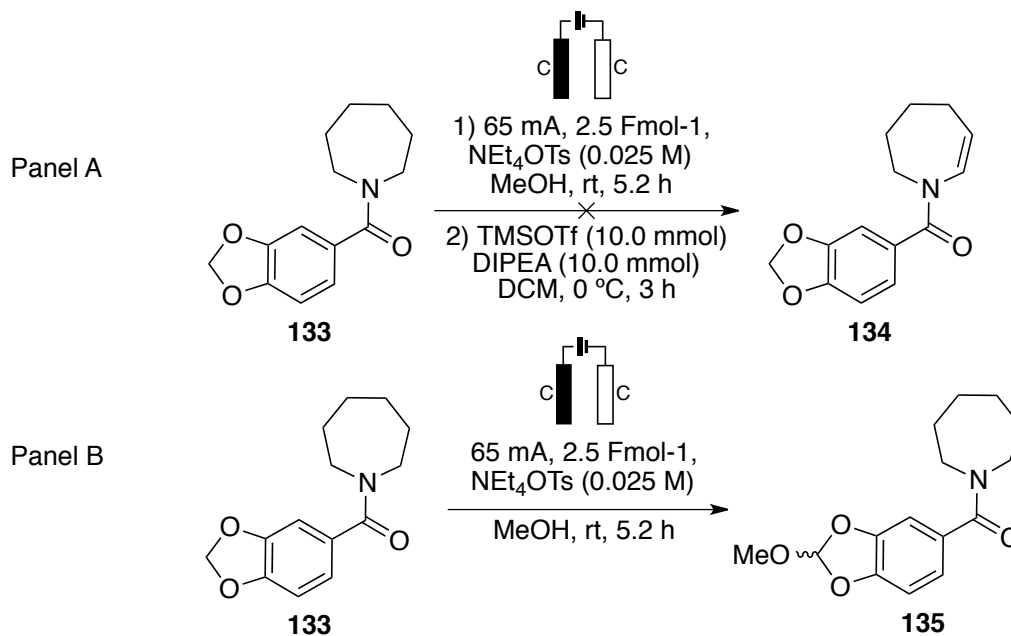


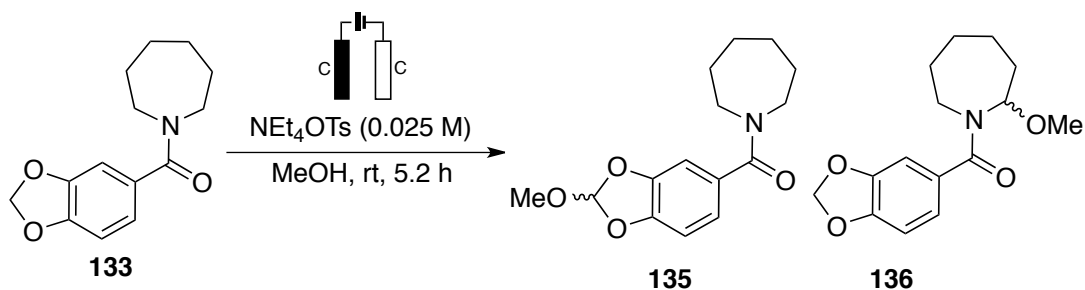
Figure 11: Fragment hit for m7GpppN-mRNA hydrolase DCP2B, **133**.¹⁵⁷

We applied our optimised procedure to piperindoyl azepane **133**; analysis of the reaction after the anodic oxidation step revealed formation of the corresponding *ortho*-ester **135**. We believe this arises from the anodic oxidation of the 1,3-benzodioxole (Scheme 24). The first report of the direct anodic oxidation of 1,3-benzodioxoles was by Thomas *et al.*, achieving installation of the methoxy motif on the heterocyclic skeleton.¹⁵⁸ Thomas reported that the reaction required an atmosphere of saturated carbon dioxide, use of platinum electrodes as well as between 3.7- 6.0 Fmol⁻¹ for full conversion. We observed complete conversion however, under a nitrogen atmosphere, utilising graphite electrodes and 2.5 Fmol⁻¹.



Scheme 24: Panel A denotes treatment of **133** using the optimised procedure was unsuccessful to yield the enecarbamate. Panel B displays the actual product of the anodic oxidation, confirmed by ¹H NMR.

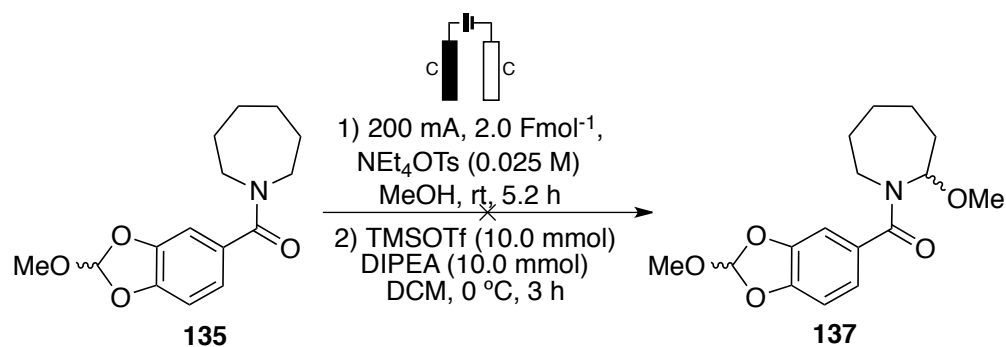
Our attention turned to modification of the electrochemical protocol in order to form the α -methoxyamide. Variation of $F\text{mol}^{-1}$ and current were both examined, but the conditions attempted did not yield the desired product (Table 15).



Entry	$F\text{mol}^{-1}$	Current / mA	Yield of 135	Yield of 136
1	2.5	100	71%	0%
2	1	100	47%	0%
3	5	100	n.d.	n.d.
4	2.5	65	68%	0%
5	2.5	50	63%	0%
6	2.5	25	56%	0%

Table 15: Modification to conditions of the anodic oxidation of 41. Yields were determined from ^1H NMR. The NMR yield is determined with respect to an internal standard, 1,3,5-trimethoxybenzene.

Following this, we attempted to take the *ortho*-ester product of the anodic oxidation and use a second anodic oxidation in an attempt to form the α -methoxycarbamate of **135**. The second anodic oxidation was unsuccessful, with only unreacted *ortho*-ester **135** observed in the crude ^1H NMR. Since the α -methoxycarbamate was not observed in any case, carbamate **134** was deprioritised for synthesis.



Scheme 25: Attempts at anodic oxidation of **135** to yield the α -methoxycarbamate.

2.8 Conclusion

A general synthesis of endocyclic enecarbamates has been presented, employing an operationally simple electrochemical oxidation and elimination procedure. This strategy has shown tolerance for variable protecting groups, ring sizes and the inclusion of beta-heteroatoms, with the sequences proceeding in moderate to excellent yields. We have shown that regioselective electrochemical oxidation was observed for both α - and β -substituted cyclic amines, with the origin of the surprisingly high regioselectivity for β -substituted substrates explored using DFT. The enecarbamates prepared have the potential to be directly elaborated with medicinally relevant functionality for use in fragment-based drug discovery projects.

2.9 Future work

With a telescoped procedure in place that enables preferential formation of the less-substituted alkene regioisomer, it would be desirable for use in fragment elaboration methodology to have a procedure which enables the synthesis of the regio-complementary enecarbamate.

Efforts by Onomura revealed that the regiochemical outcome of the electrochemical oxidation can be reversed when using cyanoamines, so the methoxylation is favoured to occur at the most substituted position. The use of cyanoamines would not be amenable to further elaboration of the formed

N-cyanoenamine in this setting and so other experimental parameters could be considered.

As the Shono oxidation takes place on the anode surface, modification of the electrode surface may vary the regiochemical outcome of the reaction. Experiments evaluating the use of glassy carbon in a regioselective reaction, such as with **122**, could lead to varying regiochemical outcome due to the difference in surface area between graphite and glassy carbon.

3 Chapter 3: Synthesis, Biological Evaluation and Elaboration of Fragments Targeting Aurora-A Kinase

3.1 Introduction

3.1.1 Post-Translational Modifications

Post-translational modifications (PTMs) are covalent processing events which change the properties of a protein by proteolytic cleavage or through the addition of a modifying group to one or more amino acids. PTM's determine a protein's activity state, localisation, turnover and interactions with other proteins. Proteomic analysis identified over 200 types of PTM, including acetylation, amidation and glycosylation.¹⁵⁹ Phosphorylation, performed by the kinase superfamily of proteins, is the most common type of PTM.¹⁶⁰ Protein kinases catalyse phosphorylation in eukaryotes, which is the transfer of the γ -phosphate of adenosine triphosphate (ATP) to a substrate, usually a partner protein. The importance of protein phosphorylation in eukaryotic signalling is reflected in the fact that protein kinase domains are found in 2% of eukaryotic genes.¹⁶¹ Protein kinases control many cellular processes, including metabolism, transcription, cell cycle progression, cytoskeletal rearrangement and cell movement, apoptosis and cell differentiation.¹⁶²

3.1.2 Protein Kinases

There are 518 protein kinases coded for in the human genome, with over a hundred of their structures determined, yielding valuable insights into their mechanisms of regulation.^{161,163–165} Protein kinase structure is composed of a smaller *N*-terminal domain and a larger *C*-terminal domain, separated by a hinge region. The *N*-terminal lobe is typically formed of a single β -sheet composed of five antiparallel β -strands and a helical subdomain comprised of α -helices and contains the activation loop. The active site is formed by a cleft between the *N*-terminal domain and *C*-terminal domain, where ATP binds and ADP is released after transfer of the γ -phosphate to the hydroxyl group of a

serine, threonine, or tyrosine. The adenosine base forms H-bonds with the kinase hinge region, the ribose moiety binds to the ribose-binding pocket and the phosphate groups interact with the Gly-rich loop which is also called the phosphate-binding loop (P-loop).

Protein kinases have been shown to exist in a range of conformations from fully inactive, to fully active. This is dependent on a number of highly conserved structural features; the activation loop, the Asp-Phe-Gly (DFG) and His-Arg-Asp (HRD) motifs, the glycine-rich loop, a lysine-glutamic acid salt bridge and a group of hydrophobic residues forming a regulatory spine (known as the R spine). In 1991 Taylor *et al.* reported the first crystal structure of a protein kinase in its active form.¹⁶⁶

The HRD and DFG motifs are defining features of protein kinases, with the aspartic acids in these motifs as essential catalytic residues. The aspartate residues of the HRD motif acts as a base catalyst that deprotonates the substrate side chain serine/threonine, and so this region of the kinase can be referred to as the catalytic loop. Situated immediately before the activation segment, the DFG motif can exist in two orientations, 'DFG-in' and 'DFG-out', which denote the positioning of the aspartate residue essential for catalytic activity. The aspartate of the DFG motif coordinates a magnesium ion, which activates the γ -phosphate of ATP, and this region of kinases is often called the magnesium (Mg^{2+})-binding loop. These residues must be positioned correctly and in the appropriate chemical environment for the kinase to catalyse phosphate transfer. In an active kinase, the DFG motif adopts the DFG-in conformation, and contacts the HRD motif through a hydrophobic interaction. Displacement of these motifs into positions incompatible for catalysis is part of the regulatory mechanism of many kinases and can be induced by small molecule inhibitors of protein kinases. Imatinib, employed in the treatment of chronic myelogenous leukaemia and gastrointestinal stromal tumours, exemplifies an inducer of DFG-out conformation of cAbl.¹⁶⁷

As the region that contains residues able to be phosphorylated, the activation segment is a crucial component in regulating kinase activity. The activation segment begins at the DFG motif and concludes at a sequence with the consensus alanine-proline-glutamic acid (APE motif). The activation segment includes several important features which are conserved in active kinase structures. The activation loop forms part of the activation segment, which contains the primary site of regulatory phosphorylation. The P + 1 loop forms a pocket that interacts with the P + 1 site of substrates and therefore must be in the correct conformation for efficient catalysis.

The phosphorylated residue on the activation loop utilises a three-point attachment to help stabilise the activation segment in the correct conformation for substrate binding. This three-point attachment is dependent on three structural features: the residue preceding the glutamic acid on αC , a residue three positions towards the C-terminal of the DFG motif on $\beta 9$ and the arginine residue of the HRD motif.¹⁶⁸

The hydrophobic spine is a feature of active kinase structures and is made up of side chains of four hydrophobic residues. The first side chain originates from the $\beta 4$ strand of the N-terminal lobe; the second comes from the adjacent αC helix; the third is a phenylalanine residue from the DFG motif and finally the fourth member of the spine is the histidine residue from the HRD motif.¹⁶⁹ The relative positions of these four residues are strikingly similar in active kinase structures where they form a continuous hydrophobic chain or 'spine'. In an inactive kinase, this side chain lacks linear organisation, allowing the kinase to adopt an inactive conformation.¹⁶⁹

The lysine-glutamate salt bridge between the ammonium group of the lysine and the carboxylate group of the glutamate is a characteristic feature of the active protein kinases. The lysine is located on the $\beta 3$ -strand and the glutamate is located on the αC -helix and the bridge thus links these two important structural elements of the N-lobe together. The lysine also interacts

with the terminal phosphate groups of ATP, holding them in the correct position for catalysis.¹⁶⁴

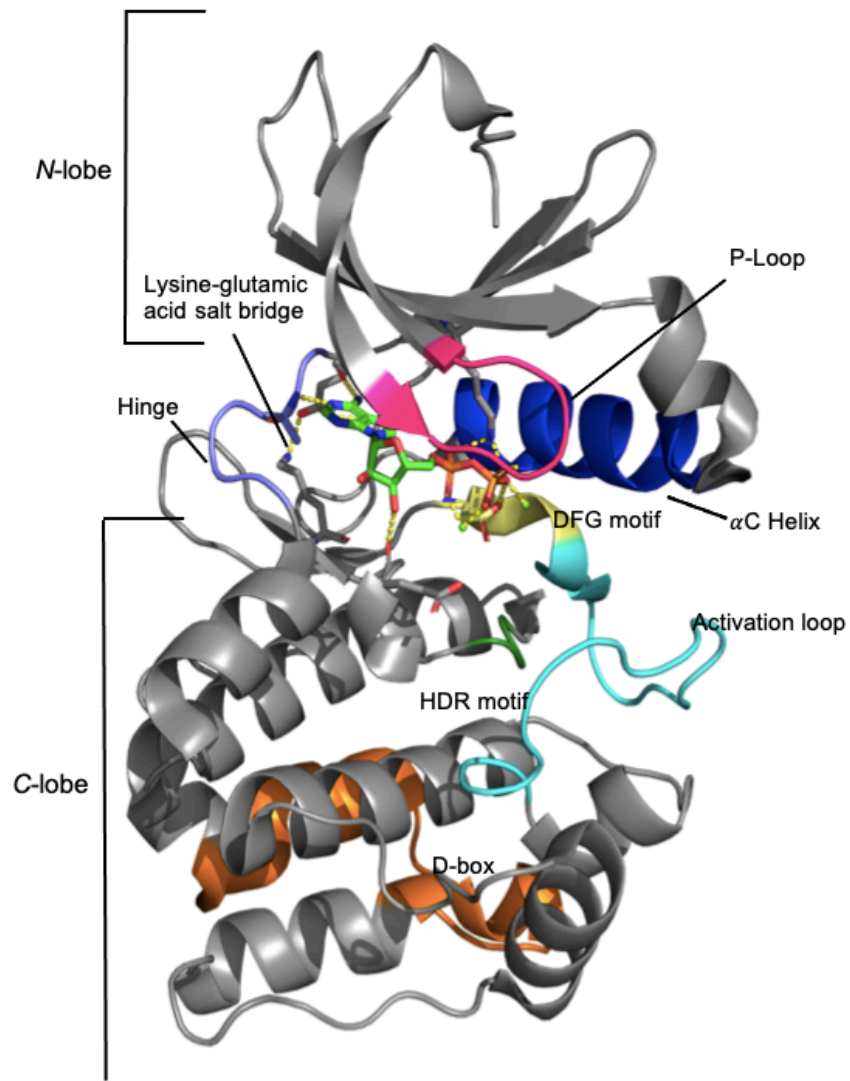


Figure 12: Conserved structural features of an active kinase conformation of a protein kinase. Structure shows Aurora-A in a complex with ADP (PDB 4DEE).

Collectively, these structures are the hallmarks of an active kinase conformation (Figure 12), determined from the crystal structures of a hundred protein kinases and subsequent comparison of catalytic centres.¹⁶⁸

3.1.3 Mitotic Kinases

The cell cycle, the mechanism by which a cell replicates its genetic material and forms two new daughter cells, is one of the fundamental and most important functions in life. The mitotic phase of the cell cycle segregates chromosomes to opposite poles, eventually resulting in two identical daughter cells.

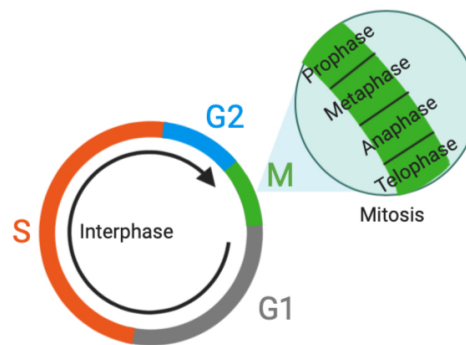


Figure 13: A schematic representation of the cell cycle. Created using Biorender.com

Mitosis is divided into five distinct stages: prophase, prometaphase, metaphase, anaphase, and telophase (Figure 13). During prophase, duplicated chromosomes resulting from interphase condense and the nuclear envelope breaks down. Throughout prometaphase, kinetochores connect chromosomes to microtubules and in metaphase the chromosomes align at the equatorial plate between the spindle poles. Chromatids can then be separated and pulled to opposite poles during anaphase. Finally, the mitotic spindle disassembles, and the chromatids decondense and are surrounded by new nuclear envelopes in telophase. The cytokinesis process results in two daughter cells via division of the parent cell cytoplasm.⁹³

The regulation of M-phase progression relies on protein-protein interactions as well as on post-translation mechanisms. Protein binding partners can stipulate subcellular localisation of a protein kinase through activating kinase activity. Two of the most common post-translation modifications are phosphorylation and ubiquitination, which can activate the protein kinase or

can direct the kinase to the proteasome for degradation (proteolysis).¹⁷⁰ Phosphorylation controls proteolytic machinery and its subsequent degradation, leading to down regulation of a particular kinase.¹⁷⁰ On the contrary, phosphatases, as the functional opposite of protein kinases, dephosphorylate their substrates. Phosphatases have been shown to play an imperative role in mitotic regulation and exit from the mitosis phase.¹⁷¹ It is unsurprising to note that since protein kinases play crucial roles throughout mitosis, their dysregulation will impact the cells ability to undergo healthy cell division and proliferation.

Mitotic kinases are an important class of drug target and through understanding their regulatory mechanisms can lead to effective new treatments for various hyperproliferative diseases. The targeting of protein kinases as potential anti-cancer therapeutics requires both characterisation and understanding of the cellular mechanism of a protein kinase. Appreciation of these factors govern whether targeting of a particular kinase will trigger apoptosis, necrosis or senescence of the cell.^{172, 173}

3.1.4 The Aurora Kinases

The Aurora kinases are a family of closely related serine-threonine protein kinases, containing three members (A, B and C) that are essential for the onset and progression of mitosis as well as genome stability. The first members of the Aurora family of serine/ threonine protein kinases were discovered in yeast and *Drosophila* by Glover *et al.* through screening for genes regulating spindle function.¹⁷⁴ The first human homologues were identified in 1998 by Bischoff *et al.*, with three homologues of Aurora kinase identified, each with distinct functions.¹⁷⁵ Amongst the Aurora kinase subfamily, there is a high level of sequence homology observed (around 70%) in all members. All three kinase share the same basic structural homology; an *N*-terminal domain of 39-132 residues and a *C*-terminal domain (15-20 residues) (Figure 14).¹⁷⁵⁻¹⁷⁷

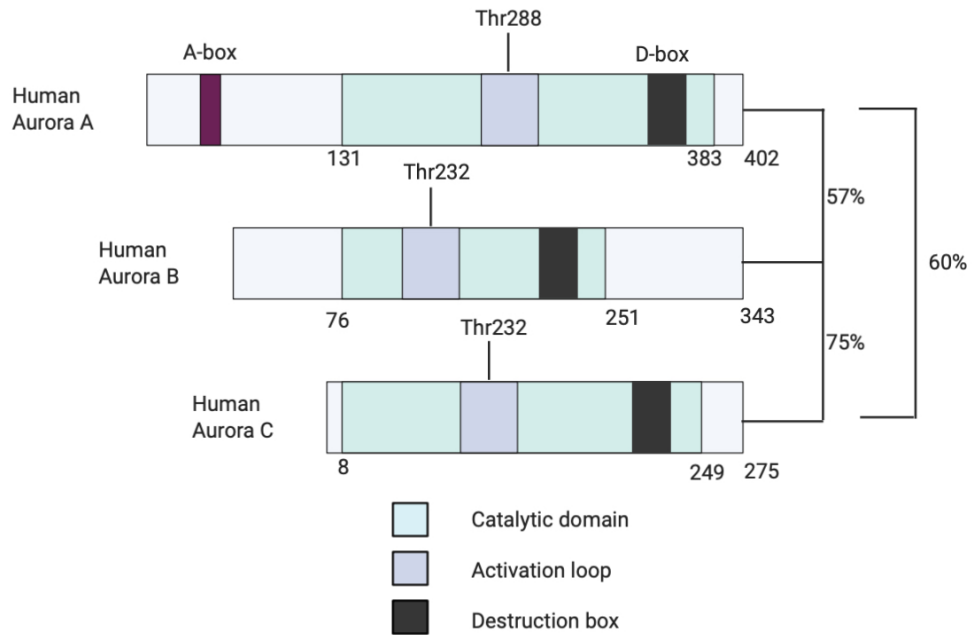


Figure 14: The structure of the Aurora kinases. Annotated with the position of the A-box and D-box. The features represented here are most thoroughly characterised in Aurora-A, with the boxes shown for Aurora B and C as approximations. Created using Biorender.com.

Within the activation loop of the Aurora kinase is a threonine residue, which when phosphorylated, enables full activation of the Aurora kinase.¹⁷⁸ Phosphorylation is regulated through interaction with co-factors, which are unique to each member of the sub-family.¹⁷⁹ These co-factors regulate aurora kinase activity outside of the catalytic domain. The *N*-terminal regions of Aurora-A and -B contain the sequence referred to as the A-box, which when used in conjunction with the *C*-terminal D-box, is required for proteolysis of Aurora-A by E3 ubiquitin-ligase, known as the anaphase promoting complex (APC).¹⁸⁰ Low levels of Aurora-A and -B in the early stages of the cell cycle are maintained by the APC and its partner protein cdh1.¹⁸⁰ Following this, the A-box and D-box structures orientate about the hinge region, directing the selectivity and position of the substrate.¹⁸¹

The ATP binding region is highly conserved between all three members of the Aurora kinase family, with only variation of three residues occurring at positions L215, T217 and R220 in Aurora-A.¹⁸² Despite the high sequence homology between all members of the Aurora kinase family, each member

has vastly different cellular spatio-temporal localisation and therefore function. This high degree of sequence conservation must be considered when designing and screening Aurora kinase substrates and inhibitors.

3.1.4.1 Aurora-A Kinase Function

Aurora-A has been shown to be a critical regulator of multiple events during mitosis. Aurora-A assists in the regulation of centrosome separation, chromosome segregation and mitotic spindle assembly through phosphorylation of its substrates and interaction with binding partners. The regulation of Aurora-A is tightly controlled with expression linked closely with progression of the cell cycle (Figure 15). Expression of Aurora-A peaks during G2 and prophase in the cell cycle, at the same time as localisation of Aurora-A at centrosomes and spindle poles.⁹³

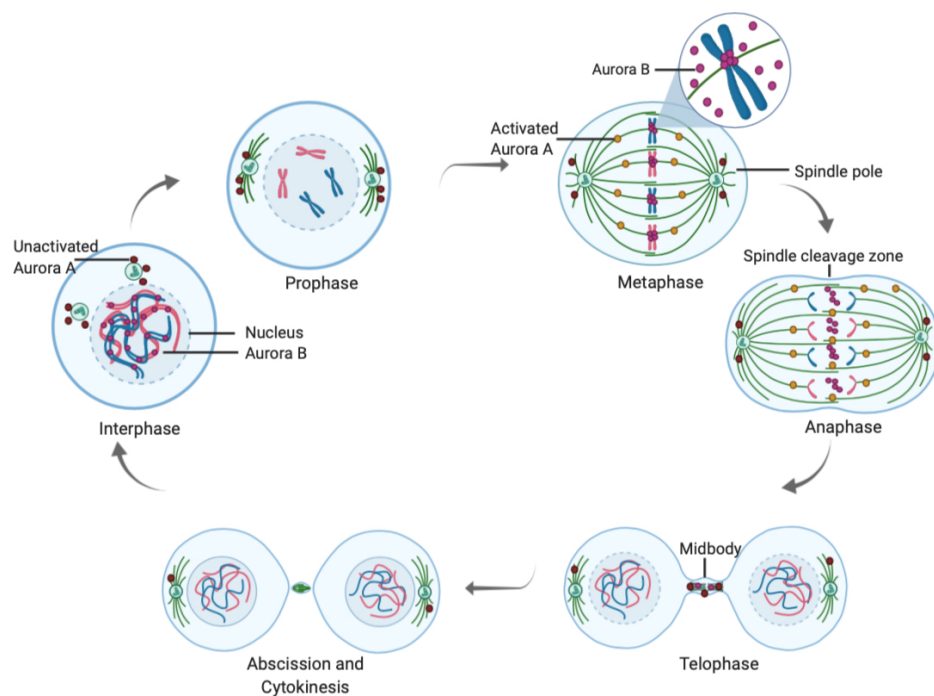


Figure 15: The relative localisation of Aurora A and B during the cell cycle. The level of both Aurora-A and B is substantially reduced during G1. By prophase, Aurora A (red circles) is concentrated around the centrosomes and Aurora B is concentrated in the nucleus. In metaphase, Aurora A localises on microtubules near spindle poles, with Aurora-B located in the inner centromere. In anaphase, Aurora A is located at the polar microtubules, with some also present in the spindle midzone. In cytokinesis both kinases are located in the midbody.⁹³Created using Biorender.com.

3.1.4.2 Aurora Kinases and The Development of Cancer

As regulators of cell cycle progression and normal cellular proliferation, the Aurora kinases have been frequently linked to oncogenesis and the progression of cancer. The *aurora-a* gene is located at chromosome site 20q13.2, with mutations in this region frequently observed in tumours, indicating a possible connection between overexpression of Aurora-A and the development of cancers.⁹³ It has been found overexpressed or amplified in a variety of cancer types, including colorectal¹⁸³, breast¹⁸⁴, lung¹⁸⁵, lymphoma¹⁸⁶, and pancreatic.¹⁸⁷ Disruption of the tightly controlled expression of the Aurora kinases through either the gain or loss of function, or overexpression can lead to altered cellular function, which can be linked to increased cancer susceptibility.

Overexpression of Aurora-A drives centrosome amplification, a hallmark of cancer, and subsequent tetraploidisation due to associated cytokinesis failure, leading to the multinucleation of cells.¹⁸⁸ Liu *et al.* reported that when Aurora-A is overexpressed, phosphorylation of p53 at Ser215 occurs promoted by Aurora-A and inhibits p53-DNA binding, disrupting the cell cycle check activities, creating opportunity for inhibitors of Aurora-A to rescue the function of tumour suppressor genes.¹⁸⁹

Additionally, the over-expression of Aurora-A has been shown to transform rodent cells *in vitro*, leading to tumour development on the introduction into a nude mice.¹⁷⁵ On the contrary, studies using transgenic mice over-expressing Aurora-A kinase displayed no formation of malignancy even following a latency period, suggesting that Aurora-A kinase alone cannot act as an oncogene but that it acts in concert with other oncogenic mutations¹⁹⁰, for example, the RAS pathway.¹⁹¹

Studies have shown that Aurora-B kinase is overexpressed in cancer cells,¹⁹² however, it is not clear whether Aurora-B overexpression is only associated with the high proliferative activity of cancer cells or if it plays a causative role

in tumorigenesis. The locus for Aurora B has been identified as 17p13.1 which has not been observed to be amplified in tumours.⁹³ The over-expression of Aurora-B in tumours may not function as an oncogenic mechanism independently and so overexpression is a feature of the highly proliferative nature of tumour cells. Therefore, due to the lack of definitive evidence that Aurora-B strictly functions as an oncogene, Aurora-A kinase represents a rational target for anti-cancer therapeutics.

3.1.4.3 Small Molecule Regulation of Aurora-A

The multi-faceted roles of Aurora-A kinase in cancer have led to it as a focus of research into anti-cancer therapeutics. Targeting of the Aurora kinases also has the additional feature of having an inbuilt selectivity for proliferating cells due to their increased expression in mitosis. As such, down-regulation of kinase function through removal of the ability to bind ATP by competing for the active site with an inhibitor would effectively starve the enzyme of the source of phosphate.¹⁹³

Regardless of the target of the kinase, inhibitors are divided into classes by the binding mode displayed during inhibition. As discussed in section 3.1.2, the kinase active site has several conformations dependent on the activation state of the kinase, and inhibitors will selectively bind these different conformations, enabling their categorisation.

Inhibitor Class	Mechanism of Action	Examples
Type I	Competes for the substrate and binds in the ATP-binding pocket of the active conformation	Bosutinib, Cabozantinib, Vandetanib
Type II	These inhibitors bind to the DFG-Asp out protein kinase conformation, which corresponds to an inactive enzyme form	Imatinib, Sorafenib
Type III (allosteric inhibitor)	Occupy a site next to the ATP-binding pocket so that both ATP and the allosteric inhibitor can bind simultaneously to the protein.	Trametinib
Type IV (substrate directed inhibitors)	Undergo a reversible interaction outside the ATP pocket and offer selectivity against targeted kinases	ONO12380
Type V (Covalent inhibitors)	Bind covalently (irreversible) to their protein kinase target	Afatinib, Ibrutinib

Table 16: Classification of molecular kinase inhibitors.

Type I inhibitors mimic the purine ring of the adenine motif of ATP, targeting the ATP binding site of the kinase in its active conformation and do not require the DFG motif in the activation loop to adopt a 'DFG-out' conformation for binding, as required for type II inhibitors.¹⁹⁴ Type I inhibitors tend to form between 1-3 hydrogen bonds with the hinge region of a kinase, which mimic those normally formed by the exocyclic amino group of adenine.¹⁹⁵ The adenine region of a protein kinase is occupied by type I inhibitors, with potential to present into other regions of the ATP-binding site, such as the hydrophobic regions I and II, the ribose region and the phosphate-binding region (Figure 16). Occupation of additional regions using diverse functionality can form the basis of inhibitor selectivity between different kinases.

A limitation of ATP-competitive inhibitors is the promiscuity observed because of the shared kinase domain homology between the kinase superfamily and also the development of drug resistance. Nonetheless, the discovery of selective ATP-competitive inhibitors is possible, shown by the seminal discovery of the tyrosine kinase bcr-abl, imatinib.¹⁶⁷

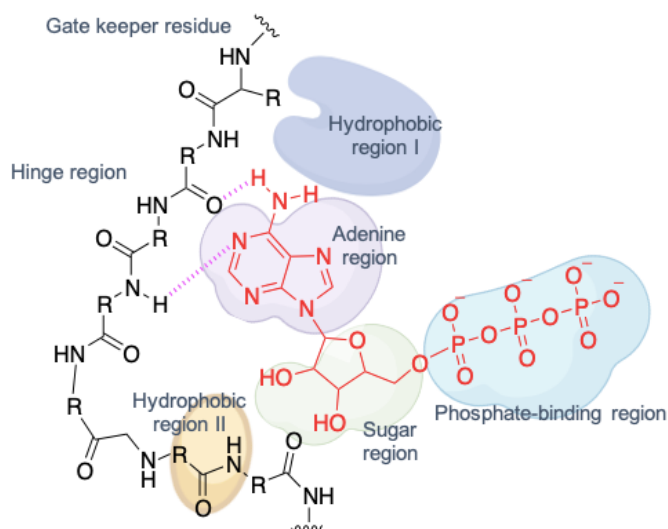


Figure 16: Schematic representation of the ATP-binding site of kinases.

Currently there are no Aurora-A inhibitors with FDA approval, despite several having entered clinical trials for a variety of cancer-types.¹⁹⁶ As sequence homology within the Aurora kinase family is high, small molecule inhibitors often modulate all three isoforms, known as pan-Aurora kinase inhibitors.¹⁹⁷ Pan-Aurora kinase inhibitors have entered the clinic, showing promising selectivity and activity against taxane-resistant cell lines.¹⁹⁸ Despite the encouraging data realised from the studies of pan-Aurora kinase inhibitors, some have been withdrawn from clinical trials due to concerns with toxicity.¹⁹⁹

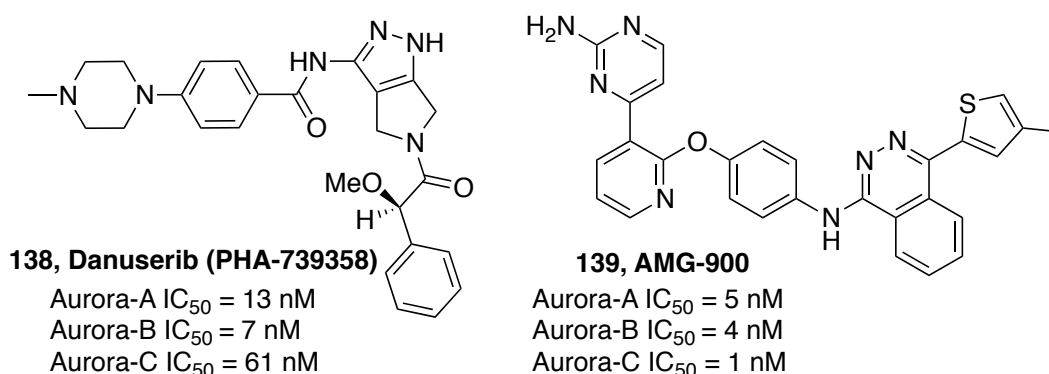


Figure 17: Pan-Aurora inhibitors Danuserib (**138**) and AMG-900 (**139**).

Danuserib (PHA-739358) is a potent pan-Aurora kinase inhibitor (Figure 17).^{197, 200} It targets a number of other kinases including ABL, RET and TRK-4.^{197,200} Danuserib progressed into the clinic and displayed an acceptable toxicity profile and promising activity in patients with advanced malignancies which were resistant to imatinib.²⁰¹ Bush and co-workers reported AMG-900, a pan-Aurora kinase inhibitor, exhibiting a phenotype typical of Aurora-B inhibition (Figure 17).¹⁹⁸ AMG-900 demonstrated potent anti-proliferative activity against a range of human tumour cell lines, including those resistant to Danuserib.^{202,203}

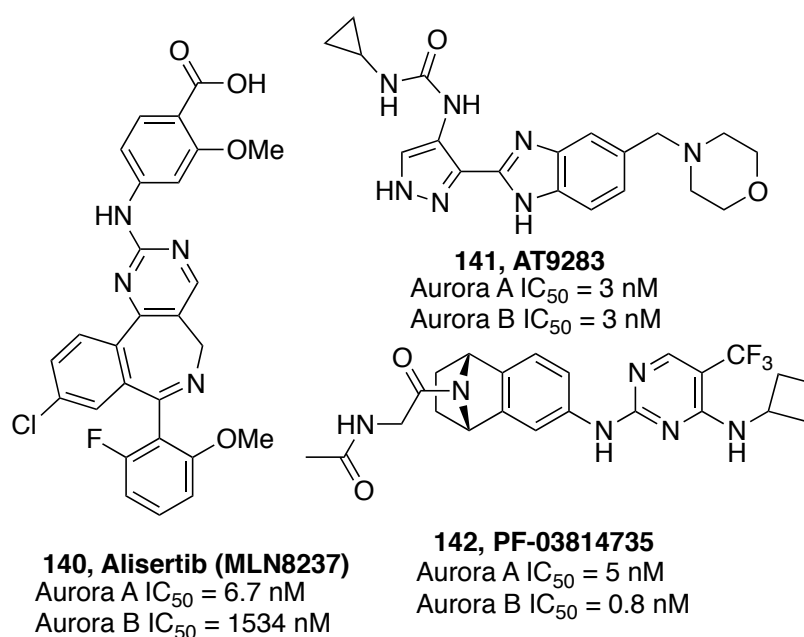


Figure 18: Dual inhibitors of Aurora-A and Aurora-B: Alisertib, AT9283 and PF-03814735.

Dual inhibitors targeting Aurora-A and Aurora-B have been reported (Figure 18).²⁰⁴ The most prominent dual Aurora-A inhibitor is Alisertib (MLN8237), an investigational Aurora-A inhibitor which has been subject to more than 30 clinical trials.^{205, 206} Alisertib has shown inhibitory activity against both Aurora A (IC_{50} = 6.7 nM) and Aurora B (IC_{50} = 1534 nM) *in vivo*. It was shown in pre-clinical models of HPV-driven cervical cancer that its dual inhibition provides selectivity and efficacy required of an *in vivo* drug in this setting.²⁰⁷ Astex describe a potent dual inhibitor, known as AT9283, of Aurora A and B (IC_{50} =

3 nM), which was also found to have activity against other kinases including JAK2, Flt-3 and Abl.^{71, 208} This broad application is understood to be due to the benzimidazole motif of AT9283 that binds to a region of the ATP-binding site which is structurally similar with Aurora-A, confirmed by X-ray crystallography. As with Aurora-A, the hinge region of JAK2 contains an extra glycine residue (Gly935), relative to the CDKs, which leads to the pocket having a particular affinity for flat heteroaromatic moieties such as a benzimidazole. This glycine residues is also common to Flt-3 and Abl, suggesting it is responsible for its strong target affinity.⁷¹ PF-03814735 was identified by scientists at Pfizer as an orally bioavailable inhibitor of Aurora-A and B achieving nanomolar affinities (Aurora A IC₅₀ = 5 nM, Aurora-B IC₅₀ = 0.8 nM).²⁰⁹ Compound **142** displayed potent inhibitory activity against a variety of human tumour cell lines and anti-proliferative activity against imatinib-resistant BCR-ABL⁺ cells, including those carrying the ABL(T315I) mutation.²¹⁰

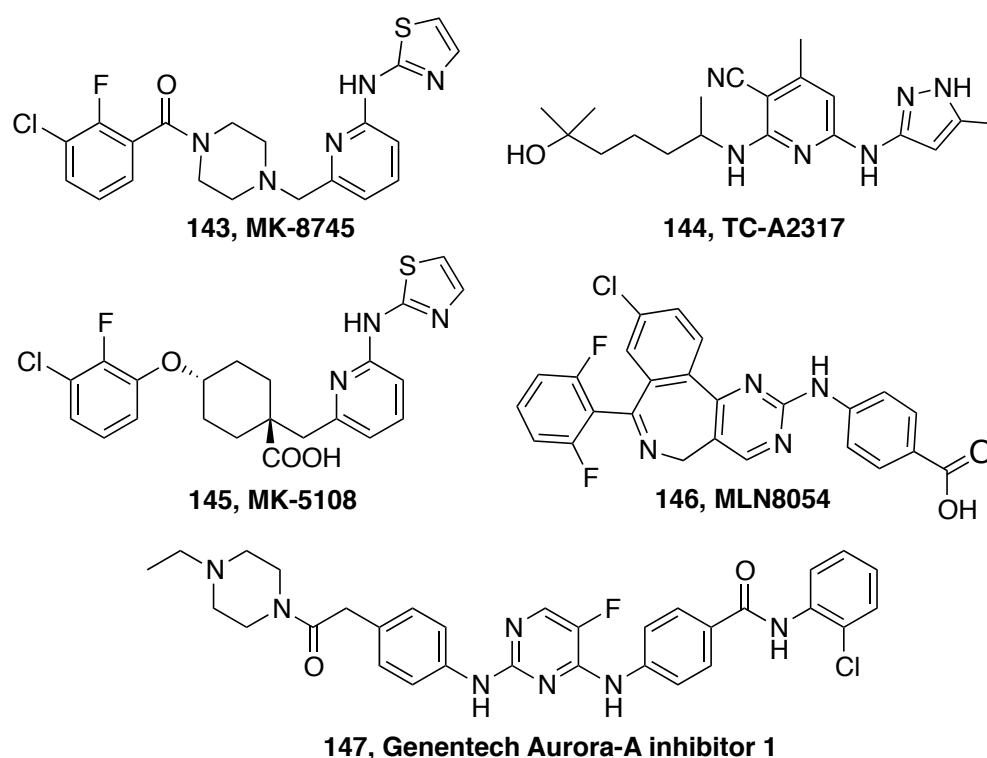


Figure 19: Structure of Aurora-A inhibitors: MK-8745 (**143**), TC-A2317 (**144**), MK-5108 (**145**), MLN8054 (**146**) and Genentech Aurora-A inhibitor 1 (**147**).

As previously discussed, type I inhibitors display promiscuity because of the targeted ATP pocket being conserved through the Aurora kinase family and so use of type I inhibitors are often accompanied by adverse effects. This low selectivity for targeted kinases has been shown to result in cardiotoxicity and deterioration in cardiac function.²¹¹ It has been possible to achieve selectivity between the Aurora kinases and the wider kinome Type I inhibitors MLN8054²⁰⁶, MK-8745²¹² and MK-5108.²¹³ all display enhanced selectivity for Aurora-A when compared to Aurora-B (Figure 19). Their displayed phenotypes were indicative of Aurora-A inhibition, through accumulation of cells stopped in the G2/M phase of the cell cycle, defective mitotic spindle formation and the inhibition of cell proliferation. Genentech Aurora-A inhibitor 1 exhibited activity against Aurora-A, with an IC₅₀ of 3.4 nM, however, off-target effects were demonstrated through toxicity in multiple cell lines.²¹⁴ Ando and co-workers reported TC-A2317 as a selective Aurora-A kinase inhibitor, constructed through transformation of a potent pan-Aurora kinase inhibitor.²¹⁵ They examined cross-reactivity with 68 typical kinases, and found activity against 60 of these kinases was much diminished (over 1000 nM).²¹⁵

3.1.5 Fragments Targeting Aurora-A

As only a small fraction of the kinome can be targeted by selective and potent inhibitors, there is a need to develop strategies for efficient discovery of novel small molecule inhibitors. Historically, ATP-competitive inhibitors are discovered by high-throughput screening (HTS) of compound collections. It is widely described that this process is becoming less effective as it has now identified a significant proportion of the applicable scaffolds which are capable of serving as ATP-competitive ligands.²¹⁶ Previous work within the field has shown that the discovery of novel ATP site-targeting ligands is achievable using fragment-based assembly strategies.⁷¹

Type I inhibitors bind at the ATP-binding pocket, which is highly conserved across the human kinome. To achieve greater selectivity than ATP, type I

inhibitors will occupy the region occupied by the adenine of ATP but can extend into different proximal regions to exploit selectivity between kinase active sites.

3.1.6 Docking Programs

Within this chapter two docking programs are utilised to predict how our active compounds bind to Aurora-A and to rationalise fragment growth points which could be pursued to increase the potency of the compounds.

3.1.6.1 Glide²¹⁷

Glide is an add-on to the Schrödinger package Maestro. Glide approximates a complete systematic search of the positional, orientation and conformational space available to the ligand.²¹⁷ The systematic search space is narrowed by an initial rough positioning and scoring phase, subsequently followed by torsionally flexible energy optimisation on an OPLS-AA, for hundreds of surviving poses. The best candidate poses are further refined by a Monte Carlo sampling of the pose conformation. Selection of the best pose uses a model energy function that combines empirical and force-field based terms.

3.1.6.2 ROCS²¹⁸

ROCS (for Rapid Overlay of Chemical Structures) is a ligand-based docking software, which uses a large database of compounds to identify potential inhibitors using shape comparison. The principle which ROCS explores is that molecules similar in shape to active molecules are more likely to be active than randomly selected molecules. ROCS considers 3D similarity and chemical functionality such as charges, hydrogen bond acceptors and donors. The results are ranked based on a ROCS scoring function, which incorporates shape and compound surface similarity.

3.2 Results and Discussion

3.2.1 Fragment Library Design Targeting Aurora-A

A virtual fragment library was designed, and the properties of the virtual fragment library analysed. Each fragment was designed to be composed of two separate chemical parts; a heterocyclic warhead attached to a cyclic amine. The heterocyclic warhead is an isosteric replacement for the adenine moiety of ATP, while the cyclic amine is predicted to stretch into the hydrophobic region of the ATP-binding pocket and enables elaboration of the fragment should hits be identified (Chapter 2).

Analysis of the literature identified three heterocyclic motifs, which would form the basis of three series of fragments to be screened against Aurora-A (Figure 20). Scaffold **148** was selected to be a purine, with previous applications in anti-tumour,²¹⁹ anti-viral and anti-microbial agents²²⁰ as well as its presence in ATP. An isoquinoline-5-sulfonyl scaffold (**149**) was chosen as the basis for a fragment series as it forms a fragment of a reported clinical ROK inhibitor, Fasudil.²²¹ Allen and co-workers reported that this motif, when functionalised with a cyclic amine in the 5-position displayed activity against a wide variety of kinase families, while retaining selectivity.²²² The final series was constructed using a 3-aminopyridine moiety (**150**), in order to incorporate variation in the size of the heterocyclic scaffold. The 3-amino pyridine scaffold contains fewer heavy atoms when compared to **148** and **149**, allowing for greater variation in the cyclic amine to be attached while still adhering to the 'rule of three' for fragments.

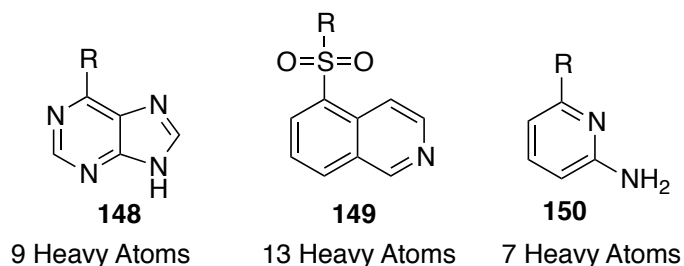


Figure 20: Aromatic warheads chosen to form the three series of fragments.

The virtual fragment library was completed through attachment of each warhead to a variety of cyclic amines, as displayed in Figure 21. The cyclic amines were selected to encompass a broad range of structural and electronic features, as well as their suitability to fragment elaboration through the aforementioned methods (Chapter 2).

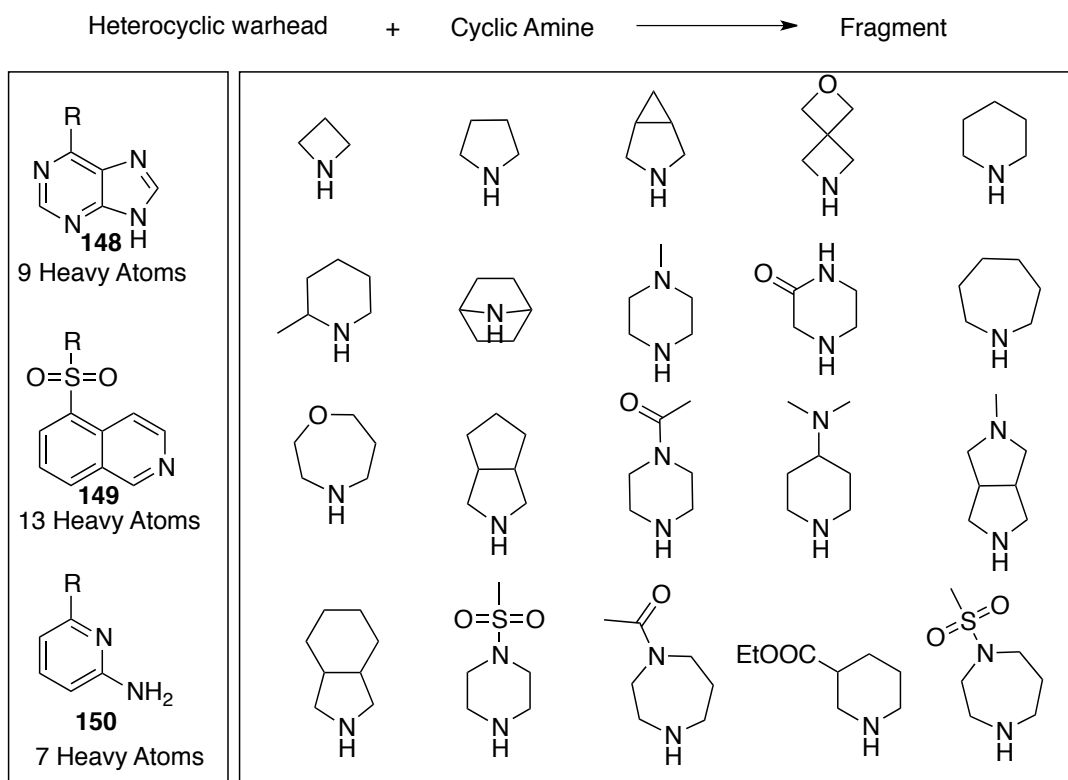


Figure 21: The selected warheads and the selected cycle amines for fragment synthesis

3.2.2 Analysis of the Virtual Fragment Library

Despite the small size, apparent simplicity and commercial availability of fragment molecules, there is a pressing need for the design and subsequent

synthesis of fragments which are in-line with guidelines reported by leading practitioners within the field.⁸³ A summary of the physicochemical criteria for this project are defined in Table 17.

Physicochemical property	Value
Number of heavy atoms	≤ 21
AlogP	$0 \leq X \leq 2$
PSA	$\geq 60 \text{ \AA}^2$

Table 17: A summary of the physicochemical properties chosen for this project.

The virtual library was assessed with respect to these criteria using the open-access computation tool, LLAMA.²²³ By doing this, we are able to confirm that the properties of the virtual library are fragment-like.⁸³ We have considered properties outside of those listed in Table 17 for the virtual library, to enable prioritisation of fragments for synthesis. The full 60-member compound library was analysed and the average, smallest and largest values were determined.

Data	MW (HAC)	AlogP	Molecular PSA / \AA^2	Fsp³	Rotatable Bonds
Average	249.1 (18)	0.98	63.9	0.49	1.6
Smallest	164.2 (12)	-0.58	50.3	0.23	1
Largest	369.5 (24)	3.13	95.1	0.69	3

Table 18: Analysis of the different physicochemical properties of the full virtual 60-member library.

Analysis of physicochemical properties (Table 18) displays that the average molecular weight (heavy atom count), AlogP and PSA fall within the desirable range specified for the fragments within this project. The smallest and largest values of molecular weight (MW) and AlogP fall outside of these criteria and so the spread of the compounds across each physicochemical parameter was investigated.

3.2.2.1 Heavy Atom Count

Heavy atom count gives an indication of molecular weight and therefore the spread of heavy atom count was analysed as a representation of the spread

of molecular weight for the virtual library. The average number of heavy atoms across the entire virtual library is 18, giving an average molecular weight of 239 g mol⁻¹. Once molecules with above 21 heavy atoms are removed from the library, this becomes 17 giving a molecular weight of 237 g mol⁻¹. Table 19 displays that a limited number of compounds exist in the extreme groups. Although some virtual fragments have a heavy atom count greater than 21, these compounds were removed from the library prior to synthesis. All of the removed compounds were part of the isoquinoline-5-sulfonyl series.

Heavy Atom number range	10-12	13-15	16-18	19-21	21 +
Percentage of total library	2	25	37	14	2

Table 19: The percentage of compounds in the library in different heavy atom count groups.

3.2.2.2 AlogP

The atomic LogP (AlogP) considers that each atom has a contribution to the LogP and that the final value of LogP for a compound is purely additive. Previous work within the literature shows a correlation between higher lipophilicity and elevated attrition rates in clinical development, therefore fragment-based assembly programmes should begin with a low AlogP fragment hit.³⁹ A high value of ALogP decreases aqueous solubility, a property important for biophysical screening of fragments, whereas fragments with a low ALogP have poorer permeability.^{23,26} Table 20 denotes that most compounds have an AlogP between 0 and 2, which is within the range for fragments as specified.

AlogP	-2	-1	0	1	2	3
Percentage of total library	0	4	32	37	23	5.3

Table 20: The percentage of compounds in the library in different AlogP groups.

3.2.2.3 Polar Surface Area

Polar surface area (PSA) defined as the surface area belonging to polar atoms, is a descriptor that has been shown to correlate positively with passive molecular transport through membranes and therefore can allow prediction of transport properties of drug candidates. Hubbard *et al.* stated that fragments should have a polar surface area of no more than 60 Å², although this has

been disputed to be an optional guideline.⁷⁹ The polar surface area of the compounds in the virtual library was assessed (Table 21). The results show the majority of the compounds have a polar surface area below 60 Å².

PSA / Å ²	50-59	60-69	70-79	80-89	90-99
Percentage of total library	52	21	12	9	7

Table 21: The percentage of compounds in the library in different PSA groups.

3.2.2.4 Fraction of sp³-Hybridised Carbons

Compounds with greater saturation are found to be more likely to succeed at each stage of development, from early discovery to market.³⁷ More highly complex molecules, as measured by saturation and the number of stereocentres, have the capacity to access greater chemical space and can aid improvement of physiochemical properties, such as aqueous solubility and lipophilicity.^{37,83} The fraction of sp³-hybridised carbons, as defined by Equation 2 is an interpretable measure of the complexity of molecules which can be applied to fragments. The virtual library was assessed for the fraction of saturation within the compounds, with results in Table 6. Most compounds within the virtual library have approximately 50% saturation, without compounds occupying the extreme groups.

$$F_{sp^3} = \left(\frac{\text{Number of } sp^3 \text{ - hybridised carbons}}{\text{Total carbon count}} \right)$$

Equation 2: Equation for the calculation of degrees of unsaturation present in a compound

F _{sp³}	0 – 0.2	0.21-0.40	0.41-0.60	0.61-0.80	0.81-1.0
Percentage of total library	0	26	70	9	0

Table 22: Distribution of saturation within the fragment library.

The 3D structures of the fragments can be visualised by use of a normalised principle moment of inertia (PMI) plot (Figure 22).²²³ The fragments are represented by graphical points and are plotted based on their rod, disk and sphere-like properties, with each fragment represented by green points. This plot clearly shows that the virtual fragment library compounds lie close to the rod-disc axis and are unsurprisingly flat and not 3-dimensional. However, it is noted that some of the fragments are beginning to extend more towards the

sphere axis, showing some 3-dimensional character, despite the simple nature of the scaffolds.

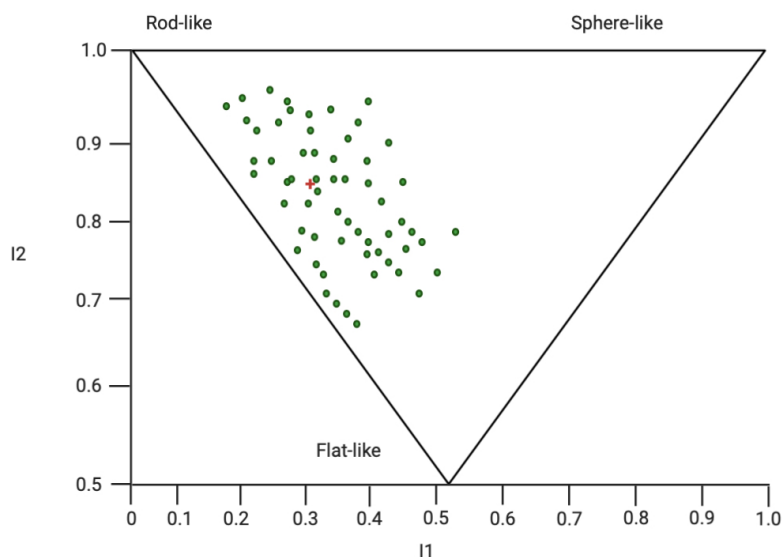


Figure 22: Principle moments of inertia plot describing the molecular shape of the virtual fragment library.

3.2.3 Summary

This analysis shows that for individual properties, a significant proportion of fragments fit within the desired criteria. However, when all the criteria are taken into consideration, only 33% of the virtual library satisfies the defined criteria. Introduction of these criteria enables focus of the synthesis in the direction of the most desirable fragments.

		HAC	AlogP	PSA	All Criteria
1	Number of Compounds	52	39	30	20
2	Percentage of total library	91	68	14	33

Table 23: The number of compounds and percentage of the library that fit with the fragment property criteria.

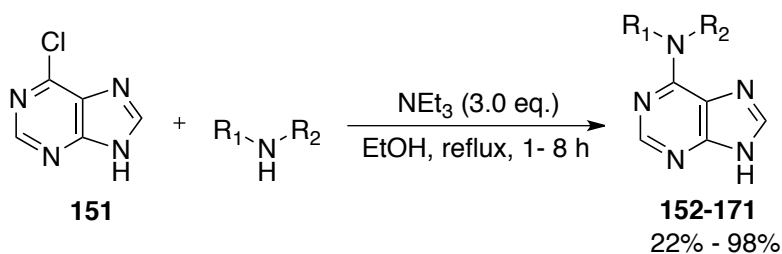
3.2.4 Synthesis of the Fragment Library

Preparation of a virtual library enables prioritisation of a fragments for synthesis. For our synthetic strategy, a prioritisation was placed on synthetic tractability. Each fragment should be synthesised in a minimum number of synthetic steps and able to provide suitable amounts (100-200 mg) for

fragment screening, analysis, and future development. The synthetic approach was grouped into each specific warhead and completed in parallel.

3.2.4.1 Purine Fragment Series

Synthesis of the purine fragment series followed a previously reported synthesis.²²² Commercially available 6-chloropurine (**151**) was refluxed in ethanol, in the presence of triethylamine and treated with each of the selected amines, in a parallel synthesis. Following the specified time, a precipitate formed, which could be isolated by filtration without additional purification (Scheme 26).



Scheme 26: General synthesis of fragments containing the purine scaffold using an S_NAr reaction.²²⁴

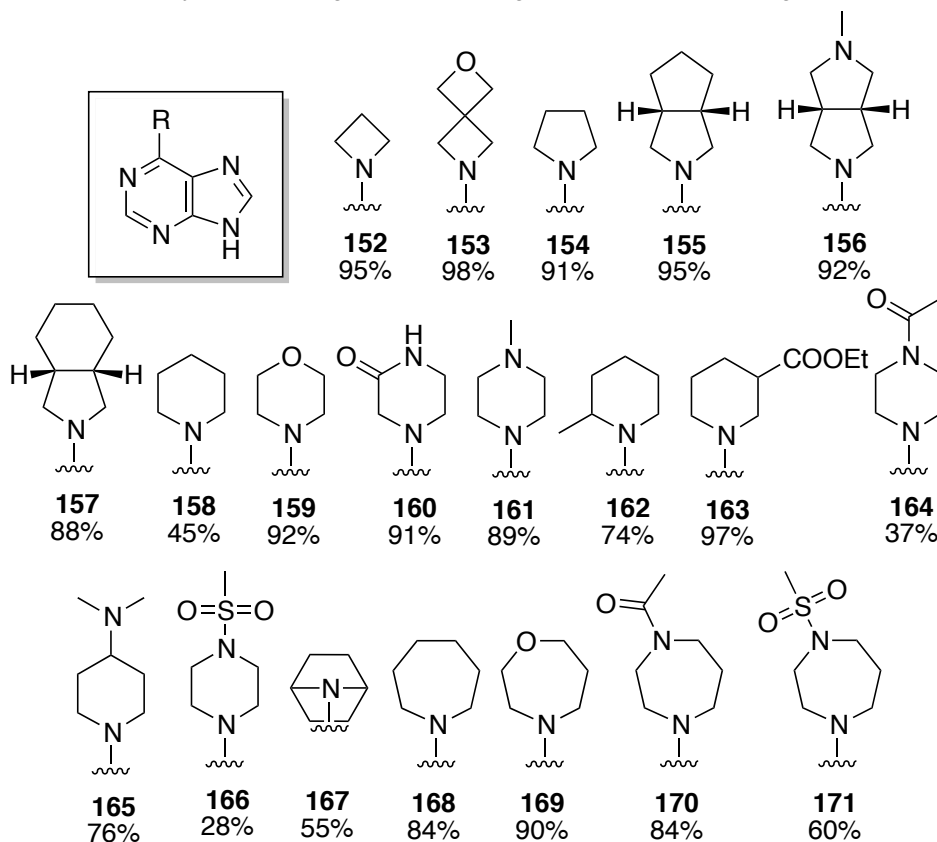
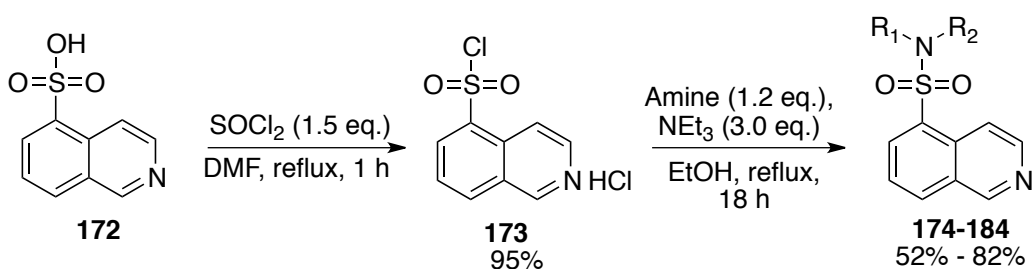


Figure 23: Purine Fragment Series.

The yields are obtained without optimisation of the procedure and since ample material was produced for biological screening, further optimisation was not required (Figure 23).

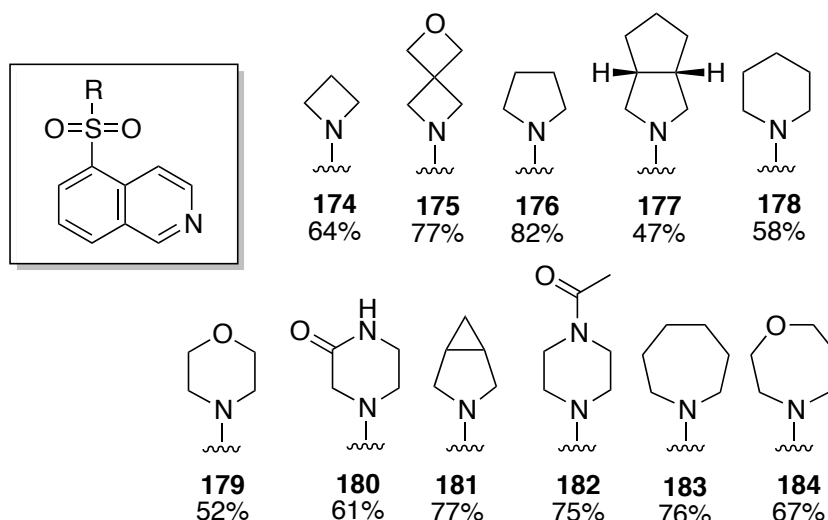
3.2.4.2 Isoquinoline-5-sulfonyl Fragment Series

As the isoquinoline-5-sulfonyl chloride (**173**) had intermittent commercial availability, a suitable synthesis of the starting material was required. It was found that refluxing isoquinoline-5-sulfonic acid (**172**) in thionyl chloride over 1 hour yielded isoquinoline-5-sulfonyl chloride in a 95% yield (Scheme 27).



Scheme 27: Synthesis of the isoquinoline-5-sulfonyl chloride and subsequent sulfonylation procedure to synthesis fragments **174-184**.²²⁵

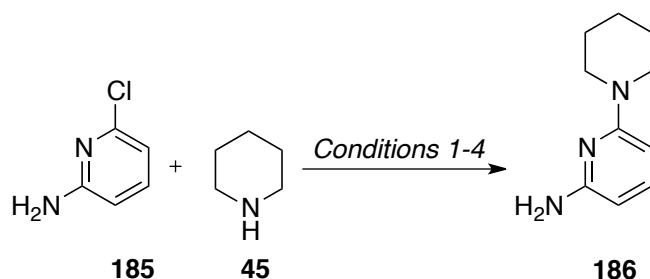
With isoquinoline-5-sulfonyl chloride in hand, a series of sulfonylation reactions were performed using previously selected amines. Conditions were analogous to those used with the purine series, suggesting amenability to parallel synthesis. Since the heavy atom count of the fragment library was restricted to 21 heavy atoms, the scope of cyclic amine used in the 5-position was limited to reflect this. All yields were obtained without optimisation and were able to produce enough material for biological screening.



Scheme 28: Synthesis of the isoquinoline-5-sulfonyl series.

3.2.4.3 3-Aminopyridine Fragment series

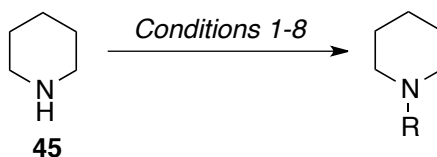
Access to the 3-aminopyridine fragment series was first attempted through an S_NAr reaction between commercially available 3-aminopyridine and the selected amines, in the presence of a non-nucleophilic base. Literature reports for this reaction were limited, therefore a range of conditions for the S_NAr were explored. Table 24 displays the conditions which were sampled.



Entry	Conditions	Outcome
1	NEt ₃ (3.0 eq.), EtOH, rt, 24 h	No reaction
2	NEt ₃ (3.0 eq.), EtOH, reflux, 24 h	No reaction
3	MW (20 W), neat, 150 °C, 2 h	Product seen in the LC-MS, unable to isolate
4	NEt ₃ (3.0 eq.), MW (20 W), neat, 150 °C, 6 h	Product seen in the LC-MS, unable to isolate

Table 24: Conditions trialled to synthesis the 3-aminopyridine series using 2-chloro-3-aminopyridine and piperidine.

Regrettably, these conditions (Table 24) did not yield a successful outcome. Although product was observed by LC-MS in the case of entry 3 and 4, it was unable to be isolated, attributed to be due to instability of the product. Consequently, a range of pyridine and pyrimidine derivatives were evaluated to replace the 3-aminopyridine series. The reactions were monitored by LC-MS and purified by flash column chromatography when the product was observed.



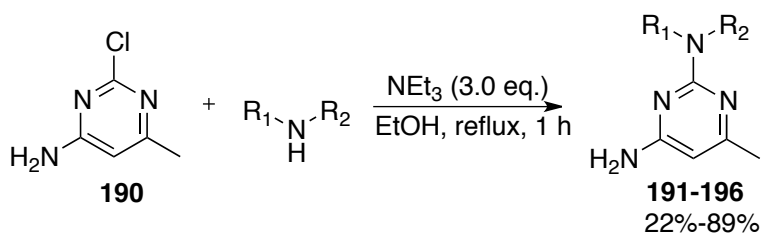
Entry	Compound	Analogue	Conditions	Outcome
1	187		NEt ₃ (3.0 eq.), reflux, EtOH, 12 h	No reaction
2			NEt ₃ (3.0 eq.), MW (20 W), 150 °C	No reaction
3	188		NEt ₃ (3.0 eq.), reflux, EtOH, 12 h	No Reaction
4			NEt ₃ (3.0 eq.), MW (20 W), 150 °C	Reaction
5	189		NEt ₃ (3.0 eq.), reflux, EtOH, 12 h	No Reaction
6			NEt ₃ (3.0 eq.), MW (20 W), 150 °C	Reaction
7	190		NEt ₃ (3.0 eq.), reflux, EtOH, 12 h	77%
8			NEt ₃ (3.0 eq.), MW (20 W), 150 °C	56%

Table 25: Screening of replacement pyridine and pyrimidine derivatives.

From considering the results displayed in Table 25, use of 2-chloro-6-methylpyrimidin-4-amine (**190**) successfully yielded the desired product applying conditions used in the parallel synthesis of the purine series and the isoquinoline-5-sulfonyl series.

With a replacement heterocyclic warhead and experimental conditions for the fragment synthesis in hand, the parallel fragment synthesis was completed

(Scheme 29). As the replacement heterocycle (**190**) had intermittent commercially availability, only limited examples could be prepared.



Scheme 29: Synthesis of the pyridine fragments **191-196**.

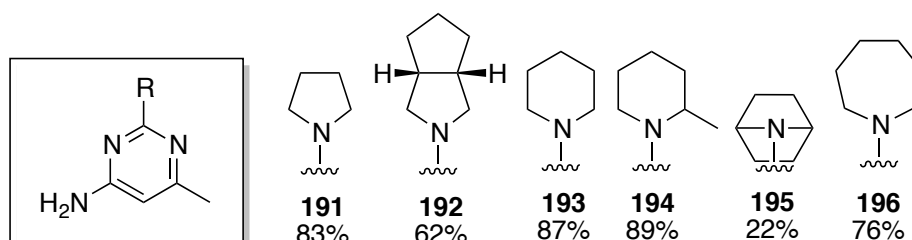


Figure 24: Pyrimidine fragment series.

3.2.5 Summary

A complete list of the fragments synthesised within this section is in Appendix 1. In summary, 37 fragments were synthesised for biological screening against Aurora-A. The original virtual library was condensed to 37 synthesised fragments, through analysis of each fragments molecular properties and commercial availability. It was concluded that at this stage, 37 fragments across three fragment series would be effective in probing the inhibition of Aurora-A phosphorylation.

3.2.6 Analysis of the fragment library

Using LLAMA, we analysed the physiochemical properties of the synthesised library with respect to the set guidelines (Section 3.2.2, Table 17).

3.2.6.1 Heavy Atom Count

All of the fragments fit within the parameter set previously (Table 26).

HAC	12-14	15-17	18-20	21	21+
Percentage of Library	11.4	42.8	37	5.7	0

Table 26: Distribution of heavy atoms throughout the synthesised library.

3.2.6.2 ALogP

The overall AlogP distribution was calculated by LLAMA²²³ where 68% of the synthesised library was within the parameters set by leading practitioners in the field $0 \leq x \leq 2$ (Table 27).

ALogP	-2	-1	0	1	2	3
Percentage of total library	0	3.50	28.6	28.6	28.6	5.7

Table 27: Distribution of AlogP throughout the synthesised library.

3.2.6.3 Three-Dimensionality of the Synthesised Library

Although a requirement for three-dimensionality was not required in our set guidelines (Table 17), we examined the three-dimensionality of the fragments by a PMI plot (Figure 25), with the purine series in green, the isoquinoline-5-sulfonyl series in red and the pyrimidine series in blue. It was found that the heterocyclic warhead which produced the most 3D fragments was the isoquinoline-5-sulfonyl motif (red), whereas the purine (green) and pyrimidine (blue) warheads produced fragments which have more rod/disc-like

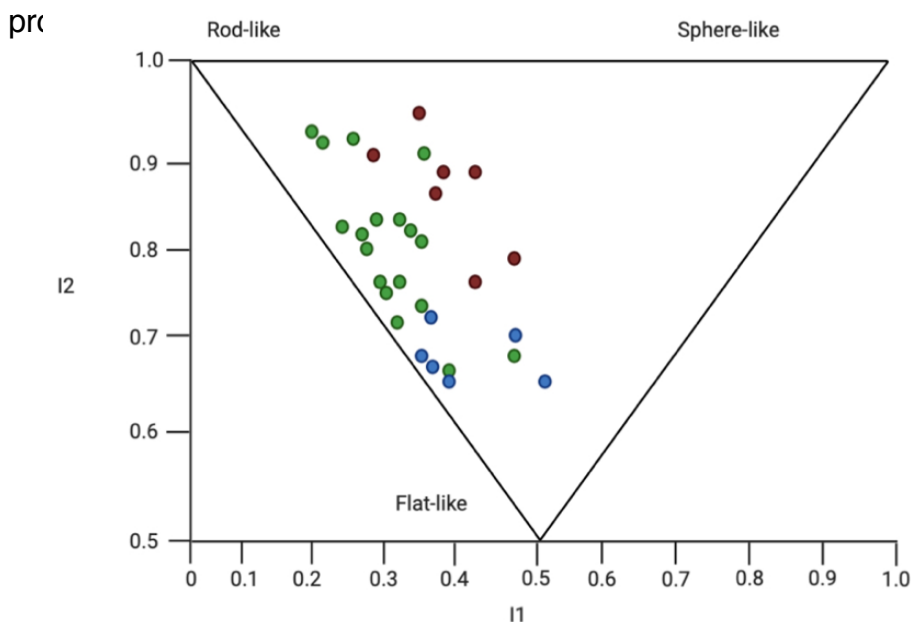


Figure 25: A PMI plot of the synthesised library, showing the purine series (green, isoquinoline-5-sulfonyl series (red) and the pyrimidine series (blue). The PMI plot was produced by use of LLAMA.

3.2.7 Summary

Overall, 37 fragments using three different aromatic warheads were synthesised from readily available starting materials. The properties of these fragments were assessed by LLAMA.²²³ The fragments synthesised in this section will be used in subsequent testing with Aurora-A.

3.2.8 Fragment Screening against Aurora-A

A variety of characterisation methods exist for the evaluation for inhibitory potency of fragments against protein targets, for example differential screening fluorimetry (DSF), surface plasmon resonance (SPR) and isothermal titration calorimetry (ITC).

In this study, the protein kinase enzymatic activity and IC₅₀ were assessed for each compound using a caliper mobility-shift assay. This method is based on the principle of electrophoresis mobility-shift, where modified products are distinguished from un-modified substrates by their relative mobilities. While several different modifications can be used for this distinction, in the context of kinase activity, the transfer of a phosphate group from ATP to a substrate peptide triggers a change in the net charge of the peptide. Aurora-A kinase catalyses the transfer of the phosphate to an appropriate peptide substrate. The product and substrate are separated by a charge potential difference drawn across pressure-driven microfluidic channels, whereby the fluorescently-labelled peptide substrate and phosphorylated product are drawn through the channels, across a viewing window, excited *via* an LED and detected by camera.^{226, 227} The relative intensities of the substrate and product allow for the determination of the percentage substrate converted, and taking these measurements over a specific time allows for the kinetics of the reaction to be obtained based on the measured initial rate of the reaction.

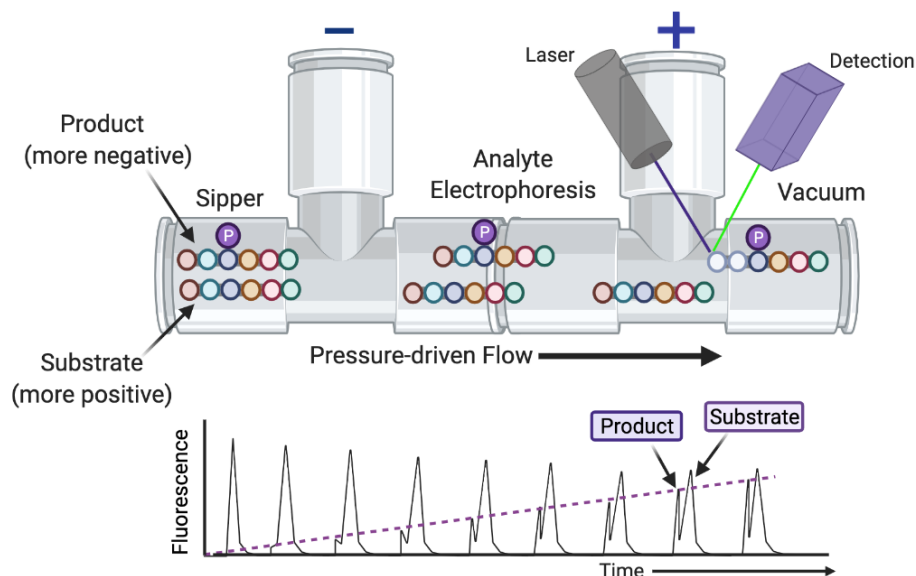


Figure 26: Schematic representation of the caliper mobility shift assay. Top: Principle of analyte electrophoresis occurring in microfluidic channels due to the electrical charge drawn across them. Bottom: The real-time output from the assay. Fluorescence output is measured and % conversion calculated as $\% \text{ conversion} = 100 \times (\text{product} / (\text{product} + \text{substrate}))$. Created using biorender.com.

Advantages of mobility-shift assays include high quality of data and high sensitivity, low protein loading requirements, low interference from compounds, no requirement for radioactive substrates, and ease of maintenance. Figure 26 shows an example setup and output for the assay. This section describes the determination of bioactivity of the fragments synthesised in section 3.2.4 using the EZ-reader II mobility-shift assay.

3.2.9 Characterisation of the Aurora-A Pseudo-WT Complex

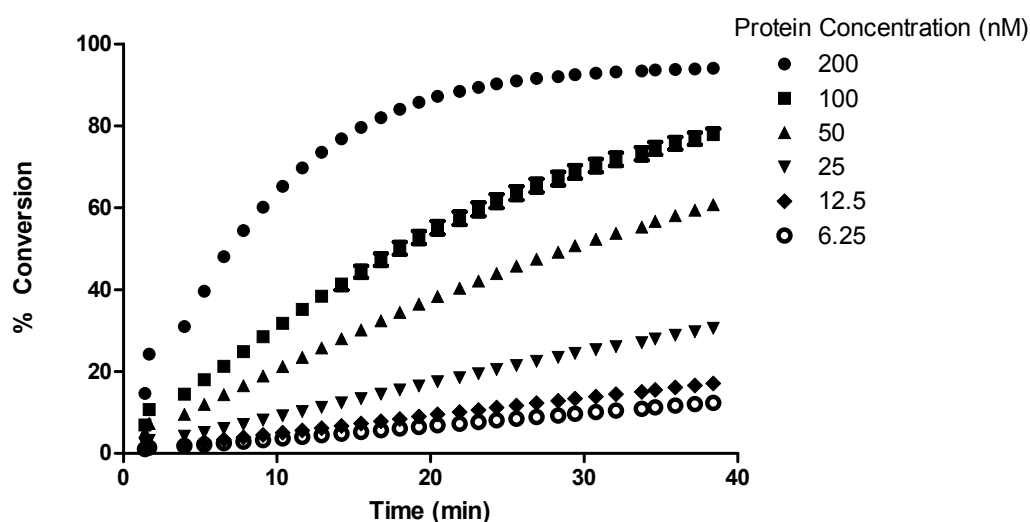
As this pseudo-WT complex would be used to perform IC_{50} determinations of fragments, full characterisation of the complex was required to ensure optimal assay conditions were obtained.

Due to the lack of stability and denaturing of the WT Aurora-A catalytic complex during previous screening within the research group²²⁸, it was a more stable complex was used, the pseudo-WT mutant. In pseudo-WT Aurora-A, two solvent exposed cysteine residues have been mutated to alanine, C292A:C393A.

This section describes the determination of ideal enzyme concentration, ATP K_M and DMSO tolerance. Once this characterisation was completed, determination of the IC_{50} of the prepared fragments could commence.

3.2.9.1 Identification of a suitable Aurora-A concentration for screening

Employing a literature K_M value for ATP of $84 \mu M$ ²²⁹ for the Aurora-A pseudo-WT complex, an enzyme titration was performed to elucidate the ideal concentration of Aurora-A for use in IC_{50} determinations. The experiment utilised six point, 2-fold serial dilution with an upper concentration of 200 nM and a $1.5 \mu M$ final substrate concentration. Using thirty-five plate cycles over forty minutes, the data is shown in Graph 1.



Graph 1: Enzyme titration of the pseudo-WT Aurora-A complex. A six-point, 2-fold serial dilution was performed to determine the ideal enzyme concentration. 31.25 nM which displayed a linear response ($R^2 = 0.9997$).

The value of enzyme concentration at 25 nM displayed the desired characteristic of linear response ($R^2 = 0.9997$) with approximately 30% conversion of the peptide substrate. Employing this concentration will enable the determination for the initial rate of the enzyme without observing a plateau in the data. This result was in accordance with previous work completed within the Nelson group by Chris Arter.²²⁸

3.2.9.2 Determination of ATP K_M

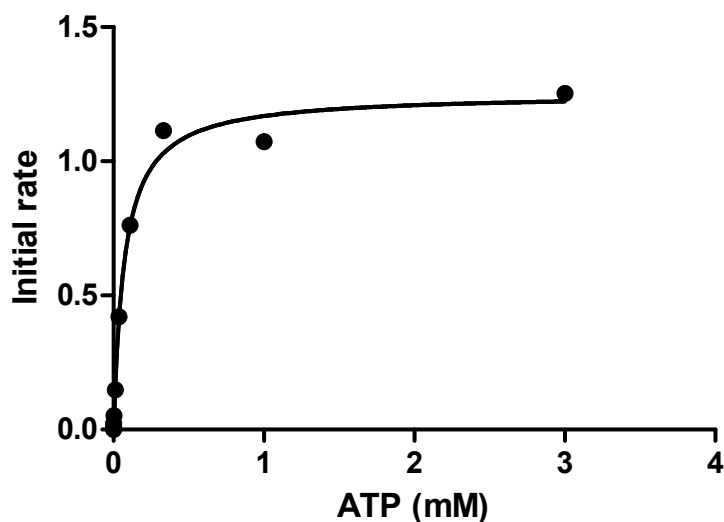
As the members of the library of fragments synthesised in section 3.2.4 are expected to be ATP competitive, the IC_{50} will depend on the intrinsic affinity of the inhibitor (K_D , the dissociation constant) as well as competition from ATP under specific assay conditions (the ATP concentration and the ATP K_M). The dependence of IC_{50} on ATP K_M is highlighted by the Cheng-Prusoff equation (Equation 3).

$$IC_{50} = K_i \left(1 + \frac{[ATP]}{K_M} \right)$$

Equation 3: Cheng-Prusoff equation.

If ATP K_M is too low, the enzyme activity is decreased and may display an overestimation of compound potency. Alternatively, if ATP K_M is too high, weakly binding fragments may be overlooked.

Utilising a final enzyme and substrate concentration of 25 nM and 1.5 μ M respectively, a twelve point 3-fold serial dilution of ATP from 3 mM in buffer was performed, with the data shown in Graph 2. The K_M of ATP for pseudo-WT Aurora-A was experimentally determined as 71.5 μ M, which is comparable to the literature value of 84 μ M.²²⁹

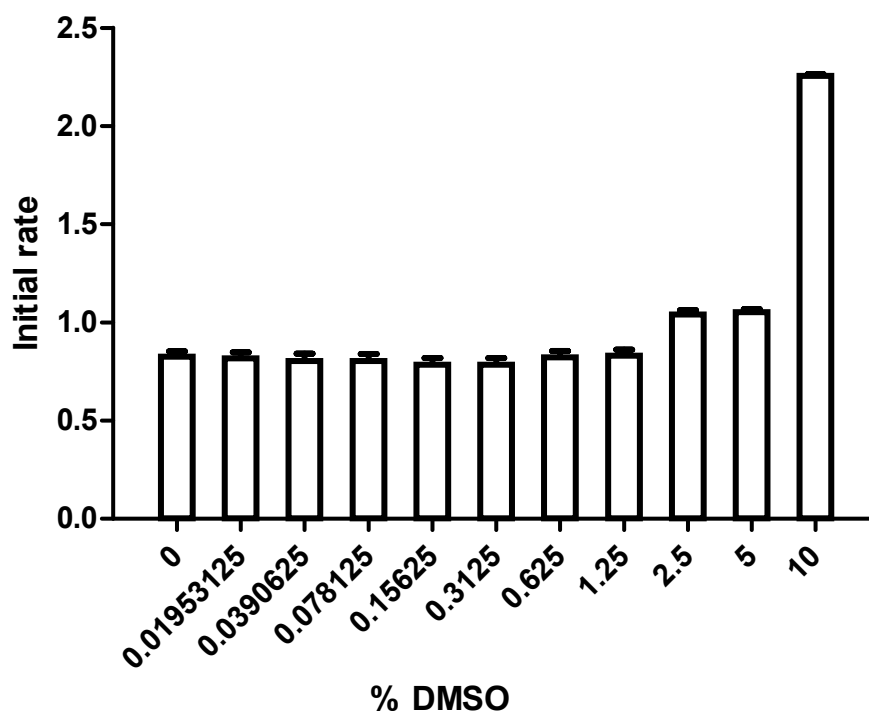


Graph 2: ATP K_M determination of pseudo-WT Aurora-A complex, where K_M is $71.5 \mu\text{M}$ and V_{max} is 1.25 mM min^{-1} . Units of initial rate are % conversion/min.

3.2.9.3 DMSO tolerance Assay

DMSO is utilised in determination of IC_{50} as a solvent for the fragment stock solutions, therefore a DMSO tolerance screen was performed to prevent interference from DMSO during the assay. An eleven point, 2-fold serial dilution of DMSO was performed from 10% DMSO constitution, including a 0% DMSO as the negative control, with the data produced plotted in Graph 3.

Concentrations above 1.25% were found to increase enzyme activity, with 10% final DMSO concentration resulting in a 2.5-fold increase in activity. This result is in accordance with work carried out within the Nelson group.²²⁸



Graph 3: DMSO tolerance assay using pseudo-WT Aurora-A. Units of initial rate are % conversion/min.

Previous work within the Nelson group by Chris Arter reported that controls run at 20 nM enzyme concentration and 2.5% DMSO display a linear conversion R^2 of 0.9978 until approximately 45 minutes and roughly 45% conversion. The conversion proceeded at a constant rate until above 40% and so deviation away from the initial rate or plateaus later in the experiment can be excluded, enabling determination of the initial rate. The observed increase in catalytic activity on addition of DMSO was accounted for by reduction of the final enzyme concentration to 20 nM.

3.2.10 Determination of Fragment bioactivity against pseudo-WT Aurora-A

Employing the enzyme concentration, ATP K_M and DMSO tolerance, the fragment bioactivity was determined. Unless otherwise discussed, the fragments were soluble at 2.5% final DMSO and the kinetic data was taken from 0-25% conversion of the fluorescent peptide substrate, capturing the

initial rate. Each IC_{50} screen was performed with both a positive and negative control consisting of no enzyme and no inhibitor, respectively, which formed the basis of the normalisation of the data. Each concentration was conducted in triplicate, with the data for a single compound obtained on the same day. A curve is then fitted to obtain the activity of each fragment.

The half maximal inhibitory concentration (IC_{50}) is defined as a measure of potency of a substance which inhibits a specific biological or biochemical function. IC_{50} can be transformed into pIC_{50} through Equation 3. The application of pIC_{50} indicates exponentially more potent inhibitors.

$$pIC_{50} = -\log_{10}(IC_{50})$$

Equation 4: Conversion of IC_{50} into pIC_{50}

Screening of the fragment library synthesised from Section 3.2.4, began with the determination of bioactivity of a single compound from each of the three series of fragments to determine the maximum concentrations to guide screening of the full fragment series. Fragments **158**, **178** and **193** were screened initially.

It was found that fragment **158** of the purine series gave an IC_{50} of $0.37 \mu\text{M}$ when screened using a 10 point 5-fold serial dilution starting at 190 mM against the Aurora-A pseudo-WT. Fragment **178** of the isoquinoline-5-sulfonyl series gave an IC_{50} of $4.8 \mu\text{M}$ when screened with 10 point 5-fold serial dilution with a top concentration of 3 mM . Finally fragment **193** of the pyrimidine series gave an IC_{50} of $45 \mu\text{M}$ when screened with a 10-point 5-fold serial dilution, with a top concentration of 24 mM . Following obtainment of these results, the full library was screened, with these concentrations utilised to guide the screening process.

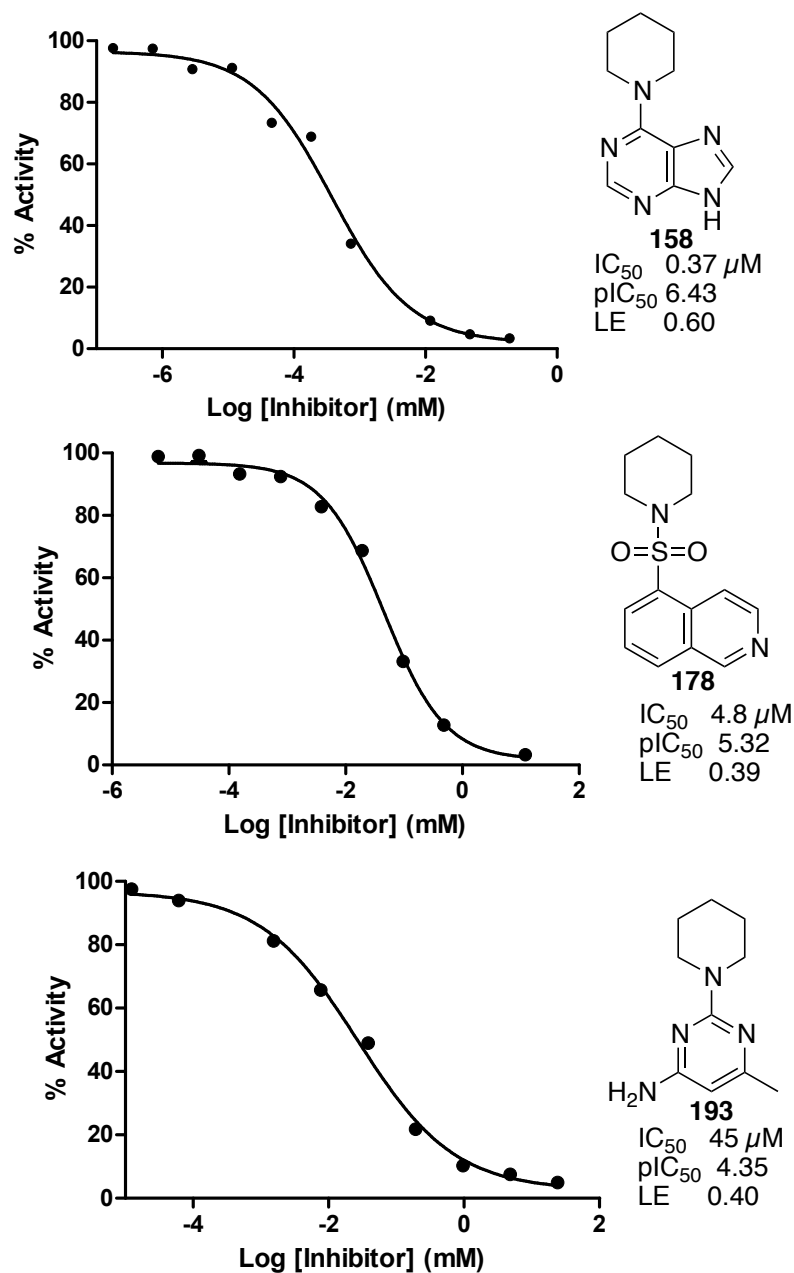


Figure 27: Determination of bioactivity of a compound from each fragment series, to determine the concentrations to guide screening of the full fragment series.

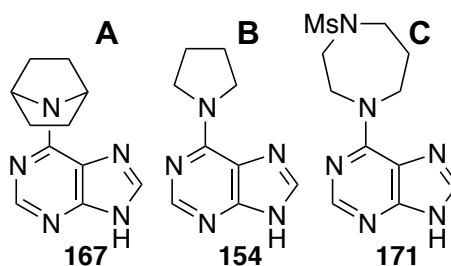
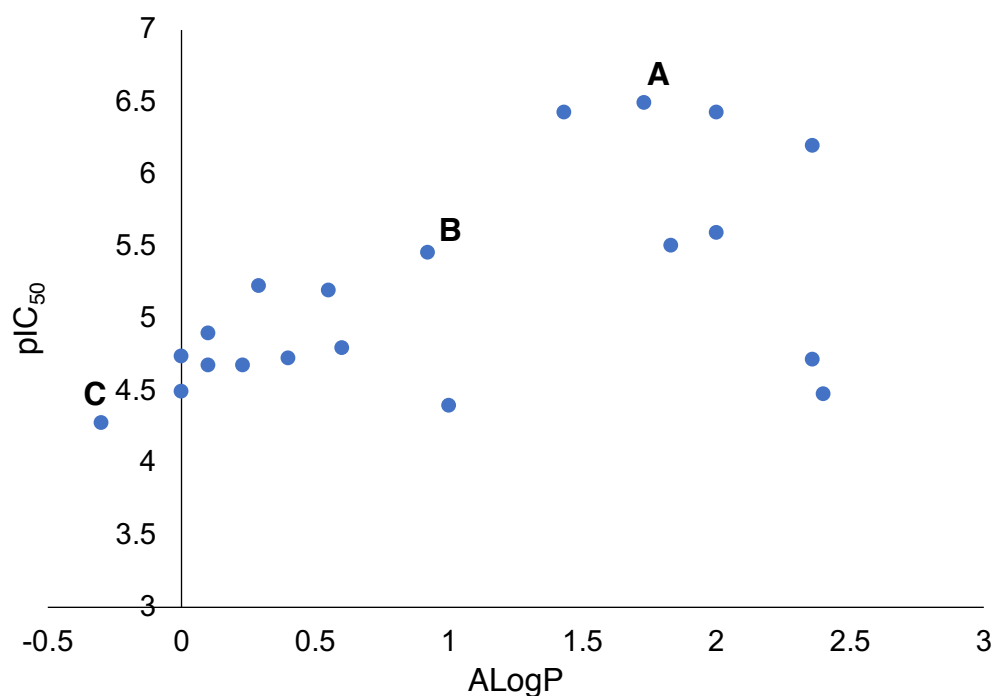
On substitution of the warhead from the purine series (**158**) to the isoquinoline-5-sulfonyl series (**178**) there is a 1.2-fold decrease in pIC_{50} (Figure 27). whereas comparing isoquinoline-5-sulfonyl **178**, to pyrimidine **193**, there is a 1.2-fold decrease in pIC_{50} . Finally, comparison of the purine series (**158**) and the pyrimidine series (**193**) saw a 1.5-fold reduction in pIC_{50} (Figure 27). The

decrease in potency with the pyrimidine (**193**) was unsurprising as it is not a previously reported motif in an Aurora-A kinase inhibitor.^{181,230}

3.2.10.1 Determination of Bioactivity for the Purine Fragment Series

Following the result with fragment **158**, the bioactivity of the remainder of the purine fragment series was determined, enabling appreciation of the effect on potency on variation of the cyclic amine. All twenty fragments of the purine series were found to target Aurora-A, with the complete analysis located in Appendix 1 and 2.

In general, a trend of increasing bioactivity was observed in those compounds with increasing value of AlogP. Those fragments with AlogP values of below 0.60 displayed poorer bioactivity against Aurora-A, while those with AlogP values of above 1.40 proved to be the most potent fragments. Additionally, it should be noted that those fragments of lower AlogP (<1.38) all contained multiple heteroatoms as part of the variable cyclic amine, signifying those multiple heteroatoms may not be tolerated by Aurora-A. Conversely, fragments with a higher value of AlogP and therefore high lipophilicity, have an increased likelihood of *in vitro* receptor promiscuity and *in vivo* toxicity.⁸⁸ Fragments with high lipophilicity frequently lead to drug candidates with rapid metabolic turnover, low solubility, and poor absorption.^{231,232} Accordingly, it is important to consult other measurements such as ligand efficiency (LE) and lipophilic ligand efficiency (LLE), which is discussed in section 3.2.11.1 and 3.2.11.2.



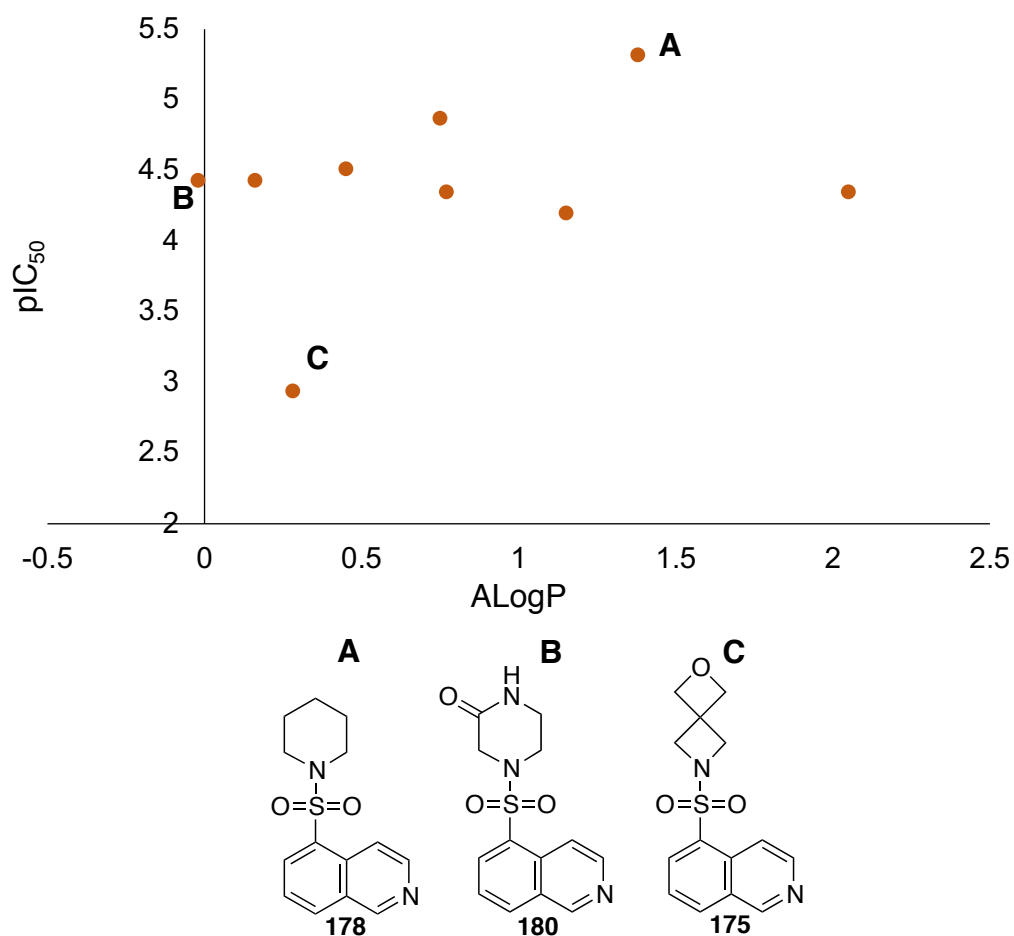
Graph 4: Variation in pIC₅₀ with AlogP within the purine fragment series

Ongoing from 4- or 5-membered ring cyclic amines (**152** and **154**) to a 6-membered ring there is a 1.2-fold improvement in bioactivity. The 6-membered ring (**158**) and 7-membered (**168**) ring analogues have similar levels of bioactivity. Addition of a methyl group in the 2-position of the piperidine ring of **162** gave a 1.2-fold reduction in pIC₅₀, whereas addition of a dimethylamino (**165**) or an ethyl ester substituent (**163**) in the 4-position or 3-position of the piperidine ring furnished a 1.5-fold decrease in pIC₅₀.

3.2.10.2 Determination of Bioactivity for the Isoquinoline-5-sulfonyl Fragment Series

Following the result with **178**, the bioactivity of the remainder of the isoquinoline-5-sulfonyl fragment series was determined. All nine fragments of the isoquinoline-5-sulfonyl series were found to target Aurora-A with varying inhibitory potency. The complete analysis located in Appendix 1 and 2.

In a similar way to the purine fragment series, an increase in ring size from a 4-membered ring to a 6-membered ring led to a 1.1-fold increase in pIC_{50} . Considering the purine fragment series, we observed a general trend between increasing pIC_{50} with increasing $AlogP$; however for the isoquinoline-5-sulfonyl series additional fragments examples would be required to confirm this trend.



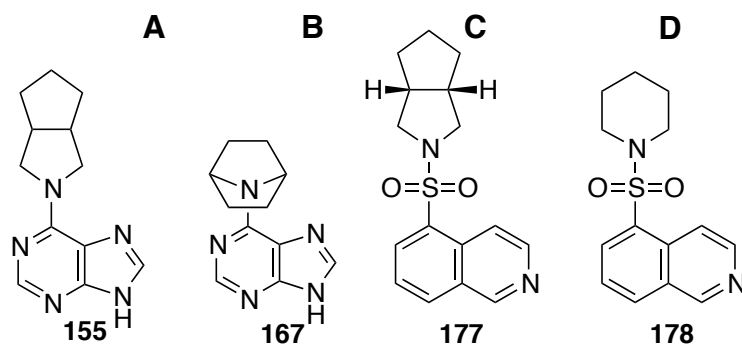
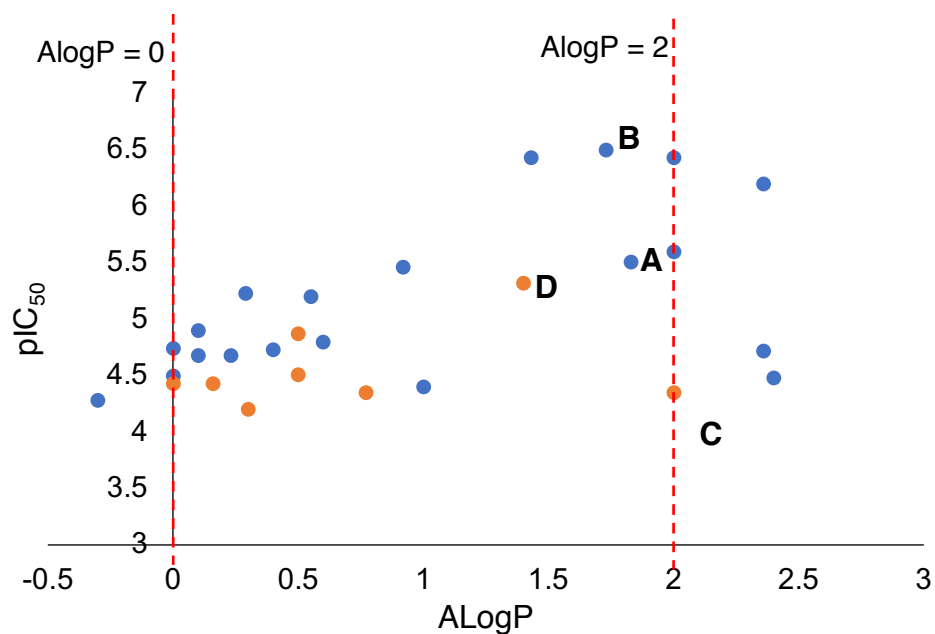
Graph 5: Variation in pIC_{50} with $AlogP$ within the isoquinoline-5-sulfonyl series.

3.2.10.3 Determination of Bioactivity for the Pyrimidine Fragment Series

Although fragment **193** of the pyrimidine series was active against Aurora-A (IC₅₀ of 45 mM), the remainder of the series were found to be inactive against Aurora-A at concentrations below 24 mM and so this series was deprioritised and was not pursued further. The results are shown in Appendix 1 and Appendix 2.

3.2.11 Analysis

A library of 35 fragments prepared in-house were screened for bioactivity against Aurora-A. The results reveal two fragment series which displayed promise in the development of an inhibitor targeting Aurora A. We were able to further prioritise fragments which would be explored for further development and elaboration by considering the physiochemical property criteria previously described. Those fragments with an ALogP > 2 have high lipophilicities, potentially leading to *in vitro* receptor promiscuity and *in vivo* toxicity (Graph 6).



Graph 6: A plot of pIC_{50} vs $ALogP$ for the purine series (blue) isoquinoline-5-sulfonyl series (orange) annotated with the desirable range of $ALogP$ for fragments.

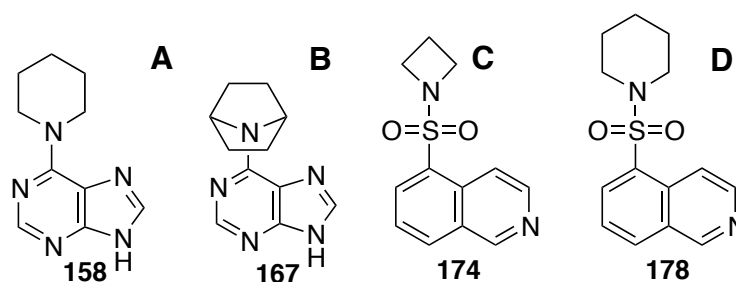
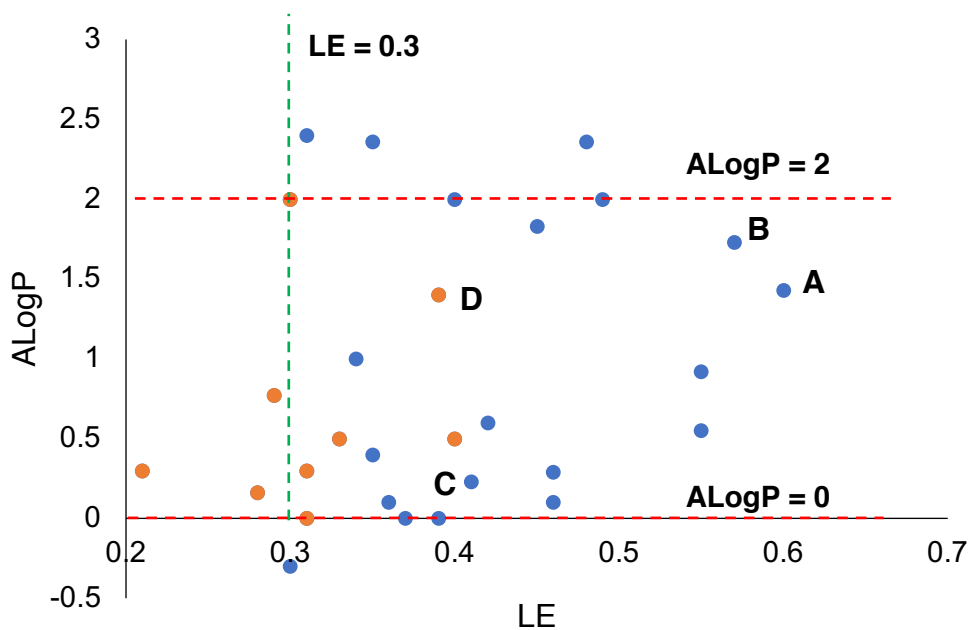
3.2.11.1 Ligand Efficiency

An additional consideration in choosing fragments for elaboration is ligand efficiency (LE). Ligand efficiency assesses binding affinity in relation to the number of heavy atoms present in a molecule (Equation 5). Monitoring of ligand efficiency throughout fragment elaboration enables assessment of whether the additional molecular mass added in the growth process has been added efficiently. A value of approximately 0.3 at this stage, should lead to a rule-of-five compliant 10 nM inhibitor on elaboration.^{88,233} At each stage of fragment growth, LE can be utilised to evaluate success.

$$LE = 1.4 \times \frac{(-\log_{10} IC_{50})}{HA}$$

Equation 5: Ligand Efficiency

In general, it is best to start with a fragment that shows a high LE since in most cases LE decreases during optimisation.⁸³ In our investigation, LE will be used as guideline in the fragment elaboration process. Graph 7 displays the variation in LE with AlogP, annotated with the desirable range for AlogP and the desirable LE a fragment would have at this stage.



Graph 7: Variation in LE with AlogP, annotated with the desirable range for AlogP and LE.

At this stage, there are twenty-one fragments which comply with both guidelines. Fragments which fall outside of the limits represented in Graph 7, were not considered for future optimisation and elaboration.

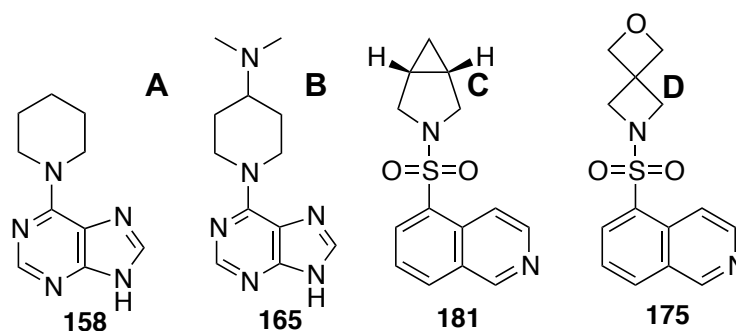
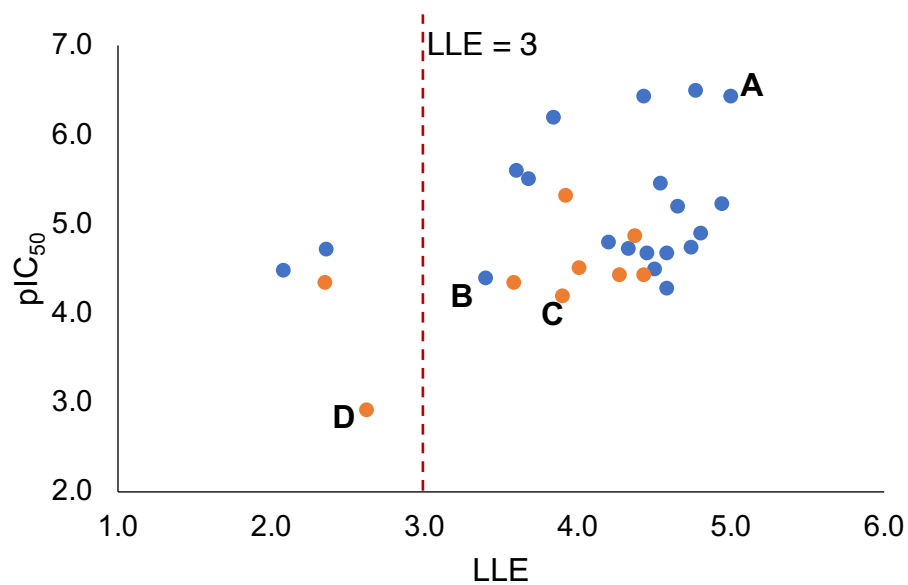
3.2.11.2 Lipophilic Ligand Efficiency

Lipophilic ligand efficiency (LLE) was first proposed by Leeson and Springthorpe and is an index that combines *in vitro* potency (pIC_{50}) and lipophilicity (AlogP) (Equation 6).³¹ A molecule with an LLE equal to zero based on LogP, where target affinity is equal to LogP, can be thought of as a fragment having the same affinity for its target as it does for 1-octanol, whereas a drug candidate with an LLE of 6 has a one-million-fold higher affinity for its target compared to 1-octanol. LLE attempts to maximize the minimally acceptable lipophilicity per unit of *in vitro* potency or more simply, to improve potency, while maintaining low lipophilicity.

$$LLE = pIC_{50} - ALogP$$

Equation 6: Lipophilic ligand efficiency

A negative value of LLE is unfavourable, indicating a fragment with a large value of AlogP. Considering the properties of an average oral drug, with a calculated AlogP (AlogP) of approximately 2.5–3.0 and potency in the range of approximately 1–10 nM, an ideal LLE value for an optimized drug candidate is approximately 5–7 units or greater.¹⁸ Fragments or lead-like molecules that are used as chemical starting points generally cannot possess drug-like LLE values as they do not possess high enough potency. Hit compounds with LLE ≤ 2 are commonly found from HTS¹⁸ and these will have to be improved by ~ 3 or more LLE units during optimisation to a candidate.³¹ Since LLE does not take into account the size of the ligand, it is potentially better suited to being used in the optimisation process of fragments selected for elaboration. Graph 8 displays that twenty-five fragments have an LLE value of 3 or above, with none of the fragments possessing a negative value.



Graph 8: Variation in pIC_{50} with LLE within the purine series (blue) and isoquinoline-5-sulfonyl series (orange), annotated with the desirable LLE for fragments.

3.2.12 Summary

A library of 35 fragments prepared in-house were screened for bioactivity against Aurora-A. The biochemical screen identified two series of fragments to be taken forward in for further analysis and potential for fragment growth. Elaboration of fragments within this library will be the subject of Section 3.2.14.

3.2.13 Molecular Docking Studies

Attempts to gain structural data *via* X-ray crystallography using our fragment library were unsuccessful. As a result, molecular docking studies were completed using Schrödinger's Glide²¹⁷ for 23 fragments employing a co-crystalised structure of Aurora-B with Reversine (PDB: 2VGO, Figure 28).²³⁴ Since the ATP binding region is highly conserved between all three members of the Aurora kinase family, use of the Aurora-B active site with Reversine active site was expected to provide insight into the binding modes of our fragments.¹⁸²

Reversine (**197**) is a substituted purine analogue, shown to bind Aurora-B at the active site, with an IC₅₀ of 150 nmol L⁻¹.²³⁴ The crystal structure of Reversine in complex with Aurora-B kinase was used to rationalise fragment potency and to indicate potential points of elaboration of the fragment library.

Reversine occupies the ATP-binding pocket at the interface between small and large lobes of Aurora-B. The purine of Reversine **197** can form hydrogen bonds with backbone residues (Glu171 and Ala173) in the hinge region of the kinase and the cyclohexyl amine motif is thought to extend into the phosphate binding region.^{234,235} The cyclohexyl moiety is modelled to adopt a twist-boat conformation. It is noted that for the co-crystalised structure of Reversine with Aurora-B that both the cyclohexyl and the morpholinoaniline motif of Reversine are not well resolved, suggesting these motifs may be partially disordered and make only weak interactions with the Aurora-B pocket. In particular, the cyclohexyl group of Reversine is solvent exposed, which can be taken into consideration when designing elaborated analogues.²³⁵

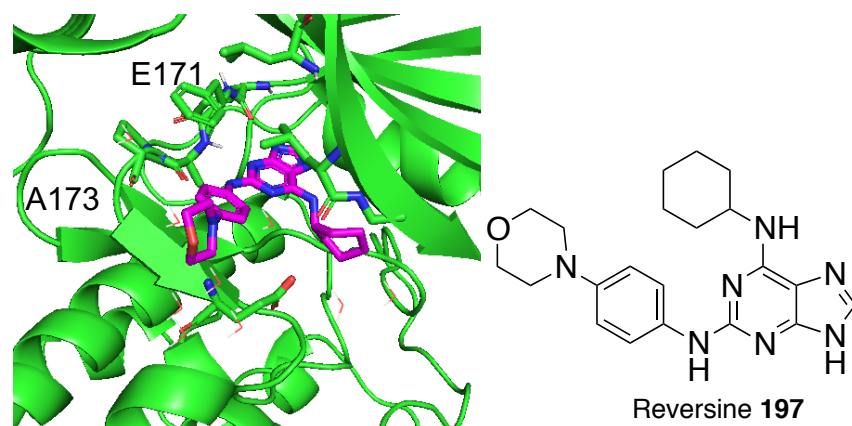


Figure 28: The structure and crystal structure of Reversine (purple) in a complex with Aurora-B (green ribbons). Key amino acids are depicted as green sticks and labelled, with A173 and E171 forming the hinge. PDB: 2VGO.²³⁴

3.2.13.1 Comparison of Molecular Docking to Biological Results

Using the co-crystallised structure of Reversine with Aurora-B as a guide, we docked fragments from Section 3.2.10 into the ATP binding pocket to identify potential points of elaboration of our fragment series. The aim of the elaboration stage was to improve the fragments potency against Aurora-A. The fragments from the purine and isoquinoline-5-sulfonyl fragment series were docked into the ATP-binding site, compounds **164** (Panel A), **167** (Panel B), **179** (Panel C) and **174** (Panel D) are displayed below (Figure 29).

Visual inspection of the top ranked docking poses of the fragments predict a consistent fragment pose, in good agreement with the proposed binding mode of Reversine, **197**.

For the purine series of fragments, the 2-aminoadenosine core is likely to recreate the hydrogen bond network with the hinge region of the kinase. The two hydrogen bond interactions between the purine and the hinge loop residues (Glu171 and Ala173) are conserved. The variable cyclic amine from the C-6 position is expected to extend into the ribose binding region of the active site.

In the isoquinoline-5-sulfonyl fragment-Aurora-B complex, the isoquinoline is predicted to occupy the same space as the adenine of ATP. The sulfonamide is predicted to stretch into the ribose-binding region and into a solvent exposed environment. The isoquinoline nitrogen accepts a hydrogen bond from Ala173, whereas the C-1 is thought to donate a hydrogen bond to the amide of Glu171.²³⁶

On examination of docking scores, we found that docking scores did not correlate with those compounds exhibiting the highest potency in the series (Figure 29). Although Glide is useful for prediction fragment poses, the scoring functions are not refined enough to enable prediction of the more active compounds within this series.

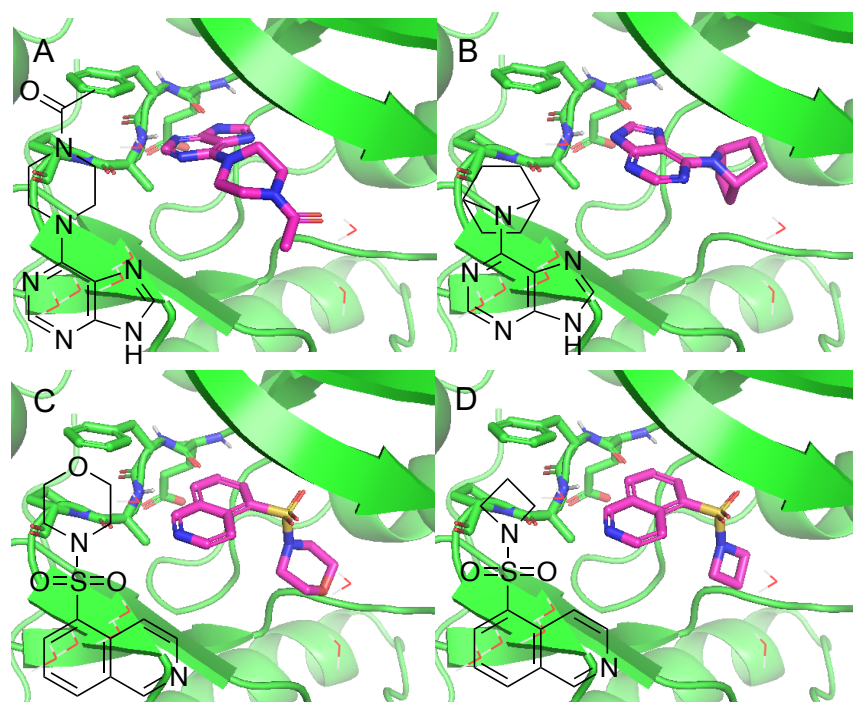


Figure 29: Molecular Docking using Glide of fragments **164**, **167**, **179** and **174** with the Aurora-B active site, using a co-crystallised crystal structure with ATP-competitive inhibitor, reversine. PDB: 2VGO.²³⁴ Panel A: Compound **164** docked into the active site, docking score: -8.23. Panel B: Purine compound **167** docked into the active site, docking score: -4.30. Panel C: Isoquinoline-5-sulfonyl fragment **179** docked into the active site, docking score -6.67. Panel D: Compound **174** docked into the active site, docking score, -5.16.

The results from this section can be used to provide insight into potential points of elaboration of the fragment library through understanding of the fragment poses.

3.2.14 Fragment Library Elaboration

From the results of section 3.2.8 we identified four suitable scaffolds for elaboration in the development of an Aurora-A inhibitor (Figure 30). The goal of the fragment elaboration stage is to increase the binding affinity by several orders of magnitude with the overall aim of developing a potent chemical tool or lead compound.

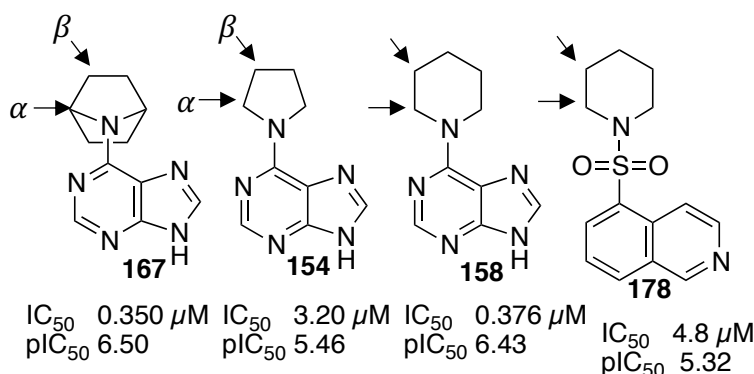


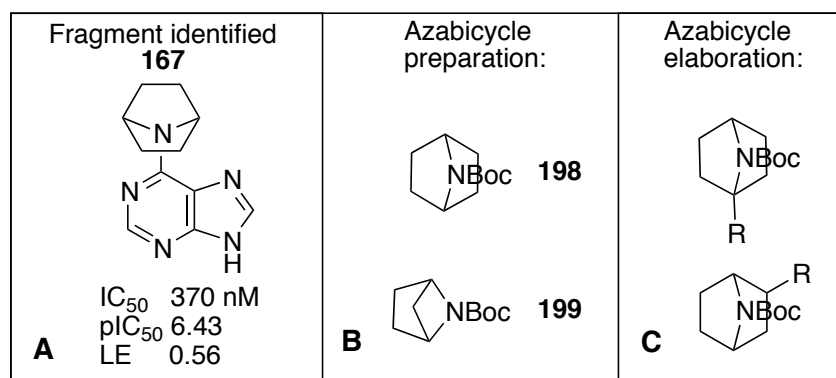
Figure 30: Fragments selected for elaboration, with vectors highlighted.

An important consideration in the elaboration of fragments is the availability of synthetically accessible growth vectors in 3-dimensions. Published methodology from the Marsden and Nelson research groups at the University of Leeds has explored the growth of cyclic amine fragments.^{105,237} Our elaboration strategy will explore the growth and decoration of the cyclic amine to explore the influence on the compounds bioactive profile.

Fragment **167** was our most potent compound and so, part 1 of our elaboration strategy explores α - and β - vectors on azabicyclic of **167** (Figure 30). By contrast, part 2 explores elaboration of simple cyclic amines of **154**, **158** and **178** using fragment growth strategies covered in Chapter 2. Discussion of the synthetic chemistry undertaken will be followed by analysis of the resulting fragment library and biochemical screening.

3.2.15 Fragment Elaboration Part 1: Towards Functionalised Azabicycles

It was found in section 3.2.10 that inclusion of azabicyclo **198** gave the most potent fragment (**167**) against Aurora-A. This section focuses on exploring methods for the preparation and elaboration of **198** as well as analogue **199**, towards generating a series of elaborated fragments which can be tested against Aurora-A. Our workflow for the studies conducted in this section is:



Workflow:

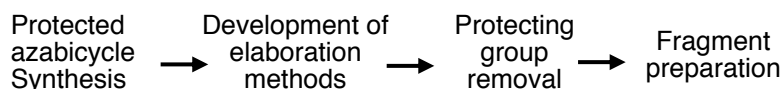
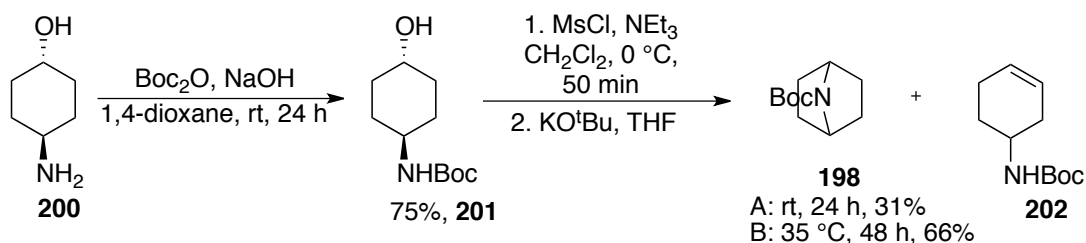


Figure 31: Panel A: Fragment **167** identified through biochemical screening yielded the highest IC₅₀ of the screen. Panel B: Azabicycles to be prepared following in this section. Panel C: Potential elaboration vectors to pursue on azabicyclo **198**. Panel D: Desired workflow for elaborated azabicyclo fragment synthesis.

3.2.16 Synthesis of Protected Azabicycles

3.2.16.1 Synthesis of *tert*-butyl 7-azabicyclo[2.2.1]heptane-7-carboxylate



Scheme 30: Synthesis of azabicyclo **198** from commercially available *trans*-4-aminocyclohexanol.²³⁸

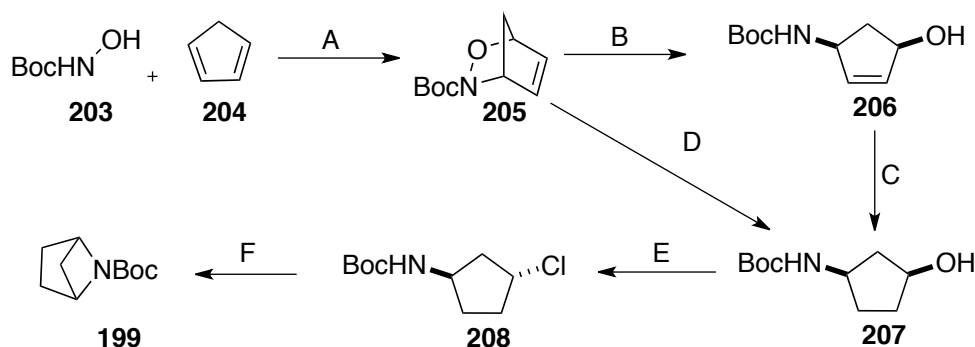
We prepared azabicyclo **198** from *trans*-4-aminocyclohexanol using a three-step protection, mesylation and base-mediated intramolecular cyclisation

strategy, as shown in Scheme 30.²³⁸ Commercially available *trans*-4-amino cyclohexanol is treated with di-*tert*-butyl dicarbonate in the presence of sodium hydroxide in 1,4-dioxane. This afforded the desired carbamate in 75% yield, comparable to literature.²³⁸ The carbamate was then subjected to mesyl chloride in the presence of triethylamine in dichloromethane to give a mesylated intermediate. Mesylated intermediate of **201** was used directly in the cyclisation step without further purification, and the crude azabicyclo **198** was purified by flash column chromatography. The presence of the elimination by-product **202** is noteworthy, but we found **198** could be used despite its presence. We were able to improve the reaction yield from 31% to 66% by increasing the temperature of the reaction to 35 °C and increasing the reaction length to 48 hours. This yield is an improvement on the literature synthesis and did not give an increase in the yield of the alkene **202**.

With azabicyclo **198** in hand, our attention turned to synthesising bicycle **199** which could be used in the synthesis of fragments and profiled against Aurora-A.

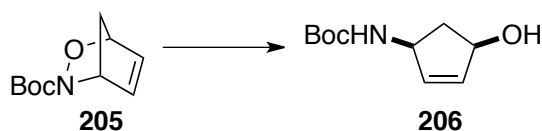
3.2.16.2 Synthesis of *tert*-butyl 5-azabicyclo[2.1.1]hexane-5-carboxylate

For the synthesis of previously unknown azabicyclo **199**, our planned route was as follows:



Scheme 31: Planned synthesis towards azabicyclo **199**. Steps A: nitroso Diels-Alder Step B: N-O reduction, Step C: Hydrogenation of alkene, Step D: potential tandem N-O and alkene reduction, Step E: Chlorination and Step F: Displacement to azabicyclo **199**.

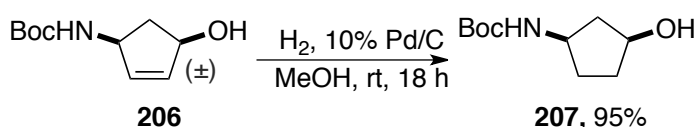
The *N*-protected hydroxylamine **203** was oxidised with sodium periodate to the transient acylnitroso species, which in the presence of cyclopentadiene gave the corresponding hetero Diels-Alder cycloadduct **205**. Conditions for the subsequent N-O bond reduction were trialled (Table 28) with molybdenum hexacarbonyl found to give moderate yields, in accordance with literature.²³⁹ Entry 4 of Table 28 explores whether the N-O and alkene reduction steps to access alcohol **207** could be achieved in a single transformation, but this was unsuccessful after 5 days, giving an inseparable mixture of **205**, **206** and **207** in the ratio (3:2:1) by crude ¹H NMR.



Entry	Conditions	Outcome
1	Zn, acetic acid, 48 h, reflux	No product
2	Mo(CO) ₆ , 15:1 CH ₃ CN:H ₂ O, 3 h, reflux	46%
3	Zn, Cp ₂ TiCl ₂	43%
4	H ₂ , 10% Pd/C, 5 days, rt	3:2:1 ^a

Table 28: Conditions for the reduction of the N-O bond of 205. ^a an inseparable mixture of starting material:alkene:alkane.

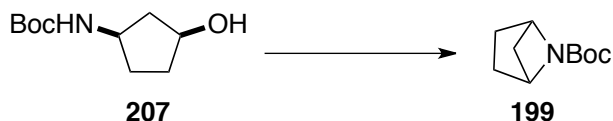
With intermediate **206** in hand, attention turned to the alkene reduction, which was completed by hydrogenation, giving alcohol **207** in high yield (Scheme 32).



Scheme 32: Hydrogenation of alcohol **206** to give **207**.

Following attainment of **207**, the synthesis of azabicyclic **199** was attempted with conditions detailed in Table 29. These conditions are analogous to literature, with the chlorination or Appel reaction inverting the stereochemistry of **207**, followed by internal substitution. In all cases, these reactions were unsuccessful. We noted the decomposition of the starting material, with the ^tBu signal absent from the crude ¹H NMR in all cases, and so it was suspected that the Boc group was cleaved by HCl generated *in situ* (Table 29, entry 1-

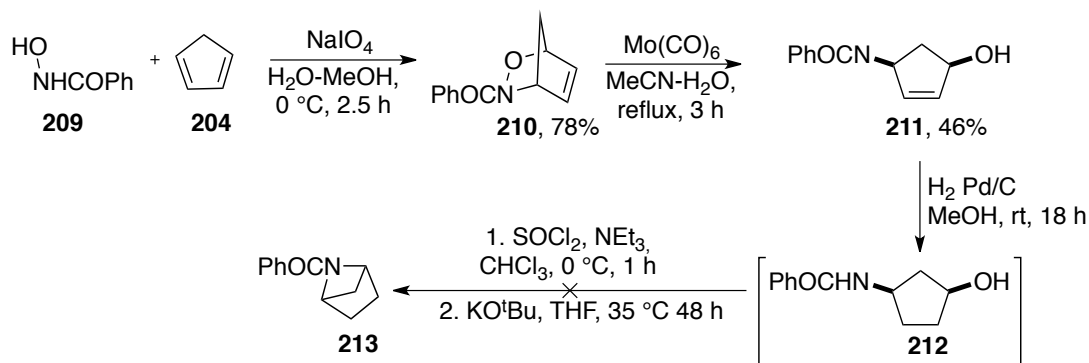
3). Therefore, we opted for an alternative synthesis to access azabicyclic **199** (Scheme 33), which was a literature reported route towards **213**.



Entry	Conditions	Outcome
1	SOCl ₂ (1.5 eq.), NEt ₃ (3 eq.), CHCl ₃ , rt	No product
2	SOCl ₂ (1.5 eq.), NEt ₃ (5 eq.), CHCl ₃ , 0 °C	No product
3	SOCl ₂ (1.5 eq.), NEt ₃ (10 eq.), CHCl ₃ , 0 °C	No product
4	NCS (2.6 eq.), PPh ₃ (2.5 eq.), CHCl ₃ , 0 °C	No product
5	NBS (1 eq.), PPh ₃ (1 eq.), CHCl ₃ , 0 °C	No product
6	CBr ₄ (1.5 eq.), PPh ₃ (2 eq.), CHCl ₃ , 0 °C	No product

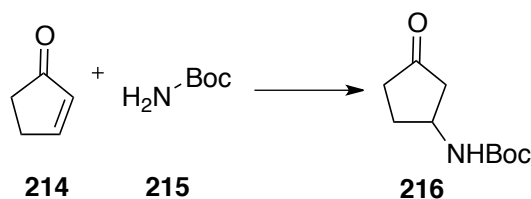
Table 29: Conditions for the synthesis of azabicyclic **199**

Following modification of the protecting group from the acid labile Boc to benzoyl, cycloadduct **210** was obtained from *in situ* oxidation of benzohydroxamic acid **209** with sodium periodate and then addition to cyclopentadiene. The N-O bond was reductively cleaved with molybdenum hexacarbonyl to give the corresponding *cis*-1,4-hydroxyamide in 21% yield, comparable to literature. In a telescoped process, the alkene of **211** was reduced, which was confirmed by TLC, and treated with thionyl chloride in the presence of triethylamine to access the *trans*-chloroamide *in situ*. Transfer by cannula of the *trans*-chloroamide into potassium *tert*-butoxide in tetrahydrofuran was expected to yield azabicyclic **213**. Analysis of the crude ¹H NMR displayed decomposition of the starting material **212**, with the aromatic peaks of the benzoyl group no longer visible in the ¹H NMR. As a result, this route was deprioritised to synthesise **213**.



Scheme 33: Alternative synthesis to access azabicyclo **213**.

The next method involved an *aza*-Michael addition between cyclopentenone **214** and *tert*-butyl carbamate **215** in the presence of a Lewis acid to give carbamate **216** (Scheme 34). The route to **199** was redesigned to access the amino alcohol **212B**, then to activate towards substitution. The synthesis was trialled using conditions reported in the literature (Table 30).^{240–242} The results display that use of a sub-stoichiometric amount of bismuth nitrate were the only conditions to yield the desired product.

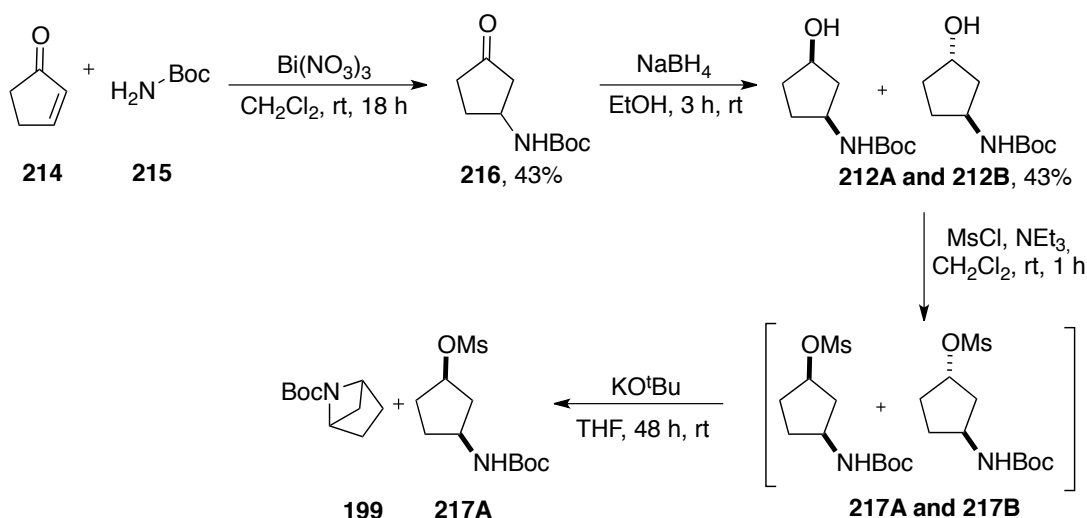


Entry	Conditions	Outcome
1	Bi(NO ₃) ₃ (1 eq.), CH ₂ Cl ₂ , rt, 24 h	No product
2	TBAB, BF ₃ ·Et ₂ O, rt 4 h	No product
3	PPh ₃ , TMSCl, CH ₂ Cl ₂ , rt, 24 h	No product
4	Bi(NO ₃) ₃ (0.1 eq.), CH ₂ Cl ₂ , rt, 48 h	43%

Table 30: Conditions trialled for the *aza*-michael reaction of **214** and **215**.

Treatment of ketone **216** with sodium borohydride gave an inseparable mixture of alcohols **212A** and **212B** (1:1). It was anticipated that only the *trans*-compound would undergo the subsequent displacement reaction to form azabicyclo **199** and therefore it could be separated by flash column chromatography from mesylated alcohol **217A**. As with the synthesis of azabicyclo **198**, the alcohols were mesylated without purification and treated with potassium *tert*-butoxide in tetrahydrofuran and warmed to 35 °C over 48 hours. The mesylation products were successfully confirmed by LC-MS. It was

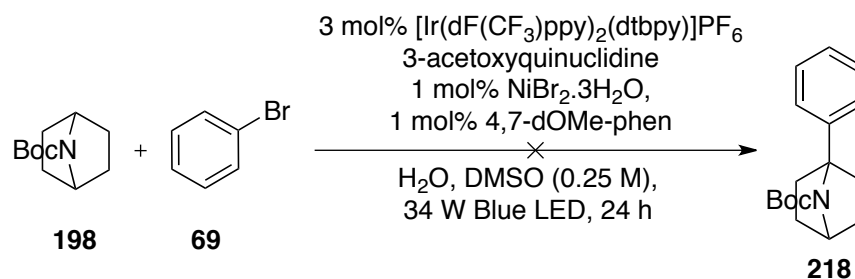
found that these conditions for the subsequent reaction step did not yield the desired product and give a complex mixture of unidentifiable products, with the diagnostic bridgehead protons absent by crude ^1H NMR. As a result, the synthesis of azabicyclo **199** was deprioritised.



Scheme 34: Synthesis towards azabicyclo **199** using the aza-Michael reaction, followed by reduction of ketone **212A/B**. Alcohols **212B** and **212A** were inseparable and were mesylated and underwent the conditions for displacement, without yielding product.

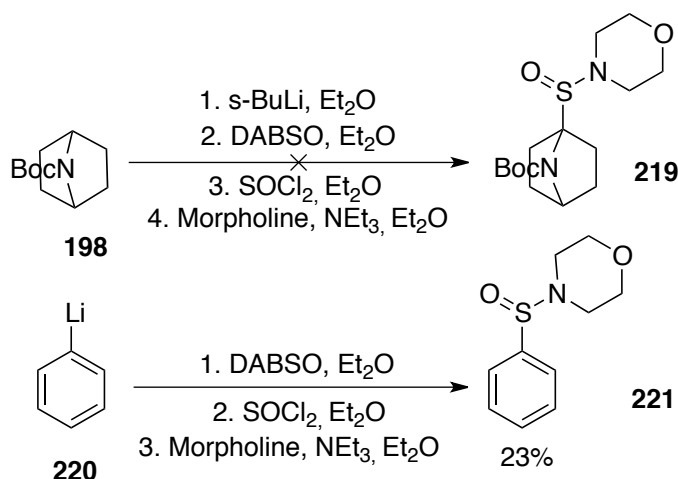
3.2.17 Elaboration of *tert*-butyl 7-azabicyclo[2.2.1]heptane-7-carboxylate

With a route to azabicyclo **198** in hand, our attention turned to elaborating the amine. In Chapter 2, Section 2.1, we identified procedures for α -arylation of cyclic amines, but we recognised that use of the Seidel method would not be applicable with this substrate, because bridgehead imine formation is not possible.¹¹³ The conditions reported by MacMillan *et al.* for photoredox-mediated HAT transfer/nickel-catalysed cross coupling¹¹⁰ to arylate the bridgehead carbon of **198** were applied. However, application of the conditions reported by MacMillan were unsuccessful with starting material recovered following purification with flash column chromatography. This result was unsurprising since this procedure has not previously been reported with sterically hindered substrates such as **198**.



Scheme 35: Applying MacMillan's photoredox C-H arylation approach to azabicyclic **198**.¹¹⁰

Our next method explored sulfinamide synthesis, with a view to functionalising the bridgehead carbon of azabicyclic **198**. Willis *et al.* reported a synthesis of sulfinamides using organometallic reagents and a nitrogen based nucleophile, using the commercially available sulfur dioxide surrogate, DABSO, as the electrophile.²⁴³ We subjected azabicyclic **198** to conditions for sulfinamide synthesis, beginning with *in situ* deprotonation of **198** by *s*-BuLi, and then treatment with DABSO was anticipated to give the metal sulfinate. This crude mixture was treated with thionyl chloride and morpholine, which was expected to give the substituted sulfinamide **219**. Regrettably, this reaction did not yield product **219** and purification by flash column chromatography recovered the starting material **198**.

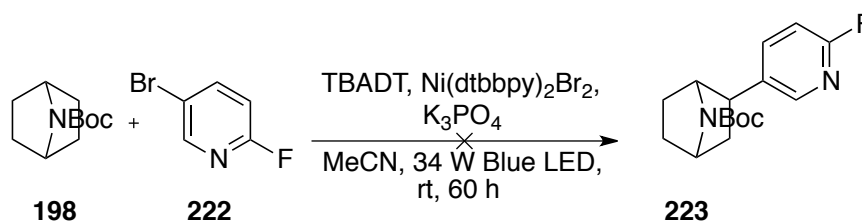


Scheme 36: Attempts to synthesise sulfinamides **219** and **221** using a procedure by Willis *et al.*²⁴³

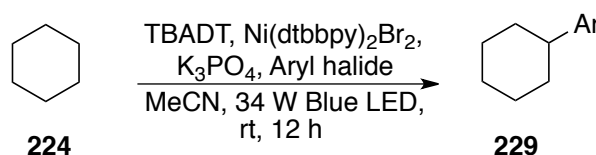
Uncertain as to why the formation of the sulfinamide was unsuccessful, efforts were made to prepare a less sterically demanding analogue which could also be analysed by LC-MS at the point of metal sulfinate generation. Previously unreported substrate, phenyllithium **220** underwent the reported conditions to give **221** in an unoptimised 23% yield, and the metal sulfinate formation was

followed by LC-MS. To determine the point of failure of the reaction of **198**, the metal sulfinate formation of **198** was followed by LC-MS and was not observed. Full repetition of the method to synthesise **219** was still unsuccessful, which we attributed due to the large sterics surrounding the azabicyclic bridgehead carbon of **198**.

Although we had established methods for β -elaboration of cyclic amines arising from enecarbamates^{104,105} previously (Chapter 2), these methods would not be possible with azabicyclic **198**. In order to access β -functionalised analogues, we employed a method for photoredox mediated C-H abstraction/Ni-Catalysed arylation by MacMillan *et al.*²⁴⁴ When 5-bromo-3-fluoropyridine and azabicyclic **198** were reacted under the reported conditions, however, we were unable to effect arylation of **198** with halide **222**.



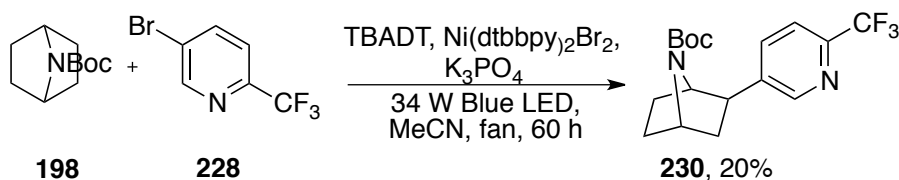
Scheme 37: Initial attempts towards arylation of azabicyclic **198**, with MacMillan and co-workers method.²⁴⁴



Entry	Substrate	Aryl Halide	Product	Outcome
1	225		-	No product
2	226		-	No product
3	227		-	No product
4	228		229	40%

Table 31: Screening of aryl halides with cyclohexane in attempts to β -functionalise azabicyclic **198**.

Unsure as to why this reaction was unsuccessful, we completed a screen of suitable aryl halides with cyclohexane as the partner. Halides **225-227** were not previously reported as substrates in the literature. We were able to attain a functionalised cyclohexane in moderate yield compared to literature using previously reported halide **228**. We then utilised halide partner **228** in a reaction with azabicyclic **198** using the reported conditions. This gave arylated carbamate **230** in reduced yield, compared to the literature.²⁴⁴ Although we were able to repeat an exact example from MacMillan, the reaction seems to be sensitive to variation in the halide partner.²⁴⁴ The reaction was *exo*-selective, owing to selective radical capture by the nickel catalyst on the less hindered face of **230**.²⁴⁴



*Scheme 38: Synthesis of protected amine **198**, employing a procedure from MacMillan *et al.*²⁴⁴*

Given the lack of success in the direct C-H elaboration of **198**, our attention turned to generating intermediates which would allow us to try additional elaboration strategies. Our initial focus was to access the bridgehead aldehyde and carboxylic acid. Based upon pioneering work of Beak²⁴⁵ on the α -lithiation of *N*-Boc carbamates, Xiong *et al.* have demonstrated lithiation and electrophilic trapping of the bridgehead positions of **198**.²⁴⁶

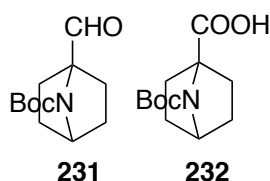
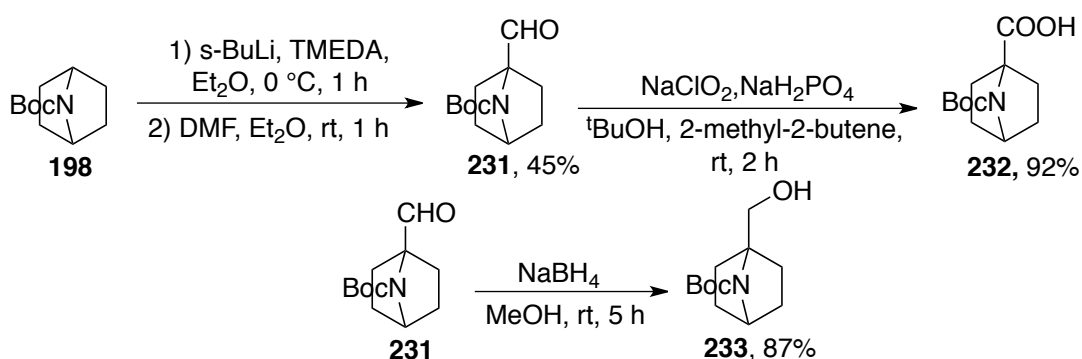


*Figure 32: Aldehyde **231** and carboxylic acid intermediates **232**.*

The synthesis of **231** was initially attempted using a procedure by Xiong *et al.*²⁴⁶ Direct carboxylation of the deprotonated bridgehead carbon using carbon dioxide was unsuccessful in our hands, with only starting material isolated. Instead, we accomplished the synthesis of **231** employing a procedure by Harty *et al.*; a two-step formylation-oxidation sequence.²³⁸ The formyl substituent was introduced through quenching of the lithiated-

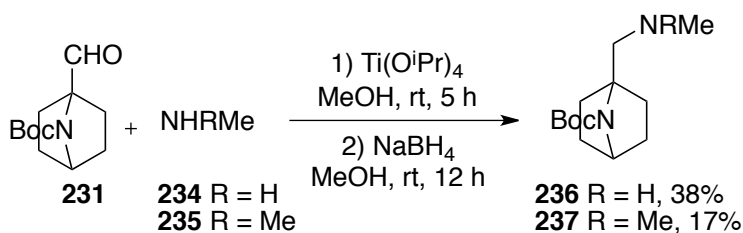
azabicyclic compound with DMF to give the aldehyde **231**, in 45% yield. The formyl substituted product could be purified by flash column chromatography and stored under nitrogen for two-weeks, without oxidation to the carboxylic acid **232**.

Formylated intermediate **231** was converted through Pinnick oxidation to give carboxylic acid **232** in high yield.²³⁸ Aldehyde **231** could also be reduced through portion-wise treatment with sodium borohydride over 5 hours, to give alcohol **233** in 87% yield.



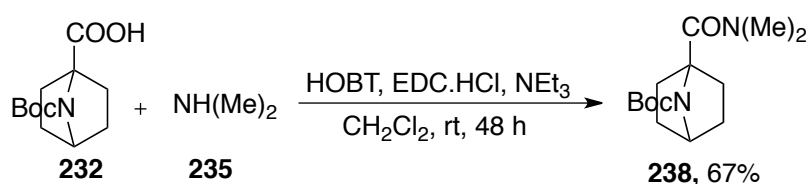
Scheme 39: Synthesis of aldehyde **231**, carboxylic acid **232** and primary alcohol **233**.

Next, we focused on the conversion of aldehyde **231** into amines **236-237** by reductive amination. Reductive amination utilising aldehyde **231** had not been reported in the literature, and we found that treatment of **231** with sodium triacetoxyborohydride and dimethylamine led to a mixture of unidentifiable products and the desired product was not isolated. Reasoning that slow formation of the requisite imine/iminium from hindered aldehyde **231** was the problem, an alternative synthesis was devised: applying conditions reported by Bhattacharyya involving dehydrative imine formation prior to reduction, we were able to access novel amines **236** and **237** in moderate yield.²⁴⁷

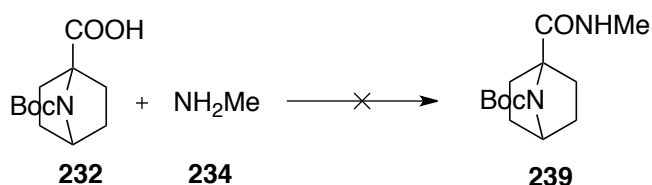


Scheme 40: Reductive amination with aldehyde **231** to access amines **236** and **237**.

As amide bonds play a crucial role in drug development, with 67% of drug candidates possessing at least one amide bond,²⁴⁸ we endeavoured to synthesise amides **238** and **239**. Treatment of carboxylic acid **232** with HOBT and EDC hydrochloride in the presence of triethylamine yielded novel amide **238** (Scheme 41). The synthesis of amide **239** was unsuccessful on multiple attempts, with no product visible in the LC-MS (Table 32), with the reason for failure unclear. This compound synthesis was deprioritised due to time constraints.



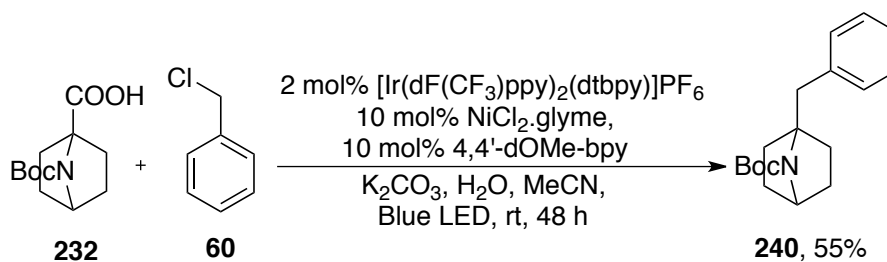
Scheme 41: Synthesis of amide **238**.



Entry	Conditions
1	HOBT, EDC.HCl, NEt ₃ , CH ₂ Cl ₂ , 60 h
2	HATU, NEt ₃ , CH ₂ Cl ₂ , 60 h
3	SOCl ₂ , NEt ₃ , CH ₂ Cl ₂ , 12 h

Table 32: Conditions trialled in the synthesis of amide **239**.

We then investigated introduction of carbon-based substituents at the bridgehead by subjecting carboxylic acid **232** to MacMillan's procedure for decarboxylative substitution using alkyl halides (Chapter 2). Applying this methodology, we were able to access novel amine **240**, bearing a benzyl-substituted bridgehead carbon atom, in moderate yield. Prior to this work, azabicyclic **232** was not a reported substrate of the reaction (Scheme 42).

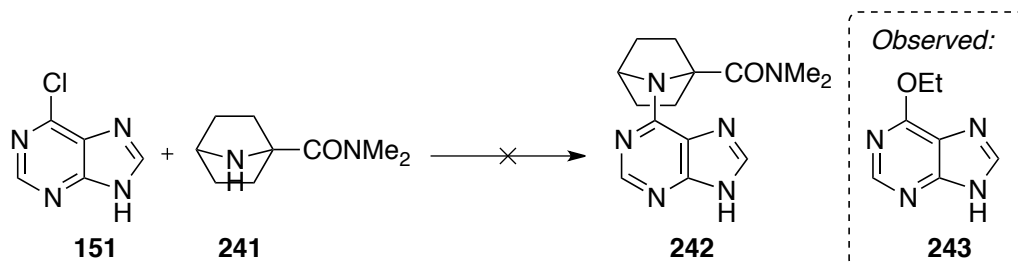


Scheme 42: Synthesis of functionalised azabicyclic 232.

3.2.18 Azabicyclic Fragment Assembly: Protecting Group Removal and Fragment Preparation

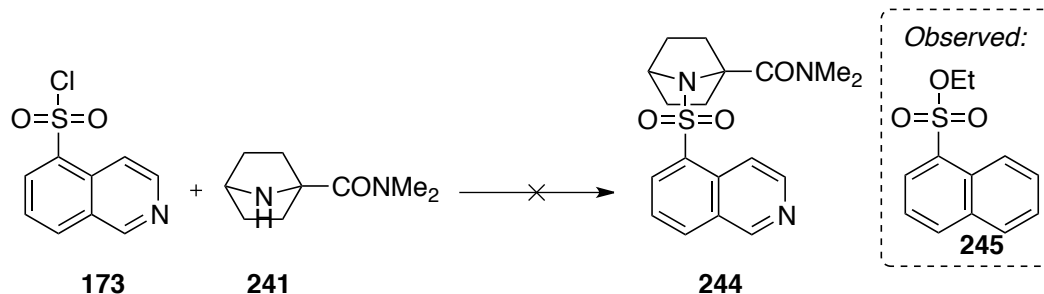
Our aim for this section was to take protected bicyclic amines prepared in section 3.2.17 and synthesise azabicyclic fragments through deprotection and attachment to the kinase-targeting warheads.

Deprotection of azabicyclic **238** was completed using neat trifluoroacetic acid over 2 hours, confirmed by both TLC and LC-MS. Following strong cation-exchange chromatography to give the free amine, we utilised conditions identified in section 3.2.4 for $\text{S}_{\text{N}}\text{Ar}$ (Table 33, entry 1) and sulfonylation (Table 34, entry 1). Both reactions were unsuccessful under these conditions, and so a range of alternative conditions were then trialled using amine **241**. For Table 33, no product could be detected and only the starting amine **241** was observed by LC-MS following treatment with coupling conditions in all entries. For entries 1-4 of Table 33, compound **243** arising from competing substitution by solvent was observed by LC-MS.



Entry	Conditions
1	NEt ₃ , EtOH 8 h, reflux
2	NEt ₃ , EtOH, 12 h, reflux
3	NEt ₃ , EtOH, 48 h, reflux
4	NEt ₃ , EtOH, 18 h reflux
5	NEt ₃ , THF, 18 h reflux
6	NEt ₃ , ⁿ BuOH, reflux
7	NaO ^t Bu, Pd ₂ (dba) ₃ , ^t Bu ₃ P, toluene
8	NEt ₃ , Pd(OAc) ₂ , ^t Bu ₃ P, DMF, 100 °C,
9	NEt ₃ , DMAc, microwave, 100 °C

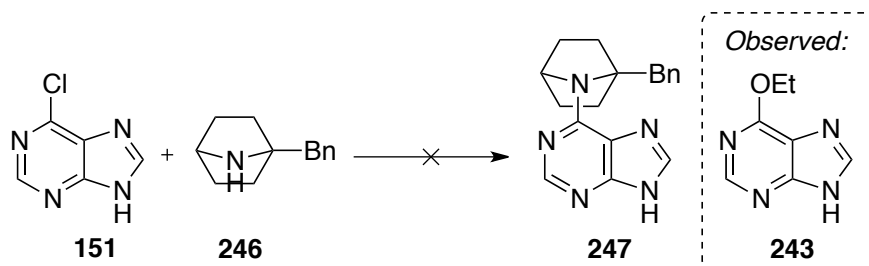
Table 33: Conditions trialled for coupling of amine **241** and 6-chloropurine **151**.



Entry	Conditions
1	NEt ₃ , EtOH, 18 h, rt
2	NEt ₃ , EtOH, 24 h, reflux
3	NEt ₃ , DMAc, microwave, 100 °C

Table 34: Conditions trialled towards fragment **244**.

Following these disappointing results, we deprotected azabicyclo **240** in the same way and attempted to attach the **151** warhead to **246**, using conditions shown in Table 35. These results were unsuccessful, with only starting materials observed. In the case of entries 1-2, the solvent-substituted **243** was identified by LC-MS.



Entry	Conditions
1	NEt ₃ , EtOH, 48 h, reflux
2	NEt ₃ , ⁿ BuOH, reflux
3	NaO ^t Bu, Pd ₂ (dba) ₃ , ^t Bu ₃ P, toluene

Table 35: Synthesis towards fragment **247**.

Following our failed attempts at *N*-decoration, the synthesis of functionalised azabicyclic fragments was deprioritised due to time constraints. It is believed the failure of these reactions could be attributed to the steric hindrance of the amine partner, although no issue was found in the S_NAr reaction to prepare initial fragment **167**.

3.2.19 Summary

A route towards azabicyclic **198** was achieved, with an improvement in yield compared to literature. We were able to apply previously reported and novel procedures towards the elaboration of azabicyclic **198**, yielding six novel amines. The aim of this section was to generate an elaborated fragment set based on **167**. Therefore, amines **240** and **238** were deprotected and a range of coupling conditions were tried with heteroaromatics **151** and **173**, with no success.

3.2.20 Fragment Elaboration Part 2: Exploring α - and β - vectors of the cyclic amine

The following section discusses elaboration of the α - and β - vectors on the cyclic amine, accessible by use of methodology discussed in Chapter 2.

3.2.20.1 Fragment Library Design

For this round of screening, a 23-member elaborated fragment library was generated using LLAMA, focusing on the growth of fragments **154**, **158** and **178** from the α - and β - vectors on the cyclic amine (Figure 30).²²³ Variation of the cyclic amine is shown in Figure 33.

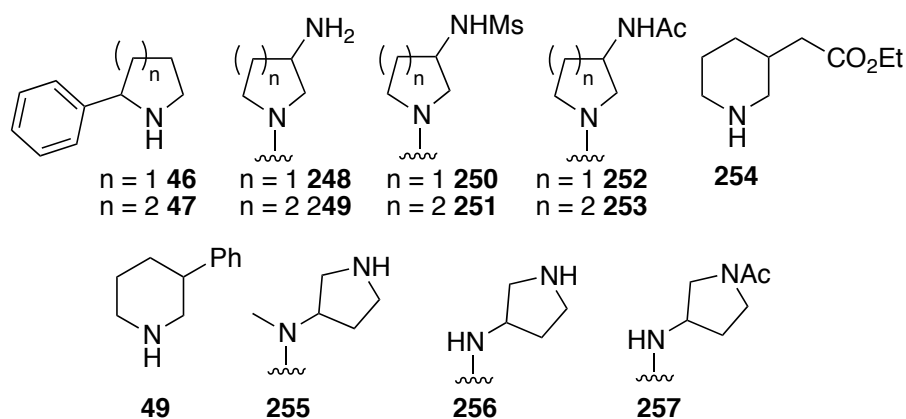


Figure 33: Amines chosen for the elaborated fragment library.

The amines were selected to incorporate both α - and β -functionalisation. In the initial library compound **162** showed that sterically small α -substituents on the cyclic amine were tolerated, this round of screening would explore a sterically bulky α -phenyl substituent. The library would also explore β -functionalised cyclic amines, bearing amines, amides, sulfonamides, and phenyl substituents, accessible using methodology discussed in Chapter 2. Lastly, we wanted to explore the attachment of the amine to the heterocyclic warhead. These amines **255-257** were included by analogy with the structure of Reversine **197**, where the C-6 position of the purine has a cyclohexylamine.²³⁴

3.2.21 Computational Analysis of Elaborated Fragments

Prior to synthesis, we conducted molecular docking studies and shape analysis of the elaborated library using the co-crystalised structure of Aurora-B with Reversine.

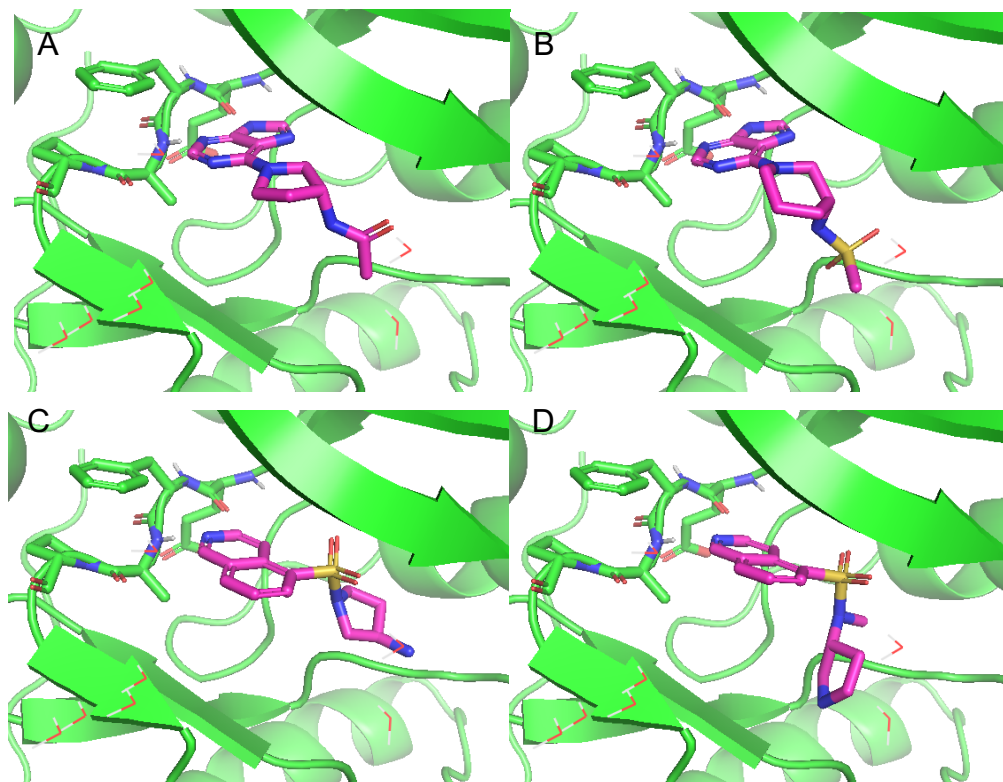


Figure 34: Elaborated Fragments docked into the Aurora-B. Panel A: **283**, docking score -9.03, Panel B: **286** docking score -8.30, Panel C: **277**, docking score -7.27 and Panel D: **270**, docking score -7.35 PDB: 2VGO.

The elaborated compounds were docked into the active site of Aurora-B in the same way as section 3.2.13 (Figure 34). The predicted binding modes for the docking results were visually inspected and the purine compounds (Figure 34, panel A and B) are thought to maintain the H-bonding pattern between the hinge residues (Glu171 and Ala173). For the isoquinoline-5-sulfonyl elaborated compounds, the isoquinoline *N* accepts a hydrogen bond from Ala173 and the isoquinoline C-1 donates a hydrogen bond to Glu171. The docking scores obtained for the elaborated library were favourable, suggesting α - and β - functionalisation of the cyclic amine may aid in the optimisation of our fragment series.

3.2.21.1 ROCS Ligand Based Screen

The ROCS analysis was completed by Dr. Martin McPhillie. In the absence of a strong docking collaboration (Section 3.2.13) between compound inhibitory potency and docking score, a ligand-based similarity screen was completed, using OpenEye's Shape-similarity software ROCS.²¹⁸ The elaborated fragment library and the structure of Reversine bound in the active site of Aurora-B were examined (Figure 35).

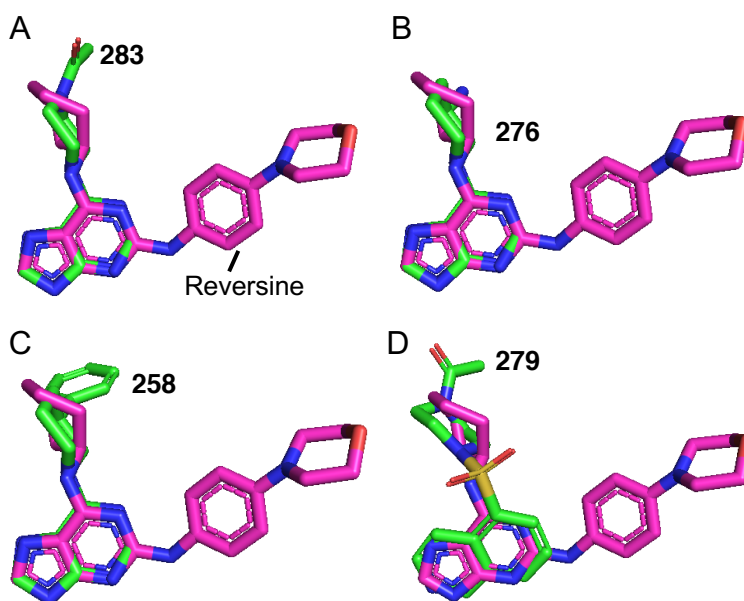


Figure 35: ROCS analysis of elaborated fragments with Reversine. Panel A: 283, ROCS Score: 1.076
Panel B: 276, ROCS score: 1.060, Panel C: 258, ROCS score: 1.290 and Panel D: Isoquinoline-5-sulfonyl 279, ROCS score 0.680. PDB: 2VGO.²³⁴

Visual inspection of the ROCS analysis for the elaborated compounds displays that the proposed elaborated fragments can mimic the binding conformation of Reversine (Figure 35). As expected, analysis of the scores showed that the purine series had higher scores than the isoquinoline-5-sulfonyl series.

The ROCS analysis and Glide docking suggested elaboration along both the α - and β -vector could support our aim of improving the potency of our compounds. However, it should be noted that following the work conducted in section 3.2.13, docking scores did not directly relate to compound potency.

Nonetheless, we decided to synthesise the 23-membered library and use the biochemical screening results to further guide our aim of improving activity of our fragments against Aurora-A.

3.2.22 Elaborated Fragment Library Synthesis: Cyclic Amine-Functionalisation

The following section details the preparation of an elaborated fragment library.

3.2.22.1 α -Functionalisation

From the initial screen against Aurora-A we identified that sterically small α -substituents were tolerated (Figure 36). Next, we wanted to explore a larger α -substituent. In response to this hypothesis we prepared fragments **258-261**.

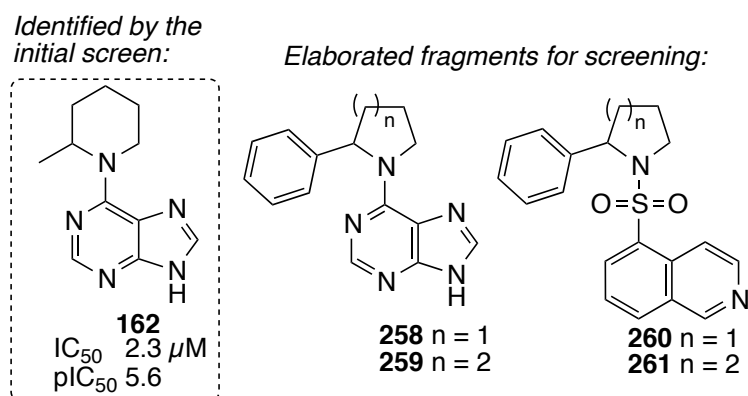
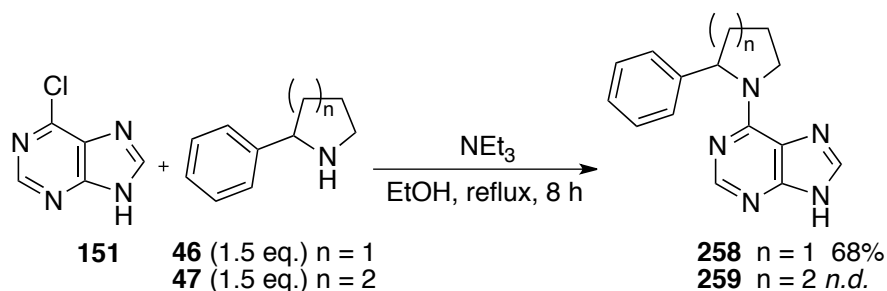


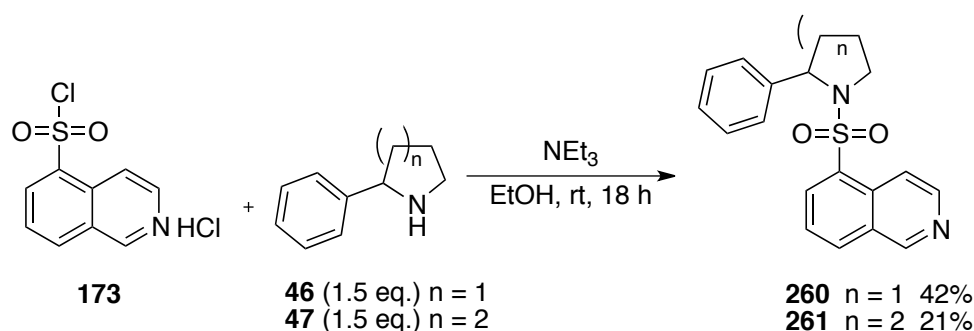
Figure 36: Elaborated fragments, functionalised in the α -position.

Fragments **258-261** were synthesised through S_NAr or sulfonylation of previously prepared (**46**, **47**) phenyl-substituted amines with the heteroaromatic precursors. For fragment **258**, commercially available 6-chloropurine was refluxed in ethanol, in the presence of triethylamine and 2-phenyl pyrrolidine. After 8 hours, a precipitate formed which was isolated by filtration in good yield. Unfortunately, **259** was unable to be isolated clean from the 6-chloropurine starting material and since we could access pyrrolidine **258**, compound **259** was deprioritised.



Scheme 43: Synthesis of α -functionalised purine fragment for screening against Aurora-A.

Following the synthesis of the purine fragment, sulfonylation reactions were performed using amines **46-47** to give previously unknown elaborated fragments **260-261**, in moderate yield (Scheme 44).

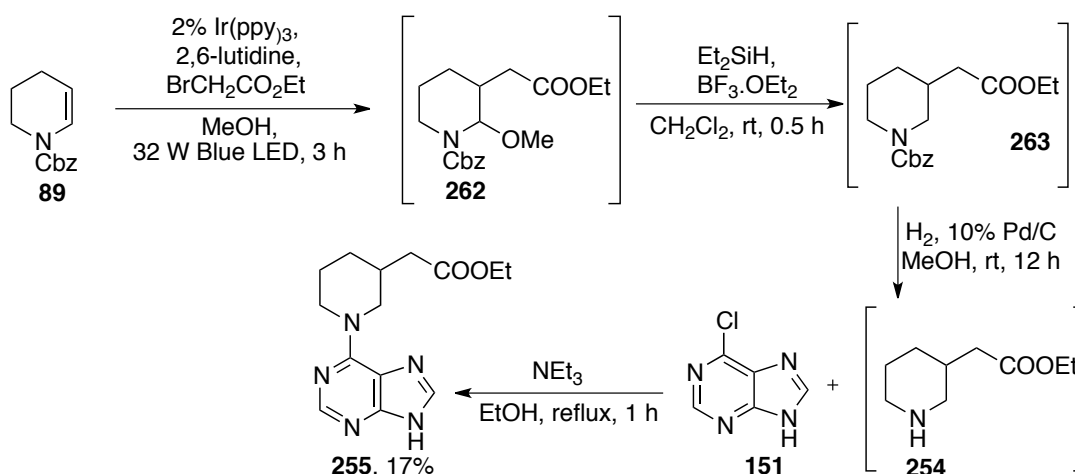


Scheme 44: Synthesis of α -functionalised sulfonyl-5-isoquinoline fragment **260**, **261** for screening against Aurora-A

A limited number of α -functionalised analogues were prepared at this point, however, should these analogues display promising activity against Aurora-A, additional α -functionalised compounds could be synthesised.^{110,113,114}

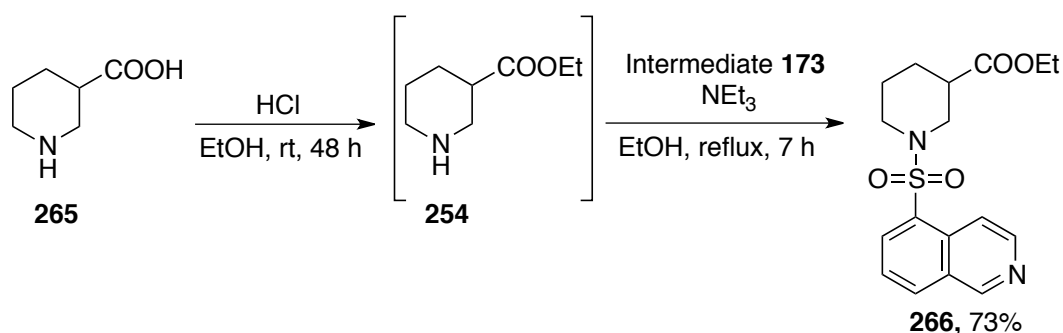
3.2.22.2 β -Functionalisation

Trindade *et al.* in the group described a procedure for the β - sp^3 alkylative functionalisation of cyclic amines.²³⁷ Substitution of an enecarbamate intermediate with a functionalised alkyl halide under photoredox catalysis yields a β -functionalised cyclic amine. Repetition of this procedure using enecarbamate **89** yielded substituted piperidine **263**, with the reaction monitored by TLC and the presence of the product confirmed by LC-MS and crude ^1H NMR (Scheme 45).



Scheme 45: Synthesis of elaborated fragment **255** by substitution of enecarbamate **89** with ethyl 2-bromoacetate.²³⁷ 17% yield from enecarbamates **89**.

Without purification, crude **254** underwent hydrogenation to furnish the free amine. The crude free amine **254** was then refluxed with triethylamine and 6-chloropurine **151** in ethanol to yield the previously unreported fragment **255** in 17% yield.



Scheme 46: Preparation of elaborated fragment **266**, 73% yield from **265**.

The isoquinoline-5-sulfonyl dehomologue was prepared from commercially-available 2-(piperidin-3-yl)acetic acid **265**, which underwent esterification using ethanol to give amine **254** (Scheme 46). This amine was subsequently used in a sulfonylation reaction with compound **173** to yield novel elaborated fragment **266**, in good yield.

Although inclusion of the C-3 ester yielded novel fragments to be tested with Aurora-A, the dehomologous fragment (**163**) had not shown promising activity against Aurora-A (Figure 37). Additionally, aliphatic esters have been flagged

as an undesirable functional group to be present in clinical candidates.¹⁰⁶ The electrophilic ester has the potential to be unintentionally reactive towards proteins and is susceptible to decomposition by solvolysis or hydrolysis. This can consequently lead to false positives that can plague screening efforts. It was therefore deemed that two elaborated fragments exploring this motif were enough to appreciate the effect on the activity of Aurora-A.

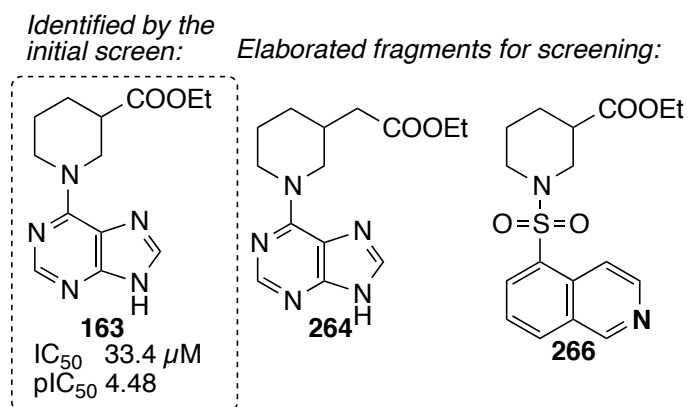
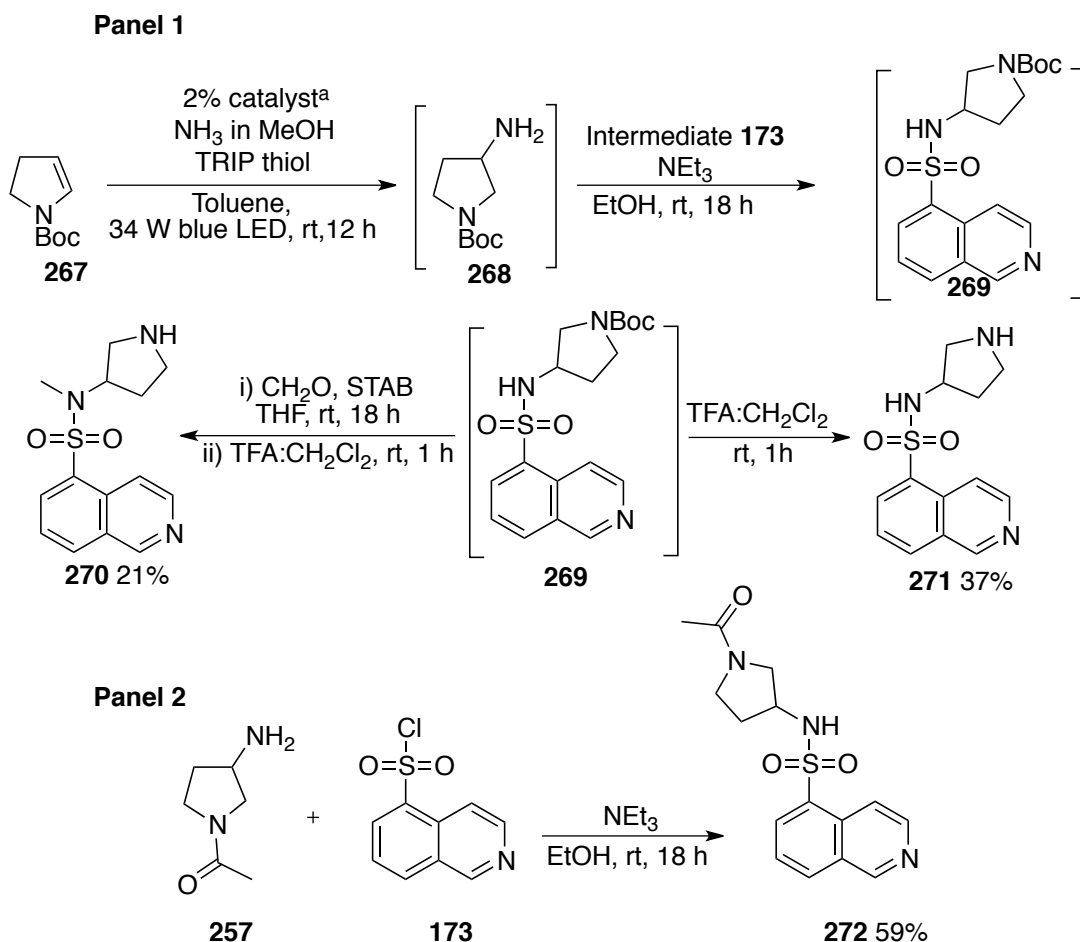


Figure 37: Fragment **163** from the initial screen and the elaborated fragments containing esters

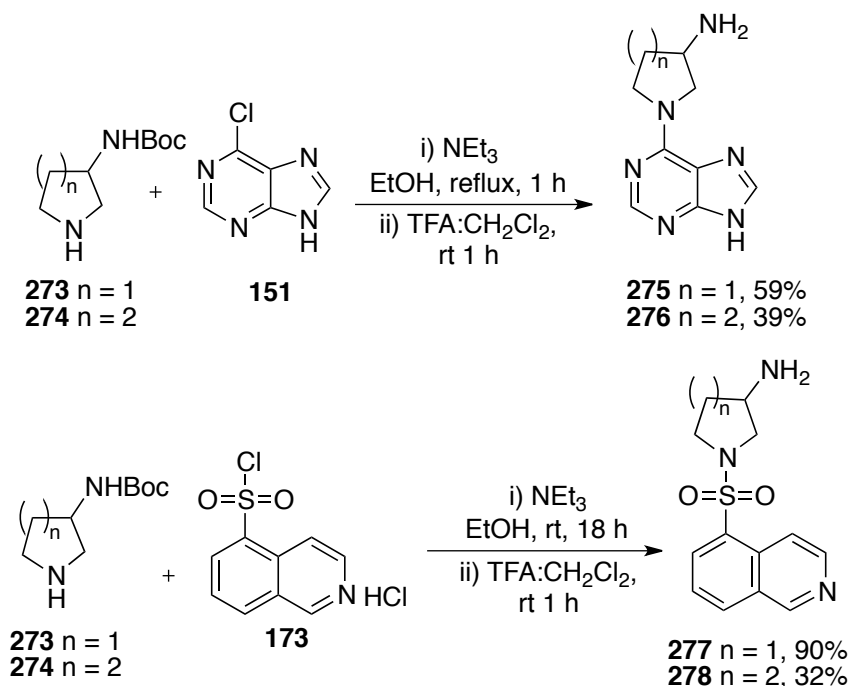
Francis *et al.* in the group reported a method for the synthesis of 3-amino substituted saturated nitrogen heterocycles using a photoredox-mediated hydroamination of an enecarbamate intermediate.¹⁰⁵ Treatment of the 5-membered cyclic enecarbamates (**267**) with an excess of methanolic ammonia under the reported conditions returned the desired primary amine **268** (Scheme 47, Panel 1). Without purification, the primary amine underwent a sulfonylation reaction with compound **173** to yield the protected amine **269**. This intermediate underwent deprotection to give the final free amine fragment **271** in moderate yield.

In parallel, intermediate **269** was methylated and deprotected to give fragment **270**. Finally, employing the conditions for sulfonylation with commercial amine **257** gave novel elaborated fragment **272** to be screened against Aurora-A (Scheme 47, Panel 2).



Scheme 47: Panel 1: Preparation of elaborated fragments **270** and **271** through hydroamination. ^a[Ir(dF(Me)ppy)₂(dtbbpy)]PF₆, yield for **271** is 37% from enecarbamates **267**. Panel 2: Preparation of fragment **272** through Sulfonylation.

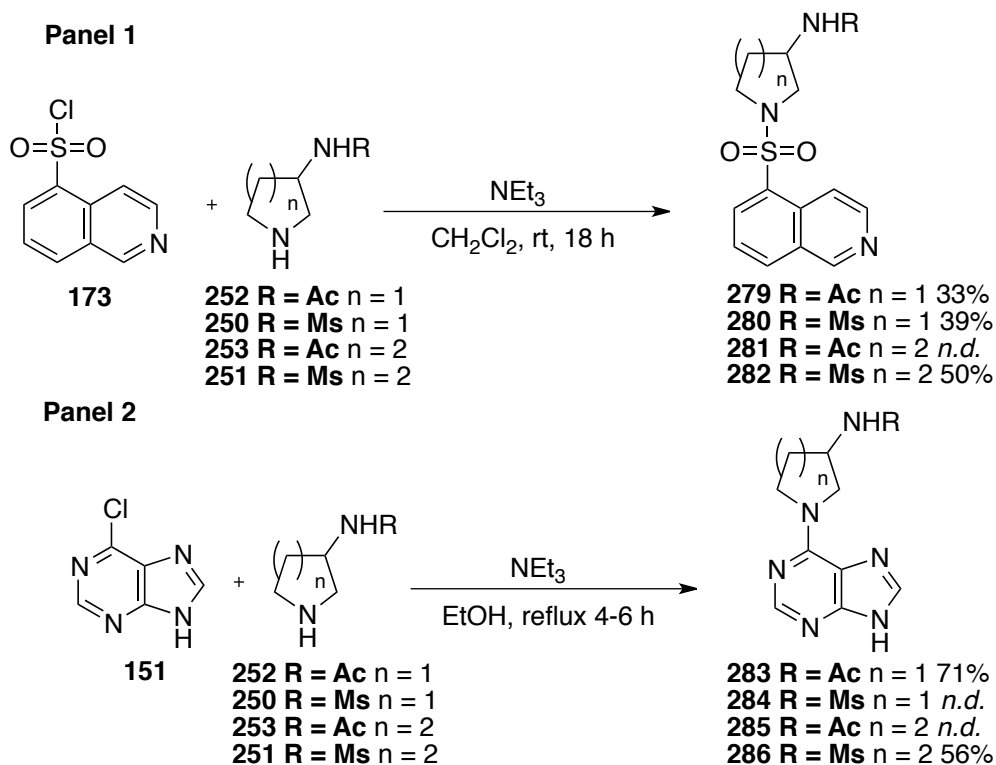
Although we could prepare amines **273-274** through hydroamination, we utilised the commercial Boc-protected amines **273-274** for the following synthesis. As before, these amines underwent substitution reactions with **151** and **173**, with analysis by LC-MS confirming completion of the reaction. The Boc-protected fragments were treated with trifluoroacetic acid in dichloromethane to give primary amine containing fragments **275-276**.



Scheme 48: Preparation of primary amine containing fragments **275-278**, through $\text{S}_{\text{N}}\text{Ar}$ reaction.

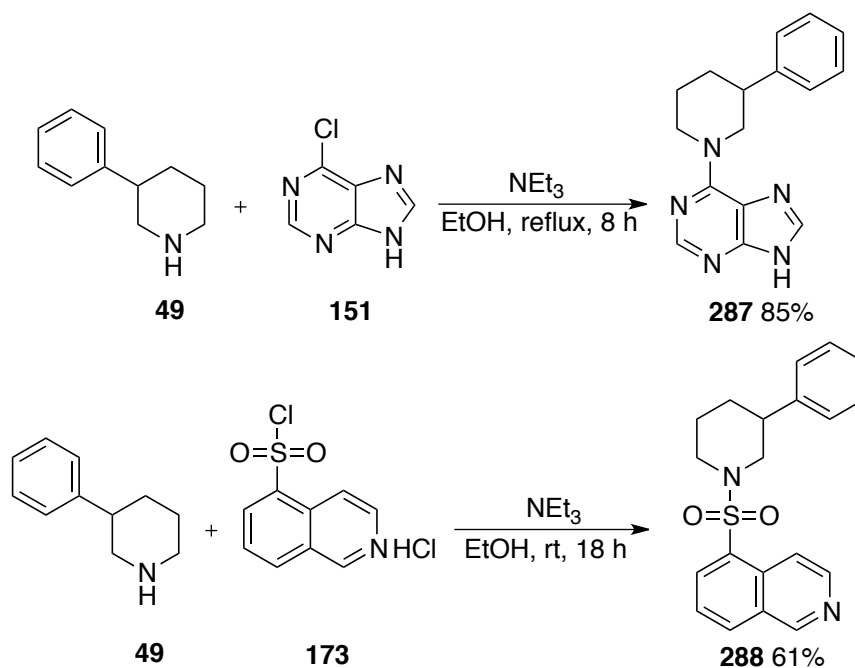
However, purification of the final elaborated fragments **276** and **278** by flash column chromatography was unable to separate 6-chloropurine and isoquinoline-5-sulfonyl chloride starting material from the final products. Starting material and product were separable by LC-MS and so automatic reverse phase column chromatography was attempted, to no avail. Finally, purification by mass directed auto-purification (MDAP), retrieved products for **276** and **278** in moderate yield (Scheme 48).

Derivatisation of amine of fragments **275-278** was originally designed to circumvent issues associated with purification of the fragments, but also enable incorporation of functionality, which may be capable of forming useful interactions with the Aurora-A binding site. In the same way as before, we prepared the fragments by $\text{S}_{\text{N}}\text{Ar}$ and sulfonylation (Scheme 49). However, on synthesis of **281**, **284** and **285**, purification issues arose, with the fragments unable to be purified by MDAP and so **281**, **284** and **285** were deprioritised for synthesis (Scheme 49, Panel 1 and Panel 2).



Scheme 49: Derivatisation of fragments 275-278.

Finally, we sought preparation of elaborated fragments bearing aromatic functionality in the β -position. The previously unknown target purine and isoquinoline-5-sulfonyl compounds were prepared from commercial **49** and either 6-chloropurine or intermediate **173**, with the fragments obtained in good yield (Scheme 50).



Scheme 50: Synthesis of functionalised aromatic fragments.

3.2.23 Summary

Overall, nineteen elaborated fragments were synthesised for screening against Aurora-A. The elaborated library explores growth of the cyclic amine motif of the fragment with α - and β - substituents. Purification issues arose which meant that some analogues could not be accessed. The biochemical screen of these compounds against Aurora-A will provide insight into future directions for the project, towards increasing the binding affinity of our initial fragments.

3.2.24 Analysis of the Elaborated Fragment Library

The elaborated fragment library was analysed using LLAMA.²²³ From this, we were able to compare the properties of the elaborated library to those of our initial fragment library. The full 19-member compound library was analysed and the average, smallest and largest values were determined.

Data	MW (HAC)	AlogP	Molecular PSA / Å²	Fsp³	Rotatable Bonds
Average	300.3 (21)	0.98	74.9	0.37	2.8
Smallest	204.2 (15)	-0.16	50.3	0.21	1
Largest	369.5 (25)	3.02	103.9	0.57	6

Table 36: Analysis of the different physicochemical properties of the 19-member elaborated library. Notably, the average AlogP remained constant from the initial library to the elaborated library (Table 36). This value offers potential for the addition of more lipophilic groups during further development of the compounds. The average PSA of the compounds has increased on elaboration.

3.2.24.1 Three-Dimensionality of the Elaborated Library

The three-dimensionality of the fragments was described by a PMI plot (Figure 38), with the purine series in green and the isoquinoline-5-sulfonyl series in red (Figure 38). From this plot, it can be concluded that the elaborated compounds explore a more distinctive three-dimensional area of the plot and are beginning to access underrepresented areas of chemical space.

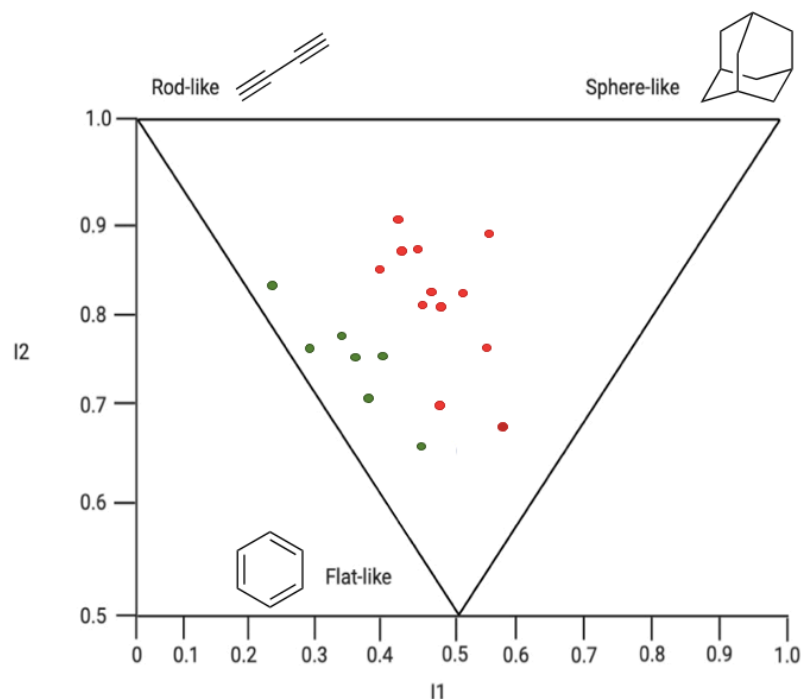


Figure 38: A PMI plot of the elaborated library, showing the purine series (green) and the isoquinoline-5-sulfonyl series (red). The PMI plot was produced by use of LLAMA.

3.2.25 Determination of Elaborated Fragment bioactivity against pseudo-WT Aurora-A

The elaborated set of compounds were screened in the same manner as Section 3.2.8. Due to issues with the instrument used to screen the compounds, the inhibitory potency of only nine of the fragments could be obtained. The results of the screen are described below.

3.2.25.1 Determination of Bioactivity for the Purine Fragment Series

The potency of the elaborated purine compounds was determined, enabling appreciation of the effect on potency on functionalisation of the cyclic amine. At this stage, five fragments from the purine series were screened against Aurora-A, with the complete results located in Appendix 3 and 4 and summarised in Table 37.

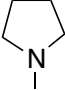
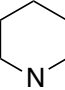
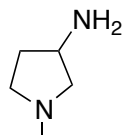
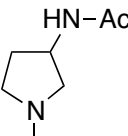
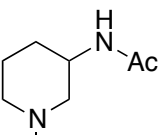
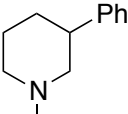
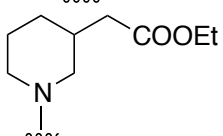
Amine	Substrate	IC ₅₀ / μM	ALogP	LE	LLE
	154	3	0.92	0.55	4.60
	158	0.370	1.43	0.60	5.00
	275	53	-0.11	0.40	4.39
	283	77	-0.14	0.32	4.25
	285	182	-0.15	0.26	3.90
	287	35	2.93	0.30	1.52
	254	43	1.46	0.29	2.90

Table 37: Determination of bioactivity for five elaborated purine compounds.

Comparing the elaborated purine compounds to their parent fragment from Section 3.2.10 for compounds **287** and **285**, the original fragment (**158**) was over 400-fold and 93-fold more potent respectively. Overall, elaboration of compounds **154** and **158** along the α - and β - vectors of the cyclic amine for these compounds led to a reduction in the potency and therefore the ligand efficiency of the compounds.

In general, for our initial purine library (Section 3.2.10.1), we observed a trend increasing bioactivity in those compounds with increasing values of AlogP. This trend is not observed with the elaborated purine compounds, suggesting

that this trend with the initial fragments is not solely due to non-specific hydrophobic properties, although additional compounds would be required to confirm this.

The lipophilic ligand efficiency was calculated to differentiate the high-quality compounds of this series, which could undergo further optimisation. In general, HTS hits have an LLE value of 2 and compounds with higher values of LLE (≤ 2) tend to possess improved ADMET characteristics.¹⁸ From Table 37 we can identify that compound **287** has a poor value of LLE at 1.5, suggesting that selection of this compound for further optimisation would be undesirable. Literature states that an ideal value for LLE for an optimised drug candidate is between 5-7. From this, we can deduce that compounds **275** and **283** would potentially be desirable candidates for further development.

3.2.25.2 Determination of Bioactivity for the Elaborated Isoquinoline-5-sulfonyl Fragment Series

The potency of the elaborated isoquinoline-5-sulfonyl compounds was determined, enabling understanding of the effect of cyclic amine functionalisation. At this stage, four fragments were screened against Aurora-A.

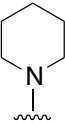
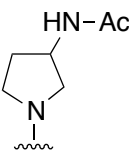
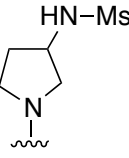
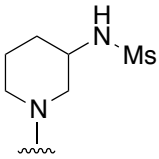
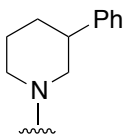
Amine	Compound No	IC ₅₀ / μ M	A _{LogP}	LE	LLE
	178	4.8	1.38	0.39	3.93
	279	189	0.47	0.24	3.25
	280	203	0.02	0.22	3.67
	282	118	0.06	0.22	3.87
	288	58	3.02	0.24	1.21

Table 38: Determination of bioactivity for five elaborated isoquinoline-5-sulfonyl compounds

All four compounds were found to have activity against Aurora-A. The parent fragment (**178**) was found to be 12-fold and 24-fold more potent **288** and **282** respectively. Unfortunately, the parent pyrrolidine-based fragment of **279** and **280** were not able to be screened due to solubility issues (**176**), so a direct comparison was unable to be made at this point. From these results, elaboration of compound **178** along the α - and β - vectors of the cyclic amine for these compounds led to a reduction in the potency and therefore the ligand efficiency of the compounds.

In general, for our initial isoquinoline-5-sulfonyl library, we observed a trend of increasing bioactivity in those compounds with increasing values of AlogP. For this library, additional compounds would be required to confirm this. However, our most potent compound from this elaborated series **288**, possessed a high value of AlogP at 3 units, and fragment **280** was our least potent and had the lowest value of AlogP of this library.

The lipophilic ligand efficiency was calculated to prioritise the compounds, which could undergo further optimisation. Table 38 displays that compound **288** has a poor value of LLE at 1.2, indicating that this compound would be a poor candidate for further optimisation. Likewise, this data displays that compound **280** and **282** would potentially be suitable contenders for further development.

3.2.26 Summary

A library of 9 elaborated fragments prepared in-house were screened for bioactivity against Aurora-A. The biochemical screen identified that functionalisation along the α - or β -carbon atom of the cyclic amine reduced activity in all cases versus the parent fragment, indicating that these may be unfavourable vectors to pursue in the elaboration of these compounds. However, more definitive conclusions would require screening of the remaining 10-compounds of the library.

3.3 Conclusion

A virtual library was developed consisting of sixty fragments across three fragment series, designed to target kinases. Each fragment consisted of a cyclic amine attached to a kinase-targeting warhead, designed through literature searching. Through analysis of predicted molecular properties, this virtual library was condensed to give 35-fragments. The 35-fragments were assembled in the minimum number of synthetic steps from readily available starting materials to give a 35-member fragment library.

The 35-member fragment library was screened against Aurora-A, yielding 30-hit fragments, with 13% of the fragments displaying sub-micromolar activity. It was decided through analysis of biological potency that the purine and isoquinoline-5-sulfonyl series would be taken forward to be elaborated. Our elaboration strategy focused on the most potent compounds arising from the biological screen.

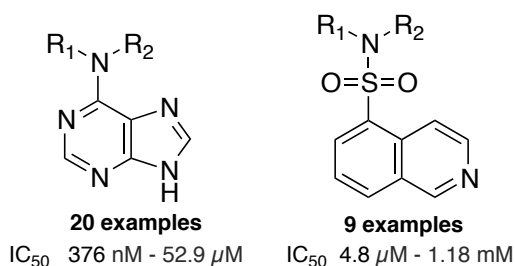


Figure 39: Summary of the two-fragment series taken forward to the elaboration stage.

From this, we moved on to the synthesis and elaboration of azabicyclic **198**, which gave our most potent compound when attached to purine (**167**). In order to access azabicyclic **198**, we employed a route proposed by Harty *et al.*²³⁸ and obtained an improved yield. We explored a variety of literature methods for the elaboration of azabicyclic **198**, enabling access to six novel amines. Following synthesis of these amines, we sought the formation of elaborated bicyclic fragments. We found we were able to deprotect the amines, but were unable to successfully effect coupling of the bicyclic amine and the heteroaromatic component in either an S_NAr , Buchwald coupling or sulfonylation. These unsuccessful reactions were postulated to be due to

steric hindrance or reduced reactivity of the amine because of the newly installed bridgehead substituents.

Next, we explored α - and β -functionalisation of the cyclic amines of the most active monocyclic fragments e.g. **167**, for which we had either identified or developed methodology to complete this task in Chapter 2. Our elaboration strategy was supported by docking structures, which suggested that α - and β functionalisation of the cyclic amine gave compounds of similar shape to a known Aurora-B inhibitor, Reversine. Biochemical screening of a 9-membered elaborated library exploiting that α - and β - vectors of the cyclic amine displayed no improvement in potency. Although we did not obtain an improvement in potency, this case study exemplifies that the underpinning chemistry developed both with Chapter 2 and previously by the Nelson and Marsden groups has enabled exploration of vectors on the cyclic amine, which will have wider use in FBDD.

3.4 Future Work

Future work for this project will focus on completing the biochemical screening and the preparation of elaborated fragments. Initially the remainder of the α - and β -functionalised library would be screened, enabling more definitive conclusions to be reached on whether these vectors are productive to pursue in the development of a potent Aurora-A inhibitor.

Next, we could explore additional methods to synthesise the desired elaborated azabicyclic fragments, given that fragment **167** was the most potent compound in the initial biochemical screen. A series of conditions were trialled to form the final fragments, but these methods were unsuccessful. In this process we trialled conditions for S_NAr , Buchwald-Hartwig and in the case of the isoquinoline-5-sulfonyl compounds, conditions for sulfonylation. For the purine series our next approach could be to protect the 6-chloropurine with -

Boc or -Cbz and use a procedure by Lakshman²⁴⁹ for palladium-catalysed amination reaction of 6-chloropurine.

Additional elaboration strategies for azabicyclic **198** could be pursued. For example, we synthesised primary alcohol **233** in Section 3.2.17. This alcohol could undergo deoxyfluorination using Selectfluor and visible light photoredox catalysis.²⁵⁰ This would be a useful functionalisation strategy since there is growing demand within medicinal chemistry for the incorporation of fluorine into organic molecules. A benefit of incorporating fluorine would be increased metabolic stability of the molecule through the replacement of an oxidisable C-H bond to a C-F bond. The addition of fluorine in this way also decreases lipophilicity, improves bioavailability and has been shown to increase binding affinity.

We could explore using decatungstate photocatalysis to directly convert the β -C-H bond of azabicyclic **198** into the corresponding alkylsulfinic acids²⁵¹ since sulfones and sulfonamides are widely found in pharmaceuticals.²⁵² These methods would extend our current toolkit of approaches to elaborate the azabicyclic **198**.

Equally, the elaboration strategy towards improving the potency of our fragments could explore different vectors on the purine and isoquinoline-5-sulfonyl compounds. For example, from examining the binding mode of the Aurora inhibitor Reversine **197**, the C-2 aniline donates a hydrogen bond to Ala173. Growth along this vector may improve the potency our fragments but may also offer opportunity to improve the physicochemical properties. The ROCS analysis from Section 3.2.14 demonstrates that in the development of Reversine this C-2 vector was pursued.

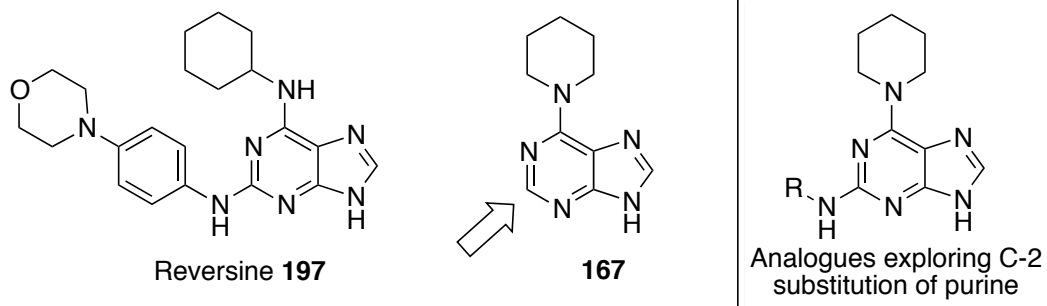


Figure 40: Potential growth vector to explore in elaboration of active fragments.

4 Chapter 4: Investigating the Selectivity of ATP-binding Site-Targeting Fragments with a Diverse Range of Kinases

4.1 Introduction

The human genome encodes 518 protein kinases, of which hundreds have been shown to have genetic links with human disease. Of the 20,000 kinase-related publications in 2009, 65% focused on the same 50 protein kinases.¹⁰⁷ The discovery of selective inhibitors of ATP-binding proteins has the potential to initiate the design of novel chemical probes, with the ability to target a broad range of kinases.²⁵³

Protein kinases can be grouped into families based on the similarity of their catalytic domain amino acid sequence.²⁵⁴ Catalytic domains are composed of an *N*- and *C*-terminal domain, where ATP binds to the backbone of the linker region between the domains, also known as the hinge region.¹⁶⁴ Protein kinases can have a catalytically active or inactive state. In an inactive state conformation, the structures of the catalytic domain are more diverse. As the kinase is activated, frequently by phosphorylation on the activation loop, it adopts a shape which can bind ATP, with the binding site open and the component residues correctly orientated for phosphate transfer. In an active kinase state conformation, part of the ATP binding site is formed from a conserved sequence of amino acids; aspartate (D), phenylalanine (F) and glycine (G) known as the DFG motif. A further conserved aspartate residue in the catalytic domain may aid in the phosphate transfer by deprotonating the substrate hydroxyl group, enabling it to more readily attack and remove the terminal phosphate from ATP.¹⁶⁴ The active conformation of the catalytic domain is well characterised. A pharmacophore model of the catalytic domain has been built to describe the ATP binding site, which has been successfully used for rational drug development.²⁵⁵ A significant proportion of kinase

inhibitors interact with the hinge motif within the ATP pocket, which is highly conserved across the kinome.²⁵³ Due to this highly conserved binding mode, it is difficult to engender selectivity across kinases.

Fragment-based drug discovery has a track record of success against protein kinases, usually from the perspective of structure-based optimisation against a single biological target. The selectivity of the fragments and the extent to which it determines the selectivity of the compounds optimised from the fragment has received less attention.²⁵³ Low -molecular weight fragments can display selectivity when they exploit very subtle differences between the highly conserved ATP-binding sites of protein kinases. This concept has previously been explored using FDA approved drugs, natural products and lead-like compounds.^{256–258} A previous study concerning fragment selectivity reported that maintaining selectivity at low-molecular weights is possible, however, the structural and biochemical data for this study was not publicly disclosed.⁷²

Traditionally, kinase inhibitors are discovered in a target-centric approach where inhibitors are identified by high-throughput screening using a target kinase. The resulting compounds can then be tested for selectivity against a representative panel of kinases. This approach is time and resource consuming. A more efficient approach would be to screen libraries of compounds in a target-blind manner against a comprehensive panel of recombinant protein kinases, to reveal the selectivity of each compound. Such an approach allows us to focus on molecules which show the desired selectivity patterns and can subsequently be structurally optimised.²⁵³ Additionally, this approach may lead to identification of unexpected kinase inhibitors or uncover multi-targeting inhibitors, where inhibitory activity is focused towards a precise range of kinases rather than a single primary target. Such multi-targeting inhibitors are unlikely to be identified using target-centric screening.

This chapter investigates the selectivity of fragments and elaborated fragments prepared in Chapter 3 against a panel of kinases. From this, we explore whether selectivity for a particular kinase can be maintained from the fragment through to corresponding elaborated compounds. The study can also reveal previously unreported inhibitor compounds.

4.2 Results and Discussion

Fragments were tested for protein kinase binding against a panel of 100 enzymes, containing representative members of each major kinome family using a thermal shift assay. This assay was performed by Dr. Benedict-Tilmen Berger of Professor Stefan Knapp's laboratory at the SGC Frankfurt.

The compounds examined within this chapter include both the fragment (Chapter 3, Section 3.2.8) and elaborated fragment (Section 3.2.14) libraries previously discussed, alongside supplementary fragments (Figure 41). Supplementary fragments were included to aid in the understanding of potential selectivity patterns, with their synthesis discussed in Chapter 6. Thirteen compounds were found not to be soluble under the conditions of this assay and therefore were not screened. Compounds were grouped according to whether they were a parent fragment or an elaborated fragment. Parent compounds have already been screened against Aurora-A in Chapter 3, Section 3.2.8. Elaborated compounds are fragments accessed from functionalisation of the cyclic amine (discussed in Chapter 2 and 3). A full list of all the compounds submitted for assay is located in Figure 42, categorised according to parent or elaborated fragment.

The compounds were tested at 200 μ M and a mean T_M value was obtained for each kinase. From that, significant binding (and therefore a hit compound) was identified by setting a threshold T_M value of >2 standard deviations above the mean. The results are displayed in a heat map located in Appendix 5; an illustrative sample of the heat map is shown in Figure 42. To determine the variability and reproducibility of the assay, the non-selective protein kinase inhibitor staurosporine and DMSO were included as an internal positive and negative control in each kinase screen.

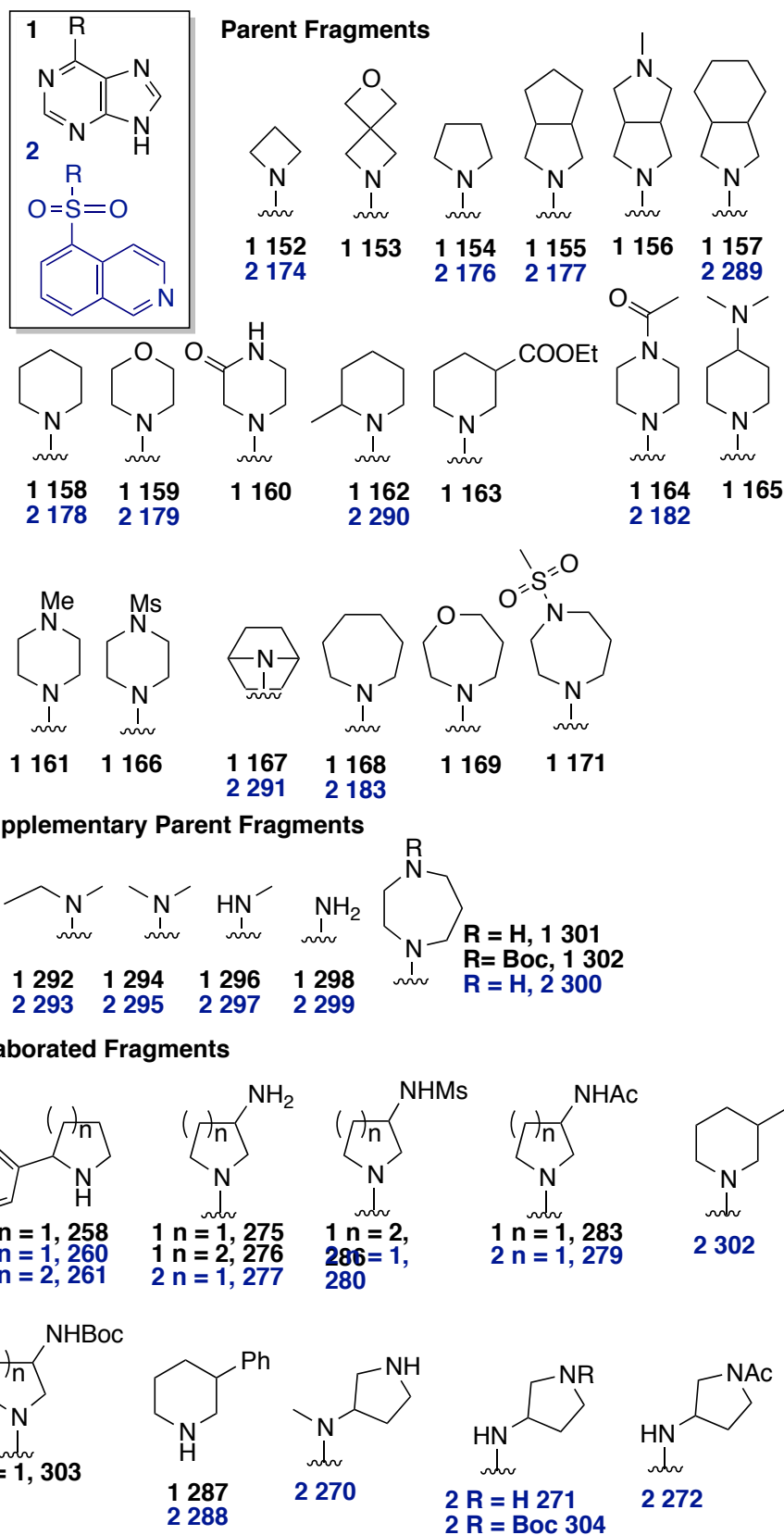


Figure 41: Structure all the fragments profiled within this chapter. **169, 296, 161, 163, 286, 302, 261, 303, 289, 304, and 279** were not screened due to poor solubility.

Compound	Purine Compounds																								
	155	159	162	167	158	154	156	166	160	171	152	292	294	168	164	275	258	287	301	283	276	153	157	298	165
AURKBA	0		1	0	1	0	2	0	-1	-1	1	2	1	1	0	-1	-1	-1	-1	-1	0	-1	2	-1	-2
BMXA	1	-1	2	1	2	0	1	1	0	0	0	1	0	2	0	0	0	0	0	0	0	0	4	0	0
BRAFA	0	-1	1	0	0	0	1	0	-1	0	0	1	1	0	0	-1	-1	-1	-1	0	0	-1	2	0	-1
AAK1A	1	0	2	1	2	1	2	1	-1	0	1	2	1	2	0	-1	0	0	-2	0	0	0	2	-1	-1
ABL1A	1	-1	2	1	3	0	1	0	-1	0	0	2	1	2	0	-1	-1	-1	-1	0	0	-1	3	0	0

Legend:

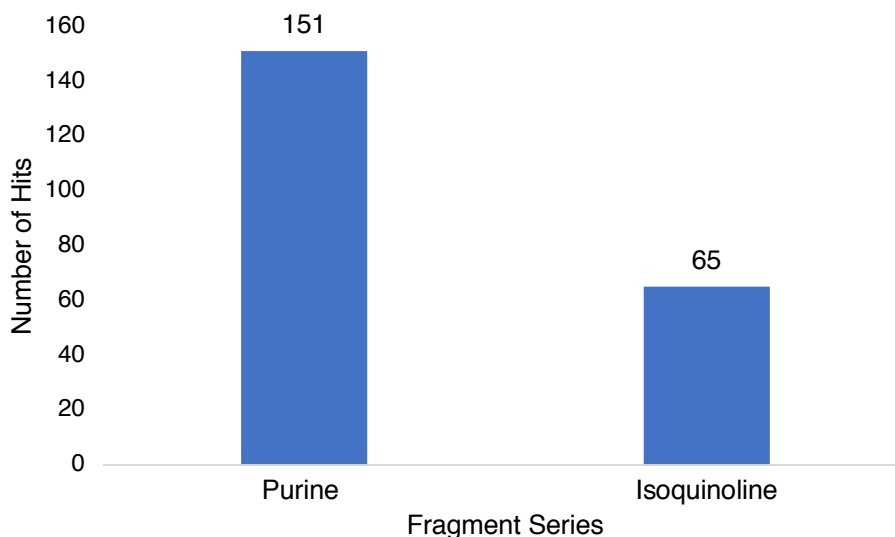
0	1	2	3	4	5	6	7
---	---	---	---	---	---	---	---

Figure 42: Sample of the kinase heat map for 48 compounds screened against 100-protein kinases. The full analysis located in appendix 5. Those values of T_M which were 2 S.D. above the mean are highlighted, with darker colours indicating more potent compounds. Values are rounded to the nearest significant figure.

The use of T_M , determined at a fixed single concentration, rather than full IC_{50} or K_D values for each compound against each kinase does impose limitations on the data interpretation. This method does not allow selectivity or activity to be accurately quantified and so we have not attempted to infer relative potency levels between compounds above the $2 \times$ S.D. threshold, even though this may be seen in a full IC_{50} determination. Nevertheless, this method provides an efficient snapshot of binding and selectivity across 100-kinases. From this, we can identify potentially useful binding across a library of compounds and to distinguish their selectivity patterns. This method will aid in the triaging of compounds that show promising binding or selectivity for full IC_{50} determination.

4.2.1 Analysis of the results

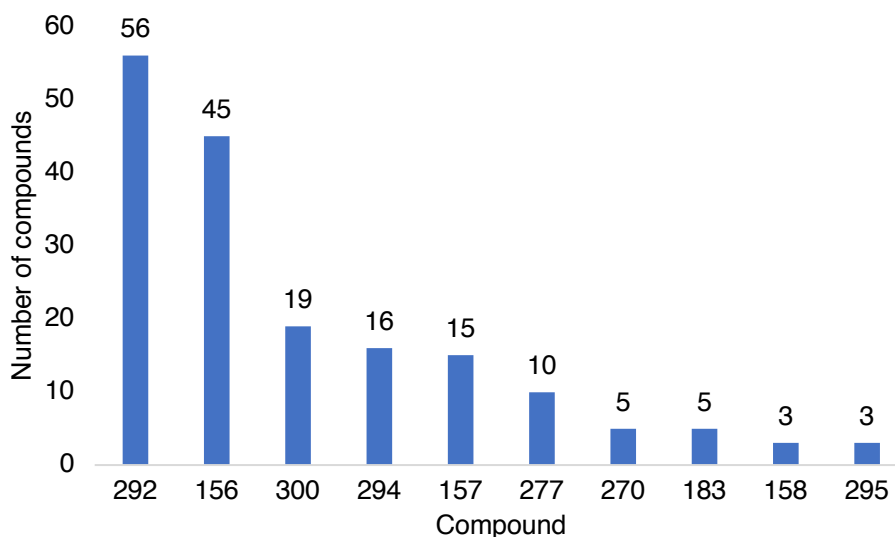
From our analysis, we identified 216 hits across 87 protein kinases exceeding the 2xSD threshold. This screen profiled 26 purine and 22 isoquinoline-5-sulfonyl compounds. The purine series delivered 2-fold more hits compared to the isoquinoline-5-sulfonyl series (Graph 9). This could be expected since the kinase substrate is ATP and the fragments were designed to be ATP-competitive inhibitors, both containing the purine motif.



Graph 9: Distribution of hits between the purine and isoquinoline-5-sulfonyl series.

4.2.1.1 Promiscuous Fragments

We analysed the ten compounds with the highest hit rates (Graph 10). Purines **292** and **156** were most promiscuous, inhibiting 56 and 45 protein kinases respectively. In total, compounds **292** and **156** account for 47% of all hits found during this screen. The top ten compounds consist of five purine and five isoquinoline-5-sulfonyl compounds and in total, they account for 81% of hits across the screen. Overall, compounds produced from the purine series appear to be the more promiscuous. Eight out of the top ten highest hits were parent compounds, with two of the top ten categorised as elaborated compounds.



Graph 10: Compounds with the highest hit rates across 100-kinases.

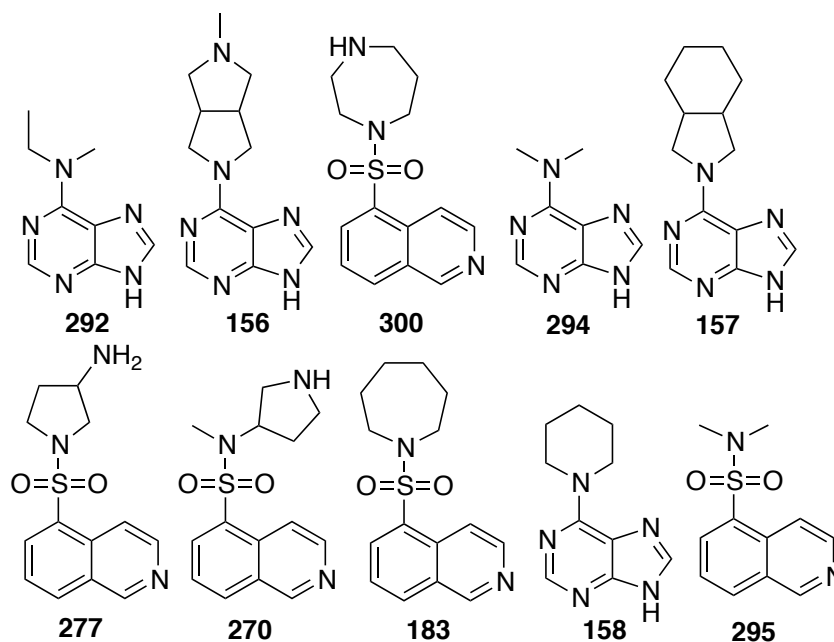
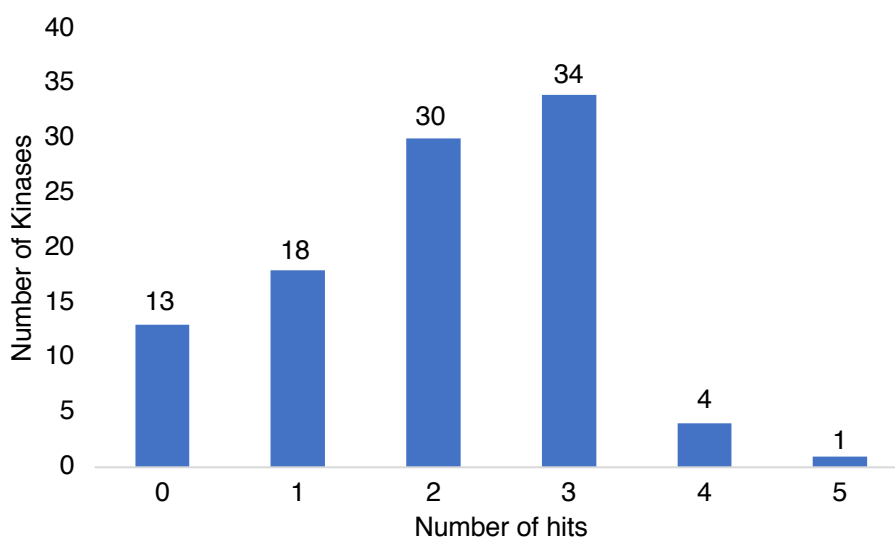


Figure 43: Structures of the most promiscuous compounds.

Since the assay is conducted at high compound concentration, compound solubility at 200 mM could be a factor in obtaining a high hit rate for certain compounds. Many of the high-hitting compounds contain additional basic nitrogen atoms (for example, compounds **156** and **300**), which could aid with solubilising the compounds at this high concentration.

4.2.1.2 Selected Kinase Targets

The screen revealed that at least one hit was found for 87% of the kinases (Graph 11). The most promiscuous kinase was ABL1A, with 5 fragments hits. For 69% of the kinases, 2 or more hit fragments were identified. To appreciate any patterns in selectivity, individual compound structures were analysed for selected kinase targets.



Graph 11: Variation in the number of hits found against the 100- kinases.

4.2.1.2.1 ABL1A

We identified five hits against the tyrosine kinase ABL1 (Figure 44). All of the identified hits contained a purine motif, and a lipophilic amine. Three out of the five hits are also found within the ten most promiscuous compounds of the screen, suggesting poor selectivity (**158**, **292**, **157**).

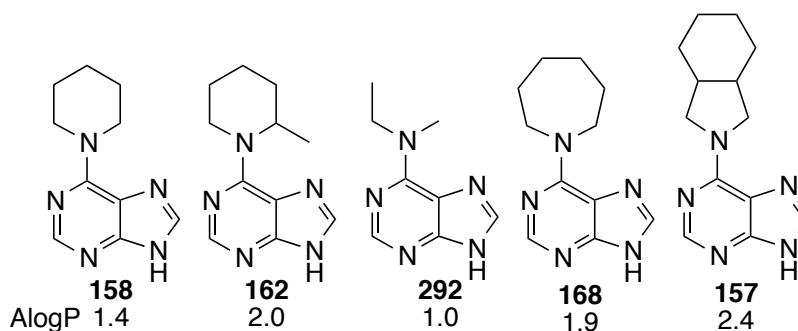


Figure 44: Fragment hits against ABL1A

4.2.1.2.2 PHKG2A

Screening against PHKG2 returned four isoquinoline-5-sulfonyl hits of related structure (Figure 45). Interestingly, all hits contain sulfonamides bearing a β -primary or secondary amine. The parent pyrrolidine-based fragment **176** was not a hit, but it is not understood whether solubility was an issue for the parent compound. However, it was previously postulated in the literature that protonated amines, in the presence of hinge binding elements, may provide a binding interaction to the kinase ribose pocket.^{222,259} Because all four compounds are structurally related, this gives confidence that this series of compounds represents genuine hits, with the potential for further development by fragment growth.

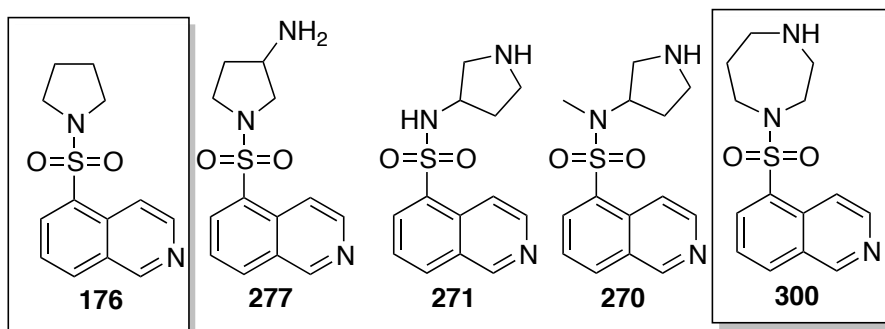


Figure 45: Fragments hits against PHKG2A. Parent compounds located in boxes.

4.2.1.2.3 AURKBA

In Chapter 3, we screened the parent fragments against Aurora-A and elucidated their activity, with some fragments displaying sub-micromolar activity. The Aurora kinases have a highly conserved active site, which has made selective inhibitor development difficult (Section 3.1.4.3). Unexpectedly, this screen reported fragment **157** as the only hit against Aurora-B, excitingly suggesting that the parent fragments display selectivity between Aurora-A and Aurora-B. To confirm this, however, full dose-dependent analysis would need to be completed.

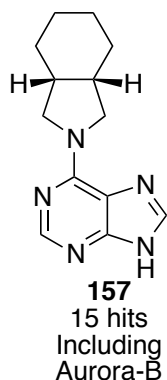


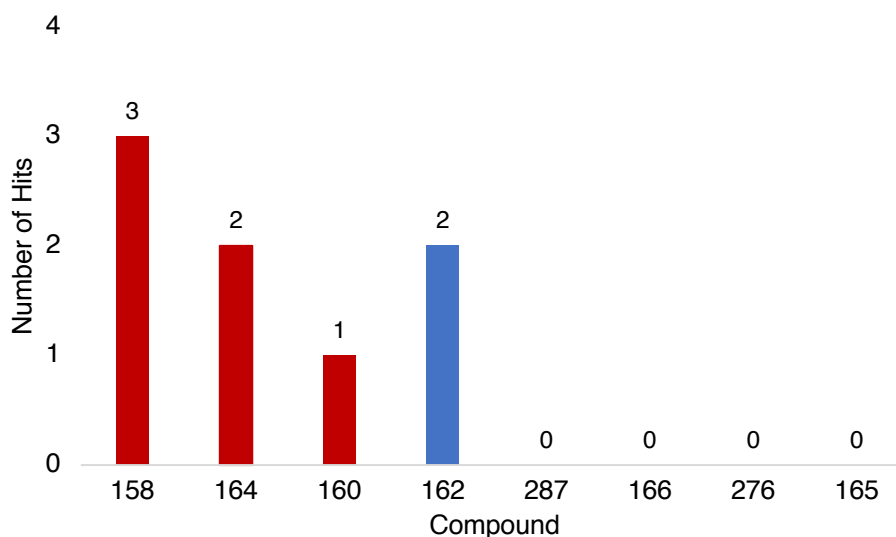
Figure 46: Structure of the Aurora-B hit.

4.2.1.3 Evaluation of Parent vs. Elaborated Fragments

In the assay, we screened 35 parent fragments and 12 elaborated fragments. For the parent fragments we identified 184 hits, while 33 hits were found for the elaborated fragments. For the parent fragments alone, we were able to obtain hits against 81 different protein kinases; the elaborated fragments returned hits against 22 kinases, of which six were not targeted by the parent fragments. We next examined selected individual parent-elaborated groups.

4.2.1.3.1 Comparison of purine-bearing fragments based on six-membered cyclic amines

The parent piperidinyl purine **158** was found to give hits against BMXA, ABL1A and CDK2A (Graph 12, Figure 47). On addition of a methyl group in the α -position (**162**), inhibition was lost for CDK2A. Analogues elaborated in the β -position (**276**, **287**) were not active against any kinase. Exploration of piperazine-type fragments **160** and **164** targeted three different kinases to **158** and **162**.



Graph 12: Comparison of the parent fragments (red), to the elaborated fragments (Blue).

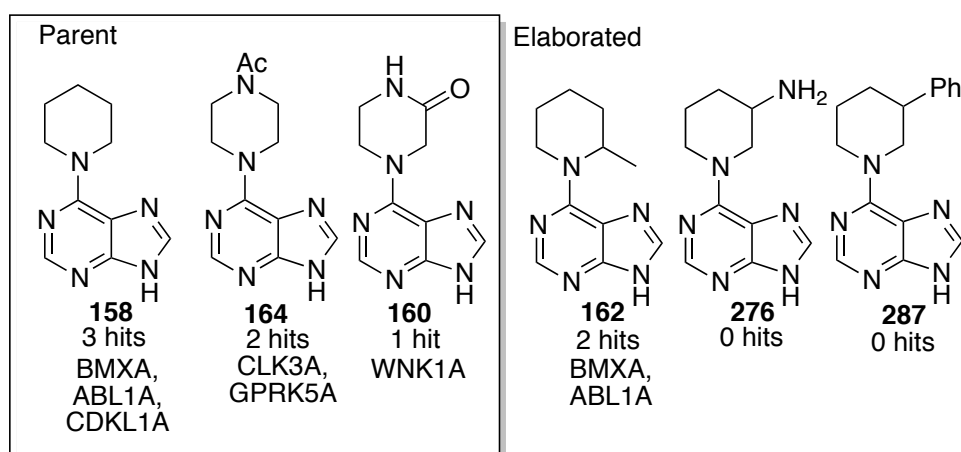
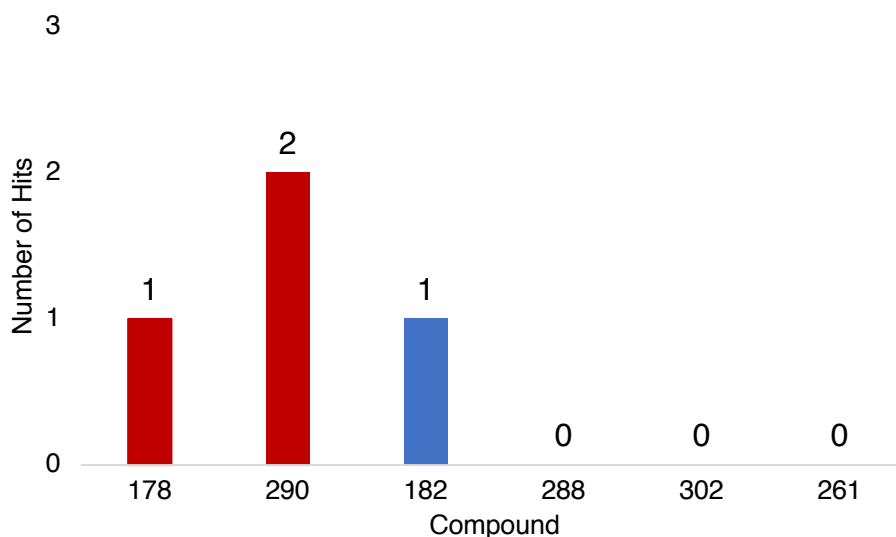


Figure 47: Representative examples with parent fragments.

4.2.1.3.2 Comparison of isoquinoline-bearing fragments based on six-membered cyclic amines

The parent fragment **178** gave a single hit against BRAFA (Graph 13, Figure 48). Incorporation of an α -methyl group gave 2 hits, not including BRAFA, indicating a variation in selectivity profile on growth from the α -position of piperidine. Binding against any of the 100-kinases was removed on incorporation of a more sterically bulky phenyl group (**261**). Fragment **302** elaborated along the β -carbon atom did not yield any hits.



Graph 13: Comparison of the parent fragments (red), to the elaborated fragments.

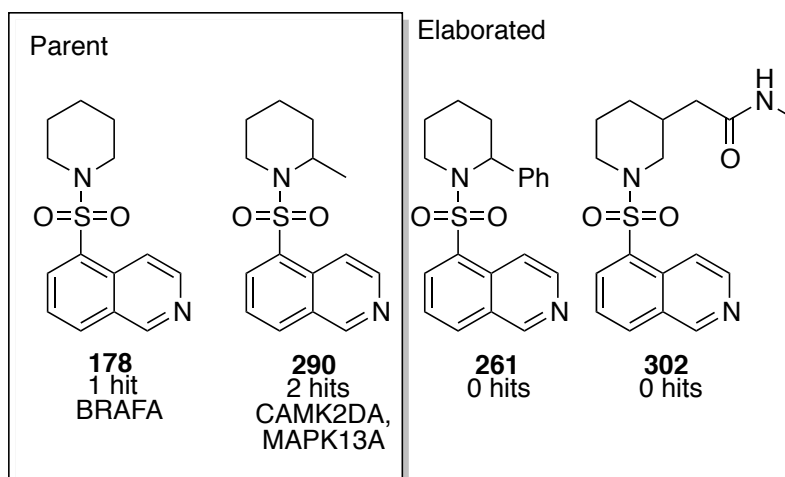


Figure 48: Selected examples with the parent fragments.

4.2.1.3.3 Pyrrolidine-containing fragments based on the sulfonylisoquinoline warhead

Parent fragment **176** did not yield any active hits. Inclusion of an amine at the β -carbon atom gave 14 hits, with all kinase binding destroyed on derivatisation of the amine to a sulfonamide, potentially indicating the importance of the free amine for binding. On reversing the attachment of the 3-aminopyrrolidine to the heteroaromatic giving **271**, a single shared hit against PHKG2A was obtained. This result suggests an improved selectivity profile, but to confirm this hypothesis, full dose-dependent activity would need to be completed.

Methylation of the sulfonamide of **271** to give **270** increased the hit rate to 10%, which included PHKG2A, but compound selectivity was reduced.

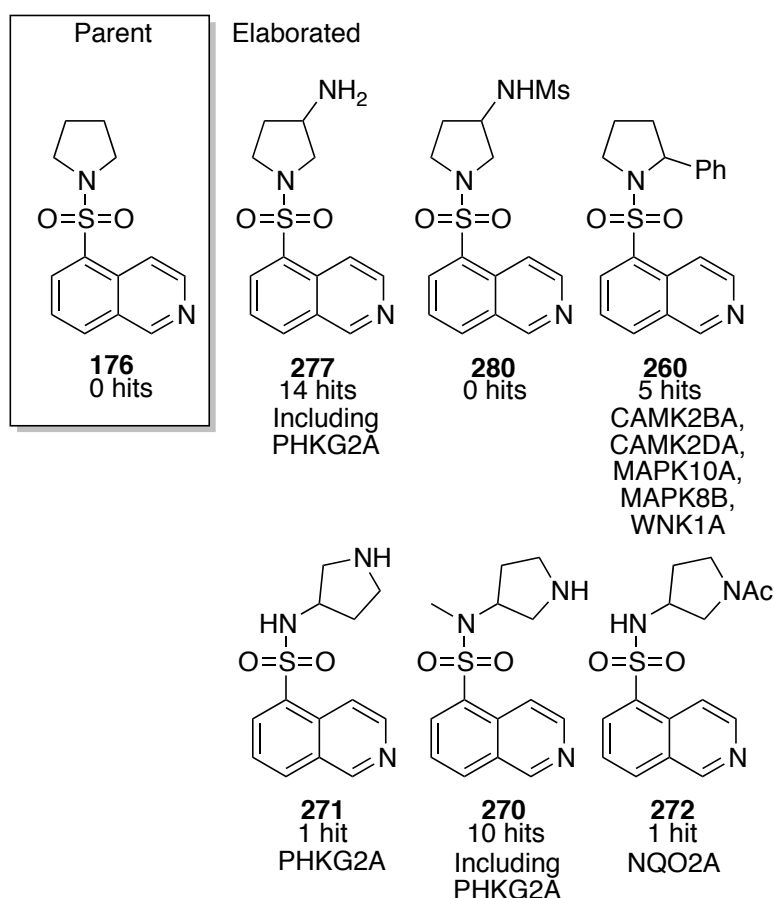


Figure 49: Selected examples with **176** as the parent fragment.

4.2.1.3.4 Acyclic Amines

Parent dimethylamino purine **294** gave 14 hits. Replacement of one of the methyl groups with an ethyl substituent (**292**) gave 56 hits, with **294** sharing 94% of its hits with **292**. The higher hit rate could be attributed to an increase in solubility of the compound since both fragments have a similar lipophilicity (AlogP of 1) but the ethyl compound may not pack as tightly in the solid form. Although the high hit rate of **292** is interesting, the fragment is not a selective compound and would not be suitable for further development towards a selective inhibitor.

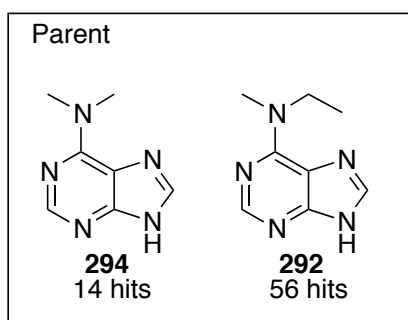


Figure 50: Structure of **294** and **292** and their hit rates.

4.2.1.3.5 Bicyclic Amines

Changing from the fused cyclopentane in **155** to the fused *N*-methylpyrrolidine in **156**, the number of kinase hits increase from 2% to 45% (Figure 51). The higher hit rate of **156** could be attributed to either an increase in compound solubility aiding screening, or the presence of a protonated amine substituent, which may provide an additional binding interaction within the kinase pocket.²⁵⁹

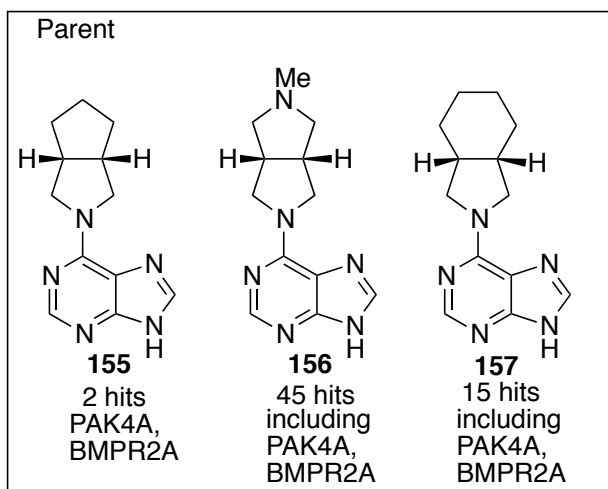


Figure 51: Parent fragment **155** and related bicycle fragments **156** and **157**.

4.2.1.4 Evaluation of Other Selected Amine Components

Fragment **167** was our most potent hit in the biochemical screen against Aurora-A (Chapter 3). In this screen, **167** displayed binding against a single kinase, TTKA. Although Aurora-A was not considered in this screen, Aurora-B was part of the kinase panel. This suggests that **167** may display selectivity

between members of the Aurora kinase family. To confirm this, full dose-dependent activity would need to be completed. Fragment **291** was not a hit against any kinases, indicating the purine motif is important for kinase binding.

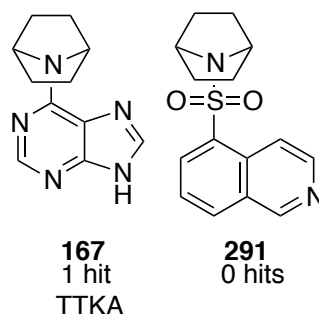


Figure 52: Structure and binding of **167** and **291**

On changing the heteroaromatic warhead from purine to isoquinoline-5-sulfonyl for a common amine (3-aminopyrrolidine) in **275** to **277**, an increased hit rate is observed. We noted previously that the purine scaffold was more promiscuous than the isoquinoline-5-sulfonyl series. An increased hit rate with **277** could be due to improved solubility relative to the purine analogue, **275**. Both fragments share a target hit with MAPKAPK2A, suggesting that the structure of the hinge binding motif is less important for this particular kinase.

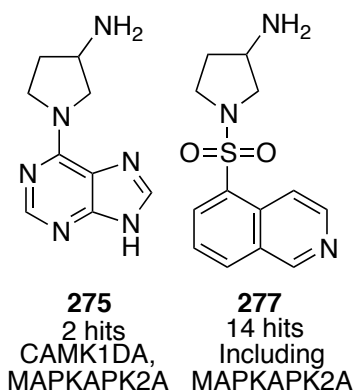


Figure 53: Structure and binding of **275** and **277**.

Fragment **292** was our most promiscuous compound, producing hits against 56 kinases. Changing the warhead to the isoquinoline-5-sulfonyl motif (**293**) there is a dramatic reduction in binding, giving one hit as CLK3A. This hit is shared between the two fragments, suggesting preference of the aromatic portion of the fragment is less important for this kinase. The isoquinoline-5-

sulfonyl compound displays a more selective profile, which is consistent with our earlier observations on the promiscuity of the purine series.

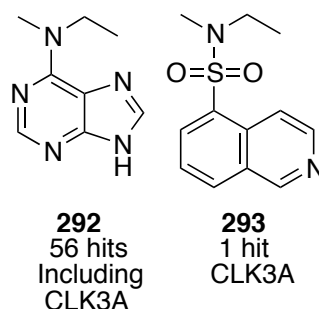


Figure 54: Structure and binding of **292** and **293**.

4.3 Conclusion

Each compound was screened at 200 mM and a T_M value was obtained for each kinase. Active compounds were identified from a T_M value 2 S.D. above the mean. T_M was determined at a fixed concentration, which limited detailed interpretation of the data. Instead, the screen provided a snapshot of the activity of 47 compounds across 100 kinases, yielding hits for 87% of kinases, with the kinase binding of each compound was shown in a heat map (Appendix 5). From this we recognised that the purine series produced the greater number of hits than the isoquinoline-5-sulfonyl series. The purine series contained the two most promiscuous fragments, accounting for 47% of all hits found in the screen.

We found that the 35-parent fragments were responsible for hits against 81 different protein kinases, with the 12-elaborated compounds responsible for accessing an additional 6 kinases. On analysis of parent fragment-elaborated fragment pairs, we saw in some cases selectivity can be tuned (**271**, **277**, **270**), but some fragments became less selective on exploration of related compounds (e.g. **292**, **293**). However, confirmation of these trends would only come with full dose-dependent analysis.

The aim of this work was to appreciate selectivity patterns within the compound libraries. However, screening our fragments in a target blind manner has meant we were able to identify inhibitors for new protein targets we had not previously considered e.g. PHKG2. We were able to identify four previously unreported compounds which target PHKG2, which were structurally related.

A critical consideration for the analysis of our data is when addressing highly promiscuous targets or those targets which are difficult to identify hits. If all fragments elicit a similar but significant change in the absolute T_M value, then 2 S.D above the mean would therefore mean these active compounds would be ignored. With this in mind, future data analysis could consider the absolute change in T_M alongside the mean and 2 S.D criteria.

Ultimately this work forms the first step in identifying compounds which could be further elaborated, towards generating selective kinase inhibitors which could have applications in inhibitor or chemical probe design. This fragment screening process has enabled the triaging of compounds for future work.

4.4 Future Work

Future work would concern the determination of solubility e.g. kinetic solubility of all of the fragments screened to ensure accurate profiling and to ensure all hits have been identified.

For the active compounds, confirmation of their activity and their binding mode would be required. An additional but narrowed panel screen could be completed to confirm the activity and selectivity found within this screen. The most active or selective compounds resulting from this panel screen could then be progressed towards IC_{50} determination. Structural studies can then uncover the mode of inhibition. The focus of the structural studies will be determined by the availability of the protein crystal, the ligand efficiency of the

elaborated fragment compound and the extent of previously reported structures, prioritising the study of underexplored kinases.

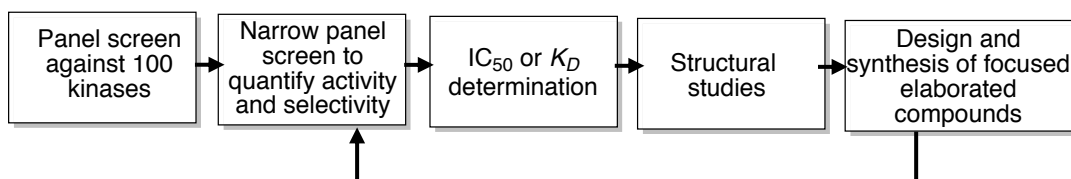
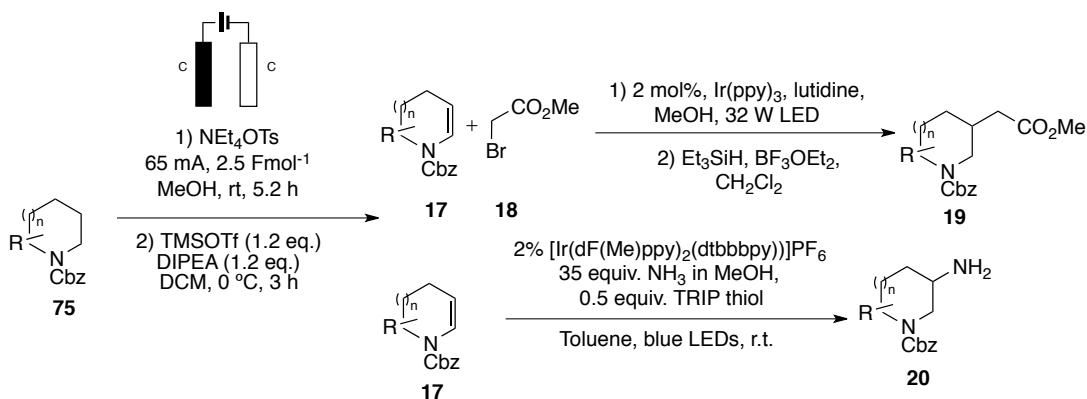


Figure 55: Workflow for the future work on this project

For example, compound **271** identified through this screen seems a rational starting point for developing a selective inhibitor of PHKG2. A next step could look at profiling **271** and the structurally related analogues against a panel of kinases to validate hits using a different assay format. If **271** was still a selective hit, it could move into full IC_{50} determination, subsequently followed by the design and synthesis of analogues of **271** towards generating a selective chemical tool for PHKG2 kinase.

5 Chapter 5: Thesis Conclusion

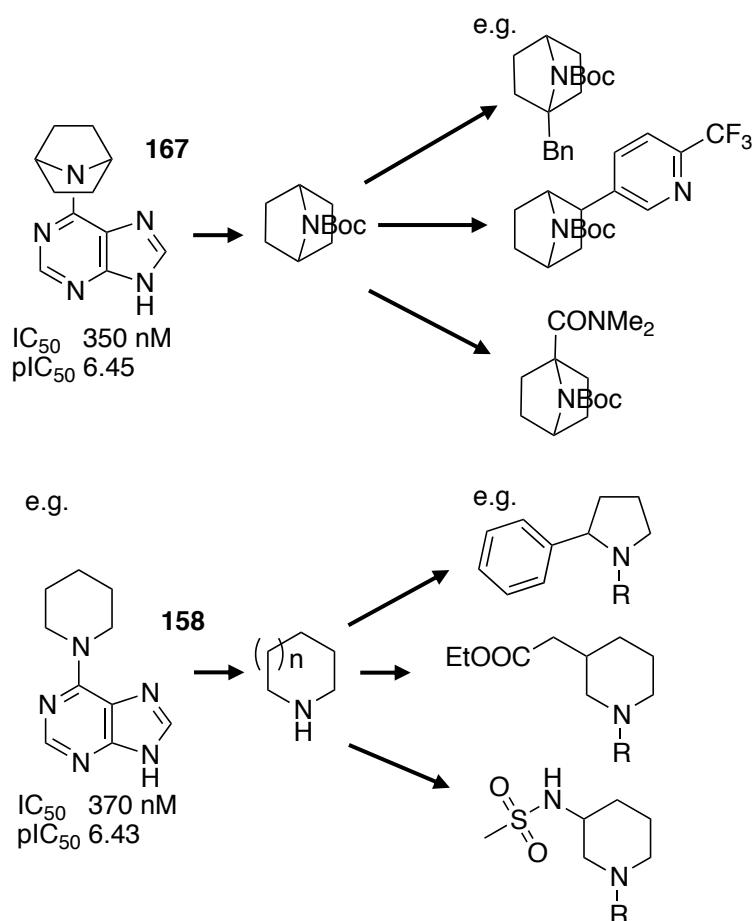
In the course of these studies, we have extended the toolkit for fragment-oriented synthesis and showcased this approach in the investigation of fragments targeting kinases. We have developed a procedure for the synthesis of endocyclic enecarbamates via electrochemical oxidation of protected cyclic amines (Chapter 2). Methodology used to access enecarbamates is well-defined, however at the outset, the synthesis of functionalised endocyclic enecarbamates including their regioselective formation, was still relatively under-explored. The method developed proved robust across a broad range of substrates, for example varying protecting groups, ring size and the inclusion of β -heteroatoms. We observed regioselective oxidation for both α - and β -substituted cyclic amines, with the origin of the surprisingly high regioselectivity for β -substituted substrates explored using DFT. The resulting enecarbamates can then feed into the fragment growth strategies reported within the Nelson and Marsden groups, to incorporate medicinally relevant functionality at the β -carbon atom.^{104,105}



Scheme 51: General workflow toward elaborated amines via enecarbamate intermediates.

To realise the importance of the developed methodology from within this project and the subsequent elaboration strategies reported within the Nelson and Marsden groups, we opted to design, synthesise and screen a library of fragments towards developing inhibitors of Aurora-A kinase (Chapter 3).

The fragments were designed through analysis of the literature to identify key warheads, to which was attached cyclic amine functionality, capable of elaboration by the above strategies, should hits have been identified. Following synthesis and screening using a functional assay (EZ-reader II mobility-shift assay), we identified 30 hits against Aurora-A kinase, a hit rate of 86%. We initially focused on the elaboration of the most potent fragment, by elaborating the azabicyclic of **167**. Since literature reported methods to functionalise azabicyclic **198** were limited, work sought to identify suitable methods to install medicinally relevant functionality along the α - and β -vectors of **198**. We obtained six novel amines, but after thorough efforts, were unable to attach the warhead needed to prepare fragments from these amines.



Methodology from Chapter 2

Figure 56: Sample Fragment hits and sample elaborated analogues. Analogues were elaborated using methodology from Chapter 2. Where R = Purine.

Our attention turned to the elaboration of simple amines, e.g. **158**, **178**. Using the methods for α - and β -elaboration of cyclic amines (Chapter 2), we created a 19-membered elaborated fragment library for screening. Screening of 9-compounds of that elaborated library were screened and had activity against Aurora-A, but with a reduction in potency observed versus the parent fragments. Although elaboration along these vectors did not yield an improvement in potency, this study exemplifies that the underpinning synthetic chemistry discussed in Chapter 2 has enabled efficient exploration of the chemical space around the cyclic amine. These synthetic strategies should have wider use in FBLD.

Lastly, we profiled the fragment libraries from Chapter 3 against a panel of 100-kinases (Chapter 4). From this, we elucidated that these fragments may show some selectivity between members of the highly conserved Aurora kinase family, offering scope for selective inhibitor development. This study also identified potential new kinase targets to which to apply our synthetic methodology (Chapter 2) with in the future. We noted that in some cases, chemical elaboration of the fragments tuned the overall kinase selectivity of the compound. Overall, this investigation has provided a foundation for more comprehensive selectivity studies on our fragments and their elaborated analogues towards not only developing Aurora-A inhibitor, but also selective inhibitors of additional kinases.

6 Experimental

6.1 General Information

Dichloromethane, toluene, methanol, THF and acetonitrile were dried under nitrogen using a PureSolv MD5 solvent purification System. All reactions were performed in oven-dried glassware under nitrogen atmosphere. All other reagents were purchased from commercial sources like Aldrich, Alpha-Aesar or Fluorochem and used without further purification, unless specified. An IKA RV 10 rotary evaporator was used to remove the solvents under reduced pressure. Electrochemical experiments were performed on an IKA Electrasyn 2.0. The Electrasyn vial was sealed with an ElectraSyn Teflon cap fitted with a graphite anode and graphite cathode, and reactions were stirred with Teflon-coated magnetic stirrer bars. The photoredox catalysts were purchased from Aldrich. Photochemical reactions were carried out using a Kessil lamp (32W, model H150) without external cooling, unless specified.

Preparative thin layer chromatography (TLC) plates were prepared with silica gel 60 GF254 Merck. Reaction mixtures were analysed by TLC using ALUGRAM® SIL G/UV254, and visualisation of TLC spots was achieved using ultraviolet (UV) and potassium permanganate solution. Nuclear magnetic resonance (NMR) spectra were recorded in a Bruker AV3 operating at 7.05 T (300 MHz ^1H , equipped with a 5 mm BBO probe), a Bruker AV3HD operating at 9.4 T (400 MHz ^1H , equipped with a 5 mm BBO probe), Bruker AV4-NEO operating at 11.7 T (500 MHz ^1H , equipped with a 5 mm DCH cryoprobe). Data was collected using CDCl_3 , CD_3OD and $(\text{CD}_3)_2\text{SO}$ as solvents and $(\text{CH}_3)_4\text{Si}$ (^1H) as internal standard. Data was collected at 300 K unless otherwise stated. Chemical shifts (δ) are given in parts per million (ppm) and they are referenced to the residual solvent peak. All coupling constants are expressed in Hz, splitting patterns are reported in an abbreviated manner: app. (apparent), s (singlet), d (doublet), t (triplet), q (quartet), m (multiplet), br (broad). Assignments were made using COSY,

DEPT, HMQC and NOESY experiments. Electrospray ionization (ESI) mass spectra were recorded in a mass spectrometer (Micromass Quattro Micro API, Waters, Ireland) with a Triple Quadrupole (TQ) and with an electrospray ion source operating in positive mode. A Bruker Daltonics micrOTOF spectrometer with electrospray (ES) ionisation source was used for high-resolution mass spectrometry (HRMS). Infrared spectra were recorded on a Bruker alpha FT-IR spectrometer using a "platinum ATR" accessory and were reported in wavenumbers (cm^{-1}). Melting points (m.p.) were determined using Stuart melting point apparatus SMP3.

6.2 General Procedures

6.2.1 General Procedure 1: α -C–H Bond Functionalization of Substituted Cyclic Amines via Intermolecular Hydride Transfer¹¹³

To a solution of the amine (1 mmol, 1.0 eq.) in anhydrous ether (2 mL) cooled to -78 °C was slowly added *n*-BuLi in hexanes (1 mmol, 1.0 eq.) under the protection of nitrogen, and the resulting solution was allowed to stir at the same temperature for 10 min. To this was then slowly added via cannula, a solution of the corresponding hydride acceptor (1.2 mmol, 1.2 eq.) in anhydrous Et₂O (1 mL). The resulting mixture was allowed to continue stirring at -78 °C for the indicated time followed by the slow addition of phenyllithium (1.5 mmol, 1.5 eq.). The reaction mixture was then allowed to warm to rt and stirring was continued for another 2 h before quenching via the addition of MeOH (1 mL) at 0 °C. The reaction mixture was diluted with ether (20 mL) and washed with H₂O (50 mL). The aqueous layer was extracted with ether (3 x 20 mL) and the combined organic layers were washed with brine (30 mL) and dried over anhydrous MgSO₄. The solvent was removed *in vacuo*. and the residue purified by flash column chromatography.

6.2.2 General Procedure 2: Metallaphotoredox-Catalysed Cross Coupling of Carboxylic Acids with Alkyl Halides Reaction¹²⁰

An oven dried 8 mL vial equipped with a Teflon septum and magnetic stir bar was charged with Ir[dF(CF₃)ppy]₂(dtbbpy)PF₆ (10.0 μ mol, 0.02 eq.), NiCl₂-glyme (0.05 mmol, 0.1 eq.), 4,4'-di-methoxy-2,2'-bipyridyl (0.05 mmol, 0.1 eq.), Boc-Pro-OH (0.75 mmol, 1.5 eq.), K₂CO₃ (1.00 mmol, 2.0 eq.) and 5 mL of MeCN. The reaction mixture was degassed by bubbling nitrogen stream for 30 min at 0 °C. Water (10.0 mmol, 20 eq.) and the alkyl halide (0.50 mmol, 1.0 eq.) were then added. The reaction mixture was then stirred and irradiated

with two 34 W blue LEDs (vials approximately 6 cm away from the light source) with a fan placed above for cooling. After 48 h, the reaction mixture was diluted with EtOAc, filtered, and concentrated *in vacuo*. Purification of the crude product by flash chromatography on silica gel using the indicated solvent system afforded the desired product.

6.2.3 General Procedure 3: for enamide synthesis via electrochemical oxidation/elimination

An Electrasyn vial (10 mL) with a stir bar was charged with Cbz-protected amine (4.57 mmol), in anhydrous methanol (10 mL) containing tetraethylammonium tosylate (83 mg, 0.28 mmol) and the mixture was electrolysed (graphite electrodes) under a constant current of 200 mA (terminal voltage 1-2 V) at 25 °C. After the passage of 2.5 Fmol⁻¹ of electricity, the mixture was concentrated *in vacuo*. The residue was taken up in anhydrous dichloromethane (0.5 M) and transferred to 100 mL RBF and placed under an inert atmosphere. Me₃SiOTf (1.8 mL, 10.0 mmol) was added dropwise over 10 minutes to the ice-cooled solution of electrolysed amine and ⁱPr₂NEt (10.0 mmol) in DCM (0.5 M) over 10 minutes. After 3 hours the reaction mixture was diluted with 40 mL of hexane. The reaction was filtered through a pad of celite and concentrated *in vacuo* to give a crude residue.

6.2.4 General Procedure 4: Synthesis of purine fragments

A solution of Et₃N (0.9 mL, 6.50 mmol), amine (3.90 mmol) and 6-chloropurine (500 mg, 3.25 mmol) in EtOH (20 mL) was heated at 80 °C (EtOH) for 1-10 h. The reaction mixture was cooled to give a crude product in a solution in EtOH.

6.2.4.1 General Procedure 5: Synthesis of sulfonyl isoquinoline fragments

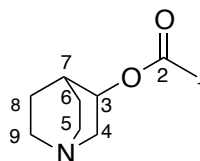
A solution of Et₃N (1.22 mL, 6.63 mmol), cyclic amine (3.32 mmol) and isoquinoline-5-sulfonyl chloride (500 mg, 2.21 mmol) in EtOH (20 mL) was stirred at room temperature for 18 h. The solvent was then removed *in vacuo* to give a solid.

6.2.4.2 General Procedure 6: Synthesis of pyrimidine fragments

A solution of Et₃N (0.9 μL, 5.25 mmol), cyclic amine (2.25 mmol) and 2-chloro-6-methylpyrimidin-4-amine (250 mg, 1.75 mmol) in THF (20 mL) and water (5 mL) was stirred at room temperature for 48 h. The solvent was then removed *in vacuo* to give a crude solid.

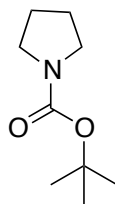
6.3 Characterisation of Compounds

Quinuclidin-3-yl acetate (22)¹¹⁰



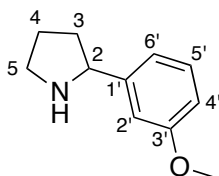
A 250 mL round-bottomed flask equipped with a magnetic stirring bar was charged with quinuclidin-3-ol (1.50 g, 11.8 mmol) and acetic anhydride (7.5 mL) and the solution was heated to reflux for 4 h. The reaction mixture was cooled to room temperature and concentrated *in vacuo*. Sat. aq. NaHCO₃ (7.5 mL) and CHCl₃ (5 mL) were added, and the solution was stirred vigorously for 20 minutes. The layers were separated, and the aqueous portion was further extracted with 10% IPA/CHCl₃ (5 × 10 mL). The organic extracts were combined, dried over Na₂SO₄ and concentrated *in vacuo*. The residue was diluted with CHCl₃ (5 mL) and stirred vigorously again with sat. aq. NaHCO₃ for 2 minutes. The layers were separated, and the aqueous portion was further extracted with 10% IPA/CHCl₃ (5 × 100 mL). The organic extracts were combined, dried over Na₂SO₄ and concentrated *in vacuo*. The residue was purified by distillation under high vacuum (65-70 °C, 100 mTorr) to provide the *title compound* as a colourless oil (1.35 g, 8.02 mmol, 68% yield). IR ν_{max} (neat) / cm⁻¹ 3870, 3621, 3328, 3200, 3003, 2944, 2628, 2098, 1726 1445 and 1376; δ_{H} (400 MHz, CDCl₃) 4.62 (1H, dtd, *J* 8.4, 3.5, 1.3, 3-H), 3.08 (1H, ddd, *J* 14.7, 8.4, 2.3, 4-H_A), 2.83 – 2.42 (5H, m, 4-H_B, 5-H, 9-H), 1.91 (3H, s, 1-H), 1.83 (1H, q, *J* 3.3, 7-H), 1.68 (1H, dddd, *J* 13.0, 10.2, 5.5, 2.8, 6-H_A), 1.63 – 1.48 (1H, m, 8-H_A), 1.40 (1H, dddd, *J* 13.3, 10.4, 5.9, 2.9, 8-H_B), 1.23 (1H, dddd, *J* 14.4, 7.2, 3.4, 1.6, 6-H_B). δ_{C} (101 MHz, CDCl₃) 170.6 (C=O C2), 71.2 (C-3), 55.4 (C-4), 47.3 (C-5 or C-9), 46.8 (C-5 or C-9), 25.1 (C-7), 24.8 (C-1), 21.0 (C-6 or C-8), 19.4 (C-6 or C-8); HRMS C₉H₁₆NO₂⁺ [M+H]⁺ calc., 170.1186 found, 170.1178. Data in accordance with literature.¹¹⁰

***N*-(*tert*-Butyl)pyrrolidine-1-carboxamide (**23**)¹¹⁰**



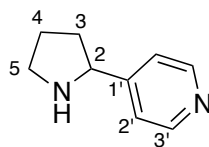
A 50 mL round-bottom flask was charged with di-*tert*-butyl dicarbonate (2.1 mL, 18 mmol, 1.5 eq.), NEt₃ (2.5 mL, 18 mmol, 1.5 eq.), and pyrrolidine (0.99 mL, 12 mmol, 1.0 eq.). Dichloromethane (24 mL) was added, and the resulting colourless solution was stirred for 5 h. The reaction mixture was diluted with H₂O (30 mL) and the aqueous layer was extracted with three portions of dichloromethane (20 mL). The combined organic layers were washed with brine (30 mL), dried over MgSO₄ filtered, and concentrated *in vacuo*. The residue was purified by flash chromatography eluting with 50:50 EtOAc–hexanes to afford the pyrrolidine **23** as a colourless oil (1.9 g, 92%). IR ν_{max} (film) / cm⁻¹ 3321, 2973, 2875, 1691 and 1609; δ_{H} (400 MHz, CDCl₃) 3.07 – 2.97 (4H, m, 2-H), 1.56 – 1.50 (4H, m, 3-H), 1.14 (9H, s, ^tBu); δ_{C} (101 MHz, CDCl₃) 154.2 (Boc C=O), 78.3 (Boc C-O), 45.6 (C-2), 28.1 (C-3), 25.4 (Boc ^tBu); HRMS [M+Na]⁺ C₉H₁₇NO₂Na⁺ calc., 194.1153, found 194.1159. Data in accordance with literature.¹¹⁰

***tert*-Butyl 2-(4-methoxyphenyl)pyrrolidine-1-carboxylate (**29**)**



An 8 mL vial equipped with a magnetic stirring bar was charged with 4-bromoanisole (94 mg, 0.50 mmol, 1.0 eq.) and Ir[dF(CF₃)ppy]₂(dtbbpy)PF₆ (5.6 mg, 5.0 μmol, 1.0 mol%). Anhydrous DMSO (1.0 mL) and 3-acetoxyquinuclidine **22** (85 μL, 0.55 mmol, 1.1 eq.) were added. 4,7-Dimethoxy-1,10-phenanthroline (1.2 mg, 5.0 μmol, 1.0 mol%) and nickel(II) bromide trihydrate (1.4 mg, 5.0 μmol, 1.0 mol%) were added as a 0.50 M stock solution in anhydrous DMSO (1 mL, sonicated for 10 minutes before addition). *N*-Boc pyrrolidine **23** (175 μL, 1.0 mmol, 2.0 eq.) and water (360 μL, 20 mmol, 40 eq.) were added before the mixture was degassed via two cycles of freeze-pump-backfill-thaw. The reaction was sealed and placed ~6 cm away from a 34 W blue LED and stirred for 24 h with cooling by fan. The reaction mixture was removed from the light, diluted with aq. NaHCO₃ and EtOAc, and the aqueous layer was extracted with three portions of EtOAc. The combined organic layers were dried over MgSO₄, filtered, and concentrated. The residue was purified by flash chromatography (5% EtOAc–hexanes) to afford a colourless oil. The residue was dissolved in dichloromethane (15 mL) and TFA (5 mL) and stirred at rt for 3 h. The solvent was removed *in vacuo* to afford pyrrolidine **29** as a colourless oil (63 mg, 63% yield). IR ν_{\max} (neat) / cm⁻¹ 13164, 3003, 2944, 2628, 2570, 2499, 2253 and 1375; δ_{H} (400 MHz, CDCl₃) 7.32 – 7.15 (1H, m, 5'-H), 7.02 – 6.88 (2H, m, 2'-H, 6'-H), 6.78 (1H, ddd, *J* 8.2, 2.6, 1.0, 4'-H₂), 4.10 (1H, t, *J* 7.7, 2-H), 3.81 (3H, s, OCH₃), 3.20 (1H, ddd, *J* 10.1, 7.7, 5.2, 5-H₂), 3.01 (1H, ddd, *J* 10.1, 8.2, 6.7, 5-H₃), 2.25 – 2.12 (1H, m, 3-H_A), 2.12 – 1.77 (2H, m, 3-H_B, 4-H₂), 1.67 (1H, ddt, *J* 12.2, 9.3, 7.8, 4-H₃). δ_{C} (101 MHz, CDCl₃) 159.7 (C-3'), 146.7 (C-1'), 129.3 (C-5'), 118.8 (C-6'), 112.2 (C-2'), 112.1 (C-4'), 62.6 (C-2), 55.2 (C-3' CH₃), 47.0 (C-5), 34.4 (C-3), 25.6 (C-4). HRMS [M+Na]⁺ C₁₁H₁₅NONa⁺ 194.1153, predicted 194.1159.

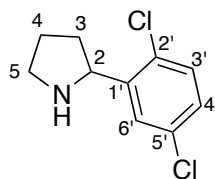
4-(pyrrolidin-2-yl)pyridine (**30**)¹¹⁰



An 8 mL vial equipped with a magnetic stirring bar was charged with 4-bromopyridine.HCl (97 mg, 0.50 mmol, 1.0 eq.) and Ir[dF(CF₃)ppy]₂(dtbbpy)PF₆ (5.6 mg, 5.0 μmol, 1.0 mol%). Anhydrous DMSO (3.0 mL) and 3-acetoxyquinuclidine (162 μL, 1.05 mmol, 2.1 eq.) were added. 4,7-Dimethoxy-1,10-phenanthroline (1.2 mg, 5.0 μmol, 1.0 mol%) and nickel(II) bromide trihydrate (1.4 mg, 5.0 μmol, 1.0 mol%) were added as a 0.50 M stock solution in anhydrous DMSO (1 mL, sonicated for 10 minutes before addition). *N*-Boc pyrrolidine (175 μL, 1.0 mmol, 2.0 eq.) and water (901 μL, 50 mmol, 100 eq.) were added before the mixture was degassed via two cycles of freeze-pump-backfill-thaw. The reaction was sealed and placed ~6 cm away from a 34 W blue LED and stirred for 8 h with cooling by fan. The reaction mixture was removed from the light, diluted with aq. NaHCO₃ and EtOAc (10 mL) and the aqueous layer was extracted with three portions of EtOAc. The combined organic layers were dried over MgSO₄, filtered, and concentrated *in vacuo*. The residue was purified by flash chromatography (20:80 EtOAc–hexane) to afford the title compound as a pale-yellow oil. The residue was dissolved in dichloromethane (15 mL) and TFA (5 mL) and stirred at rt for 3 hours. The solvent was removed *in vacuo*. The residue was dissolved in dichloromethane (2 mL) and loaded onto a 1 g SCX cartridge, and the cartridge flushed with MeOH (3 × 20 mL). The product was eluted using ammonia (1 M solution in MeOH, 3 × 20 mL) which was concentrated *in vacuo* to afford pyrrolidine **30** as a brown oil (50.0 mg, 0.34 mmol, 67%). IR ν_{max} (neat) / cm⁻¹ 2998, 2944, 2056 and 1375; δ_{H} (400 MHz, CDCl₃) 8.25 (2H, dd, *J* 3.9, 1.7, 3'-H), 7.08 – 6.99 (2H, m, 2'-H), 3.88 (1H, td, *J* 7.7, 3.3, 2-H), 2.89 (1H, m, 5-H), 2.84 – 2.72 (1H, m, 5-H), 1.96 (1H, ddd, *J* 12.2, 8.0, 3.7 Hz, 3-H), 1.70 – 1.49 (2H, m, 3-H, 4-H), 1.45 – 1.27 (1H, m, 4-H); δ_{C} (101 MHz, CDCl₃) 154.3 (C-1'), 149.6 (C-3'), 121.5 (C-2'), 60.9 (C-2), 46.8 (C-5), 34.1 (C-3), 25.3 (C-4). HRMS

[M+H]⁺ C₉H₁₃N₂⁺ calc., 149.1084, found 149.1079. Data in accordance with literature.¹¹⁰

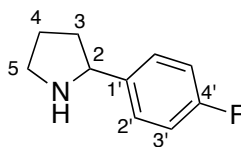
2-(2,5-Dichlorophenyl)pyrrolidine (31)



An 8 mL vial equipped with a magnetic stirring bar was charged with 12-bromo-1,4-dichlorobenzene (111.5 mg, 0.50 mmol, 1.0 eq.) and Ir[dF(CF₃)ppy]₂(dtbbpy)PF₆ (5.6 mg, 5.0 μmol, 1.0 mol%). Anhydrous DMSO (3.0 mL) and 3-acetoxyquinuclidine (162 μL, 1.05 mmol, 2.1 eq.) were added. 4,7-Dimethoxy-1,10-phenanthroline (1.2 mg, 5.0 μmol, 1.0 mol%) and nickel(II) bromide trihydrate (1.4 mg, 5.0 μmol, 1.0 mol%) were added as a 0.50 M stock solution in anhydrous DMSO (1 mL, sonicated for 10 minutes before addition). *N*-Boc pyrrolidine **23** (175 μL, 1.0 mmol, 2.0 eq.) and water (901 μL, 50 mmol, 100 eq.) were added before the mixture was degassed via two cycles of freeze-pump-backfill-thaw. The reaction was sealed and placed ~6 cm away from a 34 W blue LED and stirred for 8 h with cooling by fan. The reaction mixture was removed from the light, diluted with aq. NaHCO₃ and EtOAc, and the aqueous layer was extracted with three portions of EtOAc. The combined organic layers were dried over MgSO₄, filtered, and concentrated. The residue was purified by flash chromatography (60:40 EtOAc–hexane) to afford a pale-yellow oil. The residue was dissolved in dichloromethane (15 mL) and TFA (5 mL) and stirred at rt for 3 h. The solvent was removed *in vacuo* and residue was dissolved in dichloromethane (2 mL) and loaded onto a 1 g SCX cartridge, and the cartridge flushed with MeOH (3 × 20 mL). The product was eluted using ammonia (1 M solution in MeOH, 3 × 20 mL) which was concentrated *in vacuo* as a brown oil (37.0 mg, 34%). IR ν_{max} (neat) / cm⁻¹ 3164, 3003, 2495, 2627, 2559, 2408, 2367, 2253 and 1375. δ_{H} (400 MHz, CDCl₃) 7.91 (1H, d, *J* 2.4, 6'-H), 7.36 (1H, d, *J* 8.6, 3'-H), 7.28 (1H, dd, *J* 8.6, 2.3, 4'-H), 4.94 (1H, dd, *J* 9.1, 6.9, 2-H), 3.64 (1H, dt, *J* 11.6, 7.5 Hz, 5-H), 3.47 (1H, ddd, *J* 11.7, 8.4, 5.6, 5-H), 2.58 – 2.41 (1H, m, 4-H), 2.32 – 1.99 (3H, m, 3-H, 4-H); δ_{C} (101 MHz, CDCl₃) 134.2 (C-1'), 133.6 (C-2'

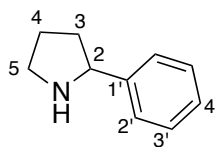
or C-5'), 131.8 (C-2' or C-5'), 131.2 (C-3'), 130.4 (C-6'), 128.2 (C-4'), 59.5 (C-2), 45.5 (C-5), 31.6 (C-4), 23.4 (C-3); HRMS (ESI): C₁₀H₁₂³⁵Cl₂N [M+H]⁺ 216.0306, predicted 216.0302.

2-(4-Fluorophenyl)pyrrolidine (**32**)



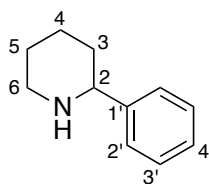
An 8 mL vial equipped with a magnetic stirring bar was charged with 1-bromo-4-fluorobenzene (86.5 mg, 0.50 mmol, 1.0 eq.) and Ir[dF(CF₃)ppy]₂(dtbbpy)PF₆ (5.6 mg, 5.0 μmol, 1.0 mol%). Anhydrous DMSO (3.0 mL) and 3-acetoxyquinuclidine (162 μL, 1.05 mmol, 2.1 eq.) were added. 4,7-Dimethoxy-1,10-phenanthroline (1.2 mg, 5.0 μmol, 1.0 mol%) and nickel(II) bromide trihydrate (1.4 mg, 5.0 μmol, 1.0 mol%) were added as a 0.50 M stock solution in anhydrous DMSO (1 mL, sonicated for 10 minutes before addition). *N*-Boc pyrrolidine (175 μL, 1.0 mmol, 2.0 eq.) and water (901 μL, 50 mmol, 100 eq.) were added before the mixture was degassed via two cycles of freeze-pump-backfill-thaw. The reaction was sealed and placed ~6 cm away from a 34 W blue LED and stirred for 8 h with cooling by fan. The reaction mixture was removed from the light, diluted with aq. NaHCO₃ and EtOAc (10 mL), and the aqueous layer was extracted with three portions of EtOAc. The combined organic layers were dried over MgSO₄, filtered, and concentrated. The residue was purified by flash chromatography (60:40 EtOAc–hexane) to afford a pale-yellow oil. The residue was dissolved in dichloromethane (2 mL) and loaded onto a 1 g SCX cartridge, and the cartridge flushed with MeOH (3 × 20 mL). The product was eluted using ammonia (1 M solution in MeOH, 3 × 20 mL) which was concentrated *in vacuo* to afford pyrrolidine **32** as a brown oil (57.6 mg, 0.35 mmol, 70%). IR ν_{\max} (film) / cm⁻¹ 3003, 2944, 2874, 2253, 1441 and 1375; δ_{H} (400 MHz, CDCl₃) 7.18 (2H, dd, *J* 5.5, 2.6, 3'-H), 6.96 – 6.77 (2H, m, 2'-H), 3.92 – 3.85 (1H, m, 2-H), 3.11 – 2.94 (1H, m, 5-H₂), 2.89 – 2.76 (1H, m, 5-H₃), 2.05 – 1.92 (1H, m, 3-H_A), 1.83 – 1.59 (2H, m, 3-H_B, 4-H₂), 1.46–1.39 (1H, m, 4-H₃); δ_{C} (101 MHz, CDCl₃, decoupled) 155.4 (C-4'), 145.8 (C-1'), 127.9 (C-2'), 124.6 (C-3'), 56.9 (C-2), 51.0 (C-5), 45.4 (C-4), 45.4 (C-3). HRMS [M+H]⁺ C₁₀H₁₃FN⁺ 166.1038, found 166.1038. Spectral data of ¹H and ¹³C in accordance with literature.²⁶⁰

2-Phenylpyrrolidine (**46**)¹¹³



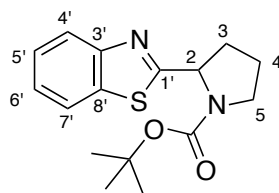
Following general procedure **1** using pyrrolidine (82 mL, 1.0 mmol, 1.0 eq.) and phenyllithium (0.20 mL, 1.5 mmol, 1.5 eq.) with benzophenone (219 mg, 1.2 mmol, 1.2 eq.) as the hydride acceptor. The hydride transfer time was 10 min. Purification by flash column chromatography eluting with 90:9:1 EtOAc–Hexanes–NEt₃, to afford pyrrolidine **46** as a yellow oil (96.3 mg, 0.65 mmol, 65%). IR ν_{max} (film) / cm⁻¹ 3000, 2944, 2097, 1603 and 1508; δ_{H} (400 MHz, CDCl₃) 7.43 – 7.06 (5H, m, 1'-H, 2'-H, 3'-H, 4'-H), 4.03 – 3.97 (1H, m, 2-H), 3.14 – 3.05 (1H, m, 5-H), 2.97 – 2.82 (1H, m, 5-H), 2.25 (1H, s, NH), 2.18 – 2.01 (1H, m, 3-H_A), 1.93 – 1.70 (2H, m, 3-H_A, 4-H₂), 1.66 – 1.50 (1H, m, 4-H₃); δ_{C} (101 MHz, CDCl₃) 144.9 (C-1'), 128.3 (C-2', C-3'), 126.6 (C-2', C-3'), 126.5 (C-4'), 62.5 (C-2), 46.9 (C-5), 34.3 (C-3), 22.7 (C-4); HRMS C₁₀H₁₄N⁺ [M+H]⁺ calc., 148.1125, found 148.1120. Spectral data in accordance with literature.¹¹³

2-Phenylpiperidine (**47**)¹¹³



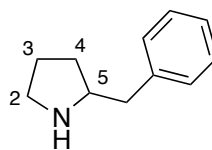
Following the general procedure **1**, 2-phenylpiperidine was obtained from piperidine (99 mL, 1.00 mmol, 1.0 eq.) and phenyllithium (0.2 mL, 1.5 mmol, 1.5 eq.) using benzophenone (0.20 mL, 1.2 mmol, 1.2 eq.) as the hydride acceptor. The hydride transfer time was 1.5 h. Purification by flash column chromatography eluting with 90:9:1 EtOAc–hexanes–NEt₃, to afford piperidine **47** as a colourless oil (122 mg, 0.72 mmol, 75%). δ_{H} (400 MHz, CDCl₃) : 7.48 – 7.19 (5H, m, 2'-H, 3'-H, 4'-H), 3.72 – 3.40 (1H, m, 2-H), 3.22 – 3.16 (1H, m, 6-H), 2.82 – 2.77 (1H, m, 6-H), 1.92 – 1.89 (1H, m, 3-H), 1.83 – 1.79 (1H, m, 3-H), 1.73 – 1.44 (4H, m, 4-H, 5-H). δ_{C} (101 MHz, CDCl₃) 145.6 (C-1'), 128.4 (C-2'), 127.0 (C-3'), 126.6 (C-4'), 62.4 (C-2), 47.8 (C-6), 35.1 (C-3), 26.0 (C-4), 25.5 (C-5). IR ν_{max} (neat) / cm⁻¹ 3253, 3061, 3026, 3001, 2929, 2837, 2929, 2837, 2790, 2717. HRMS: C₁₁H₁₆N [M+H⁺] 162.1286, predicted 168.1238. Spectral data in accordance with literature.

***tert*-Butyl 2-(benzo[*d*]thiazol-2-yl)azepane-1-carboxylate (52)**



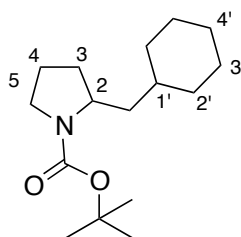
To a 10 mL glass vial was added Ir[dF(CF₃)ppy]₂(dtbbpy)PF₆ (2.24 mg, 0.002 mmol, 1 mol%), *t*-BPA (105.6 mg, 0.4 mmol, 2.0 eq., 50 wt.% solution in aromatic free mineral spirit), *N*-Boc pyrrolidine (68.5 mg, 0.4 mmol, 2.0 eq.), 2.0 mL acetone, benzo[*d*]thiazole (27.0 mg, 0.2 mmol, 1 eq.) and TFA (30 μL, 0.4 mmol, 2.0 eq.). The reaction was degassed by bubbling with nitrogen for 5 minutes with an outlet needle and sealed with a PTFE cap. The mixture was stirred and irradiated with a 36 W blue LED (approximately 2cm away from the light source) at room temperature for 24 h. The reaction was concentrated in vacuum to remove the acetone. The mixture was diluted with 2.5 mL of aqueous 1M NaOH solution and extracted with dichloromethane (3 × 10 mL). The combined organic extracts were washed with brine (20 mL) dried over MgSO₄ and concentrated *in vacuo*. Purification of the crude product by flash column chromatography eluting with 20:80 EtOAc–hexane to afford pyrrolidine **52** (35.9 mg, 59%) as a yellow oil, *R*_f 0.48 (EtOAc); $\nu_{\text{max}}/\text{cm}^{-1}$ 1743; δ_{H} (400 MHz, CDCl₃) 7.91 (1H, dd, *J* 10.5, 8.0, 4'-H), 7.87 – 7.69 (1H, m, 7'-H), 7.49 – 7.26 (2H, m, 5'-H, 6'-H), 5.36 – 5.06 (1H, m, 2-H), 4.15 – 4.11 (2H, m, 5-H), 3.72 – 3.45 (2H, m, 3-H), 2.53 – 2.10 (2H, m, 4-H), 1.33 (9H, br, ^tBu rotamers); δ_{C} (101 MHz, CDCl₃) 180.4 (C-1'), 154.8 (Boc C=O), 154.3 (C-3'), 135.2 (C-8'), 126.1 (C-5' or C-6'), 125.0 (C-5' or C-6'), 124.9 (C-4' or C-8'), 122.8 (C-4' or C-8'), 80.5 (Boc C-O), 60.0 (C-2), 47.1 (C-5), 34.2 (C-3), 33.0 (C-4), 30.8, 28.2 (Boc ^tBu), 24.1, 23.4. 17 signals observed, owing to rotamers; HRMS: C₁₆H₂₁N₂O₂S⁺ [M+H⁺] 305.1329, predicted 305.1321. Data is in accordance with literature.¹¹⁴

2-Benzylpyrrolidine (**64**)¹¹⁸



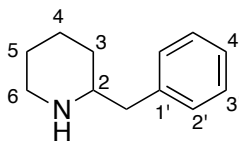
Following general procedure **2**, Ir[dF(CF₃)ppy]₂(dtbbpy)PF₆ (11.2 mg, 10.0 μmol 0.02 eq.), NiCl₂-glyme (11.0 mg, 0.05 mmol, 0.1 eq.), 4,4'-di-methoxy-2,2'-bipyridyl (10.8 mg, 0.05 mmol, 0.1 eq.), benzyl chloride (58 μL, 0.5 mmol, 1.0 eq.), Boc-Pro-OH (161 mg, 0.75 mmol, 1.5 eq.), K₂CO₃ (138 mg, 1.00 mmol, 2.0 eq.), water (180 μL, 10 mmol, 20 eq.), and 5 mL of MeCN were used. Purification by flash column chromatography eluting with 10:90 EtOAc–Hexane afforded a colourless oil. The oil was dissolved in dichloromethane (3 mL) and TFA (1 mL) and stirred for 3 h and concentrated *in vacuo*. The residue was dissolved in dichloromethane (2 mL) and loaded onto a 1 g SCX cartridge, and the cartridge flushed with MeOH (3 × 20 mL). The product was eluted using ammonia (1 M solution in MeOH, 3 × 20 mL) which was concentrated *in vacuo*, eluting with saturated NH₃/MeOH (10 mL) to afford pyrrolidine **64** as a colourless oil (41.2 mg, 56%). IR ν_{max} (neat) / cm⁻¹ 2978, 2930, 2722, 2612, 2539, 2298, 2229, 2189, 2163, 2043 and 2003; δ_{H} (400 MHz, CDCl₃) 7.38 – 6.94 (5H, m, 2'-H, 3'-H, 4'-H), 3.18 (1H, br, 2-H), 2.98 (1H, d, *J* 10.5, 7.6, 5.1, 5-H₂), 2.86 – 2.59 (3H, m, 5-H₃, benzyl CH₂), 2.42 (1H, s, NH), 1.84 – 1.49 (4H, m, 3-H, 4-H). δ_{C} (125 MHz, CDCl₃) 140.0 (C-1'), 129.0 (C-2'), 128.7 (C-3'), 126.1 (C-4'), 77.2 (C-2), 60.6 (Benzyl CH₂), 46.1 (C-5), 31.2 (C-3), 24.8 (C-4). HRMS [M+Na]⁺ C₁₁H₁₅NNa calc., 184.1107, found, 184.1104.

***tert*-Butyl 2-(cyclohexylmethyl)pyrrolidine-1-carboxylate (65)**¹¹⁸



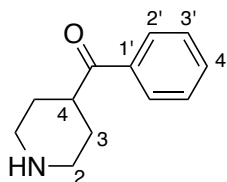
According to the general procedure **2**, Ir[dF(CF₃ppy)]₂(dtbbpy)PF₆ (11.2 mg, 10.0 μmol 0.02 eq.), NiCl₂-glyme (11.0 mg, 0.05 mmol, 0.1 eq.), 4,4'-dimethoxy-2,2'-bipyridyl (10.8 mg, 0.05 mmol, 0.1 eq.), (bromomethyl)cyclohexane (69 μL, 0.5 mmol, 1.0 eq.), Boc-Pro-OH (161 mg, 0.75 mmol, 1.5 eq.), K₂CO₃ (138 mg, 1.00 mmol, 2.0 eq.), water (180 μL, 10 mmol, 20 eq.), and 5 mL of MeCN were used. Purification by flash column chromatography eluting with 10:90 EtOAc–hexanes to give pyrrolidine **65** as a colourless oil (100 mg, 75%). IR ν_{max} (neat) / cm⁻¹ 2980, 2254, 1731, 1683 and 1478; δ_{H} (400 MHz, CDCl₃) 3.77 (1H, m, 2-H rotamers), 3.23 (2H, s, 4-H₂), 1.90 – 1.67 (4H, m), 1.67 – 1.45 (5H, m), 1.39 (9H, s, Boc ^tBu), 1.28 – 1.01 (6H, m), 0.98 – 0.73 (2H, m, 4'-H); δ_{C} (125 MHz, CDCl₃) 154.6 (Boc C=O), 78.9 (Boc C-O), 55.1 (C-2), 46.2 (C-4), 42.5, 35.3, 34.5, 32.8, 30.9, 28.6, 26.7, 26.6, 23.7. HRMS [M+Na]⁺ C₁₆H₂₉NO₂Na⁺ calc., 290.2101, found 290.2098. Spectral data in accordance with literature.¹¹⁸

2-Benzylpiperidine (67)



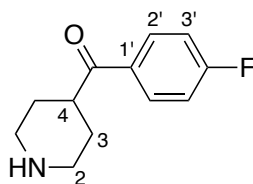
According to the general procedure **2**, Ir[dF(CF₃)ppy]₂(dtbbpy)PF₆ (13.5 mg, 12.0 μmol 0.02 eq.), NiCl₂-glyme (13.2 mg, 0.06 mmol, 0.1 eq.), 4,4'-dimethoxy-2,2'-bipyridyl (13 mg, 0.06 mmol, 0.1 eq.), benzyl chloride (68.7 μL, 0.6 mmol, 1.0 eq.), *N*-Boc-2-piperidinecarboxylic acid (110 mg, 0.6 mmol, 1.0 eq.), K₂CO₃ (166 mg, 1.2 mmol, 2.0 eq.), water (216 μL, 12 mmol, 20 eq.), and 6 mL of MeCN were used. Purification by flash column chromatography eluting with 10:90 Et₂O–Hexane to give the Boc-protected piperidine as a colourless oil. The residue was dissolved in DCM (15 mL) and TFA (5 mL), stirred at rt for 2 h and concentrated *in vacuo* to give piperidine **67** as a colourless oil (12.6 mg, 12%). IR ν_{\max} (neat) / cm⁻¹ 3357, 3048, 2877, 2293, 2253, 1500 and 1376; δ_{H} (400 MHz, CDCl₃) 7.41 – 7.11 (5H, m, 2'-H, 3'-H, 4'-H), 3.56 (2H, m, Benzyl CH₂), 3.17 (1H, tt, *J* 11.5, 3.3, 2-H), 3.06 – 2.79 (2H, m, 6-H), 2.24 – 1.93 (1H, br s, NH), 1.93 – 1.59 (4H, m, 5-H, 3-H), 1.45 – 1.21 (2H, m, 4-H); δ_{C} (125 MHz, CDCl₃) 135.7 (C-1'), 129.5 (C-2'), 128.7 (C-4'), 127.1 (C-3'), 77.3 (Benzyl CH₂), 58.6 (C-2), 44.8 (C-6), 39.6 (C-3), 27.5 (C-5), 22.3 (C-4). HRMS (ESI): C₁₂H₁₈N⁺ [M+H]⁺ 176.1453, predicted 176.1439. Data in accordance with literature.²⁶¹

4-Phenyl(piperidin-4-yl)methanone (71)



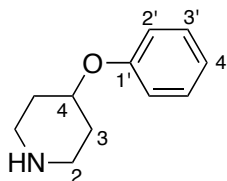
To an 8 mL vial equipped with a stir bar was added Ir[dF(CF₃)ppy]₂(dtbbpy)PF₆ (6.4 mg, 5.7 μmol, 0.01 eq.), bromobenzene (77.5 mg, 0.57 mmol, 1.0 eq.), *N*-Boc-4-piperidinecarboxaldehyde (243 mg, 1.14 mmol, 2.0 eq.), quinuclidine (6.3 mg, 5.7 μmol, 0.10 eq.), and anhydrous K₂CO₃ (118 mg, 0.86 mmol, 1.5 eq.). The vial was sealed and placed under nitrogen before 1,4-dioxane (1 mL) was added. To a separate vial was added NiBr₂.glyme (17.6 mg, 5.7 μmmol, 0.10 eq.) and 4,4'-di-*tert*-butyl-2,2'-bipyridine (15.3 mg, 5.7 μmol, 0.10 eq.). The pre-catalyst vial was sealed, purged with nitrogen, dissolved in 1,4-dioxane (2 mL) and then sonicated until it became homogeneous. Subsequently, the precatalyst solution was syringed into the reaction vessel and the solution was degassed by sparging with nitrogen for 15 minutes before sealing with parafilm. The reaction was stirred and irradiated using 34 W blue LED lamps for 24 h. The reaction was quenched by exposure to air, concentrated *in vacuo*. and dissolved in dichloromethane (10 mL) and TFA (10 mL) and stirred at rt for 1 h. The product was purified by flash column chromatography, eluting with 40:60 EtOAc–Hexane, to yield piperidine **71** as a white solid (202 mg, 84%). Mp 89 °C (EtOH); IR ν_{max} (film) / cm⁻¹ 3394, 2641, 2483, 2257, 1987 and 1290. ¹H NMR (400 MHz, CDCl₃) δ 7.34 – 7.23 (2H, m, 2'-H), 7.00 – 6.90 (3H, m, 3'-H, 4'-H), 4.39 (1H, tt, *J* 8.3, 3.8, 4-H), 3.17 (2H, dt, *J* 12.7, 4.4, 2H, 2-H₂), 2.74 (2H, ddd, *J* 12.6, 9.4, 3.2, 2-H₃), 2.03 (2H, dddd, *J* 11.8, 5.9, 3.8, 1.9, 3-H₂), 1.68 (2H, dtd, *J* 12.9, 8.9, 3.8, 3-H₃). ¹³C NMR (101 MHz, CDCl₃) δ 157.4 (C-1'), 129.5 (C-2'), 120.8 (C-4'), 116.2 (C-3'), 77.2 (C-4), 44.0 (C-2), 32.5 (C-3). HRMS [M+H]⁺ C₁₂H₁₆NO⁺ calc., 190.1237, found 190.1237. Spectral data in accordance with literature.²⁶²

4-Fluorophenyl(piperidin-4-yl)methanone (**72**)



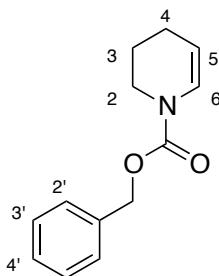
To an 8 mL vial equipped with a stir bar was added Ir[dF(CF₃)ppy]₂(dtbbpy)PF₆ (6.4 mg, 5.7 μmol, 0.01 eq.), 1-bromo-4-fluorobenzene (100 mg, 0.57 mmol, 1.0 eq.), *N*-Boc-4-piperidinecarboxaldehyde (242.8 mg, 1.14 mmol, 2.0 eq.), quinuclidine (6.3 mg, 5.7 μmol, 0.10 eq.), and K₂CO₃ (118 mg, 0.86 mmol, 1.5 eq.). The vial was sealed and placed under nitrogen before 1,4-dioxane (1 mL) was added. To a separate vial was added NiBr₂.glyme (17.6 mg, 5.7 μmol, 0.10 eq.) and 4,4'-di-*tert*-butyl-2,2'-bipyridine (15.3 mg, 5.7 μmol, 0.10 eq.). The precatalyst vial was sealed, purged with nitrogen, dissolved in 1,4-dioxane (2 mL) and then sonicated until it became homogeneous. Subsequently, the precatalyst solution was syringed into the reaction vessel and the solution was degassed by sparging with nitrogen for 15 minutes before sealing with parafilm. The reaction was stirred and irradiated using 34 W blue LED lamps for 20 hours. The reaction was quenched by exposure to air, concentrated *in vacuo*. and dissolved in DCM (1 mL) and TFA (3 mL) and stirred at rt for 1 h. The product was purified by flash column chromatography eluting with 10:90 hexane–EtOAc, to yield the piperidine **72** as a white solid (88.8 mg, 53.9%). Mp 238 °C (EtOH); IR ν_{\max} (film) / cm⁻¹ 2927, 2788, 2712, 2570 and 1284; δ_{H} (400 MHz, DMSO-*d*₆): 8.16 – 8.06 (2H, m, H-8), 7.38 (2H, dd, *J* 10.0, 7.7, 8-H), 3.79 (1H, tt, *J* 11.0, 3.6, 4-H), 3.28 (2H, dt, *J* 12.9, 3.6, 2-H₂), 3.03 (2H, td, *J* 12.6, 3.2, 2-H₃), 1.92 (2H, dd, *J* 14.5, 3.6, 3-H₂), 1.80 (2H, qd, *J* 14.5, 13.2, 4.0, 3-H₃). δ_{C} (101 MHz, DMSO-*d*₆) 200.4 (Ketone C=O), 166.9 (C-1'), 164.4 (C-4'), 132.3 (C-2' and C-3'), 70.2 (C-4), 42.7 (C-2), 25.4 (C-3). HRMS C₁₂H₁₅FNO⁺ [M+H]⁺ calc., 208.1143, found 208.1150. Spectral data in accordance with literature.²⁶³

4-Phenoxypiperidine (**74**)



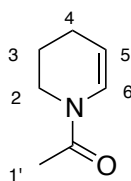
To an 8 mL vial containing a solution of the bromobenzene (157 mg, 1.00 mmol, 1.0 eq.), quinuclidine (11.1 mg, 0.100 mmol, 0.1 eq.), Ir[dF(Ir[dF(CF₃)ppy]₂(dtbbpy)PF₆ (11.2 mg, 0.01 mmol, 0.01 eq.) and K₂CO₃ (138 mg, 1.00 mmol, 1.0 eq) in MeCN (2.0 mL) was added a solution of NiCl₂.DME (11.0 mg, 0.05 mmol, 0.05 eq.) and 4,4'-di-methoxy-2,2'-bipyridyl (13.4 mg, 0.05 mmol, 0.05 eq.) in MeCN (4 mL). The vial was placed under an atmosphere of nitrogen, then the was *tert*-butyl 4-hydroxypiperidine-1-carboxylate (300 mg, 1.0 mmol, 1.0 eq.) was added. The reaction mixture was then cooled to -78 °C and degassed by vacuum evacuation (5 min), backfilled with nitrogen, and then warmed to rt. This process was repeated three times, then the vial was sealed with parafilm, placed 1 cm away from a 34 W blue LED, and irradiated with 2 X 34W blue LEDs under fan cooling. After 24 h, the reaction mixture was diluted with EtOAc (10 mL) then poured into a separatory funnel containing H₂O (10 mL). The aqueous phase was separated and extracted with EtOAc (3 × 10 mL). The organics were concentrated *in vacuo* and dissolved in dichloromethane (1 mL) and TFA (3 mL) and stirred at rt for 1 h. Purification of the crude material by flash column chromatography, eluting with 10:90 Hexane–EtOAc, afforded piperidine **74** (67.5 mg, 24%). Mp 64.2 °C (EtOH); IR ν_{max} (neat) / cm⁻¹ 3313, 3061, 3038, 2943, 2856, 2822, 2735, 2201 and 1597. δ_{H} (400 MHz, CDCl₃) 7.42 – 7.14 (2H, m, 2'-H), 6.95 (3H, m, 3'-H, 4'-H), 4.39 (1H, tt, *J* 8.3, 3.8, 4-H), 3.17 (2H, dt, *J* 12.8, 4.5, 2-H₂), 2.74 (2H, ddd, *J* 12.6, 9.3, 3.2, 2-H₃), 2.08 – 1.96 (2H, m, 3-H₂), 1.68 (2H, dtd, *J* 12.9, 8.9, 3.8, 3-H₃). δ_{C} (125 MHz, CDCl₃) 157.4 (C-1'), 129.5 (C-3'), 120.8 (C-4'), 116.2 (C-2'), 77.2 (C-4), 44.0 (C-3), 32.5 (C-2). HRMS [M+H]⁺ C₁₁H₁₆NO⁺ calc., 178.1233, found 178.1237. Spectral data in accordance with literature.²⁶⁴

Benzyl 3,4-dihydropyridine-1(2*H*)-carboxylate (**89**)



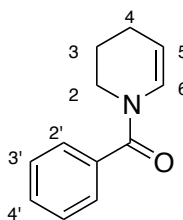
Following general procedure **3** employing benzyl piperidine-1-carboxylate (1.0 g, 4.57 mmol) to give a crude residue. Purification of the crude by flash column chromatography (5:95 EtOAc–hexane) gave enecarbamate **89** as a viscous colourless oil (891mg, 90%, 6:4 mixture of rotamers). R_f 0.30 (10:90 Hexane–EtOAc); $\nu_{\max}/\text{cm}^{-1}$ (film) 1710, 1655; δ_{H} (500 MHz, CDCl_3) 7.51 – 7.29 (5H, m, 2'-H, 3'-H, 4'-H), 6.95 – 6.92 (0.4H, br s, 6-H), 6.85 – 8.82 (0.6H, br s, 6-H), 5.21 (2H, s, Cbz CH_2), 5.01 – 4.95 (0.4H, m, 5-H), 4.90 – 4.84 (0.6H, m, 5-H), 3.69 – 3.59 (2H, m, 2-H), 2.09 – 1.99 (2H, m, 4-H), 1.97 – 1.78 (2H, m, 3-H); δ_{C} (125 MHz, CDCl_3) 153.6 (Cbz C=O rotamers), 153.2 (Cbz C=O rotamers), 136.4 (C-1'), 128.6 (C-2'), 128.2 (C-2'), 128.04 (C-3'), 127.98 (C-4'), 125.4 (C-6 rotamers), 124.9 (C-6 rotamers), 106.7 (C-5 rotamers), 106.4 (C-5 rotamers), 67.5 (Cbz CH_2 rotamers), 67.4 (Cbz CH_2 rotamers), 42.4 (C-2 rotamers), 42.2 (C-2 rotamers), 21.7 (C-4 rotamers), 21.5 (C-4 rotamers), 21.2 (C-3 rotamers). (18 signals observed); HRMS $[\text{M}+\text{H}]^+$ $\text{C}_{13}\text{H}_{16}\text{NO}_2^+$ calc. 218.1186 found, 218.1196. Spectral data in accordance with literature values.²⁶⁵

1-(3,4-Dihydropyridin-1(2*H*)-yl)ethanone (**90**)



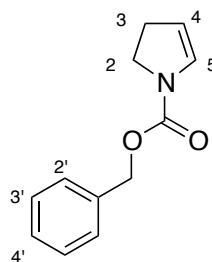
Following general procedure **3**, employing benzyl 1-(piperidin-1-yl)ethanone (580 mg, 4.57 mmol) to give a crude residue. Purification of the crude by flash column chromatography eluting with 5:95 EtOAc–hexane to give enecarbamate **90** as a viscous brown oil (428 mg, 75%, mixture of rotamers). $\nu_{\max}/\text{cm}^{-1}$ (film) 1680; δ_{H} (400 MHz, CDCl_3) 6.58 (1H, dt, J 8.4, 2.0, 6-H), 4.98 (1H, dt, J 8.1, 3.9, 5-H), 3.75 – 3.68 (2H, m, 2-H), 2.17 (3H, s, 1'-H), 2.10 (2H, tdd, J 6.2, 3.9, 2.0, 4-H), 1.89 – 1.77 (2H, m, 3-H). δ_{C} (101 MHz, CDCl_3) 173.2 (Acetyl C=O), 168.1, 167.9, 125.7 (C-6), 123.8, 108.6 (C-5 rotamers), 108.3 (C-5 rotamers), 44.3 (C-2), 40.1 (C-4), 21.68 (Acetyl CH_3), 21.66 (Acetyl CH_3), 21.4 (C-3) (12 signals observed). **HRMS** $[\text{M}+\text{H}]^+$ $\text{C}_7\text{H}_{12}\text{NO}^+$ calc. 126.0913 found 126.0909. Spectral data is in accordance with literature.²⁶⁶

(3,4-Dihydropyridin-1(2H)-yl)(phenyl)methanone (91)



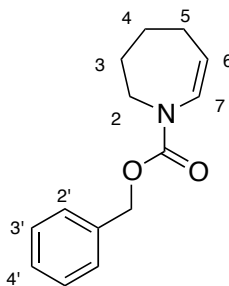
Following general procedure **3**, employing phenyl(piperidin-1-yl)methanone (864 mg, 4.57 mmol) to give a crude residue. Purification of the crude by flash column chromatography eluting with 5:95 EtOAc–hexane to give enecarbamate **91** as a viscous colourless oil (675 mg, 79%, mixture of rotamers). $\nu_{\max}/\text{cm}^{-1}$ (film) 1691; δ_{H} (400 MHz, CDCl_3) 7.47 – 7.29 (5H, m, 2'-H, 3'-H, 4'-H), 6.38 (1H, d, J 8.2, 6-H), 4.80 – 4.76 (1H, m, 5-H), 3.79 – 3.76 (2H, m, 2-H), 2.08 – 2.04 (2H, m, 4-H), 1.90 – 1.85 (2H, m, 3-H); δ_{C} (101 MHz, CDCl_3) 169.3 (Amide C=O), 135.2 (C-1'), 130.2 (C-2'), 128.4 (C-3'), 127.5 (C-4'), 124.8 (C-6), 107.6 (C-5), 41.1 (C-2), 30.9 (C-4), 21.9 (C-3); HRMS $[\text{M}+\text{H}]^+$ $\text{C}_{12}\text{H}_{14}\text{NO}^+$ calc. 188.1070 found 188.1071. Spectral data in accordance with literature.²⁶⁷

Benzyl 2,3-dihydro-1*H*-pyrrole-1-carboxylate (**97**)



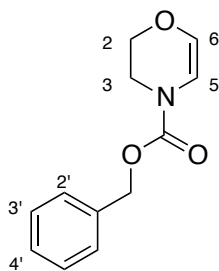
Following general procedure **3**, employing benzyl pyrrolidine-1-carboxylate (937 mg, 4.57 mmol) to give a crude residue. Purification of the crude by flash column chromatography (5:95 EtOAc–hexane) gave enecarbamate **97** as a viscous colourless oil (705 mg, 76% as a 6:4 mixture of rotamers). R_f 0.30 (10:90 hexane–EtOAc); $\nu_{\max}/\text{cm}^{-1}$ (film) 1702, 1635; δ_{H} (400 MHz, CDCl_3) 7.34 – 7.21 (m, 5H, 2'-H, 3'-H, 4'-H), 6.56 (0.4H, br, 5-H), 6.47 (0.6H, br, 5-H), 5.10 (2H, s, Cbz CH_2), 5.02 (0.4H, br, 4-H), 4.99 (0.6H, br, 4-H), 3.66 – 3.59 (2H, m, 2-H), 2.55 – 2.45 (2H, m, 3-H). δ_{C} (101 MHz, CDCl_3) 153.6 (Cbz $\text{C}=\text{O}$ rotamers), 153.2 (Cbz $\text{C}=\text{O}$ rotamers), 136.6 (C-1'), 129.7 (C-2'), 129.1 (C-3'), 128.5 (C-4'), 128.1, 128.0 (C-5 rotamers), 127.9 (C-5 rotamers), 108.8 (C-4 rotamers), 108.7 (C-4 rotamers), 67.1 (Cbz CH_2 rotamers), 66.9 (Cbz CH_2 rotamers), 45.3 (C-2 rotamers), 45.1 (C-2 rotamers), 29.7 (C-3 rotamers), 28.7 (C-3 rotamers) (17 signals observed); HRMS $[\text{M}+\text{H}]^+$ $\text{C}_{12}\text{H}_{14}\text{NO}_2^+$ calc. 204.1030 found, 204.1023. Spectral data in accordance with literature values.²⁶⁸

Benzyl 2,3,4,5-tetrahydro-1*H*-azepine-1-carboxylate (**98**)



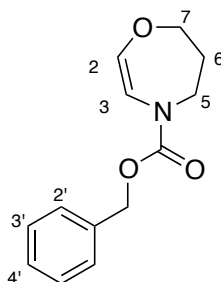
Following general procedure **3**, employing benzyl azepane-1-carboxylate (1.06 g, 4.57 mmol) to give a crude residue. Purification of the crude by flash column chromatography (5:95 EtOAc–hexane) gave *enecarbamate* **98** as a viscous colourless oil (760 mg, 72%, 1:1 mixture of rotamers). R_f 0.31 (10:90 Hexane–EtOAc); $\nu_{\max}/\text{cm}^{-1}$ (film) 1713, 1624; δ_{H} (400 MHz, CDCl_3) 7.25 – 7.08 (5H, m, 2'-H, 3'-H, 4'-H), 6.35 (1H, m, 7-H), 4.96 (2H, s, Cbz CH_2), 4.92 – 4.78 (1H, m, 6-H), 3.50 (2H, m, 2-H), 2.02 – 1.93 (2H, m, 5-H), 1.66 – 1.46 (4H, m, 3-H). δ_{C} (101 MHz, CDCl_3) 154.4 (Cbz C=O), 136.6 (C-1'), 130.7 (C-2' rotamers), 129.9 (C-2' rotamers), 128.5 (C-3' rotamers), 128.1 (C-3' rotamers), 127.9 (C-4'), 115.9 (C-7), 77.3 (C-6), 67.4 (Cbz CH_2), 47.7 (C-2), 28.1 (C-5), 26.3 (C-3 rotamers), 26.0 (C-3 rotamers), 25.1 (C-4) (15 signals observed owing to rotamers). HRMS $[\text{M}+\text{Na}]^+$ $\text{C}_{14}\text{H}_{17}\text{NNaO}_2^+$ calc., 254.1151 found, 254.1151.

Benzyl 2*H*-1,4-oxazine-4(3*H*)-carboxylate (106)



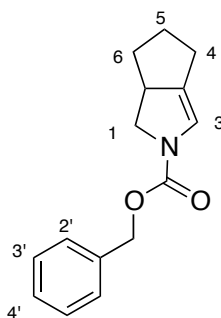
Following general procedure **3**, employing benzyl morpholine-4-carboxylate (1.00 g, 4.57 mmol) to give a crude residue. Purification of the crude by flash column chromatography (5:95 EtOAc–hexane) gave *enecarbamate* **106** as a viscous colourless oil (640 mg, 64%, 6:4 mixture of rotamers). R_f 0.32 (10:90 hexane–EtOAc); $\nu_{\max}/\text{cm}^{-1}$ (film) 1702, 1605; δ_{H} (400 MHz, CDCl_3) 7.38-7.26 (5H, m, 2'-H, 3'-H, 4'-H), 6.34 (0.4H, br s, 6-H), 6.21 (0.6H, m, 6-H), 6.03 (0.4H, m, 5-H), 5.89 (0.6H, m, 5-H), 5.19-5.18 (2H, m, Cbz CH_2), 4.09-4.03 (2H, m, 2-H), 3.75-3.73 (2H, m, 3-H); δ_{C} (101 MHz, CDCl_3) 152.2 (Cbz C=O rotamers), 151.9 (Cbz C=O rotamers), 136.26 (C-1' rotamers), 136.22 (C-1' rotamers), 130.3 (C-6 rotamers), 129.2 (C-6 rotamers), 128.7 (C-2' rotamers), 128.4 (C-2' rotamers), 128.3 (C-3'), 128.2 (C-4'), 106.2 (C-5 rotamers), 105.7 (C-5 rotamers), 67.8 (Cbz CH_2), 67.7 (Cbz CH_2), 64.8 (C-2 rotamers), 64.3 (C-2 rotamers), 42.3 (C-3 rotamers), 41.6 (C-3 rotamers) (19 signals observed); HRMS $[\text{M}+\text{Na}]^+$ $\text{C}_{12}\text{H}_{13}\text{NNaO}_3$ calc. 242.0787 found 242.0784.

Benzyl 6,7-dihydro-1,4-oxazepine-4(5*H*)-carboxylate (**108**)



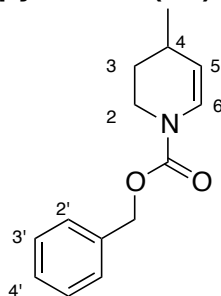
Following general procedure **3**, employing benzyl 1,4-oxazepane-4-carboxylate (1.07 g, 4.57 mmol) to give a crude residue. Purification of the crude by flash column chromatography (5:95 EtOAc–hexane) gave *enecarbamate* **108** as a viscous colourless oil (618 mg, 58%, mixture of rotamers). R_f 0.25 (10:90 hexane–EtOAc); $\nu_{\max}/\text{cm}^{-1}$ (film) 1717, 1626; δ_{H} (400 MHz, CDCl_3) 7.33 – 7.19 (5H, m, 2'-H, 3'-H, 4'-H), 5.88 – 5.74 (1H, m, 2-H), 5.68 – 5.59 (1H, m, 3-H), 5.07 (2H, s, Cbz CH_2), 4.06 – 3.93 (2H, m, 7-H), 3.82 – 3.72 (2H, m, 5-H), 1.93 – 1.82 (2H, m, 6-H); δ_{C} (101 MHz, CDCl_3) 153.9 (Cbz C=O), 136.3 (C-1'), 134.8 (C-2), 128.6 (C-2'), 128.0 (C-3'), 120.0 (C-4'), 110.3 (C-3), 70.8 (C-7), 68.9 (Cbz CH_2 rotamers), 67.8 (Cbz CH_2 rotamers), 46.6 (C-5), 28.5 (C-6) 12 signals observed, owing to rotamers. HRMS $[\text{M}+\text{Na}]^+$ $\text{C}_{13}\text{H}_{15}\text{NNaO}_3^+$ calc. 256.0944 found 256.0944.

Benzyl 4,5,6,6a-tetrahydrocyclopenta[*c*]pyrrole-2(1*H*)-carboxylate (**110**)



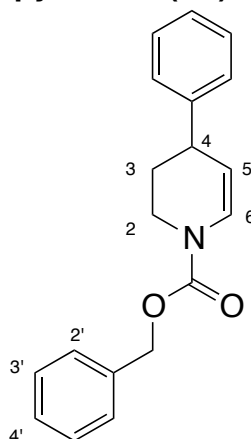
Following general procedure **3**, employing benzyl hexahydrocyclopenta[*c*]pyrrole-2(1*H*)-carboxylate (1.20 g, 4.57 mmol) to give a crude residue. Purification of the crude by flash column chromatography (5:95 EtOAc–hexane) gave *enecarbamate* **110** as a viscous colourless oil (776 mg, 69%, 6:4 mixture of rotamers). R_f 0.41 (10:90 hexane–EtOAc); $\nu_{\max}/\text{cm}^{-1}$ (film) 1741, 1604; δ_{H} (400 MHz, CDCl_3) 7.25 – 6.96 (5H, m, 2'-H, 3'-H, 4'-H), 6.05 (0.4H, br, 3-H), 5.97 (0.6H, m, 3-H), 4.93 (2H, s, 1-H), 3.86 – 3.69 (1H, m, 6a-H), 3.24 – 2.88 (2H, m, 1-H), 2.15 – 1.87 (2H, m, 4-H), 1.87 – 1.50 (2H, m, 6-H), 1.12 – 0.90 (2H, m, 5-H); δ_{C} (101 MHz, CDCl_3) 152.5 (Cbz C=O rotamers), 151.9 (Cbz C=O rotamers), 136.9 (C-1' rotamers), 136.8 (C-1' rotamers), 133.2 (C-3a), 132.7 (C-1'), 128.5 (C-2' rotamers), 128.4 (C-2' rotamers) 128.0 (C-3'), 127.9 (C-4'), 119.2 (C-3 rotamers), 118.6 (C-3 rotamers), 66.8 (Cbz CH_2 rotamers), 66.7 (Cbz CH_2 rotamers), 52.2 (C-6a rotamers), 52.1 (C-6a rotamers), 49.2 (C-1 rotamers), 48.1 (C-1 rotamers), 31.32 (C-4 rotamers), 31.29 (C-4 rotamers), 27.6 (C-6), 21.70 (C-5 rotamers), 21.67 (C-5 rotamers) (23 signals observed, owing to rotamers). HRMS $[\text{M}+\text{H}]^+$ $\text{C}_{15}\text{H}_{18}\text{NO}_2^+$ calc., 244.1332 found 244.1332.

Benzyl 4-methyl-3,4-dihydropyridine-1(2*H*)-carboxylate (**113**)



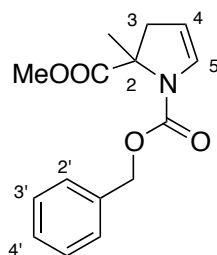
Following general procedure **3**, employing benzyl 4-methylpiperidine-1-carboxylate (1.06 g, 4.57 mmol) to give a crude residue. Purification of the crude by flash column chromatography (5:95 EtOAc–hexane) gave *enecarbamate* **113** as a viscous colourless oil (718 mg, 68%, 6:4 mixture of rotamers). R_f 0.35 (10:90 hexane–EtOAc); $\nu_{\max}/\text{cm}^{-1}$ (film) 1724, 1621; δ_{H} (400 MHz, CDCl_3) 7.29 – 7.04 (5H, m, 2'-H, 3'-H, 4'-H), 6.77 (0.4H, br, 6-H), 6.68 (0.6H, br, 6-H), 5.04 (2H, s, 1-H), 4.80 – 4.75 (0.4H, m, 5-H), 4.69 – 4.62 (0.6H, m, 5-H), 3.77 – 3.66 (1H, m, 2-H), 3.42 – 3.34 (1H, m, 2-H), 2.26 – 2.16 (1H, m, 4-H), 1.89 – 1.51 (1H, m, 3-H₂), 1.36 – 1.20 (1H, m, 3-H₃), 0.94 (3H, m, J 7.0, CH₃). δ_{C} (101 MHz, CDCl_3) 153.5 (Cbz C=O rotamers), 153.1 (Cbz C=O rotamers), 136.4 (C-1'), 128.5 (C-2'), 128.2 (C-3'), 128.1 (C-4'), 124.2 (C-6 rotamers), 123.7 (C-6 rotamers), 113.2 (C-5 rotamers), 112.8 (C-5 rotamers), 77.3, 67.5 (Cbz CH₂), 67.4 (Cbz CH₂), 41.0 (C-2 rotamers), 40.8 (C-2 rotamers), 29.9 (C-4), 26.8 (C-3 rotamers), 26.2 (C-3 rotamers), 21.3 (C-4 CH₃) (19 signals observed). HRMS $[\text{M}+\text{H}]^+$ C₁₄H₁₈NO₂⁺ calc., 232.1332 found 232.1332.

Benzyl 4-phenyl-3,4-dihydropyridine-1(2H)-carboxylate (**114**)



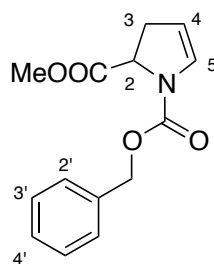
Following general procedure **3**, employing benzyl 4-phenylpiperidine-1-carboxylate (1.35 g, 4.57 mmol) to give a crude residue. Purification of the crude by flash column chromatography (5:95 EtOAc–hexane) gave *enecarbamate* **114** (1.11 g, 83%, 6:4 mixture of rotamers. R_f 0.40 (10:90 hexane–EtOAc); $\nu_{\max}/\text{cm}^{-1}$ (film) 1743, 1660, 1620; δ_{H} (400 MHz, CDCl_3) 7.43–7.23 (10H, m, 2'-H, 3'-H, 4'-H and 4-Ph), 7.14 (0.4H, d, J 8.3, 6-H), 7.04 (0.6H, d, J 8.3, 6-H), 5.24 (2H, s, Cbz CH_2), 5.08 (0.6H, dd, J 8.2, 2.8 Hz, 5-H), 4.96 (0.4H, dd, J 8.2, 2.8, 5-H), 3.75 – 3.51 (3H, m, 2-H, 4-H), 2.18 – 2.16 (1H, m, 3-H), 1.85 – 1.84 (1H, m, 3-H); δ_{C} (101 MHz, CDCl_3) 153.7 (Cbz C=O rotamers), 153.2 (Cbz C=O rotamers), 145.1 (C-1' rotamers), 136.4 (C-4 phenyl, C-1), 128.7 (C-2' rotamers), 128.6 (C-4 phenyl), 128.4 (C-3' rotamers), 128.3 (C-3' rotamers), 127.8 (C-4' rotamers), 126.6 (C-6 rotamers), 126.3 (C-6 rotamers), 125.8 (C-4 phenyl), 109.4 (C-5 rotamers), 109.1 (C-4 phenyl, C-4), 67.8 (Cbz CH_2), 40.5 (C-2), 38.3 (C-4 rotamers), 38.0 (C-4 rotamers), 31.2 (C-3) (19 signals observed, owing to rotamers); HRMS $[\text{M}+\text{H}]^+$ $\text{C}_{19}\text{H}_{20}\text{NO}_2^+$ calc. 294.1486 found 294.1487.

1-Benzyl 2-methyl 2-methyl-2,3-dihydro-1H-pyrrole-1,2-dicarboxylate (118)



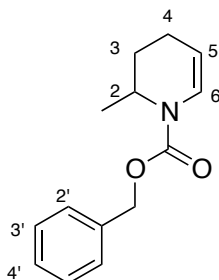
Following general procedure **3**, employing 1-benzyl 2-methyl 2-methylpyrrolidine-1,2-dicarboxylate (1.27 g, 4.57 mmol) to give a crude residue. Purification of the crude by flash column chromatography (10:90 EtOAc–Hexane) gave *enecarbamate* **118** as a viscous yellow oil (264 mg, 21%, 55:45 mixture of rotamers). R_f 0.40 (30:70 hexane–EtOAc); $\nu_{\max}/\text{cm}^{-1}$ (film) 1740, 1707, 1612; δ_{H} (400 MHz, CDCl_3) 7.36–7.30 (5H, m, 2'-H, 3'-H, 4'-H), 6.65 (0.45H, dt, J 4.3, 2.1, 5-H), 6.56 (0.55H, dt, J 4.3, 2.1, 5-H), 5.26–5.03 (2H, m Cbz CH_2), 4.97 (0.45H, dt, J 4.7, 2.5, 4-H), 4.89 (0.55H, dt, J 4.7, 2.5, 4-H), 3.74 (1.6H, s, Ester CH_3), 3.47 (1.4H, s, Ester CH_3), 3.03–2.95 (1H, m, 3-H), 2.62–2.55 (1H, m, 3-H), 1.68 (1.6H, s, C-2 CH_3), 1.59 (1.4H, s, C-2 CH_3); δ_{C} (101 MHz, CDCl_3) 173.7 (ester C=O), 173.6 (ester C=O), 152.3 (Cbz C=O), 151.7 (Cbz C=O), 136.4 (C-1' rotamers), 136.0 (C-1' rotamers), 129.9 (C-5 rotamers), 129.2 (C-5 rotamers), 128.7 (C-2' rotamers), 128.6 (C-2' rotamers), 128.41 (C-4' rotamers), 128.43, (C-4' rotamers) 128.3 (C-3' rotamers), 128.3 (C-3' rotamers), 104.8 (C-4 rotamers), 104.7 (C-4 rotamers), 67.5 (Cbz CH_2 rotamers), 67.3 (Cbz CH_2 rotamers), 65.9 (C-1 rotamers), 65.5 (C-1 rotamers), 52.8 (Ester C-O rotamers), 52.5 (Ester C-O), 45.7 (C-3 rotamers), 44.2 (C-3 rotamers), 23.4 (C-2 CH_3), 22.5 (C-2 CH_3) (28 signals observed); HRMS $[\text{M}+\text{H}]^+$ $\text{C}_{15}\text{H}_{18}\text{NO}_4^+$ calc. 276.1230 found 276.1226.

1-Benzyl 2-methyl 2,3-dihydro-1*H*-pyrrole-1,2-dicarboxylate (117)



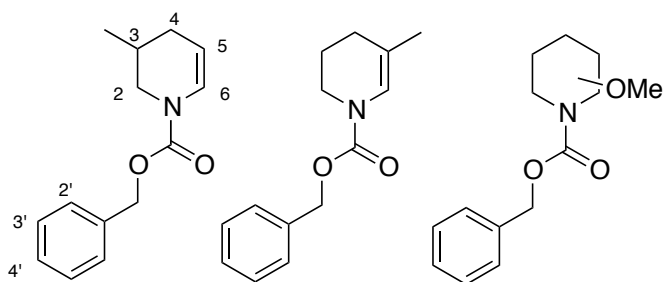
Following general procedure **3**, employing 1-benzyl 2-methyl pyrrolidine-1,2-dicarboxylate (1.20 g, 4.57 mmol) to give a crude residue. Purification of the crude by flash column chromatography (5:95 EtOAc–hexane) gave *enecarbamate* **117** as a viscous colourless oil (800 mg, 67%, mixture of rotamers). R_f 0.30 (10:90 hexane–EtOAc); $\nu_{\max}/\text{cm}^{-1}$ (film) 1755, 1708, 1621; δ_{H} (400 MHz, CDCl_3) 7.44–7.29 (5H, m, 2'-H, 3'-H, 4'-H), 6.70 (0.45H, m, 5-H), 6.60 (0.55H, m, 5-H), 5.27–5.05 (2H, m, Cbz CH_2), 4.98 – 4.95 (0.45H, m, 4-H), 4.73 – 4.69 (0.55H, m, 4-H), 3.77 (1.65H, s, Ester CH_3), 3.60 (1.35H, s, Ester CH_3), 3.19 – 2.97 (2H, m, 2-H, 3-H_A), 2.78 – 2.58 (1H, m, 3-H_B). δ_{C} (101 MHz, CDCl_3) 172.1 (ester C=O rotamers), 171.9 (ester C=O rotamers), 152.2 (Cbz C=O rotamers), 152.2 (Cbz C=O rotamers), 136.2 (C-1' rotamers), 136.1 (C-1' rotamers), 130.0 (C-5), 129.3 (C-5), 128.54 (C-2' rotamers), 128.50 (C-2' rotamers), 128.22 (C-4' rotamers), 128.18 (C-4' rotamers), 128.1 (C-3' rotamers), 128.0 (C-3' rotamers), 106.4 (C-4 rotamers), 106.2 (C-4 rotamers), 67.5 (Cbz CH_2), 67.3 (Cbz CH_2), 58.1 (Ester C-O), 58.8 (Ester C-O), 52.5 (C-2 rotamers), 52.3 (C-2 rotamers), 35.5 (C-3 rotamers), 34.3 (C-3 rotamers). HRMS $[\text{M}+\text{H}]^+$ $\text{C}_{14}\text{H}_{16}\text{NO}_4^+$ calc. 262.1079, found 262.1079.

Benzyl 2-methyl-3,4-dihydropyridine-1(2*H*)-carboxylate (**120**)



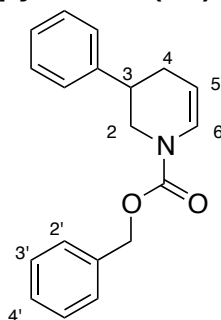
Following general procedure **3**, employing benzyl 2-methylpiperidine-1-carboxylate (1.06 g, 4.57 mmol) to give a crude residue. Purification of the crude by flash column chromatography (5:95 EtOAc–Hexane) gave *enecarbamate* **120** as a viscous colourless oil (749 mg, 71%, 6:4 mixture of rotamers). R_f 0.40 (10:90 hexane–EtOAc); $\nu_{\max}/\text{cm}^{-1}$ (film) 1701, 1605; δ_{H} (400 MHz, CDCl_3) 7.34–7.19 (5H, m, 2'-H, 3'-H, 4'-H), 6.75 – 6.68 (0.4H, m, 6-H), 6.68 – 6.60 (0.6H, m, 6-H), 5.17 – 5.01 (2H, m, Cbz CH_2), 4.89 – 4.80 (0.4H, m, 5-H), 4.77 – 4.70 (0.6H, m, 5-H), 4.43 – 4.24 (1H, m, 2-H), 2.12 – 2.09 – 1.95 (1H, m, 4- H_A), 1.95 – 1.78 (1H, m, 4- H_B), 1.78 – 1.45 (2H, m, 3-H), 1.03 (3H, d, J 7.0, CH_3). δ_{C} (101 MHz, CDCl_3) 153.4 (Cbz C=O), 152.7 (Cbz C=O), 136.9 (C-1' rotamers), 128.5 (C-2' rotamers), 128.1 (C-4'), 127.99 (C-3' rotamers), 127.95 (C-3' rotamers), 123.8 (C-6 rotamers), 123.4 (C-6 rotamers), 105.8 (C-5 rotamers), 105.4 (C-5 rotamers), 67.2 (Cbz CH_2), 46.5 (C-2), 46.3 (C-4), 26.4 (C-3) 17.3 (CH_3) (16 signals observed, owing to rotamers). HRMS $[\text{M}+\text{H}]^+$ $\text{C}_{14}\text{H}_{18}\text{NO}_2^+$ calc. 232.1332 found 232.1332.

Benzyl 3-methyl-3,4-dihydropyridine-1(2*H*)-carboxylate (**126**)



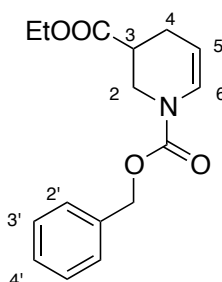
Following general procedure **3**, employing benzyl 3-methylpiperidine-1-carboxylate (1.06 g, 4.57 mmol) to give a crude residue. Additional Me₃SiOTf (1.0 eq.) was added dropwise over 10 minutes to the ice-cooled solution of crude and ⁱPr₂NEt (1.0 eq.) in DCM (0.5 M) over 10 minutes. Purification of the crude by flash column chromatography (5:95 EtOAc–hexane) gave an inseparable mixture of regioisomers **126A** and **126B** and aminoacetals (1:0.5:1) equating to a 40% yield of **126** (major regioisomer showed a 0.7:1 ratio of rotamers, minor showed a 1:1 mixture of rotamers, methylamino acetal showed a mixture of 3:1 regioisomers). $\nu_{\max}/\text{cm}^{-1}$ (film) 1755, 1708, 1621, 1229; δ_{H} (500 MHz, CDCl₃) 7.27 – 7.12 (12.5H, m), 6.81 (0.4H, d, J = 8.3 Hz, 6-H), 6.71 (0.60H, d, J 8.3, H-6), 6.62 (0.25H, br s), 6.61 (0.25H, br s), 5.03 (5.8H, m, CH₂), 4.79 (0.4H, m, 5-H), 4.68 (0.6H, m, 5-H), 3.85–3.67 (2H, m, H-2), 3.53–3.39 (1H, m), 3.11 (1.5H, s), 3.02 (1.5H, s), 2.78 (1.7H, m, 4-H), 1.95 (1.3H, m, 3-H), 1.82-1.20 (10.5H, m, 3-H), 0.84 (6H, m, CH₃); δ_{C} (101 MHz, CDCl₃) 155.7, 155.3, 153.7 (amide C=O rotamers), 153.3 (amide C-O rotamers), 153.1, 153.0, 136.7, 136.63, 136.55, 136.4, 128.5, 128.1, 128.00, 127.97, 127.7, 125.0 (C-6 rotamers), 124.5 (C-6 rotamers), 120.1, 115.5, 115.1, 106.0 (C-5), 105.8 (C-5), 85.8, 85.7, 67.4 (ether C-O), 67.2, 67.1, 66.9, 55.0, 54.6, 48.5 (C-2 rotamers or C-4), 48.3 (C-2 rotamers or C-4), 41.6, 38.2, 38.0, 35.7, 35.5, 29.8 (C-3), 29.6 (C-3), 26.9, 25.6, 25.5, 25.1, 21.7, 20.9, 18.7 (CH₃), 17.7, 17.6 (48 signals observed). HRMS [M+H]⁺ C₁₄H₁₈NO₂⁺ calc., 232.1332 found 232.1332.

Benzyl 3-phenyl-3,4-dihydropyridine-1(2H)-carboxylate (**127**)



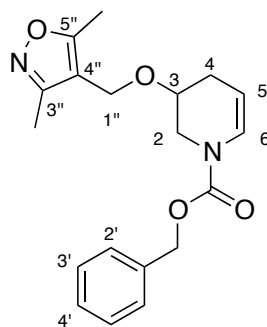
Following general procedure **3**, employing benzyl 3-phenylpiperidine-1-carboxylate (1.35 g, 4.57 mmol) to give a crude residue. Purification of the crude by flash column chromatography (5:95 EtOAc–hexane) gave *enecarbamate* **127** as a viscous colourless oil (897 mg, 67%, 1:1 mixture of rotamers). R_f 0.42 (10:90 hexane–EtOAc); $\nu_{\max}/\text{cm}^{-1}$ (film) 1712, 1603; δ_{H} (400 MHz, CDCl_3) 7.38–7.09 (10H, m, 2'-H, 3'-H, 4'-H and 3-Ph), 6.94 – 6.90 (0.5H, m, 6-H), 6.85 – 6.80 (0.5H, m, 6-H), 5.21 – 5.04 (2H, m, Cbz CH_2), 4.95 – 4.90 (0.5H, m, 5-H), 4.20 – 4.16 (0.5H, m, 5-H), 4.06 – 4.00 (1H, m, 3-H), 3.23 – 3.18 (1H, m, 2-H_A), 2.95 – 2.90 (1H, m, 2-H_B), 2.25 – 2.20 (2H, m, 4-H). δ_{C} (101 MHz, CDCl_3) 153.5 (Cbz C=O), 153.1 (Cbz C=O), 143.0 (C-1' rotamers), 142.8 (C-1' rotamers), 136.3 (C-4 Phenyl, C-1), 136.2 (C-4 Phenyl, C-1), 128.72 (aromatic), 128.68 (aromatic), 128.57 (aromatic), 128.5 (aromatic), 128.25 (aromatic), 128.21 (aromatic), 128.14 (aromatic), 128.08 (aromatic), 127.3 (aromatic), 127.2 (aromatic), 126.9 (aromatic), 126.1 (aromatic), 125.3 (C-6 rotamers), 124.9 (C-6 rotamers), 106.6 (C-5 rotamers), 106.3 (C-5 rotamers), 67.7 (C-1 rotamers), 67.6 (C-1 rotamers), 47.9 (C-2 rotamers), 47.7 (C-2 rotamers), 38.6 (C-3 rotamers), 38.5 (C-3 rotamers), 31.6 (C-4) (29 signals observed, owing to rotamers). HRMS $[\text{M}+\text{H}]^+$ $\text{C}_{19}\text{H}_{20}\text{NO}_2^+$ 294.1489 found 294.1487.

1-Benzyl 3-ethyl 3,4-dihydropyridine-1,3(2H)-dicarboxylate (128)



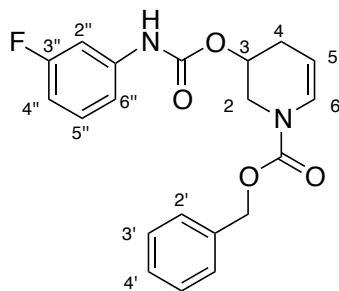
Following general procedure **3**, employing 1-benzyl 3-ethyl piperidine-1,3-dicarboxylate (1.33 g, 4.57 mmol) to give a crude residue. Purification of the crude by flash column chromatography (5:95 EtOAc–Hexane) gave *enecarbamate* **128** as a viscous colourless oil (964 mg, 73%, 1:1 mixture of rotamers). R_f 0.31 (10:90 hexane–EtOAc); $\nu_{\max}/\text{cm}^{-1}$ (film) 1748, 1702, 1621; δ_{H} (400 MHz, CDCl_3) 7.56–6.95 (5H, m, 2'-H, 3'-H, 4'-H), 6.87 – 6.84 (0.5H, m, 6-H), 6.78 – 6.74 (0.5H, m, 6-H), 5.03 (2H, s, Cbz CH_2), 4.91 – 4.88 (0.5H, m, 5-H), 4.79 – 4.75 (0.5H, m, 5-H), 4.00 (2H, q, J 7.1, ester CH_2CH_3), 3.58 – 3.53 (2H, m, 2-H), 3.01 – 2.91 (1H, m, 3-H), 1.95 – 1.90 (1H, m, 4-H_A), 1.81 (1H, m, 4-H_B), 1.10 (3H, t, J 7.1, ester CH_2CH_3); δ_{C} (101 MHz, CDCl_3) 173.2 (Ester C=O), 153.4 (Cbz C=O), 152.9 (Cbz C=O), 136.1 (C-1'), 129.6 (C-2'), 128.6 (C-4' rotamers), 128.3 (C-4' rotamers), 128.1 (C-3'), 126.6 (C-6 rotamers), 126.2 (C-6 rotamers), 103.3 (C-5 rotamers), 103.0 (C-5 rotamers), 67.7 (Cbz CH_2), 60.9 (Ester C-O), 40.3 (C-2 rotamers), 40.2 (C-2 rotamers), 37.5 (C-3 rotamers), 37.2 (C-3 rotamers), 23.9 (C-4 rotamers), 23.8 (C-4 rotamers), 14.2 (CH_3) (21 signals observed). HRMS $[\text{M}+\text{Na}]^+$ $\text{C}_{16}\text{H}_{19}\text{NNaO}_4^+$ calc., 312.1206 found, 312.1203.

Benzyl 3-((3,5-dimethylisoxazol-4-yl)methoxy)-3,4-dihydropyridine-1(2H)-carboxylate (129)



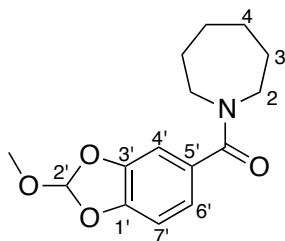
Following general procedure **3**, employing benzyl 3-((3,5-dimethylisoxazol-4-yl)methoxy)piperidine-1-carboxylate (1.57 g, 4.57 mmol) to give a crude residue. Purification of the crude by flash column chromatography (10:90 EtOAc–Hexane) gave *enecarbamate* **129** as a viscous colourless oil (641 mg, 641%, 7:3 mixture of rotamers). R_f 0.37 (10:90 hexane–EtOAc); $\nu_{\max}/\text{cm}^{-1}$ (film) 1719, 1634; δ_{H} (400 MHz, CDCl_3) 7.37 – 7.36 (5H, m, 2'-H, 3'-H, 4'-H), 6.89 (0.3H, d, J 8.3, 6-H), 6.80 (0.7H, d, J 8.3, 6-H), 5.22 – 5.17 (2H, m, Cbz CH_2), 4.81 – 4.79 (1H, m, 5-H), 4.40 – 4.27 (2H, m, 1''-H), 3.79 – 3.56 (3H, m, 2-H, 3-H), 2.38 – 2.08 (8H, m, 4-H, 3''-H CH_3 , 5''-H CH_3). δ_{C} (101 MHz, CDCl_3) 167.1 (C-3''), 159.8 (C-5''), 153.4 (Cbz C=O), 136.1 (C-1'), 128.6 (Cbz aromatics), 128.3 (Cbz aromatics), 128.2 (Cbz aromatics), 128.1 (Cbz aromatics), 125.5 (C-6 rotamers), 125.0 (C-6 rotamers), 111.0 (C-4''), 103.4 (C-5 rotamers), 103.2 (C-5 rotamers), 69.9 (C-3 rotamers), 69.8 (C-3 rotamers), 67.8 (Cbz CH_2), 67.7 (Cbz CH_2), 59.4 (C-1''), 45.0 (C-2 rotamers), 44.0 (C-2 rotamers), 28.5 (C-4 rotamers), 27.9 (C-4 rotamers), 10.9 (C-5'' CH_3), 10.0 (C-3'' CH_3) (24 signals observed). HRMS $[\text{M}+\text{H}]^+$ $\text{C}_{19}\text{H}_{23}\text{N}_2\text{O}_4^+$ calc. 343.1652 found 343.1659.

Benzyl 3-(((3-fluorophenyl)carbamoyl)oxy)-3,4-dihydropyridine-1(2H)-carboxylate (130)



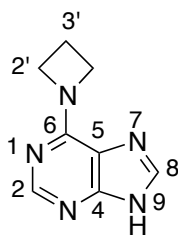
Following general procedure **3**, employing benzyl 3-(((3-fluorophenyl)carbamoyl)oxy)piperidine-1-carboxylate (1.70 g, 4.57 mmol) to give a crude residue. Purification of the crude by flash column chromatography (5:95 EtOAc–hexane) gave *enecarbamate* **130** as a viscous colourless oil (1.07 g, 63%, mixture of rotamers). R_f 0.27 (10:90 Hexane–EtOAc); $\nu_{\max}/\text{cm}^{-1}$ (film) 1760, 1702, 1600; δ_{H} (400 MHz, CDCl_3) 7.39–7.22 (6H, m, 2'-H, 3'-H, 4'-H and 5''-H), 7.00–6.98 (1H, m, 6''-H), 6.92 (1H, dd, J 8.4, 6-H), 6.77–6.74 (1H, m, 4''-H), 6.68 (1H, bs, 2''-H), 5.30–5.18 (3H, m, Cbz CH_2 , 3-H), 4.93–4.81 (1H, m, 5-H), 4.03 (1H, dd, J 13.1, 4.6, 2-H), 3.58 (1H, d, J 13.2, 2-H), 2.48–2.44 (1H, m, 4-H_A), 2.27–2.23 (1H, m, 4-H_B); δ_{C} (101 MHz, CDCl_3) 164.3 (d, $J_{\text{C-F}}$ 244.1, C-3''), 153.7 (C-3 carbamate C=O), 153.4 (Cbz C=O), 152.3 (Cbz C=O), 139.3 (d, $J_{\text{C-F}}$ 11, C-2'' rotamers), 139.2 (C-1'' rotamers), 136.0 (C-1'), 130.2 (d, J 8.8, C-5''), 128.6 (Cbz aromatic), 128.3 (Cbz aromatic), 128.2 (Cbz aromatic), 128.1 (Cbz aromatic), 125.5 (C-6 rotamers), 125.0 (C-6 rotamers), 113.8 (C-5 rotamers), 110.3 (d, J 20.1, C-4''), 106.1 (d, J 20.1, C-2''), 102.9 (C-5 rotamers), 102.5 (C-5 rotamers), 67.9 (Cbz CH_2), 67.7 (Cbz CH_2), 66.3 (C-3), 45.2 (C-2 rotamers), 45.0 (C-2 rotamers), 27.4 (C-4 rotamers), 27.2 (C-4 rotamers) (26 signals observed); HRMS $[\text{M}+\text{Na}]^+$ $\text{C}_{20}\text{H}_{19}\text{FN}_2\text{NaO}_4^+$ calc. 393.1221 found 393.1215.

Azepan-1-yl(2-methoxybenzo[d][1,3]dioxol-5-yl)methanone (135)



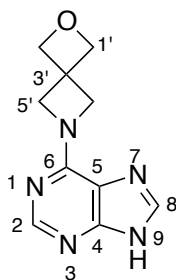
Following general procedure **3**, employing azepan-1-yl(benzo[d][1,3]dioxol-5-yl)methanone (1.13 g, 4.57 mmol) to give a crude residue. Purification of the crude by flash column chromatography eluting with 5:95 EtOAc–hexane to give enecarbamate **135** as a viscous colourless oil (899 mg, 71%, mixture of rotamers). $\nu_{\max}/\text{cm}^{-1}$ (film) 1754, 1676; δ_{H} (400 MHz, CDCl_3) 6.87 (1H, s, 4'-H), 6.87 (1H, s, 6'-H), 6.85 (1H, s, 2'-H), 6.81 (1H, s, 7'-H), 3.62 – 3.51 (4H, m, H-2), 3.34 (3H, s, ether CH_3), 1.75-1.54 (8H, m, 3'-H, 4'-H); δ_{C} (101 MHz, CDCl_3) 170.8 (Amide $\text{C}=\text{O}$), 146.7 (C-3'), 145.9 (C-1'), 131.2 (C-5'), 120.7 (C-6'), 119.5 (C-2'), 107.9 (C-4' or C-7'), 107.2 (C-4' or C-7'), 50.1 (Ether C-O, CH_3), 46.5 (C-2), 28.0 (C-3 or C-4), 27.3 (C-3 or C-4); HRMS $[\text{M}+\text{H}]^+$ $\text{C}_{15}\text{H}_{20}\text{NO}_4^+$ calc. 278.1398 found 278.1390.

6-(azetidin-1-yl)-9H-purine (152)



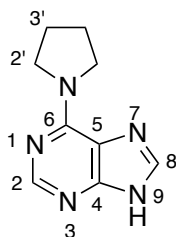
Following general procedure **4**, employing azetidine hydrochloride (362 mg, 3.90 mmol) and heated at reflux for 1 h. The solid was isolated through filtration using a sintered funnel. The crude solid was washed with MeOH (2 × 25 mL) and dichloromethane (2 × 25 mL) to give *purine* **152** as a brown solid (540 mg, 95%). mp 198°C (EtOH); $\nu_{\max}/\text{cm}^{-1}$ (film) 3052, 2993, 2577 and 1367; δ_{H} (500 MHz, DMSO- d_6) 8.17 (1H, s, 2-H), 8.07 (1H, s, 8-H), 4.34 (4H, m, 2'-H), 2.42 (2H, tt, J 8.5, 7.0, 3'-H); δ_{C} (125 MHz DMSO- d_6) 155.0 (C-6), 152.6 (C-2), 150.9 (C-4), 139.7 (C-8), 119.4 (C-5), 51.8 (C-2'), 17.6 (C-3'); HRMS $[\text{M}+\text{H}]^+$ $\text{C}_8\text{H}_{10}\text{N}_5^+$ calc. 176.0941, found 176.0940.

6-(9*H*-purin-6-yl)-2-oxa-6-azaspiro[3.3]heptane (153)



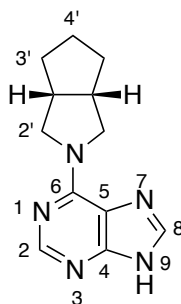
Following general procedure **4**, employing 2-oxa-6-azaspiro[3.3]heptane hydrochloride (526 mg, 3.90 mmol) and heated at reflux for 2 h. The solid was isolated by filtration using a sintered funnel. The crude solid was washed with MeOH (2 × 25 mL) and dichloromethane (2 × 25 mL) to give *purine* **153** as a colourless solid (691 mg, 98%). mp 231 °C (EtOH); $\nu_{\text{max}}/\text{cm}^{-1}$ (film) 3066, 3017, 2948, 2591 and 1573; δ_{H} (500 MHz, DMSO- d_6) 12.96 (1H, s, 9-H), 8.19 (1H, s, 2-H), 8.11 (1H, s, 8-H), 4.75 (4H, s, 1'-H), 4.60 (4H, s, 5'-H); δ_{C} (125 MHz DMSO- d_6) 154.8 (C-6), 152.6 (C-2), 151.0 (C-4), 139.9 (C-8), 119.6 (C-5), 80.3 (C-1'), 61.0 (C-3'), 39.9 (C-2'); HRMS $[\text{M}+\text{H}]^+$ $\text{C}_{10}\text{H}_{12}\text{N}_5\text{O}^+$ calc 218.1036, found 218.1031.

6-(pyrrolidin-1-yl)-9H-purine (154)



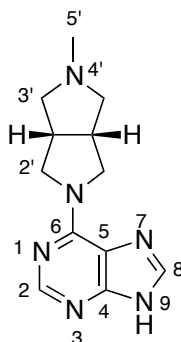
Following general procedure **4**, employing pyrrolidine (737 mg, 3.90 mmol) and heated at reflux for 3 h. The solid was isolated through filtration using a sintered funnel. The crude solid was washed with MeOH (2 × 25 mL) and dichloromethane (2 × 25 mL) to give *purine 154* as a colourless solid (559 mg, 91%). mp 204 °C (EtOH); $\nu_{\max}/\text{cm}^{-1}$ (film) 3178, 3005, 2863 and 1628; δ_{H} (500 MHz, DMSO- d_6) 8.21 (1H, s, 2-H), 8.12 (1H, s, 8-H), 5.21 (2H, br s, 2'-H₂), 2.72 (2H, m, 2'-H₃), 1.94 (2H, m, 3'-H₂), 1.56 (2H, m, 3'-H₃); δ_{C} (125 MHz DMSO- d_6) 153.0 (C-6), 152.9 (C-2), 151.5 (C-4), 139.2 (C-8), 119.3 (C-5), 60.4 (C-2'), 28.3 (C-3'); HRMS [M+H]⁺ C₉H₁₂N₅⁺ calc., 190.1098 found 190.1094.

6-((3a*R*,6a*S*)-hexahydrocyclopenta[*c*]pyrrol-2(1*H*)-yl)-9*H*-purine (155)



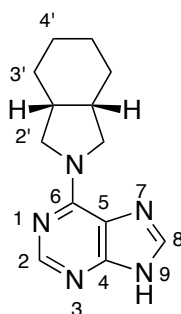
Following general procedure **4**, employing (3a*R*,6a*S*)-octahydrocyclopenta[*c*]pyrrole (432 mg, 3.90 mmol) and heated at reflux for 2.5 h. The solid was isolated through filtration using a sintered funnel. The crude solid was washed with MeOH (2 × 25 mL) and dichloromethane (2 × 25 mL) to give *purine 155* as a colourless solid (707 mg, 95%). mp 212 °C (EtOH); $\nu_{\max}/\text{cm}^{-1}$ (film) 3057, 2947, 2859, 2673 and 1581; δ_{H} (500 MHz, DMSO-*d*₆) 12.96 – 12.82 (1H, m, 9-H), 8.16 (1H, s, 2-H), 8.04 (1H, s, 8-H), 4.16 – 3.94 (2H, m, 2'-H₂), 3.68 – 3.46 (2H, m, 2'-H₃), 2.31 (2H, m, 3a'-H), 1.72 – 1.27 (6H, m, 3'-H, 4'-H); δ_{C} (125 MHz DMSO-*d*₆) 153.5 (C-6), 152.6 (C-2), 151.1 (C-4), 138.6 (C-8), 119.6 (C-5), 52.9 (C-2'), 37.6 (C-3a'), 26.0 (C-3'), 22.9 (C-4'); HRMS [M+H]⁺ C₁₂H₁₆N₅⁺ calc., 230.1411 found 230.1409.

6-((3a*R*,6a*S*)-5-methylhexahydropyrrolo[3,4-*c*]pyrrol-2(1*H*)-yl)-9*H*-purine (156)



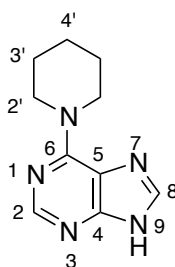
Following general procedure **4**, employing 2-methyloctahydropyrrolo[3,4-*c*]pyrrole (491 mg, 3.90 mmol) and heated at reflux for 2.5 h. The solid was isolated through filtration using a sintered funnel. The crude solid was washed with MeOH (2 × 25 mL) and dichloromethane (2 × 25 mL) to give *purine 156* as a as a colourless solid (729 mg, 92%). mp 254 °C (EtOH); $\nu_{\max}/\text{cm}^{-1}$ (film) 3105, 3005, 2863 and 1579; δ_{H} (500 MHz, MeOD) 8.09 (1H, s, 2-H), 7.92 (1H, s, 8-H), 4.62- 3.97 (4H, m, 2'-H), 3.07 – 2.90 (2H, m, 3'-H₂), 2.85 – 2.68 (2H, m, 3'-H₃), 2.47 – 2.33 (2H, m, 3a'-H), 2.24 (3H, s, 5'-H); δ_{C} (500 MHz, MeOD) 153.8 (C-6), 152.5 (C-2), 151.2 (C-4), 138.9 (C-8), 119.6 (C-5), 50.9 (C-1'), 49.5 (C-3'), 16.7 (C-2') 10.1 (C-5'); HRMS [M+H]⁺ C₁₂H₁₇N₆⁺ calc. 245.1509, found 245.1503.

6-((3a*R*,7a*S*)-hexahydro-1*H*-isoindol-2(3*H*)-yl)-9*H*-purine (157)



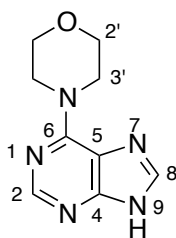
Following general procedure **4**, employing 2 octahydro-1*H*-isoindole (487 mg, 3.90 mmol) and heated at reflux for 4 h. The solid was isolated through filtration using a sintered funnel. The crude solid was washed with MeOH (2 × 25 mL) and dichloromethane (2 × 25 mL) to give *purine 157* as a colourless solid (789 mg, 88%). mp 213 °C (EtOH); $\nu_{\text{max}}/\text{cm}^{-1}$ (film) 3165, 3015, 2822 and 1674; δ_{H} (500 MHz, DMSO- d_6) 12.98 – 12.76 (1H, m, 9-H), 8.16 (1H, s, 2-H), 8.04 (1H, s, 8-H), 4.10 – 3.93 (2H, m, 2'-H), 3.66 – 3.47 (2H, m, 2'-H), 2.31 (2H, m, 3a'-H), 1.70 – 1.29 (8H, m, 3'-H, 4'-H); δ_{C} (125 MHz DMSO- d_6) 153.5 (C-6), 152.6 (C-2), 151.1 (C-4), 138.6 (C-8), 119.6 (C-5), 52.9 (C-1'), 37.6 (C-2'), 35.6 (C-3'), 22.9 (C-4'); HRMS $[\text{M}+\text{H}]^+$ C₁₃H₁₈N₅⁺ calc 244.1567, found 244.1577.

6-(piperidin-1-yl)-9*H*-purine (158)



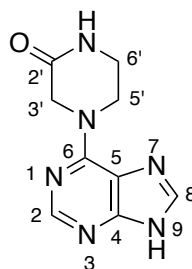
Following general procedure **4**, employing piperidine (659 mg, 3.90 mmol) and heated at reflux for 1 h. The solid was isolated through filtration using a sintered funnel. The crude solid was washed with MeOH (2 × 25 mL) and dichloromethane (2 × 25 mL) to give purine **158** as an off-white solid (297 mg, 45%). mp 232 °C (EtOH); $\nu_{\text{max}}/\text{cm}^{-1}$ (film) 2973, 2920 and 1570; δ_{H} (500 MHz, DMSO- d_6) 8.18 (1H, s, 2-H), 8.08 (1H, s, 8-H), 4.20 (4H, m, 2'-H), 1.68 (2H, m, 4'-H), 1.58 (4H, m, 3'-H); δ_{C} (125 MHz DMSO- d_6) 153.6 (C-6), 152.3 (C-2), 151.8 (C-4), 138.2 (C-8), 119.1 (C-5), 46.0 (C-2'), 26.2 (C-4'), 24.8 (C-3'); HRMS $[\text{M}+\text{H}]^+$ $\text{C}_{10}\text{H}_{14}\text{N}_5$ calc. 204.1244 found 204.1244. Data in accordance with literature.²²⁰

4-(9*H*-purin-6-yl)morpholine (159)



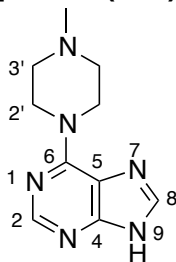
Following general procedure **4**, employing morpholine (339 mg, 3.90 mmol) and heated at reflux for 1 h. The solid was isolated through filtration using a sintered funnel. The crude solid was washed with MeOH (2 × 25 mL) and dichloromethane (2 × 25 mL) to give *purine 159* as a as a colourless solid (712 mg, 92%). mp 212 °C (EtOH); $\nu_{\max}/\text{cm}^{-1}$ (film) 3076, 2974, 2961, 2689 and 1628; δ_{H} (500 MHz, DMSO- d_6) δ 13.07 (1H, s, 9-H), 8.23 (1H, s, 2-H), 8.14 (1H, s, 8-H), 4.21 (4H, m, 2'-H), 3.72 (4H, m, 3'-H); δ_{C} (125 MHz DMSO- d_6) 153.7 (C-6), 152.2 (C-2), 151.9 (C-4), 138.8 (C-8), 119.3 (C-5), 66.7 (C-2'), 45.6 (C-3'); HRMS $[\text{M}+\text{H}]^+$ $\text{C}_9\text{H}_{12}\text{N}_5\text{O}^+$ calc., 206.1047, found 206.1043. Data in accordance with reported spectra.²²⁰

4-(9*H*-purin-6-yl)piperazin-2-one (**160**)



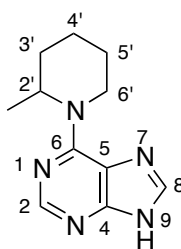
Following general procedure **4**, employing piperazin-2-one (390 mg, 3.90 mmol) and heated at reflux for 5 h. The solid was isolated through filtration using a sintered funnel. The crude solid was washed with MeOH (2 × 25 mL) and dichloromethane (2 × 25 mL) to give *purine* **160** as a yellow solid (644 mg, 91%). mp 196 °C (EtOH); $\nu_{\max}/\text{cm}^{-1}$ (film) 3156, 3000, 2823 1753 and 1628; δ_{H} (500 MHz, DMSO- d_6) 13.00 (1H, s, 9-H), 8.21 (1H, s, 2-H), 8.11 (1H, s, 8-H), 4.47 (2H, s, 3'-H), 3.77 (2H, t, J 5.1, 5'-H), 3.63 (2H, t, J 5.6, 6'-H), 3.33 (1H, s, NH); δ_{C} (125 MHz DMSO- d_6) 167.2 (C-2'), 153.0 (C-6), 151.9 (C-2), 151.8 (C-4), 139.2 (C-8), 119.3 (C-5), 56.5 (C-3'), 48.8 (C-5'), 40.6 (C-6'); HRMS $[\text{M}+\text{H}]^+$ $\text{C}_9\text{H}_{11}\text{N}_6\text{O}^+$ calc 219.0999, found 219.0997.

6-(4-methylpiperazin-1-yl)-9H-purine (161)



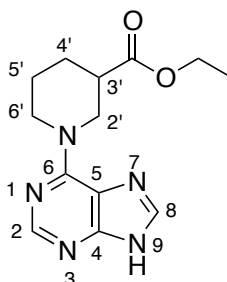
Following general procedure **4**, employing 1-methyl piperazine (390 mg, 3.90 mmol) and heated at reflux for 5 h. The solid was isolated through filtration using a sintered funnel. The crude solid was washed with MeOH (2 × 25 mL) and dichloromethane (2 × 25 mL) to give *purine 161* as a colourless solid (630 mg, 89%). mp 241 °C (EtOH); $\nu_{\max}/\text{cm}^{-1}$ (film) 3531, 3065, 2941, 2780, 2673 and 1699; δ_{H} (500 MHz, DMSO- d_6) 12.97 (s, 1H, 9-H), 8.18 (1H, s, 2-H), 8.09 (1H, s, 8-H), 3.03 (2H, t, J 12.9, 2'-H₂), 1.70 (4H, m, 2'-H₃ 3'-H₂), 1.16 – 1.04 (2H, m, 3'-H₃), 0.92 (3H, s, CH₃); δ_{C} (125 MHz DMSO- d_6) 153.6 (C-6), 152.3 (C-2), 151.8 (C-4), 138.2 (C-8), 119.2 (C-5), 45.3 (C-2'), 34.4 (C-3'), 31.1, (CH₃). HRMS [M+H]⁺ C₁₀H₁₅N₆⁺ calc., 219.1353, found 219.1363.

6-(2-methylpiperidin-1-yl)-9H-purine (162)



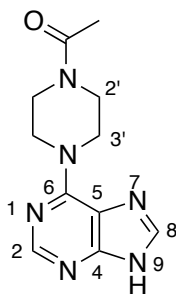
Following general procedure **4**, employing 2-methyl piperidine (386 mg, 3.90 mmol) and heated at reflux for 5 h. The solid was isolated through filtration using a sintered funnel. The crude solid was washed with MeOH (2 × 25 mL) and dichloromethane (2 × 25 mL) to give *purine* **562** as a colourless needles (846 mg, 74%). mp 264 °C (EtOH); $\nu_{\max}/\text{cm}^{-1}$ (film) 3417, 3081, 2945, 2804 and 1519; δ_{H} (400 MHz, DMSO- d_6) 12.97 (1H, s, 9-H), 8.18 (1H, s, 2-H), 8.09 (1H, s, 8-H), 3.15 – 2.99 (1H, m, 2'-H), 2.78 (2H, s, 6'-H), 1.85 – 1.38 (4H, m, 5'-H, 4'-H), 1.21 (2H, m, 3'-H), 0.91 (3H, d, J 6.6, CH₃); δ_{C} (125 MHz DMSO- d_6) 153.6 (C-6), 152.3 (C-2), 151.8 (C-4), 138.2 (C-8), 119.1 (C-5), 52.2 (C-2'), 45.5 (C-6'), 33.3 (C-5'), 31.3 (C-3'), 25.5 (C-4'), 19.4 (CH₃); HRMS [M+H]⁺ C₁₁H₁₆N₅⁺ calc. 218.1411, found 218.1406.

Ethyl 1-(9*H*-purin-6-yl)piperidine-3-carboxylate (**163**)



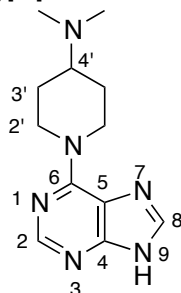
Following general procedure **4**, employing ethyl piperidine-3-carboxylate (612 mg, 3.90 mmol) and heated at reflux for 5 h. The solid was isolated through filtration using a sintered funnel. The crude solid was washed with MeOH (2 × 25 mL) and dichloromethane (2 × 25 mL) to give *purine* **163** as a colourless solid (867 mg, 97%). mp 215 °C (EtOH); $\nu_{\max}/\text{cm}^{-1}$ (film) 3288, 3069, 3019, 2994, 2204, 2042, 1765 and 1641; δ_{H} (500 MHz, DMSO- d_6) 8.21 (1H, s, H-1), 8.12 (1H, s, 8-H), 5.21 (2H, app s, 2'-H), 4.08 (2H, q, J 7, OCH₂), 3.32 (2H, m, 6'-H), 2.71 (1H, app. tt, J 11.0, 4.0, 3'-H), 1.94 (2H, app. dt, J 13.3, 3.7, 5'-H), 1.56 (2H, app. dtd, J 13.2, 11.3, 4.1, 4'-H), 1.19 (3H, br, OCH₂CH₃); δ_{C} (125 MHz DMSO- d_6) 174.5 (ester C=O), 153.6 (C-6) 152.3 (C-2), 151.9 (C-4), 138.5 (C-8), 119.3 (C-5), 60.4 (ester OCH₂), 44.4 (C-2'), 40.8 (C-6'), 40.2 (C-3'), 39.8 (C-4') 28.3 (C-5'), 14.6 (ester OCH₂CH₃); HRMS [M+H]⁺ C₁₃H₁₈N₅O₂⁺ calc. 276.1465, found 276.1478.

1-(4-(9H-purin-6-yl)piperazin-1-yl)ethanone (164)



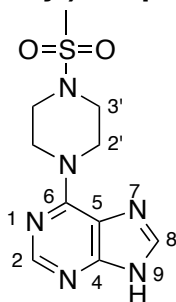
Following general procedure **4**, employing 1-(piperazin-1-yl)ethanone (499 mg, 3.90 mmol) and heated at reflux for 2 h. The solid was isolated through filtration using a sintered funnel. The crude solid was washed with MeOH (2 × 25 mL) and dichloromethane (2 × 25 mL) to give *purine* **164** as a colourless solid (295 mg, 37%). mp 219 °C (EtOH); $\nu_{\max}/\text{cm}^{-1}$ (film) 3123, 3001, 2821, 1762 and 1628; δ_{H} (500 MHz, DMSO- d_6) 8.26 (1H, s, 2-H), 8.18 (1H, s, 8-H), 4.35 (4H, m, 3'-H), 3.25 (4H, m, 2'-H), 2.89 (3H, s, acetyl CH₃); δ_{C} (125 MHz DMSO- d_6) 210.03 (amide C=O) 153.4 (C-6), 152.2 (C-2), 152.1 (C-4) 139.1 (C-8), 119.4 (C-5), 46.1 (C-3'), 45.8 (C-2'), 34.3 (acetyl CH₃); HRMS [M+H]⁺ C₁₁H₁₅N₆O calc. 247.1302 found 247.1302.

***N,N*-dimethyl-1-(9*H*-purin-6-yl)piperidin-4-amine (165)**



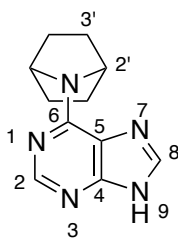
Following general procedure **4**, employing *N,N*-dimethylpiperidin-4-amine (499 mg, 3.90 mmol) and heated at reflux for 7 h. The solid was isolated through filtration using a sintered funnel. The crude solid was washed with MeOH (2 × 25 mL) and dichloromethane (2 × 25 mL) to give *purine 165* as a yellow solid (607 mg, 76%). mp 213 °C (EtOH); $\nu_{\max}/\text{cm}^{-1}$ (film) 3129, 3016, 2758 and 1599; δ_{H} (500 MHz, DMSO- d_6) 12.99 (1H, s, 9-H), 8.19 (1H, s, 2-H), 8.10 (1H, s, 8-H), 5.37 (4H, br s, 2'-H), 3.07 (4H, br s, 3'-H), 2.41 (1H, tt, J 11.0, 3.7, 4'-H), 2.17 (6H, s, N-CH₃); δ_{C} (125 MHz DMSO- d_6) 153.5 (C-6), 152.3 (C-2), 151.9 (C-4), 138.4 (C-8), 119.2 (C-5), 62.0 (C-2'), 44.3 (C-4'), 41.8 (N-CH₃), 28.6 (C-3'); HRMS [M+H]⁺ C₁₂H₁₉N₆⁺ calc. 247.1667, found 247.1680.

6-(4-(methylsulfonyl)piperazin-1-yl)-9H-purine (166)



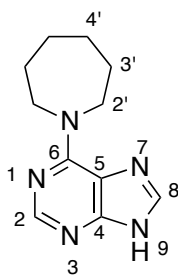
Following general procedure **4**, employing 1-(methylsulfonyl)piperazine (640 mg, 3.90 mmol) and heated at reflux for 7 h. The solid was isolated through filtration using a sintered funnel. The crude solid was washed with MeOH (2 × 25 mL) and dichloromethane (2 × 25 mL) to give *purine 166* as a brown solid (257 mg, 28%). mp 243 °C (EtOH); $\nu_{\max}/\text{cm}^{-1}$ (film) 3020, 2951, 2691 and 1574; δ_{H} (500 MHz, DMSO- d_6) 8.26 (1H, s, 2-H), 8.18 (1H, s, 8-H), 4.35 (4H, m, 2'-H), 3.25 (4H, m, 3'-H), 2.89 (3H, s, mesyl CH₃); δ_{C} (125 MHz DMSO- d_6) 153.4 (C-6), 152.1 (C-2), 151.1 (C-4) 139.1 (C-8), 119.4 (C-5), 45.8 (C-2'), 44.1 (C-3'), 34.3 (mesyl CH₃); HRMS [M+H]⁺ C₁₀H₁₅N₆O₂S⁺ calc. 283.0982, found 283.0982.

6-(7-azabicyclo[2.2.1]heptan-7-yl)-9H-purine (167)



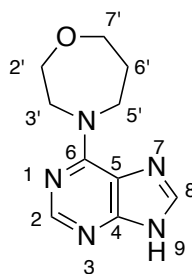
Following general procedure **4**, employing 7-azabicyclo[2.2.1]heptane (378 mg, 3.90 mmol) and heated at reflux for 6 h. The solid was isolated through filtration using a sintered funnel. The crude solid was washed with MeOH (2 × 25 mL) and dichloromethane (2 × 25 mL) to give *purine 167* as a colourless solid (384 mg, 55%). mp 223 °C (EtOH); $\nu_{\max}/\text{cm}^{-1}$ (film) 3188, 3010, 2861 and 1654; δ_{H} (500 MHz, DMSO- d_6) 8.25 (1H, s, 2-H), 8.17 (1H, s, 8-H), 3.33 (2H, s, 2'-H), 1.79 – 1.61 (4H, m, 3'-H₂), 1.52 (4H, m, 3'-H₃); δ_{C} (125 MHz DMSO- d_6) 154.0 (C-6), 152.6 (C-2), 151.7 (C-4), 139.9 (C-8), 120.3 (C-5), 56.5 (C-2'), 29.9 (C-3'); HRMS [M+H]⁺ C₁₁H₁₄N₅⁺ calc. 216.1254 found 216.1255.

6-(azepan-1-yl)-9H-purine (168)



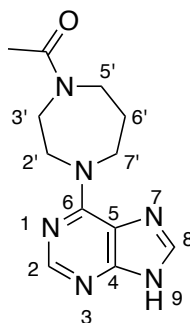
Following general procedure **4**, employing azepane (386 mg, 3.90 mmol) and heated at reflux for 2 h. The crude solid was washed with MeOH (2 × 25 mL) and dichloromethane (2 × 25 mL) to give *purine 168* as a colourless solid (592 mg, 84%). mp 207 °C (EtOH); $\nu_{\text{max}}/\text{cm}^{-1}$ (film) 3066, 2918, 2847, 2763, 2553 and 1571; δ_{H} (500 MHz, DMSO- d_6) 12.92 (1H, s, 9-H), 8.17 (1H, s, 2-H), 8.07 (1H, s, 8-H), 4.34 (2H, br s, 2'-H₂), 3.84 (2H, br s, 2'-H₃), 1.83 – 1.73 (4H, m, 3'-H₂, 4'-H₃), 1.50 (4H, m, 3'-H₃, 4'-H₃); δ_{C} (125 MHz DMSO- d_6) 154.0 (C-6), 152.4 (C-2), 151.6 (C-4), 138.4 (C-8), 119.0 (C-5), 49.5 (C-2'), 29.2 (C-3'), 27.2 (C-4'); HRMS [M+H]⁺ C₁₁H₁₆N₅⁺ calc. 218.1411 found, 218.1400.

4-(9*H*-purin-6-yl)-1,4-oxazepane (**169**)



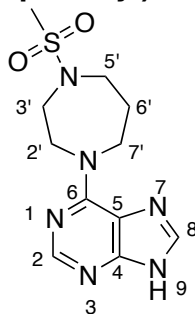
Following general procedure **4**, employing 1,4-oxazepane (393 mg, 3.90 mmol) and heated at reflux for 4 h. The solid was isolated through filtration using a sintered funnel. The crude solid was washed with MeOH (2 × 25 mL) and dichloromethane (2 × 25 mL) to give *purine* **169** as a colourless solid (640 mg, 90%). mp 285 °C (EtOH); $\nu_{\max}/\text{cm}^{-1}$ (film) 3076, 3002, 2950, 2700 and 1696; δ_{H} (500 MHz, DMSO- d_6) 13.00 (1H, s, 9-H), 8.21 (1H, s, 2-H), 8.11 (1H, s, 8-H), 4.47 (2H, s, 2'-H), 3.98 (2H, s, 7'-H), 3.77 (2H, t, J 5.1, 3'-H), 3.63 (2H, t, J 5.6, 5'-H), 1.97 – 1.89 (2H, m, 6'-H); δ_{C} (125 MHz DMSO- d_6) 153.9 (C-6), 152.4 (C-2), 151.7 (C-4), 138.8 (C-8), 119.1 (C-5), 70.7 (C-2'), 69.3 (C-7'), 49.7 (C-3') 47.9 (C-5'), 29.0 (C-6'); HRMS $[M]^+$ C₁₀H₁₃N₅O⁺ calc., 219.1125, found 219.1126.

1-(4-(9H-purin-6-yl)-1,4-diazepan-1-yl)ethanone (170)



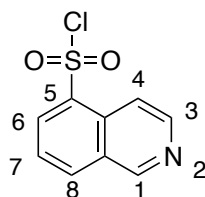
Following general procedure **4**, employing 1-(1,4-diazepan-1-yl)ethanone (553 mg, 3.90 mmol) and heated at reflux for 4 h. The solid was isolated through filtration using a sintered funnel. The crude solid was washed with MeOH (2 × 25 mL) and dichloromethane (2 × 25 mL) to give *purine 170* as a colourless solid (710 mg, 84%). mp 229 °C (EtOH); $\nu_{\max}/\text{cm}^{-1}$ (film) 3187, 3012, 2812, 1782 and 1628; δ_{H} (500 MHz, DMSO- d_6) 8.21 (1H, s, 2-H), 8.13 (1H, s, 8-H), 4.73 – 3.75 (4H, m, 2'-H, 7'-H), 3.68 (2H, m, 3'-H), 3.43 (2H, m, 5'-H), 2.05 – 1.71 (5H, m, 6'-H, acetyl CH₃); δ_{C} (125 MHz DMSO- d_6) 210.1 (acetyl C=O), 153.6 (C-6), 152.4 (C-2), 151.7 (C-4), 139.0 (C-8), 119.1 (C-5), 50.0 (C-2'), 49.5 (C-7'), 47.2 (C-3'), 44.7 (C-5'), 36.4 (C-6'), 21.5 (acetyl CH₃); HRMS [M+H]⁺ C₁₂H₁₇N₆O⁺ calc. 261.1458, found 261.1460.

6-(4-(methylsulfonyl)-1,4-diazepan-1-yl)-9H-purine (171)



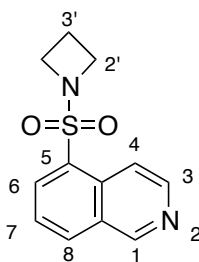
Following general procedure 4, employing 1-(methylsulfonyl)-1,4-diazepane (694 mg, 3.90 mmol) and heated at reflux for 4 h. The solid was isolated through filtration using a sintered funnel. The crude solid was washed with MeOH (2 × 25 mL) and dichloromethane (2 × 25 mL) to give *purine 171* as a colourless solid (577 mg, 60%). mp 232 °C (EtOH); $\nu_{\max}/\text{cm}^{-1}$ (film) 3006, 2949, 2567 and 1575; δ_{H} (500 MHz, DMSO- d_6) 8.23 (1H, s, 2-H), 8.14 (1H, s, 8-H), 4.70 – 3.78 (4H, m, 7-H', 5'-H), 3.50 (2H, t, J 5.5, 2'-H), 3.41 – 3.17 (2H, t, J 5.5, 3'-H), 2.82 (3H, s, mesyl CH₃), 1.92 (2H, app. s, 6'-H); δ_{C} (125 MHz DMSO- d_6) 153.6 (C-6), 152.4 (C-2), 151.8 (C-4), 139.1 (C-8), 119.1 (C-5), 50.5 (C-2'), 46.9 (C-7'), 46.0 (C-3'), 44.5 (C-5'), 37.3 (mesyl CH₃), 29.6 (C-6'); HRMS [M+H]⁺ C₁₁H₁₇N₆O₂S⁺ calc. 297.1139, found 297.1148.

Isoquinoline-5-sulfonyl chloride (173)



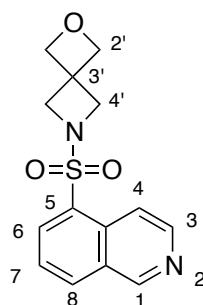
A flask was charged with isoquinoline-5-sulfonic acid (3.20 g, 15.30 mmol) dissolved in SOCl_2 (20 mL), After addition of DMF (0.5 mL) the mixture was heated to reflux for 1 h. Excess SOCl_2 was removed under pressure, the resulting solid was re-suspended in DCM, filtered over a glass-filter and washed with CH_2Cl_2 to yield the product (3.83 g, 95%. $\nu_{\text{max}}/\text{cm}^{-1}$ (film) 1201; δ_{H} (500 MHz, $\text{DMSO-}d_6$ 10.15 (br, 1H, 1-H), 9.22 – 9.11 (m, 1H, 4-H), 8.86 (dd, $J = 7.1, 1.5$ Hz, 1H, 3-H), 8.59 – 8.44 (m, 2H, 6-H, 8-H), 7.98 (ddd, $J = 10.7, 8.3, 7.2$ Hz, 1H, 7-H). δ_{C} (125 MHz, $\text{DMSO-}d_6$) 147.8 (C-1), 144.2 (C-3), 134.6 (C-6, C-8), 134.3 (C-6, C-8), 132.9 (C-5), 132.3 (C-4a), 130.8 (C-7), 128.0 (C-7), 125.2 (C-4). Spectral data in accordance with literature.²²⁵

5-(azetidin-1-ylsulfonyl)isoquinoline (174)



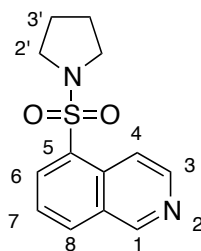
Following general procedure **5**, employing azetidine hydrochloride (299 mg, 3.21 mmol) and stirred at room temperature for 18 h. The solid was dissolved in CH₂Cl₂ (5 mL), dry loaded onto silica and purified by flash column chromatography eluting with EtOAc, to give *fragment 174* was isolated as a yellow solid (438 mg, 80%). R_f 0.40 (EtOAc). mp 233 °C (EtOH); $\nu_{\text{max}}/\text{cm}^{-1}$ (film) 2946, 2920, 2402, 2074, 1657 and 1351; δ_{H} (500 MHz, DMSO-*d*₆) 9.31 (1H, app. d, *J* 1.0, 1-H), 8.54 (1H, d, *J* 6.2, 4-H), 8.47 (1H, dt, *J* 6.2, 1.0, 3-H), 8.39 – 8.33 (2H, m, 6-H, 8-H), 7.77 (1H, d, 7.4, 7-H), 3.81 – 3.76 (4H, d, *J* 7.7, 2'-H), 2.04 (2H, d, *J* 7.7, 3'-H). δ_{C} (125 MHz, DMSO-*d*₆) 152.9 (C-1), 143.5 (C-3), 134.7 (C-6, C-8), 134.3 (C-6, C-8), 132.4 (C-5), 131.3 (C-8a), 129.3 (C-4a), 126.4 (C-7), 118.3 (C-4), 50.2 (C-2'), 14.6 (C-3'). HRMS [M+H]⁺ C₁₂H₁₃N₂O₂S⁺ 249.0698 found, 249.0708.

6-(isoquinolin-5-ylsulfonyl)-2-oxa-6-azaspiro[3.3]heptane (175)



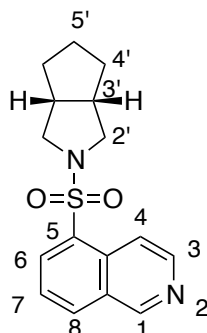
Following general procedure **5**, employing 2-oxa-6-azaspiro[3.3]heptane hydrochloride (433 mg, 3.21 mmol) and stirred at room temperature for 18 h. The solid was dissolved in CH₂Cl₂ (5 mL), dry loaded onto silica and purified by flash column chromatography eluting with EtOAc, to give *fragment 175* was isolated as a white solid (717 mg, 77%). R_f0.41 (EtOAc). mp 221 °C (EtOH); $\nu_{\max}/\text{cm}^{-1}$ (film) 2951, 2923, 2485, 1701 and 1328; δ_{H} (500 MHz, DMSO-*d*₆) 9.21 (1H, app. d, *J* 1.0, 1-H), 8.45 (1H, d, *J* 6.2, 4-H), 8.34 (1H, dt, *J* 6.2, 1.0, 3-H), 8.27 (2H, m, 6-H, 8-H), 7.67 (1H, m, 6-H), 4.46 (4H, s, 2'-H), 3.88 (4H, s, 4'-H); δ_{C} (125 MHz, DMSO-*d*₆) 152.9 (C-1), 143.7 (C-3), 134.7 (C-6, C-8), 134.5 (C-6, C-8), 127.1 (C-5), 126.3 (C-8a), 125.4 (C-4a) 124.3 (C-7), 118.2 (C-4), 80.0 (C-2'), 58.7 (C-4'), 37.3 (C-3'); HRMS [M+H]⁺ C₁₄H₁₆N₂O₃S⁺ calc. 292.0887 found, 292.0886.

5-(pyrrolidin-1-ylsulfonyl)isoquinoline (176)



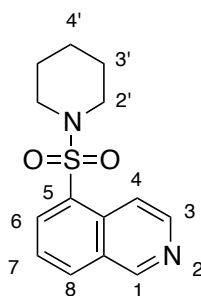
Following general procedure **5**, employing pyrrolidine (228 mg, 3.21 mmol) and stirred at room temperature for 18 h. The solid was dissolved in CH₂Cl₂ (5 mL), dry loaded onto silica and purified by flash column chromatography eluting with EtOAc, to give *fragment 176* as a white solid (382 mg, 66%). R_f 0.28 (EtOAc). mp 230 °C (EtOH); $\nu_{\max}/\text{cm}^{-1}$ (film) 3433, 3225 2985, 2923, 2866, 2727, 2678, 1813 and 1372; δ_{H} (500 MHz, MeOD) 9.28 (1H, app. d, J 1.0, 1-H), 8.56 (1H, dt, J 6.2, 1.0, 3-H), 8.51 (1H, d, J 6.2, 4-H), 8.36 – 8.28 (2H, m, 6-H, 8-H), 7.74 (1H, dd, J 8.2, 7.4, 7-H), 3.23 (4H, td, J 4.4, 2.5, 2'-H), 1.77 – 1.66 (4H, m, 3'-H); δ_{C} (125 MHz, DMSO-*d*₆) 152.9 (C-1), 143.5 (C-3), 133.70 (C-6, C-8), 133.69 (C-6, C-8), 133.3 (C-5), 132.1 (C-4a), 129.4 (C-8a), 126.4 (C-7), 118.2 (C-4), 47.4 (C-2'), 25.1 (C-3'); HRMS [M+H]⁺ C₁₃H₁₅N₂O₂S⁺ calc., 263.0859 found, 263.0859.

5-(((3a*R*,6a*S*)-hexahydrocyclopenta[*c*]pyrrol-2(1*H*)-yl)sulfonyl)-isoquinoline (177)



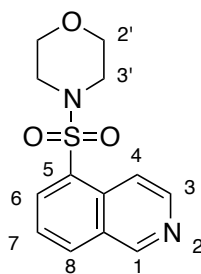
Following general procedure **5**, employing (3a*R*,6a*S*)-octahydrocyclopenta[*c*]pyrrole hydrochloride (417 mg, 3.21 mmol) and stirred at room temperature for 18 h. The solid was dissolved in CH₂Cl₂ (5 mL), dry loaded onto silica and purified by flash column chromatography eluting with EtOAc, to give *fragment 177* was isolated as a brown solid (437 mg, 71%). *R_f* 0.50 (EtOAc). mp 199 °C (EtOH); $\nu_{\max}/\text{cm}^{-1}$ (film) 3497, 3441, 2956, 2618, 2087, 1652 and 1356; δ_{H} (500 MHz, MeOD) 9.40 (1H, s, 1-H), 8.73 – 8.65 (1H, m, 3-H), 8.63 (1H, m, 4-H), 8.45 (2H, m, 6-H, 8-H), 7.87 (1H, m, 7-H), 3.25 (2H, dq, *J* 10.8, 6.5, 2'-H₂), 3.03 (2H, dd, *J* 9.8, 3.1, 2'-H₃), 2.59 (2H, m, 4'-H₂), 1.84 – 1.69 (2H, m, 4'-H₃), 1.61 – 1.50 (1H, m, 5'-H₂), 1.44 (1H, m, 5'-H₃), 1.31 (2H, m, 3'-H). δ_{C} (125 MHz, DMSO-*d*₆) 152.9 (C-1), 143.5 (C-3), 134.5 (C-6, C-8), 134.0 (C-7, C-8), 131.2 (C-5), 130.5 (C-8a), 129.1 (C-4a), 126.3 (C-7), 118.3 (C-4), 54.0 (C-2'), 42.7 (C-3'), 32.4 (C-4'), 25.6 (C-5'). HRMS [M+H]⁺ C₁₆H₁₉N₂O₂S⁺ 303.1173 found 303.1182.

5-(piperidin-1-ylsulfonyl)isoquinoline (178)



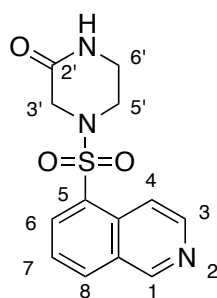
Following general procedure **5**, employing piperidine (272 mg, 3.21 mmol) and stirred at room temperature for 18 h. **178** was isolated as white needles (201 mg, 33%). R_f 0.30 (EtOAc). mp 228 °C (EtOH); $\nu_{\max}/\text{cm}^{-1}$ (film) 3356, 3073, 2952, 1685 and 1342; δ_{H} (500 MHz, DMSO- d_6) 9.55 (1H, br, 1-H), 8.71 (1H, app. d, J 7.2, 3-H), 8.51 (1H, d, J 7.2, 4-H), 8.40 – 8.36 (2H, m, 6-H, 8-H), 7.91 – 7.88 (1H, m, 7-H), 3.09 (4H, t, J 5.4, 2'-H), 1.49 (4H, m, 3'-H), 1.38 (2H, m, 4'-H); δ_{C} (125 MHz, DMSO- d_6) 156.9 (C-1), 147.4 (C-3), 138.3 (C-6, C-8), 137.7 (C-6, C-8), 136.7 (C-5), 135.9 (C-8a), 133.3 (C-4a), 130.3 (C-7) 122.0 (C-4), 46.5 (C-2'), 25.4 (C-3'), 23.3 (C-4'); HRMS $[\text{M}+\text{H}]^+$ $\text{C}_{14}\text{H}_{17}\text{N}_2\text{O}_2\text{S}^+$ 277.1016, found 277.1012.

4-(isoquinolin-5-ylsulfonyl)morpholine (179)



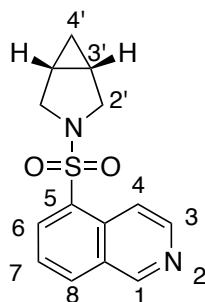
Following general procedure **5**, employing piperidine (279 mg, 3.21 mmol) and stirred at room temperature for 18 h. The solid was dissolved in CH₂Cl₂ (5 mL), dry loaded onto silica and purified by flash column chromatography eluting with EtOAc, to give *fragment 179* was isolated as a brown oil (381 mg, 62%). *R_f* 0.25 (EtOAc). mp 219 °C (EtOH); $\nu_{\max}/\text{cm}^{-1}$ (film) 3099, 2854, 1696 and 1340; δ_{H} (500 MHz, DMSO-*d*₆) 9.52 (1H, dd, *J* 1.2, 0.9, 1-H), 8.71 (1H, d, *J* 6.2, 4-H), 8.54 (1H, dt, *J* 8.2, 1.0, 3-H), 8.45 (1H, dd, *J* 6.2, 1.0, 6-H), 8.38 (1H, app. dd, *J* 7.4, 1.2, 8-H), 7.91 (1H, m, 7-H), 3.66 – 3.55 (4H, m, 2'-H), 3.12 – 2.98 (4H, m, 3'-H). δ_{C} (125 MHz, DMSO-*d*₆) 153.6 (C-1), 144.4 (C-3), 134.8 (C-6, C-8), 134.8 (C-6, C-8), 132.3 (C-8a), 131.7 (C-5), 129.2 (C-4a), 127.3 (C-7), 117.6 (C-4), 66.0 (C-2'), 45.9 (C-3'). HRMS [M+H]⁺ C₁₃H₁₅N₂O₃S⁺ calc., 279.0808 found 279.0813.

4-(isoquinolin-5-ylsulfonyl)piperazin-2-one (180)



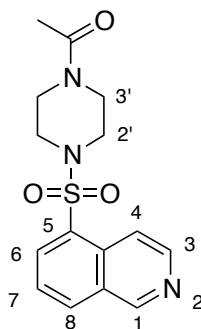
Following general procedure **5**, employing piperazin-2-one (321 mg, 3.21 mmol) and stirred at room temperature for 18 h. The solid was dissolved in CH_2Cl_2 (5 mL), dry loaded onto silica and purified by flash column chromatography eluting with EtOAc, to give *fragment 180* was isolated as a yellow solid (495 mg, 77%). R_f 0.22 (EtOAc). mp 182 °C (EtOH); $\nu_{\text{max}}/\text{cm}^{-1}$ (film) 3301, 2912, 2893, 2421, 2056, 1682 and 1336; δ_{H} (500 MHz, MeOD) 9.31 (1H, app. d, J 0.9, 1-H), 8.55 (1H, d, J 6.2, 4-H), 8.47 (1H, dt, J 6.2, 0.9, 3-H), 8.44 – 8.34 (2H, m, 6-H, 8-H), 7.78 (1H, dd, J 8.2, 7.4, 7-H), 4.75 (2H, m, 3'-H), 3.71 (2H, m, 6'-H), 3.44 – 3.38 (2H, m, 5'-H). δ_{C} (125 MHz, MeOD) 166.8 (amide C=O), 153.1 (C-1), 143.9 (C-3), 134.5 (C-6, C-8), 133.6 (C-6, C-8) 133.1 (C-5), 131.8 (C-8a), 129.4 (C-4a), 126.4 (C-7), 118.0 (C-4), 41.7 (C-3'), 40.6 (C-6'), 40.2 (C-5'). HRMS $[\text{M}+\text{H}]^+$ $\text{C}_{13}\text{H}_{14}\text{N}_3\text{O}_3\text{S}^+$ calc., 292.0761 found, 292.0762.

5-((1*R*,5*S*)-3-azabicyclo[3.1.0]hexan-3-ylsulfonyl)isoquinoline (181)



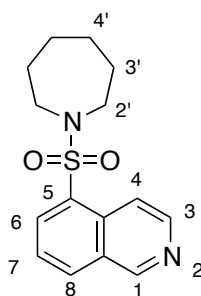
Following general procedure **5**, employing (1*R*,5*S*)-3-azabicyclo[3.1.0]hexane hydrochloride (382 mg, 3.21 mmol) and stirred at room temperature for 18 h. **181** was isolated as a white solid (284 mg, 47%). *R*_f 0.41 (EtOAc). mp 192 °C (EtOH); $\nu_{\text{max}}/\text{cm}^{-1}$ (film) 3263, 2941, 2856, 2412, 2073, 1676 and 1375; δ_{H} (500 MHz, DMSO-*d*₆) 9.48 (1H, br, 1-H), 8.69 (1H, d, *J* 6.1, 4-H), 8.48 (1H, dt, *J* 8.3, 1.1, 3-H), 8.42 – 8.32 (2H, m, 6-H, 8-H), 7.86 (1H, d, *J* 8.2, 7.4, 7-H), 3.44 (2H, d, *J* 8.5, 7.4, 1'-H), 3.18 (2H, dt, *J* 9.6, 1.7, 2'-H), 1.47 (2H, dddd, *J* 7.6, 3.9, 2.3, 1.2, 3'-H), 0.51 (2H, m, *J* 7.7, 4.8, 4'-H); δ_{C} (125 MHz, DMSO-*d*₆) 154.0 (C-1), 145.4 (C-3), 134.6 (C-6, C-8), 134.1 (C-6, C-8), 132.5 (C-5), 131.5 (C-8a), 129.2 (C-4a), 127.1 (C-7), 117.6 (C-4), 49.8 (C-2'), 15.6 (C-3'), 7.5 (C-4'); HRMS [M+H]⁺ C₁₄H₁₅N₂O₂S⁺ calc., 275.0860 found 275.0866.

1-(4-(isoquinolin-5-ylsulfonyl)piperazin-1-yl)ethanone (182)



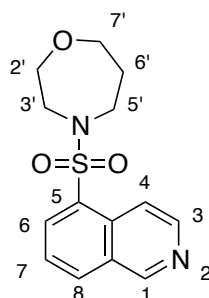
Following general procedure **5**, employing 1-(piperazin-1-yl)ethanone (410 mg, 3.21 mmol) and stirred at room temperature for 18 h. The solid was dissolved in CH₂Cl₂ (5 mL), dry loaded onto silica and purified by flash column chromatography eluting with EtOAc, to give *fragment 182* was isolated as a white solid (535 mg, 76%). R_f 0.30 (10% MeOH in EtOAc). mp 189 °C (EtOH); $\nu_{\text{max}}/\text{cm}^{-1}$ (film) 3190, 2952, 2880, 2492, 1780 1620 and 1351; δ_{H} (500 MHz, MeOD) 9.29 (1H, dd, J 1.1, 0.9, 1-H), 8.56 – 8.47 (2H, m, 3-H, 4-H), 8.37 – 8.33 (2H, m, 6-H, 7-H), 7.76 (1H, app. dd, J 8.2, 1.1, 8-H), 3.50 (2H, dt, J 5.2, 2'-H₂), 3.46 (2H, dt, J 5.2, 2'-H₃) 3.15 – 3.09 (2H, m, 3'-H₂), 3.09 – 3.03 (2H, m, 3'-H₃), 1.91 (3H, s, CH₃). δ_{C} (125 MHz, MeOD) 170.4 (acetyl C=O), 153.1 (C-1), 143.8 (C-3), 134.8 (C-6, C-8), 134.4 (C-6, C-8), 131.9 (C-5), 131.8 (C-4a), 129.3 (C-8a), 126.4 (C-7), 118.0 (C-4), 45.4 (C-2', C-3'), 45.2 (C-2', C-3'), 19.6 (acetyl CH₃). HRMS [M+H]⁺ C₁₅H₁₈N₃O₃S⁺ calc. 320.1074 found, 320.1069.

5-(azepan-1-ylsulfonyl)isoquinoline (**183**)



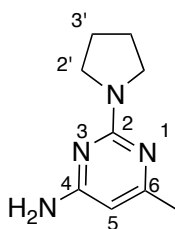
Following general procedure **5**, employing azepane (449 mg, 3.21 mmol) and stirred at room temperature for 18 h. The solid was dissolved in CH₂Cl₂ (5 mL), dry loaded onto silica and purified by flash column chromatography eluting with EtOAc, to give fragment **183** as a brown solid (69.1 mg, 70%). *R_f* 0.43 (EtOAc). mp 231 °C (EtOH); $\nu_{\text{max}}/\text{cm}^{-1}$ (film) 2922, 2855 and 1351; δ_{H} (500 MHz, MeOD) 9.27 (1H, d, *J* 1.0, 1-H), 8.51 (1H, dd, *J* 6.2, 1.5, 4-H), 8.44 (1H, d, *J* 6.2, 3-H), 8.26 (2H, m, 6-H, 8-H), 7.71 (1H, app. d, *J* 7.4, 7-H), 3.32 (4H, td, *J* 6.0, 1.7, 2'-H), 1.68 – 1.58 (4H, m, 3'-H), 1.58 – 1.48 (4H, m, 4'-H). δ_{C} (125 MHz, MeOD) 152.9 (C-1), 143.4 (C-3), 134.9 (C-5), 133.3 (C-6, C-8), 132.7 (C-6, C-8), 131.7 (C-4a), 129.4 (C-8a), 126.4 (C-7), 118.2 (C-4), 29.1–29.0 (C-2', C-3'), 26.5 (C-4'). HRMS [M+H]⁺ C₁₅H₁₉N₂O₂S⁺ 291.1172 found, 291.1186.

4-(isoquinolin-5-ylsulfonyl)-1,4-oxazepane (**184**)



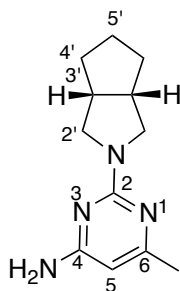
Following general procedure **5**, employing 1,4-oxazepane (324 mg, 3.21 mmol) and stirred at room temperature for 18 h. The solid was dissolved in CH_2Cl_2 (5 mL), dry loaded onto silica and purified by flash column chromatography eluting with EtOAc, to give *fragment 184* was isolated as a white solid (509 mg, 79%). R_f 0.48 (10:90 MeOH–EtOAc). mp 190 °C (EtOH); $\nu_{\text{max}}/\text{cm}^{-1}$ (film) 2823, 2620, 2419, 2021, 1660 and 1335; δ_{H} (500 MHz, MeOD) 9.27 (1H, app. d, J 1.0, 1-H), 8.51 (1H, d, J 6.2, 4-H), 8.41 (1H, dt, J 6.2, 1.0, 3-H), 8.28 – 8.25 (2H, m, 6-H, 8-H), 7.71 (1H, dd, J 8.3, 7.4, 7-H), 3.69 – 3.61 (4H, m, 2'-H, 7'-H), 3.46 – 3.40 (4H, m, 3'-H, 5'-H), 1.85 – 1.76 (2H, m, 6'-H). δ_{C} (125 MHz, MeOD) 153.0 (C-1), 143.6 (C-3), 133.6 (C-6, C-8), 133.1 (C-6, C-8), 131.6 (C-8a), 129.4 (C-5), 126.4 (C-4a), 118.0 (C-7), 117.8 (C-4), 70.7 (C-2'), 69.2 (C-7'), 50.5 (C3'), 46.4 (C5'), 30.6 (C6'). HRMS $[\text{M}+\text{H}]^+$ $\text{C}_{14}\text{H}_{17}\text{N}_2\text{O}_3\text{S}^+$ calc. 293.0965 found, 293.0973.

6-methyl-2-(pyrrolidin-1-yl)pyrimidin-4-amine (191)



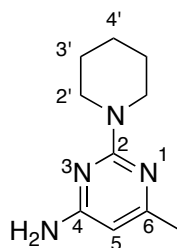
191 was isolated through procedure **6** employing pyrrolidine (160 mg, 2.25 mmol). The solid was washed with acetone (2 × 25 mL) and dichloromethane (2 × 25 mL) to give the product *fragment 191* as a brown solid (246 mg, 79%). mp 131 °C (EtOH); $\nu_{\max}/\text{cm}^{-1}$ (film) 3423, 3355, 2963, 2870, 2422 and 1671; δ_{H} (500 MHz, CDCl_3) 5.68 (1H, s, 5-H), 3.64 – 3.41 (4H, m, 2'-H), 2.15 (3H, d, J 2.0, pyrimidine CH_3), 2.02 – 1.88 (4H, m, 3'-H); δ_{C} (125 MHz, CDCl_3) 169.1 (C-4), 168.6 (C-6), 164.4 (C-2), 96.8 (C-5), 52.1 (C-2'), 29.1 (C-3'), 25.9 (pyrimidine CH_3); HRMS $[\text{M}+\text{H}]^+$ $\text{C}_9\text{H}_{15}\text{N}_4^+$ calc., 179.1302 found 179.1311.

2-((3a*R*,6a*S*)-hexahydrocyclopenta[*c*]pyrrol-2(1*H*)-yl)-6-methylpyrimidin-4-amine (192)



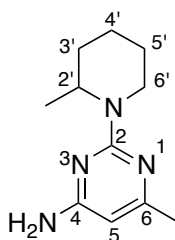
192 was isolated through procedure **6** employing (3a*R*,6a*S*)-octahydrocyclopenta[*c*]pyrrole (330 mg, 2.25 mmol). The solid was washed with acetone (2 × 25 mL) and dichloromethane (2 × 25 mL) to give the product *fragment 192* as a white solid (317 mg, 83%). mp 141 °C (EtOH); $\nu_{\text{max}}/\text{cm}^{-1}$ (film) 3483, 3390, 2344, 2450, 2392 and 1636; δ_{H} (500 MHz, DMSO-*d*₆) 6.14 (1H, s, 5-H), 3.57 (2H, dd, *J* 11.5, 6.9, 2'-H₂), 3.20 (2H, dd, *J* 11.1, 3.8, 2'-H₃), 2.63 (4H, m, 4'-H), 2.02 (3H, d, *J* 1.4, CH₃), 1.77 (1H, m, 5'-H₂), 1.72 – 1.61 (1H, m, 5'-H₃), 1.42 (2H, m, 3'-H); δ_{C} (125 MHz, DMSO-*d*₆) 164.6 (C-4), 164.6 (C-6), 161.2 (C-2), 93.3 (C-5), 53.1 (C-2'), 42.6 (C-3'), 32.6 (C-4'), 25.7 (C-5'), 24.2 (pyrimidine CH₃); HRMS [M+H]⁺ C₁₂H₁₉N₄⁺ calc., 219.1615, found 219.1604.

6-methyl-2-(piperidin-1-yl)pyrimidin-4-amine (193)



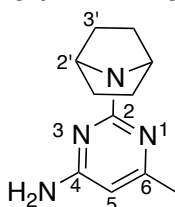
193 was isolated through procedure **6** employing piperidine (191 mg, 2.25 mmol). The solid was isolated through filtration using a sintered funnel. The solid was washed with acetone (2 × 25 mL) and dichloromethane (2 × 25 mL) to give the product *fragment 193* as a brown oil (259 mg, 77%). mp 131 °C (EtOH); $\nu_{\max}/\text{cm}^{-1}$ (film) 3450, 3365, 2991, 2900, 2389 and 1690 δ_{H} (500 MHz, CDCl_3) 5.56 (1H, s, 5-H), 3.64 – 3.49 (4H, m, 2'-H), 2.02 (3H, s, CH_3), 1.64 – 1.51 (2H, m, 4'-H), 1.51 – 1.35 (4H, m, 3'-H). δ_{C} (125 MHz, CDCl_3) 166.6 (C-4), 163.8 (C-6), 162.0 (C-2), 92.9 (C-5), 44.8 (C-2'), 25.5 (C-3'), 24.6 (C-4'), 23.2 (pyrimidine CH_3). HRMS $[\text{M}+\text{H}]^+$ $\text{C}_{10}\text{H}_{17}\text{N}_4^+$ calc., 193.1458, found 193.1456.

6-methyl-2-(2-methylpiperidin-1-yl)pyrimidin-4-amine (194)



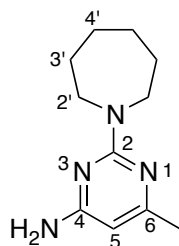
194 was isolated through procedure **6** employing 2-methyl piperidine (223 mg, 2.25 mmol). The solid was isolated through filtration using a sintered funnel. The solid was washed with acetone (2 × 25 mL) and dichloromethane (2 × 25 mL) to give the product *fragment 194* as a brown oil (292 mg, 81%). mp 120 °C (EtOH); $\nu_{\max}/\text{cm}^{-1}$ (film) 3398, 3332, 2909, 2821, 2761 and 1680; δ_{H} (500 MHz, CDCl_3) 5.50 (1H, s, 5-H), 4.62 – 4.40 (2H, m, 6'-H), 2.64 (1H, m, 2'-H) 2.32 (2H, m, 5'-H), 2.11 (3H, s, CH_3), 1.72– 1.52 (2H, m, 3'-H), 1.52 – 1.47 (2H, m, 4'-H), 1.47 – 1.01 (3H, br, CH_3); δ_{C} (125 MHz, CDCl_3) 166.6 (C-4), 163.8 (C-6), 162.0 (C-2), 92.8 (C-5), 51.3 (C-6'), 44.1 (C-2'), 33.6 (C-5'), 31.0 (C-3'), 25.4 (C-4'), 24.2 (pyrimidine CH_3), 19.4 (CH_3); HRMS $[\text{M}+\text{H}]^+$ $\text{C}_{11}\text{H}_{19}\text{N}_4^+$ 207.1615 found, 207.1620.

2-(7-azabicyclo[2.2.1]heptan-7-yl)-6-methylpyrimidin-4-amine (195)



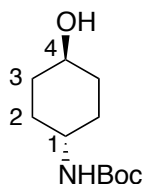
195 was isolated through procedure **6** employing 7-azabicyclo[2.2.1]heptane (218 mg, 2.25 mmol). The solid was isolated through filtration using a sintered funnel. The solid was washed with acetone (2 × 25 mL) and dichloromethane (2 × 25 mL) to give the product *fragment 195* as a white solid (357 mg, 64%). mp 131 °C (EtOH); 3378, 3345, 2803, 2730, 2515 and 1676; δ_{H} (500 MHz, CDCl_3) 5.68 (1H, s, 5-H), 4.46 (2H, m, 2'-H), 2.04 (3H, d, J 0.6, CH_3), 1.71 – 1.57 (4H, m, 3'-H₂), 1.36 (4H, m, 3'-H₃); δ_{C} (125 MHz, CDCl_3) 165.3 (C-4), 165.1 (C-6), 162.8 (C-2), 94.8 (C-5), 56.4 (C-2'), 48.1 (C-3'), 21.9 (CH_3); HRMS $[\text{M}+\text{H}]^+$ $\text{C}_{11}\text{H}_{17}\text{N}_4^+$ calc. 205.1459 found, 205.1452.

2-(azepan-1-yl)-6-methylpyrimidin-4-amine (196)



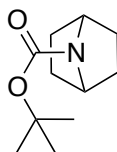
196 was isolated through procedure **6** employing azepane (223 mg, 2.25 mmol). The solid was isolated through filtration using a sintered funnel. The solid was washed with acetone (2 × 25 mL) and dichloromethane (2 × 25 mL) to give the product *fragment 196* as a brown solid (278 mg, 77%). mp 140 °C (EtOH); 3540, 3471, 2987, 2801, 2358 and 1640; δ_{H} (500 MHz, MeOD) 5.55 (1H, s, H5), 3.60 – 3.54 (4H, m, H2'), 2.03 (3H, d, J 0.6, CH₃), 1.69 – 1.60 (4H, m, H2'), 1.44 (4H, dt, J 7.5, 2.7, H3'). δ_{C} (125 MHz, CDCl₃) 165.1 (C-4), 164.8 (C-6), 161.7 (C-2), 92.5 (C-5), 48.1 (C-2'), 46.6 (C-3'), 27.9 (C-4'), 26.9 (pyrimidine CH₃). HRMS [M+H]⁺ C₁₁H₁₉N₄⁺ calc., 207.1615 found, 207.1617.

***tert*-Butyl((1*R*,4*R*)-4-hydroxycyclohexyl)carbamate (201)** ²³⁸



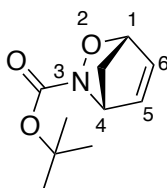
A solution of *trans*-4-aminocyclohexanol (5.00 g, 33 mmol) in 1,4-dioxane (100 mL) was cooled to 0 °C. After 15 min, sodium hydroxide (1.60 g, 40 mmol) dissolved in water (40 mL) was added and allowed to cool for an additional 15 min. A solution of di-*tert*-butyl dicarbonate (7.9 g, 36 mmol) dissolved in 1,4-dioxane (65 mL) was then added to the solution of amino alcohol and allowed to stir at rt for 18 h. The reaction was quenched by the addition of 1 M HCl (100 mL) followed by EtOAc (150 mL). The layers were separated, and the aqueous layer was extracted further with EtOAc (2 × 150 mL). The combined organic layers were washed sequentially with water (100 mL), brine (100 mL), and dried (MgSO₄) before being concentrated *in vacuo* to give a white solid (5.30 g, 75%). Note: The product can be carried forward to the mesylation step without further purification. *R*_f 0.23 (50:50 EtOAc–hexane; KMnO₄); $\nu_{\text{max}}/\text{cm}^{-1}$ (film): 2932, 2921, 1700, and 1210; ¹H-NMR (500 MHz, CDCl₃) 4.43 – 4.23 (1H, br s, NH), 3.52 (1H, tt, *J* 10.6, 4.4, 1-H), 3.43 – 3.27 (1H, br m, 4-H), 1.94 – 1.90 (4H, m, H-2, H-3), 1.73 (1H, s, OH), 1.37 (9H, s, ^tBu), 1.36 – 1.24 (2H, m, 2-H), 1.16 – 1.02 (2H, m, 3-H); ¹³C-NMR (100 MHz, CDCl₃) 155.4 (Carbonyl), 79.4 (C-O), 69.9 (C4), 49.0 (C-1), 34.1 (C-3), 31.3(C-2), 28.5 (^tBu). HRMS [M+H]⁺ C₁₁H₂₂N₁O₃⁺ calc., 215.1527 found, 215.1521. The spectral data for this compound is in accordance with literature. ²³⁸

***tert*-Butyl 7-azabicyclo[2.2.1]heptane-7-carboxylate (198)**²³⁸



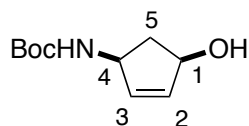
To a solution of *tert*-butyl((1*R*,4*R*)-4-hydroxycyclohexyl)carbamate (3.01 g, 13.9 mmol) in DCM (120 mL) was added triethylamine (2.9 mL, 20.9 mmol, 1.5 eq.). The resulting solution was then cooled to 0 °C followed by the dropwise addition of methanesulfonyl chloride (1.6 mL, 20.9 mmol, 1.5 eq.) followed by stirring for 50 min at 0 °C. The reaction was quenched by the slow addition of sat aq. NaHCO₃ solution (120 mL) with vigorous stirring. The reaction was then further diluted with DCM (40 mL) and sat aq. NaHCO₃ (40 mL) and then separated. The organic layer was then washed with water (60 mL) and dried (MgSO₄) before being concentrated *in vacuo* to give a white solid. The resulting product was then dissolved in dry THF (120 mL) followed by the addition of potassium *tert*-butoxide (770 mg, 7.00 mmol, 1.5 eq.). After 2 h, an additional portion of potassium *tert*-butoxide was added (2.32 g, 20.7 mmol, 1.5 eq.) and heated to 30 °C for 48 h. The reaction was cooled to 0 °C, quenched by the addition of 1 M HCl (50 mL), and separated. The organic layer was then washed with brine (30 mL), dried (MgSO₄), and concentrated *in vacuo*. Flash chromatography (10:90 EtOAc–hexane) yielded the desired product as a clear, colourless oil (1.80 g, 66%). Note: 95% purity by ¹H NMR; major impurity in reaction is the eliminated by-product Boc-3-amino cyclohexene. *R*_f 0.49 (10:90 EtOAc–hexane, KMnO₄); *v*_{max}/cm⁻¹ (film): 2965, 2943, 1700, 1386, 1700, 1386, 1373, 1331, 1192, 1157 and 1100; ¹H-NMR (500 MHz, CDCl₃) 4.10 (2H, br, 1-H), 1.76 (4H, m, 2-H), 1.47 (9H, s, ^tBu), 1.45 (4H, m, 2-H); ¹³C-NMR (100 MHz) 155.7 (carbonyl), 79.1 (C-O), 56.3 (C-1), 29.54 (C-2, C-3), 29.49 (C-2, C-3), 27.3 (^tBu). HRMS [M+Na]⁺ C₁₁H₁₉NO₂Na⁺ calc., 220.1319, found 220.1324. The spectral data for this compound is in accordance with literature.

***tert*-Butyl-2-oxa-3-azabicyclo[2.2.1]hept-5-ene-3-carboxylate (205)²⁶⁹**



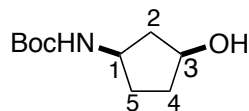
tert-Butyl hydroxycarbamate (811 mg, 6.1 mmol) was dissolved in MeOH-H₂O (3:1, 40 mL) and cooled to 0-5 °C. Freshly distilled cyclopentadiene (1.4 mL, 17.4 mmol) and then NaIO₄ (1.26 g, 5.9 mmol) were added, and the reaction was allowed to warm to room temperature and stirred 2 h. The reaction was cooled to 0-5 °C, more cyclopentadiene (1.0 mL, 12.5 mmol) and NaIO₄ (0.76 g, 3.5 mmol) were added, and the mixture was stirred for 30 min. The mixture was concentrated *in vacuo* to a slurry, H₂O was added (2 × 20 mL), and the solution was extracted with EtOAc (3 × 20 mL). The combined organic layers were washed with saturated sodium thiosulfate (20 mL), H₂O (20 mL), and brine (10 mL), dried over MgSO₄, vacuum-filtered through Celite, and concentrated *in vacuo* to give a tan oil (697 mg, 58%). This material was used in the next reaction without further purification. *R*_f 0.35 (10% EtOAc–hexane; KMnO₄); *v*_{max}/cm⁻¹ (film) 1740; ¹H-NMR (500 MHz, CDCl₃) 6.33 (2H, m, 5-H, 6-H), 5.13 (1H, app. q, *J* 2.1, 4-H), 4.90 (1H, app. t, *J* 1.9, 1-H), 1.89 (1H, app. dt, *J* 8.7, 2.0, 7-H), 1.66 (1H, app. dt, *J* 8.6, 1.0, 7-H), 1.36 (9H, s, ^tBu). ¹³C-NMR (100 MHz) 158.4 (carbonyl), 134.0 (C-5, C-6), 132.8 (C-5, C-6), 83.4 (C-4), 81.8 (C-O), 64.9 (C-1), 48.0 (C-7), 28.0 (^tBu). HRMS [M+Na]⁺ C₁₀H₁₅NO₃Na⁺ calc., 220.0955 found, 220.0947. Spectral data of the crude material was consistent with that reported in the literature.²⁷⁰

(1*RS*,4*RS*)-4-Aminocyclopent-2-enol (206**)**



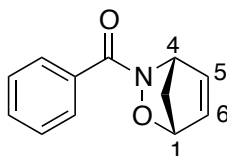
A 15:1 CH₃CN:H₂O solution of cycloadduct **205** (1.34 g, 6.73 mmol) was charged with Mo(CO)₆ (1.95 g, 7.40 mmol, 1.1 eq.) and refluxed under N₂ for 3 h and the solution turned black. The heat was then removed, and the solution allowed to cool to rt. The mixture was concentrated *in vacuo*, the crude mixture filtered through a celite pad and concentrated to give **206** as a brown solid (603 mg, 45%) which was used without further purification. R_f0.51 (40:60 EtOAc–hexane; KMnO₄). $\nu_{\text{max}}/\text{cm}^{-1}$ (film): 3324, 3056, 2979, 2871, 1700, 1675 and 1514; ¹H-NMR (500 MHz, CDCl₃) 6.39 – 6.36 (2H, m 2-H, 3-H), 5.21 – 5.13 (1H, m, 1-H), 4.94 (1H, m, 4-H), 1.95 (1H, ddd, *J* 14.4, 8.7, 2.1, 5-H_{ax}), 1.70 (1H, ddd, *J* 14.4, 8.7, 1.5, 5-H_{eq}), 1.53 – 1.37 (9H, br, ^tBu rotameric). ¹³C-NMR (100 MHz) 158.5 (carbonyl), 134.1 (C-2), 132.9 (C-3), 83.5 (C-O), 82.0 (C-1), 65.0 (C-4), 48.1 (C-5), 28.1 (^tBu). HRMS [M+Na]⁺ C₁₀H₁₇NNaO₃⁺ calc., 222.1111 found, 222.1114. Spectral data in accordance with literature.²⁷¹

***tert*-Butyl-((1*RS*,4*RS*)-4-hydroxycyclopent-2-en-1-yl)carbamate (207)**



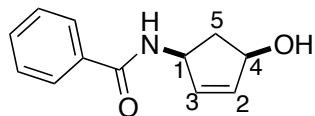
Pd/C (10% w/w, 100 mg) was added to a solution of the amine (1.10 g, 5.53 mmol) in MeOH (50 mL), the flask was evacuated and put under a hydrogen atmosphere, the mixture was stirred at room temp for 18 h. The crude mixture was filtered through celite and concentrated *in vacuo*. to give a crude product as a tan oil, which was used without further purification (1.11 g, 95%). R_f 0.40 (40:60 EtOAc–hexane; KMnO_4). $\nu_{\text{max}}/\text{cm}^{-1}$ (film): 3029, 2846, 2852 and 1702; $^1\text{H-NMR}$ (500 MHz, CDCl_3) 5.22 (1H, s, NH), 4.36 (1H, app. dh, J 5.0, 2.5, 3-H), 4.04 (1H, app. d, J 9.0 Hz, 1-H), 2.68 (1H, s OH), 2.12 – 1.87 (2H, m, 2-H, 5-H), 1.82 – 1.70 (3H, m, 4-H, 5-H), 1.62 (1H, app. dt, J 14.3, 2.6, 2-H), 1.44 (9H, s, ^tBu); $^{13}\text{C-NMR}$ (100 MHz) 155.5 (carbonyl), 79.1 (C-O), 73.0 (C-1), 50.9 (C-4), 42.3 (C-5), 34.3 (C-2), 31.6 (C-3), 28.5 (^tBu); HRMS $[\text{M}+\text{Na}]^+$ $\text{C}_{10}\text{H}_{19}\text{NNaO}_3^+$ calc., 224.1268 found, 224.1270. Spectral data in accordance with literature. ²⁷²

2-Oxa-3-azabicyclo[2.2.1]hept-5-en-3-yl(phenyl)methanone (210)



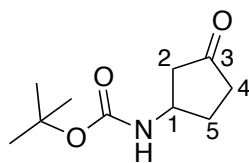
tert-Butyl hydroxycarbamate (5.00 g, 40.0 mmol) was dissolved in MeOH-H₂O (3:1, 40 mL) and cooled to 0-5 °C. Freshly distilled cyclopentadiene (4.0 mL, 60.6 mmol) and then NaIO₄ (4.25 g, 10 mmol) were added, and the reaction was allowed to warm to room temperature and stirred 2 h. The reaction was cooled to 0-5 °C, more cyclopentadiene (4.0 mL, 60.6 mmol) and NaIO₄ (4.25 g, 10 mmol) were added, and the mixture was stirred for 30 min. The mixture was concentrated *in vacuo* to a slurry, H₂O was added (2 × 20 mL), and the solution was extracted with EtOAc (3 × 20 mL). The combined organic layers were washed with saturated sodium thiosulfate (20 mL), H₂O (20 mL), and brine (10 mL), dried over MgSO₄, vacuum-filtered through Celite, and concentrated *in vacuo* to give a colourless oil (3.70 g, 46%). R_f 0.37 (50:50 EtOAc–hexane; KMnO₄). $\nu_{\max}/\text{cm}^{-1}$ (film): 1639; ¹H-NMR (500 MHz, CDCl₃) 7.68 (2H, d, *J* 7.4, 2'-H), 7.36 (3H, m, 3'-H, 4'-H), 6.28 (2H, m, 1-H, 6-H), 5.22 (2H, m, 4-H, 5-H), 2.03 (1H, d, *J* 9.0, 7-H), 1.74 (1H, d, *J* 8.5, 7-H). ¹³C-NMR (100 MHz) 170.6 (carbonyl), 134.2 (C-1'), 132.6 (C-4'), 131.2 (C-2'), 129.8 (C-3'), 126.9 (C-6), 126.4 (C-5), 82.92 (C-1, C-4), 89.90 (C-1, C-4) 46.4 (C-7) 19 peaks in spectrum, owing to rotamers. HRMS [M+Na]⁺ C₁₂H₁₁NNaO₂⁺ calc. 224.0692 found, 224.0693. Spectral data of the crude material was consistent with that reported in the literature.²⁷³

***N*-((1*RS*,4*RS*)-4-Hydroxycyclopent-2-en-1-yl)benzamide (211)**



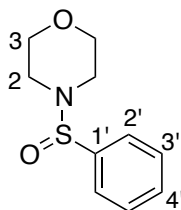
A 15:1 CH₃CN:H₂O solution of cycloadduct **210** (1.18 g, 5.85 mmol) was charged with Mo(CO)₆ (1.58 g, 6.44 mmol, 1.1 eq.) and refluxed under N₂ for 3 h and the solution turned black. The heat was then removed, and the solution allowed to cool to rt. The mixture was concentrated *in vacuo*, the crude mixture filtered through a celite pad and concentrated to give **211** as a brown solid (300 mg, 21%) which was used without further purification. R_f0.35 (50:50 EtOAc–hexane; KMnO₄). $\nu_{\text{max}}/\text{cm}^{-1}$ (film): 3295, 2360, 1642, 1561, 1587 and 1469; ¹H-NMR (500 MHz, CDCl₃) 7.72 – 7.61 (2H, m, 2'-H), 7.43 – 7.35 (1H, m, 4'-H), 7.33 (2H, dd, *J* 8.2, 6.7, 3'-H), 6.52 (1H, d, *J* 8.3, NH), 5.99 (1H, app. dt, *J* 5.4, 1.8, 2-H), 5.86 (1H, dd, *J* 5.4, 2.0, 3-H), 4.87 (1H, tdd, *J* 8.4, 3.9, 1.9, 4-H), 4.71 (2H, m, 1-H, OH), 2.74 (1H, app. dt, *J* 15.0, 7.7, 5-H_{eq}), 1.61 (1H, app. dt, *J* 14.5, 3.4, 5-H_{ax}). ¹³C-NMR (100 MHz) 167.1 (carbonyl), 136.7 (C-2'), 134.4 (C-1'), 133.9 (C-3'), 131.6 (C-4'), 128.6 (C-2), 127.0 (C-3), 75.4 (C-1), 54.3 (C-4), 41.2 (C-5). HRMS [M+Na]⁺ C₁₂H₁₃NNaO₂⁺ calc., 226.0849 found, 226.0852. Spectral data of the crude material was consistent with that reported in the literature.²⁷⁴

***tert*-Butyl (3-oxocyclopentyl)carbamate (216)**



To a stirred suspension of cyclopent-2-en-1-one 36 (2.50 g, 3.05 mmol) in CH_2Cl_2 (60 mL), was added *tert*-butyl carbamate (3.60 g, 3.05 mmol) and stirred for 30 min. Bismuth nitrate (14.7 g, 3.05 mmol) was added portionwise and allowed to stir at rt for 18 h. After completion of reaction, the reaction mixture was diluted with CH_2Cl_2 and filtered through a celite pad. The filtrate was quenched with saturated NaHCO_3 solution and the organic layer was separated. The aqueous layer was extracted with CH_2Cl_2 and the combined organic extracts were dried over MgSO_4 and concentrated in vacuo. to obtain a crude residue. Flash chromatography (20:80 EtOAc–hexane) yielded the desired product as a white solid (261 mg, 43%). R_f 0.31 (20% EtOAc–hexane; KMnO_4). $\nu_{\text{max}}/\text{cm}^{-1}$ (film): 1730; $^1\text{H-NMR}$ (500 MHz, CDCl_3) 4.87 (1H, s, NH), 4.23 (1H, s, 1-H), 2.61 (1H, m, 2-H), 2.45 – 2.27 (2H, m, 5-H, 4-H), 2.27 – 2.18 (1H, m, 5-H), 2.18 – 2.09 (1H, m, 2-H), 1.86 (1H, br, 4-H), 1.45 (9H, s, ^tBu). $^{13}\text{C-NMR}$ (100 MHz) 216.4 (carbonyl), 156.4 (boc carbonyl), 79.6 (C-O), 48.9 (C2), 45.3 (C-5), 37.1 (C-3), 30.0 (C-4), 28.3 (^tBu). Spectral data of the crude material was consistent with that reported in the literature.²⁷⁵

4-(Phenylsulfinyl)morpholine (221)

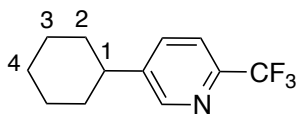


Predried DABSO (60 mg, 0.25 mmol, 0.5 eq.) was added to an oven-dried 10 mL reaction vial. The vial was then sealed with a rubber septum, evacuated, and filled with N₂ (×3). Anhydrous THF (2 mL) was added. Phenylmagnesium bromide (90 μL of an 2 M solution in Et₂O, 0.50 mmol, 1.0 eq.) was added dropwise to the resulting suspension at rt, and the reaction mixture was stirred for 30 min. SOCl₂ (40 μL, 0.55 mmol, 1.1 eq.) was then added dropwise, and the mixture was stirred at rt for 30 min. After this, triethylamine (110 μL, 0.75 mmol, 1.5 eq.) was added followed by the morpholine (65 μL, 0.75 mmol, 1.5 eq.). The mixture was stirred at rt for 30 min, quenched with brine (10 mL), and extracted with EtOAc (3 × 10 mL). A few drops of water were added to dissolve any solid formed during the workup. The combined organic phases were dried with MgSO₄, filtered, and concentrated. Flash chromatography (50:50 EtOAc–hexane) yielded the desired product as a white solid (26.0 mg, 23%). R_f 0.50 (50:50 EtOAc–Hexane; KMnO₄). ν_{max}/cm⁻¹ (film): 1600, 1432, 1587 1245 and 1040; ¹H-NMR (500 MHz, CDCl₃) 7.66 – 7.55 (2H, m, 2'-H), 7.51 – 7.39 (3H, m, 3'-H, 4'-H), 3.70 – 3.55 (4H, m, 3-H), 3.16 – 3.04 (2H, m, 2-H), 2.90 (2H, m, 2-H). ¹³C-NMR (100 MHz) 142.3 (C-1'), 131.1 (C-3, C-4), 129.0 (C-3, C-4), 126.2 (C-2'), 66.9 (C-1), 45.9 (C-2).

Preparation of NiBr₂•dtbbpy²⁴⁴

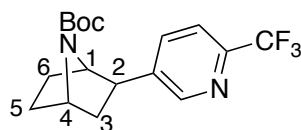
An adapted procedure originally reported by MacMillan.⁴ To a 500 mL round-bottom flask equipped with a Teflon stir bar were added nickel(II) bromide ethylene glycol dimethyl ether adduct (NiBr₂•DME, 1.54 g, 5.0 mmol, 1.0 equiv.) and 4,4'-di-*tert*-butyl-2,2'-dipyridyl (1.35 g, 5.03 mmol, 1.00 equiv.). The vessel was sealed and purged with nitrogen for 10 min. 250 mL dry MeCN was added and the reaction mixture was stirred at 65 °C for 1 h. The solvent was removed, and the residue was dried under vacuum for 12 h at rt. The solid was suspended in pentane, sonicated, and isolated using a sintered glass funnel, washed with pentane, and dried under high vacuum. The complex was isolated as a green solid (1.90 g, 4.59 mmol, 87% yield). No further characterisation was completed. This complex is used in the synthesis of **229** and **230**.

5-Cyclohexyl-2-(trifluoromethyl)pyridine (**229**)²⁴⁴



To an oven-dried 8-mL vial equipped with a stir bar were added anhydrous K_3PO_4 (117 mg, 0.55 mmol, 1.1 eq.) and the vial was sealed with a cap equipped with a Teflon-lined septum and sparged with nitrogen. 5-Bromo-2-(trifluoromethyl)pyridine (113 mg, 0.5 mmol, 1.0 eq.) $NiBr_2 \cdot dtbbpy$ (12.0 mg, 0.025 mmol, 5.0 mol%), and tetrabutylammonium decatungstate (17 mg, 0.005 mmol, 1.0 mol%) were added as a stock solution in dry MeCN (5 mL). Subsequently, the reaction vessel was placed in an ice bath and deoxygenated by sparging with nitrogen for 10 minutes. Cyclohexane (270 μ L, 2.5 mmol, 5.0 eq.) was added before sealing the reaction vessel with parafilm. The reaction mixture was then stirred and irradiated with two 34 W blue LEDs (vials approximately 6 cm away from the light source) with a fan placed above for cooling for 18 h. The reaction mixture was removed from light and quenched by stirring open to air for 15 min. The reaction mixture was diluted with ethyl acetate and passed through a pad of celite. The celite plug was washed with additional ethyl acetate. Solvent was removed *in vacuo* from the filtrate, and the residue was purified by flash chromatography (1:99–10:90, EtOAc–Hexane) to yield the product **229** as a clear colourless oil (115 mg, 41%). R_f 0.30 (10:90 EtOAc–hexane). 1H -NMR (500 MHz, $CDCl_3$) 8.51 (1H, d, J 2.1, 2'-H), 7.61 (1H, dd, J 8.1, 2.2, 5'-H), 7.53 (1H, d, J 8.1, 6'-H), 2.56 (1H, app. tt, J 11.3, 3.1, 1-H), 1.82 (4H, app. tt, J 9.1, 3.3, 2-H), 1.45 – 1.27 (4H, m, 3-H), 1.29 – 1.10 (2H, m, 4-H). ^{13}C -NMR (100 MHz) 149.3 (C-2'), 146.2 (C-4'), 135.2 (C-6'), 122.2 (C-1') 120.20 (C-5', CF_3), 120.17 (C-5', CF_3), 41.9 (C-1), 33.9 (C-2), 26.5 (C-3), 25.8 (C-4). Spectral data in accordance with literature.²⁴⁴

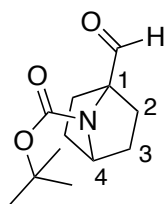
***tert*-Butyl-2-(6-(trifluoromethyl)pyridin-3-yl)-7-azabicyclo[2.2.1]heptane-7-carboxylate (230)**



To an oven-dried 40-mL vial equipped with a stir bar were added amine **198** (493 mg, 2.50 mmol, 5.0 eq.) and Na₃PO₄ (85 mg, 0.55 mmol, 1.1 eq.). The vial was sealed with a cap equipped with a Teflon-lined septum and purged with nitrogen. 5-bromo-2-(trifluoromethyl)pyridine (113 mg, 0.5 mmol, 1 eq.), NiBr₂·dtbbpy (12 mg, 0.025 mmol, 5.0 mol%), and tetrabutylammonium decatungstate (17 mg, 0.005 mmol, 1.0 mol%) were added as a stock solution in dry MeCN (12.5 mL, 0.04 M). Subsequently, the reaction vessel was placed in an ice bath and deoxygenated by sparging with nitrogen for 10 minutes. The reaction mixture was then stirred and irradiated with two 34 W blue LEDs (vials approximately 6 cm away from the light source) with a fan placed above for cooling. After 18 h, a second portion of TBADT (17 mg, 0.005 mmol, 1.0 mol%) in 0.2 mL degassed MeCN was added, and the reaction was subjected once again to irradiation for 18 h. After another 18 h, a third portion of TBADT (17 mg, 0.005 mmol, 1.0 mol%) in 0.2 mL degassed MeCN was added, and the reaction was subjected once again to irradiation for 18 h. At this point, the reaction mixture was removed from light and quenched by stirring open to air for 15 minutes. The reaction mixture was diluted with ethyl acetate and passed through a pad of celite. The celite plug was washed thoroughly with additional ethyl acetate. Filtrate was concentrated *in vacuo*. Residue was purified by mass-directed preparative purification (20-minute run time; 5-95% water containing 0.1 M formic acid/MeCN; target *m/z* 342, 286; product eluted at 15.3 minutes) to give the product as a clear colourless oil, (34.2 mg, 20%). $\nu_{\max}/\text{cm}^{-1}$ (film): 3346, 2912, 1576, 1325 and 1241; ¹H-NMR (500 MHz, CDCl₃) 8.58 – 8.46 (1H, m, 2'-H), 7.77 (1H, d, *J* 8.1, 5'-H), 7.54 (1H, d, *J* 8.2, 6'-H), 4.33 (1H, br, 4-H), 4.25 – 4.09 (1H, m, 1-H), 2.89 (1H, app. dd, *J* 9.1, 4.8, 2-

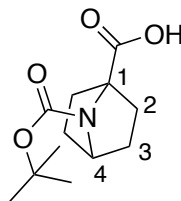
H_{endo}), 2.02 – 1.91 (2H, m, 3-H), 1.78 – 1.75 (2H, m, 6-H), 1.73 – 1.46 (2H, m, 5-H), 1.39 (9H, br, ^tBu rotamers); ¹³C-NMR (100 MHz, decoupled) 155.2 (carbonyl), 149.3 (C-2'), 146.1 (C-4'), 144.4 (C-1'), 135.6 (C-5' or CF₃), 135.5 (C-5' or CF₃) 120.4 (C-6'), 80.1 (C-O), 62.0 (C-1), 56.0 (C-4), 45.0 (C-2), 40.2 (C-3), 29.7 (C-5, C-6), 29.4 (C-5, C-6), 28.3 (^tBu) (17 peaks in spectrum owing to rotamers). HRMS [M+Na]⁺ C₁₇H₂₁F₃N₂NaO₂⁺ calc., 365.1458 found, 365.1459. The spectroscopic properties of this compound are consistent with data reported in the literature.²⁴⁴

***tert*-Butyl-1-Formyl-7-azabicyclo[2.2.1]heptane-7-carboxylate (231)**²³⁸



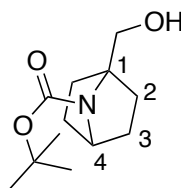
The starting material (*tert*-butyl 7-azabicyclo[2.2.1]heptane-7-carboxylate, 1.26 g, 6.4 mmol) was rigorously dried under high vacuum for 1 h prior to reaction, dissolved in Et₂O (5 mL), and then transferred into a suspension of freshly Et₂O (20 mL) via a cannula. The solution was transferred to a dry flask (100 mL) via a cannula followed by N,N,N',N'-tetramethylethylenediamine (1.40 mL, 9.6 mmol, 1.5 eq.). The solution was then cooled to 0 °C. After 15 min, *sec*-butyllithium (9.1 mL, 12.7 mmol, 2 eq., (1.4 M solution in cyclohexane) was added dropwise over 5 min. The reaction was maintained at 0 °C for 1 h during which time the solution turned pale yellow. After this time, dry DMF (2 mL, 25.5 mmol, 4 eq.) was added dropwise and the solution turned cloudy. This solution was warmed to rt and left to stir for 18 h. The reaction was quenched by the addition of sat aq. NH₄Cl (2 mL), partitioned between EtOAc (50 mL) and 1 M HCl (50 mL), and separated. The aqueous layer was extracted with additional EtOAc (2 × 30 mL). The combined organic layers were dried (MgSO₄) and concentrated *in vacuo*. Purification by flash chromatography (10:90 EtOAc–hexane) yielded a clear, colourless liquid that solidified upon standing to a white powder (646 mg, 45%). R_f 0.28 (10:90 EtOAc–hexane; KMnO₄); ν_{max}/cm⁻¹ (film) 2981, 1720 and 1434; ¹H-NMR (500 MHz, CDCl₃) 9.94 (1H, s, CHO), 4.37 – 4.21 (1H, m, 4-H), 2.07 – 1.86 (4H, m, 2-H, 3-H), 1.68 – 1.49 (4H, m, 2-H, 3-H), 1.43 (9H, s, ^tBu). ¹³C-NMR (100 MHz) 197.3 (Carbonyl), 156.1 (Boc), 81.3 (C-1), 73.5 (C-O), 58.9 (C-4), 30.3 (C-2, C-3), 29.1 (C-2, C-3), 28.1 (^tBu). HRMS [M+Na]⁺ C₁₂H₁₉NNaO₃⁺ calc., 248.1268 found 248.1257. The spectral data is in accordance with literature.

7-(*tert*-Butoxycarbonyl)-7-azabicyclo[2.2.1]heptane-1-carboxylic acid (232)



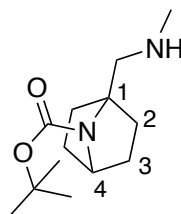
The Boc-protected formyl-bicyclic compound (**231**) (1.00 g, 4.40 mmol) was dissolved in *tert*-butanol (30 mL) and 2-methyl-2-butene (3 mL). In a separate solution, sodium chlorite (NaClO₂, 1.99 g, 22.0 mmol, 5 eq.) and sodium hydrogen phosphate-monohydrate (NaH₂PO₄·H₂O, 6.07 g, 44.0 mmol, 10 eq.) were dissolved in distilled water (1 mL) to produce a yellow solution. The yellow aqueous solution was added to the solution of starting material and left to stir at rt for 1.5 h. The reaction was quenched by the addition of brine (10 mL) and EtOAc (10 mL). The mixture was separated, and the aqueous layer was washed further with EtOAc (2 × 10 mL). The organic extracts were then combined, dried (MgSO₄), and concentrated *in vacuo*. to produce acid **232** as a white solid (975 mg, 92%). Used without further purification; $\nu_{\max}/\text{cm}^{-1}$ (film): 2961, 2921, 1740 and 1420; ¹H-NMR (500 MHz, CDCl₃) 4.15 (1H, app. t, *J* 4.7, 4-H), 1.97 (2H, app. tt, *J* 12.6, 2.9, 2-H), 1.79 – 1.57 (4H, m, 2-H, 3-H), 1.37 – 1.13 (11H, m, 9-H, 3-H). ¹³C-NMR (100 MHz) 175.4 (acid carbonyl), 157.0 (carbonyl), 81.8 (C-O), 69.3 (C-1), 59.8 (C-4), 34.0 (C-2), 29.0 (C-3), 28.0 (^tBu). HRMS [M+Na]⁺ C₁₂H₁₉NNaO₄⁺ calc., 264.1217 found 264.1206. Spectral data is in accordance with literature.²³⁸

***tert*-Butyl-1-(hydroxymethyl)-7-azabicyclo[2.2.1]heptane-7-carboxylate (233)**



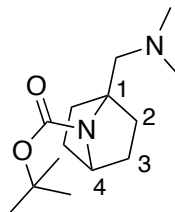
Aldehyde **231** (300 mg, 1.3 mmol) was dissolved in MeOH (20 mL) and stirred at 0 °C for 15 min. Sodium borohydride (72.2 mg, 2.0 mmol) was added portion-wise over 5 min. The reaction was allowed to warm to rt and stirred for 5 h. The reaction was quenched with water (10 mL) followed by EtOAc (20 mL). The layers were separated, and the aqueous layer was extracted further with EtOAc (2 × 15 mL). The combined organic layers were washed sequentially with water (10 mL), brine (10 mL), and dried (MgSO₄) before being concentrated *in vacuo*. to give *alcohol 233* as a white solid (257 mg, 87%). *R_f* 0.20 (50:50 EtOAc–Hexane; KMnO₄); $\nu_{\max}/\text{cm}^{-1}$ (film): 3240, and 2911; ¹H-NMR (500 MHz, CDCl₃) 4.17 (1H, app. t, *J* 4.8, 4-H), 3.83 (2H, s, CH₂), 1.83 – 1.71 (2H, m, 2-H), 1.75 – 1.63 (2H, m, 2-H), 1.47 – 1.25 (13H, m, 3-H, ^tBu). ¹³C-NMR (100 MHz) 155.2 (carbonyl), 80.2 (C-O), 69.1 (C-1), 62.0 (C-4), 58.4 (CH₂), 31.8 (C-2), 29.3 (C-3), 28.4 (^tBu). HRMS [M+Na]⁺ C₁₂H₂₁NNaO₃⁺ calc., 250.1424 found, 250.1418.

***tert*-Butyl-1-((methylamino)methyl)-7-azabicyclo[2.2.1]heptane-7-carboxylate (**236**)**



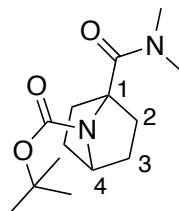
Aldehyde **231** (100 mg, 0.44 mmol) was dissolved in MeOH (8 mL) and then methylamine (1 M in methanol, 41 μ L, 1.32 mmol) and titanium isopropoxide (0.16 mL, 0.57 mmol) were added and the reaction stirred at rt for 6 h. The reaction was cooled to 0 °C and sodium borohydride (16.3 mg, 0.44 mmol) was added. The reaction was allowed to warm to room temperature and stir for 18 h. MeOH (50 mL) was added, the reaction filtered through celite and concentrated *in vacuo*. to yield a colourless oil. Flash chromatography (100%) yielded *azabicyclo* **236** as a colourless oil (19.0 mg, 17%). R_f 0.10 (50:50 EtOAc–KMnO₄); $\nu_{\max}/\text{cm}^{-1}$ (film): 3248, and 2965; ¹H-NMR (500 MHz, CDCl₃) 4.20 (1H, app. t, J 4.9, 4-H), 3.35 (2H, s, CH₂), 2.73 (3H, s, NCH₃), 1.90 (2H, ddd, J 11.7, 9.9, 4.1, 2-H_{exo}), 1.80 – 1.71 (2H, m, 3-H_{exo}), 1.64 (2H, ddd, J 11.5, 9.1, 4.3, 2-H_{endo}), 1.44 (2H, ddd, J 11.5, 9.1, 4.0, 3-H_{endo}), 1.38 (9H, s, ^tBu); ¹³C-NMR (100 MHz) 156.7 (carbonyl), 81.7 (C-O), 65.1 (C-1), 58.9 (C-4), 51.0 (CH₂), 34.2 (NCH₃), 33.8 (C-2), 29.0 (C-3), 28.3 (^tBu). HRMS [M+H]⁺ C₁₃H₂₅N₂O₂⁺ calc., 241.1921 found, 241.1911.

***tert*-Butyl-1-((dimethylamino)methyl)-7-azabicyclo[2.2.1]heptane-7-carboxylate (**237**)**



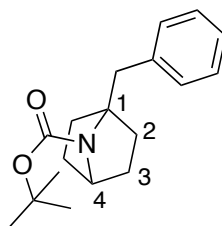
Aldehyde **231** (100 mg, 0.44 mmol) was dissolved in MeOH (8 mL) and then dimethylamine (2 M in ethanol, 60 μ L, 1.32 mmol) and titanium isopropoxide (0.16 mL, 0.57 mmol) were added and the reaction stirred at rt for 6 h. The reaction was cooled to 0 °C and sodium borohydride (16.3 mg, 0.44 mmol) was added. The reaction was allowed to warm to room temperature and stir for 18 h. MeOH (50 mL) was added, the reaction filtered through celite and concentrated *in vacuo*. to yield a colourless oil. Flash chromatography (50:50 EtOAc–hexane) yielded *azabicyclo* **237** as a colourless oil (19.0 mg, 17%). R_f 0.25 (50:50 EtOAc–hexane; KMnO_4); $\nu_{\text{max}}/\text{cm}^{-1}$ (film): 3226, and 2968; $^1\text{H-NMR}$ (500 MHz, CDCl_3) 4.18 (1H, dd, J 5.3, 4.0, 4-H), 3.41 (2H, s, CH_2), 2.28 (6H, s, $(\text{CH}_3)_2$), 1.77 – 1.65 (4H, m, 2- H_{exo} , 3- H_{exo}), 1.60 – 1.54 (4H, m, 2- H_{endo} , 3- H_{endo}), 1.37 (9H, br, ^tBu). $^{13}\text{C-NMR}$ (100 MHz) 156.1 (carbonyl), 79.4 (C-O), 68.3 (C-1), 67.0 (C-4), 62.4 (CH_2), 47.3 ($\text{N}(\text{CH}_3)_2$), 34.4 (C-2), 28.9 (C-3), 28.4 (^tBu). HRMS $[\text{M}+\text{H}]^+$ $\text{C}_{14}\text{H}_{27}\text{N}_2\text{O}_2^+$ Calc., 255.2078 found, 255.2082.

***tert*-Butyl-1-(dimethylcarbamoyl)-7-azabicyclo[2.2.1]heptane-7-carboxylate (238)**



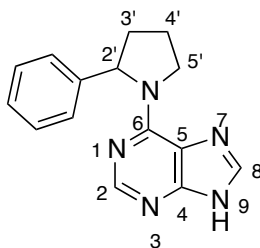
Carboxylic acid **232** (100 mg, 0.41 mmol) was dissolved in CH₂Cl₂ (15 mL) and HOBT (108 mg, 0.80 mmol), EDC.HCl (229 mg, 1.20 mmol), NEt₃ (172 μL, 1.2 mmol) and dimethylamine (2 M in ethanol, 51.6 μL, 1.20 mmol) were added and stirred at rt for 18 h. The reaction was quenched by the addition of 1 M HCl (10 mL) followed by EtOAc (15 mL). The layers were separated, and the aqueous layer was extracted further with EtOAc (2 × 15 mL). The combined organic layers were washed sequentially with water (10 mL), brine (10 mL), and dried (MgSO₄) before being concentrated *in vacuo* to give *bicycle 238* as an orange oil. Flash chromatography (EtOAc) yielded the desired product as a tan oil (73.6 mg, 67%). R_f 0.20 (30:70 EtOAc–hexane; KMnO₄); ν_{max}/cm⁻¹ (film): 3361, 2981 and 1700; ¹H-NMR (500 MHz, CDCl₃) 4.33 (1H, app. t, *J* 4.6, 4-H), 3.19 (3H, s, CH₃), 2.95 (3H, s, CH₃), 2.12 (2H, br, 2-H), 1.78 – 1.73 (4H, m, 2-H, 3-H), 1.43 – 1.40 (11H, m, 3-H, ^tBu). ¹³C-NMR (100 MHz) 170.4 (amide), 156.6 (carbonyl), 80.3 (C-O), 70.0 (C-1), 59.4 (C-4), 36.8 (CH₃), 36.3 (CH₃), 34.4 (C-2, C-3), 34.0 (C-2, C-3), 28.0 (^tBu). HRMS [M+Na]⁺ C₁₄H₂₄N₂NaO₃⁺ calc., 291.1690 found 290.1687.

***tert*-Butyl 1-benzyl-7-azabicyclo[2.2.1]heptane-7-carboxylate (**240**)**



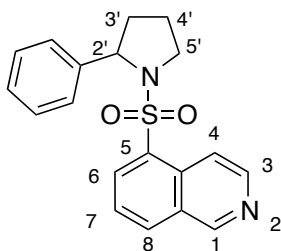
Synthesis of **240** utilises a modified procedure from MacMillan.² An oven dried 8 mL vial equipped with a Teflon septum and magnetic stir bar was charged with Ir[dF(CF₃)ppy]₂(dtbbpy)PF₆ (11.2 mg, 10.0 μmol, 0.02 eq.), NiCl₂•glyme (11.0 mg, 0.05 mmol, 0.1 eq.), 4,4'-di-methoxy-2,2'-bipyridyl (10.8 mg, 0.05 mmol, 0.1 eq.), carboxylic acid **232** (181 mg, 0.75 mmol, 1.5 eq.), K₂CO₃ (138 mg, 1.00 mmol, 2.0 eq.), and 5 mL of MeCN. The reaction mixture was degassed by bubbling nitrogen stream for 15 min at 0 °C. Water (170 μL, 10.0 mmol, 20 eq.) and benzyl chloride (58 μL, 0.50 mmol, 1.0 eq.) were then added. The reaction mixture was then stirred and irradiated with two 34 W blue LEDs (vials approximately 6 cm away from the light source) with a fan placed above for cooling. After 24 h, the reaction mixture was diluted with EtOAc, filtered, and concentrated *in vacuo*. Flash chromatography (10:90 EtOAc–Hexane) yielded *azabicyclo* **240** as a yellow oil (77.5 mg, 36%). R_f 0.20 (10:90 EtOAc–Hexane; KMnO₄). $\nu_{\max}/\text{cm}^{-1}$ (film): 3248, 2965, 1567, 1445 and 1230; ¹H-NMR (500 MHz, CDCl₃) 7.41 – 7.21 (5H, m, Ph), 5.17 (2H, s, CH₂), 4.24 (1H, t, *J* 4.8, 4-H), 2.20 – 2.06 (2H, m, 2-H_{exo}), 1.85 (2H, app. dddt, *J* 12.5, 7.4, 4.7, 2.9, 3-H_{exo}), 1.68 (2H, ddd, *J* 11.5, 9.2, 4.4, 2-H_{endo}), 1.42 (2H, ddd, *J* 11.5, 9.2, 4.2, 3-H_{endo}), 1.34 (9H, s, ^tBu). ¹³C-NMR (100 MHz) 171.3, 156.5 (carbonyl), 136.0 (ipso), 128.5 (Ph), 128.0 (Ph), 80.7 (Ph), 68.8 (C-1), 66.6 (C-4), 59.8 (CH₂), 33.3 (C-2), 29.4 (C-3), 28.1 (^tBu). HRMS [M+2H-^tBu]²⁺ C₁₄H₁₈NO₂²⁺ calc., 232.1333 found, 232.1332.

6-(2-phenylpyrrolidin-1-yl)-9H-purine (258)



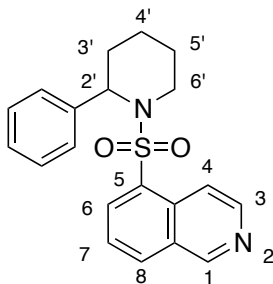
Following general procedure **4**, employing 2-phenylpyrrolidine (**46**, 573 mg, 3.90 mmol) and heated at reflux for 6 h. The solid was isolated through filtration using a sintered funnel. The crude solid was washed with MeOH (2 × 25 mL) and dichloromethane (2 × 25 mL) to give *purine 258* as a colourless solid (585 mg, 68%). mp 199 °C (EtOH); $\nu_{\max}/\text{cm}^{-1}$ (film) 3064, 2932 and 1602; δ_{H} (500 MHz, DMSO- d_6) 13.00 (1H, s, 9-H), 8.20 (1H, s, 8-H), 8.09 (1H, s, 2-H), 7.41 – 7.29 (4H, m, phenyl 2-H, phenyl 3-H), 7.29 – 7.20 (1H, m, phenyl 4-H), 3.12 (2H, m, 2'-H, 4'-H), 2.75 (1H, app. tt, J 11.4, 3.8, 5'-H), 2.02 – 1.94 (1H, m, 3'-H₂), 1.91 – 1.78 (2H, m, 3'-H₃, 4'-H₂), 1.60 (1H, m, 4'-H₂); δ_{C} (125 MHz DMSO- d_6) 153.6 (C-6), 152.4 (C-2), 151.9 (C-4), 144.2 (phenyl C-1), 138.4 (C-8), 128.9 (phenyl), 127.6 (phenyl), 127.0 (phenyl), 119.3 (C-5), 42.8 (C-1'), 32.1 (C-2'), 31.2 (C-4'), 25.8 (C-3'); HRMS $[\text{M}+\text{H}]^+$ C₁₅H₁₆N₅⁺ calc. 266.1406, found, 266.1000.

5-((2-phenylpyrrolidin-1-yl)sulfonyl)isoquinoline (**260**)



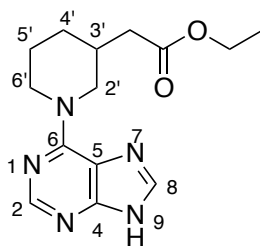
Following general procedure **5**, employing 2-phenylpyrrolidine (**46**, 228 mg, 3.21 mmol) and stirred at room temperature for 18 h. The solid was dissolved in CH₂Cl₂ (5 mL), dry loaded onto silica and purified by flash column chromatography eluting with EtOAc, to give *fragment 260* as a grey solid (136 mg, 42%). *R*_f 0.28 (EtOAc). mp 216 °C (EtOH); $\nu_{\max}/\text{cm}^{-1}$ (film) 2226 and 1351; δ_{H} (500 MHz, CDCl₃) 9.24 (1H, d, *J* 1.0, 1-H), 8.50 – 8.47 (2H, m, 3-H, 4-H), 8.23 – 8.16 (2H, m, 6-H, 8-H), 7.58 (1H, dd, *J* 8.2, 7.8, 7-H), 7.04 – 6.85 (5H, m, Ph), 4.90 – 4.82 (2H, m, 2-H, 5'-H_A), 3.86 – 3.75 (1H, m, 5'-H_B), 3.65 (1H, dt, *J* 13.3, 4.9, 3.3, 3'-H_A), 2.31 – 2.18 (1H, m, 3'-H_B), 2.01 – 1.93 (1H, m, 4'-H₂), 1.89 – 1.70 (1H, m, 4'-H₃); δ_{C} (125 MHz, CDCl₃) 156.6 (C-1), 147.2 (C-3), 145.8 (phenyl C-1), 138.1 (C-6, C-8), 138.0 (C-6, C-8) 137.6 (phenyl C-2), 135.8 (phenyl C-3), 135.4 (C-5), 133.0 (C-4a), 131.5 (C-8a), 130.7 (phenyl C-4), 130.1 (C-7), 122.1 (C-4), 67.5 (C-2'), 53.1 (C-5'), 40.3 (C-3'), 28.1 (C-4'); HRMS [M+H]⁺ C₁₉H₁₉N₂O₂S⁺ calc., 339.1172 found, 339.1182.

5-((2-phenylpiperidin-1-yl)sulfonyl)isoquinoline (261)



Following general procedure **5**, employing 2-phenyl piperidine (**47**, 517 mg, 3.21 mmol) and stirred at room temperature for 18 h. The solid was dissolved in CH₂Cl₂ (5 mL), dry loaded onto silica and purified by flash column chromatography eluting with EtOAc, to give fragment **261** as a white solid (163 mg, 21%). *R_f* 0.38 (EtOAc). mp 205 °C (EtOH); $\nu_{\max}/\text{cm}^{-1}$ (film) 3066, 2956, 2866, 2761 and 1332; δ_{H} (500 MHz, DMSO-*d*₆) 9.52 (1H, dd, *J* 1.1, 0.9, 1-H), 8.74 (1H, d, *J* 6.1, 4-H), 8.48 (2H, m, 3-H, 6-H), 8.41 (1H, app. dt, *J* 6.1, 1.0, 8-H), 7.84 (1H, dd, *J* 8.1, 7.4, 7-H), 7.30 (4H, m, phenyl 2-H, phenyl 3-H), 7.25 – 7.20 (4H, m, phenyl 4-H), 5.32 – 5.28 (1H, m, 2'-H), 3.82 – 3.72 (1H, m, 6'-H_A), 3.04 (1H, m, 6'-H_B), 2.24 – 2.22 (1H, m, 3'-H_A), 1.50 – 1.46 (1H, m, 3'-H_B), 1.40 – 1.31 (2H, m, 4'-H_A, 5'-H_A), 1.15 – 1.20 (1H, m, 5'-H_B), 0.92 – 0.90 (1H, m, 4'-H_A). δ_{C} (125 MHz, DMSO-*d*₆) 154.2 (C-1), 145.5 (C-3), 139.1 (phenyl C-1), 135.0 (C-6, C-8), 136.0 (C-5), 134.4 (C-6, C-8), 130.7 (C-4a), 129.3 (C-8a), 129.0 (phenyl C-2), 127.3 (phenyl C-4), 127.2 (phenyl C-3), 127.1 (C-7), 117.5 (C-4), 55.5 (C-2'), 41.9 (C-6'), 28.3 (C-3'), 24.6 (C-5'), 18.9 (C-4'). HRMS [M+H]⁺ C₂₀H₂₁N₂O₂S⁺ calc., 353.1329 found, 353.1335.

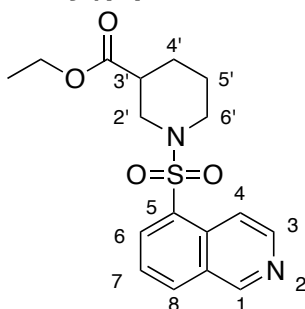
Ethyl 2-(1-(9*H*-purin-6-yl)piperidin-3-yl)acetate (**264**)



Into an oven-dried 4 × 7 mL Supelco vial fitted with a Teflon septum was weighed lutidine (29 mg, 0.27 mmol), ethyl bromoacetate (240 mg, 1.56 mmol), and the *tert*-butyl 3,4-dihydropyridine-1(2*H*)-carboxylate (100 mg, 0.52 mmol). The vial was then purged with nitrogen for 5 minutes, before the addition of a dry MeOH solution of Ir(ppy)₃ (2 mg in 2 mL, prepared in an oven-dried vial under nitrogen flow). The vial was sealed and stirred for 3 hours under blue LED irradiation (32W blue LED Kessil H150). After this period the solvent was removed under reduced pressure and replaced with dry dichloromethane under nitrogen. Et₃SiH (0.8 mL) was added followed by BF₃·Et₂O (0.68 mL). Once the intermediate *N,O*-aminal have been completely reduced, as judged by LC-MS, the reaction mixtures were combined and concentrated *in vacuo*, dissolved in dichloromethane (5 mL) and TFA (2.5 mL) and stirred at rt for 1 hour. Following this, the residue was concentrated *in vacuo* and purified by flash column chromatography to give a brown ethyl 2-(piperidin-3-yl)acetate as a brown oil (66.7 mg). Following general procedure **4**, employing ethyl 2-(piperidin-3-yl)acetate (66.7 mg, 0.390 mmol) and heated at reflux for 7 h. The solid was isolated through filtration using a sintered funnel. The crude solid was washed with MeOH (2 × 25 mL) and dichloromethane (2 × 25 mL) to give *purine* **264** (38.5 mg, 41%) as a light yellow solid. mp 218 °C (EtOH); $\nu_{\max}/\text{cm}^{-1}$ (film) 3523, 3334, 3132, 1759 and 1687; δ_{H} (500 MHz, DMSO-*d*₆) 12.99 (1H, s, H-9), 8.18 (1H, s, 2-H), 8.10 (1H, s, 8-H), 4.08 (2H, app. qd, *J* 7.1, 0.9, OCH₂CH₃), 3.09 (1H, app. s, 3'-H), 2.32 (1H, dd, *J* 15.2, 7.0, 2'-H_A), 2.24 (1H, dd, *J* 15.2, 7.2, 2'-H_B), 1.95 (2H, m, 5'-H), 1.85 (1H, dt, *J* 13.0, 4.0, 1H, 6'-H_A), 1.73 (1H, dp, *J* 11.5, 3.6 Hz, 4'-H_A), 1.55 – 1.44 (1H, m, 4'-H_B), 1.42 – 1.29 (1H, m, 6'-H_B), 1.19 (3H, t, *J* 7.1, OCH₂CH₃); δ_{C} (125 MHz DMSO-*d*₆) 187.6 (Ester C=O), 153.6 (C-6), 143.8

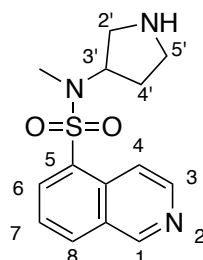
(C-2), 138.3 (C-4), 120.2 (C-5), 118.9 (C-8), 60.3 (OCH₂CH₃), 39.3 (C-3'), 38.3 (C-2'), 33.4 (C-5'), 30.7 (C-6'), 25.0 (C-3' or C-4') 24.9 (C-3' or C-4'), 14.6 (OCH₂CH₃); HRMS [M+H]⁺ C₁₄H₂₀N₅O₂⁺ calc. 290.1622, found 290.1628.

ethyl 1-(isoquinolin-5-ylsulfonyl)piperidine-3-carboxylate (**266**)



Following general procedure **5**, employing ethyl piperidine-3-carboxylate (503 mg, 3.21 mmol) and stirred at room temperature for 18 h. The solid was dissolved in CH₂Cl₂ (5 mL), dry loaded onto silica and purified by flash column chromatography eluting with EtOAc, to give *fragment 266* was isolated as a white solid (475 mg, 73%). R_f 0.24 (EtOAc). mp 214 °C (EtOH); ν_{max}/cm⁻¹ (film) 3287, 2789, 2598, 2109, 1720 and 1351; δ_H (500 MHz, Acetone-*d*₆) 9.35 (1H, dd, *J* 1.1, 1.0, 1-H), 8.60 (1H, d, *J* 6.2, 4-H), 8.42 (1H, dt, *J* 6.1, 1.0, 3-H), 8.36 (1H, app. dd, *J* 8.2, 1.1, 6-H), 8.33 (1H, dd, *J* 7.4, 1.2, 8-H), 7.78 (1H, dd, *J* 8.2, 7.4, 7-H), 4.07 – 3.82 (2H, br, CH₂CH₃), 3.68 (1H, ddt, *J* 12.1, 4.0, 1.3, 2'-H_A), 3.53 – 3.40 (1H, m, 6'-H_A), 2.85 (1H, dd, *J* 12.2, 9.4, 2'-H_B), 2.73 (1H, ddd, *J* 12.3, 9.9, 3.2, 6'-H_B), 2.47 – 2.43 (1H, m, 3'-H), 1.86 – 1.71 (2H, m, 4'-H), 1.52 – 1.38 (2H, m, 5'-H), 1.07 (3H, t, *J* 7.2, CH₂CH₃); δ_C (125 MHz, Acetone-*d*₆) 205.3 (ester C=O), 153.5 (C-1), 145.0 (C-3), 134.1 (C-6, C-8), 134.0 (C-6, C-8), 132.5 (C-5), 131.7 (C-4a), 129.3 (C-8a), 126.2 (C-7), 117.5 (C-4), 60.2 (CH₂CH₃), 47.1 (C-2'), 45.7 (C-6'), 40.7 (C-3'), 25.9 (C-5'), 23.8 (C-4'), 13.5 (CH₂CH₃); HRMS [M+H]⁺ C₁₇H₂₁N₂O₄S⁺ calc., 349.1228 found, 349.1235.

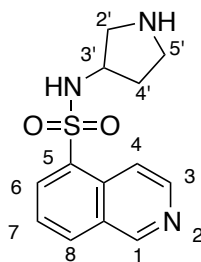
***N*-methyl-*N*-(pyrrolidin-3-yl)isoquinoline-5-sulfonamide (270)**



Following general procedure **5**, employing *tert*-butyl 3-aminopyrrolidine-1-carboxylate (642 mg, 3.21 mmol) and stirred at room temperature for 18 h. The reaction mixture was concentrated *in vacuo* to give a crude solid. The solid was dissolved in tetrahydrofuran (20 mL) to which was added formaldehyde (165 μ L, 4.42 mmol) and sodium triacetoxyborohydride (932 mg, 4.42 mmol) and stirred at room temperature for 18 h. The reaction was quenched by the addition of 1 M HCl (1 mL) followed by EtOAc (10 mL). The layers were separated, and the aqueous layer was extracted further with EtOAc (2 \times 10 mL). The combined organic layers were washed sequentially with water (10 mL), brine (10 mL), and dried (MgSO₄) before being concentrated *in vacuo* to give a brown solid. The solid was dissolved in dichloromethane (50 mL) and TFA (25 mL) and stirred at room temperature for 4.5 h. Subsequently the reaction was concentrated *in vacuo* to give a crude residue. The residue was dissolved in dichloromethane (2 mL) and loaded onto a 1 g SCX cartridge, and the cartridge flushed with MeOH (3 \times 20 mL). The product was eluted using ammonia (1 M solution in MeOH, 3 \times 20 mL) which was concentrated *in vacuo* to give a crude residue. The crude was purified by flash column chromatography (EtOAc) and subsequently concentrated *in vacuo* to yield **270** as a white solid (135 mg, 21%). *R*_f 0.29 (EtOAc). mp 225 °C (EtOH); $\nu_{\text{max}}/\text{cm}^{-1}$ (film) 3323, 3087, 2975, 2043, 1620 and 1381; δ_{H} (500 MHz, DMSO-*d*₆) 9.50 (1H, dd, *J* 1.1, 0.9, 1-H), 8.71 (1H, d, *J* 6.1, 4-H), 8.49 (1H, app. dd, *J* 8.2, 1.0, 8-H), 8.42 – 8.33 (2H, m, 3-H, 6-H), 7.87 (1H, dd, *J* 8.2, 7.4, 7-H), 4.50 (1H, tt, *J* 8.6, 6.2, 3'-H), 2.82 – 2.70 (5H, m, 2'-H, CH₃), 2.64 (2H, dt, *J* 10.8, 7.4, 5'-H), 1.70 – 1.59 (1H, m, 4'-H_A), 1.53 – 1.39 (1H, m, 4'-H_B); δ_{C} (125 MHz, DMSO-*d*₆) 153.1 (C-1), 143.7 (C-3), 134.3

(C-6, C-8), 133.9 (C-6, C-8), 133.7 (C-5), 131.5 (C-4a), 129.3 (C-8a), 126.4 (C-7), 117.8 (C-4), 56.8 (C-3'), 47.4 (C-2'), 45.3 (C-5'), 28.7 (C-4'), 27.7 (CH₃);
HRMS [M+H]⁺ C₁₄H₁₈N₃O₂S⁺ calc., 292.1125 found, 292.1117.

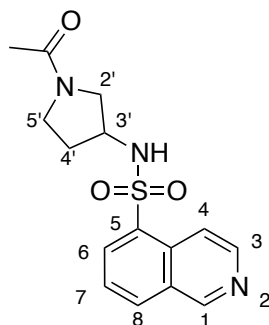
***N*-(pyrrolidin-3-yl)isoquinoline-5-sulfonamide (271)**



To an 4 × 8mL reaction vial equipped with a septum and stirrer bar was added *tert*-butyl 2,3-dihydro-1*H*-pyrrole-1-carboxylate (169 mg, 1 mmol), 2,4,6-triisopropylthiophenol (4 × 0.125 mmol; 50 mol%) and [Ir(dF(Me)ppy)₂(dtbbpy)]PF₆ (20 mg) The vial was purged with nitrogen for 5 minutes followed by the addition of anhydrous toluene (16 mL) and ammonia (7 M in methanol, 4 mL). The reaction was irradiated with a 32 W blue LED for 16 hours. The reactions were combined and the solvent was removed *in vacuo*. The residue dissolved in dichloromethane (5 ml) and TFA (2.5 mL) and stirred for 1 h. The solvent was removed *in vacuo* and telecoped into the next reaction. Following general procedure 5, employing *tert*-butyl 3-aminopyrrolidine-1-carboxylate (59.7 mg, 0.321 mmol) and stirred at room temperature for 18 h. The reaction mixture was concentrated *in vacuo* to give a crude solid. The solid was dissolved in dichloromethane (15 mL) and TFA (7 mL) and stirred at room temperature for 3 h. Subsequently the reaction was concentrated *in vacuo* to give a crude residue. The residue was dissolved in dichloromethane (2 mL) and loaded onto a 1 g SCX cartridge, and the cartridge flushed with MeOH (3 × 20 mL). The product was eluted using ammonia (1 M solution in MeOH, 3 × 20 mL) which was concentrated *in vacuo* to give **271** as a yellow solid (61.2 mg, 37%). mp 222 °C (EtOH); $\nu_{\max}/\text{cm}^{-1}$ (film) 3229, 2977, 2889 and 1300; δ_{H} (500 MHz, DMSO-*d*₆) 9.54 (1H, app. d, *J* 1.0, 1-H), 8.76 (1H, dd, *J* 6.0, 1.0 3-H), 8.59 – 8.41 (3H, m, 4-H, 6-H, 8-H), 8.03 – 7.76 (1H, m, 7-H), 3.03 (1H, tt, *J* 9.1, 4.0, 3'-H), 2.69 (2H, m, 2'-H), 2.32 (1H, td, *J* 10.2, 5.3, 5'-H_A), 2.29 – 2.22 (1H, m, 5'-H_B), 1.57 – 1.41 (1H, m, 4'-H_A), 1.30 – 1.15 (1H, m, 4'-H_B); δ_{C} (125 MHz, DMSO-*d*₆) 153.9 (C-1), 145.0 (C-3), 136.2 (C-5), 133.9 (C-6, C-8), 132.8 (C-6, C-8), 130.8 (C-4a),

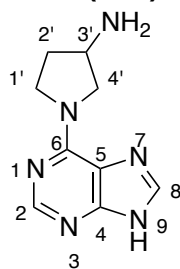
129.1 (C-8a), 126.9 (C-7), 117.7 (C-4), 51.9 (C-3'), 50.5 (C-2'), 45.3 (C-5'),
44.3 (C-6'); HRMS [M+H]⁺ C₁₃H₁₆N₃O₂S⁺ calc., 278.0969 found, 278.0958.

***N*-(1-acetylpyrrolidin-3-yl)isoquinoline-5-sulfonamide (272)**



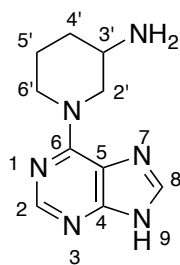
Following general procedure **5**, employing 1-(3-aminopyrrolidin-1-yl)ethanone (410 mg, 3.21 mmol) and stirred at room temperature for 18 h. The solid was dissolved in CH₂Cl₂ (5 mL), dry loaded onto silica and purified by flash column chromatography eluting with EtOAc, to give *fragment 272* was isolated as an off-white solid (415 mg, 59%). *R_f* 0.46 (10:90 MeOH–EtOAc). mp 197 °C (EtOH); $\nu_{\max}/\text{cm}^{-1}$ (film) 3229, 2977, 2889 and 1300; δ_{H} (500 MHz, DMSO-*d*₆) 9.50 (1H, app. t, *J* 0.8, 1-H), 8.72 (1H, dd, *J* 6.1, 1.7, 3-H), 8.57 – 8.41 (2H, m, 4-H, 6-H), 8.40 (1H, app. dd, *J* 7.4, 1.2, 8-H), 7.86 (1H, ddd, *J* 8.2, 7.4, 3.0, 7-H), 3.75 (0.5H, app. p, *J* 5.9, 3'-H), 3.68 (0.5H, app. p, *J* 5.6, 3'-H), 3.46 – 3.40 0.5H, m, 2'-H_A), 3.40 – 3.35 (0.5H, m, 5'-H_A), 3.32 – 3.23 (1H, m, 5'-H_A) 3.18 (1H, dd, *J* 12.0, 6.5, 5'-H_B), 3.14 – 3.07 (1H, m, 2'-H), 2.96 (0.5H, dd, *J* 12.0, 5.2, 2'-H), 1.86 (0.5H, ddt, *J* 12.4, 7.7, 6.1, 4'-H), 1.81 (1.5H, s, CH₃ rotamers), 1.78 – 1.62 (2.5 H, m, CH₃ rotamers, 4'-H). δ_{C} (125 MHz, DMSO-*d*₆) 168.6 (acetyl C=O rotamers), 168.3 (acetyl C=O rotamers), 153.97 (C-1 rotamers), 153.95 (C-1 rotamers), 145.13 (C-3 rotamers), 145.09 (C-3 rotamers), 135.38 (C-5 rotamers), 135.37 (C-5 rotamers), 134.2 (C-6, C-8 rotamers), 134.1 (C-6, C-8 rotamers), 133.21 (C-6, C-8 rotamers), 133.19 (C-6, C-8 rotamers), 130.74 (C-4a rotamers), 130.73 (C-4a rotamers), 129.13 (C-8a rotamers), 129.12 (C-8a rotamers), 127.01 (C-7 rotamers), 127.0 (C-7 rotamers) 117.49 (C-4 rotamers), 117.49 (C-4 rotamers), 53.0 (C-3' rotamers), 52.4 (C-3' rotamers), 51.7 (C-2' rotamers), 50.6 (C-2' rotamers), 44.9 (C-5' rotamers), 43.4 (C-5' rotamers), 32.1 (C-4' rotamers), 30.6 (C-4' rotamers), 22.6 (CH₃ rotamers), 22.2 (CH₃ rotamers). HRMS [M+H]⁺ C₁₅H₁₈N₃O₃S⁺ calc., 320.1074 found 320.1079.

1-(9*H*-purin-6-yl)pyrrolidin-3-amine (275)



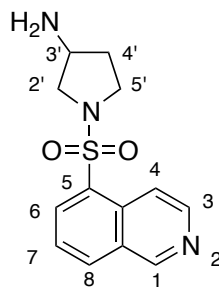
Following general procedure 4, employing *tert*-butyl pyrrolidin-3-ylcarbamate (725 mg, 3.90 mmol) and heated at reflux for 6 h. Following this, the solid was isolated through filtration using a sintered funnel. The solid was dissolved in dichloromethane (50 mL) and TFA (25 mL) and stirred at room temperature for 1 h. Subsequently the reaction was concentrated *in vacuo* to give a crude residue. The residue was dissolved in dichloromethane (2 mL) and loaded onto a 1 g SCX cartridge, and the cartridge flushed with MeOH (3 × 20 mL). The product was eluted using ammonia (1 M solution in MeOH, 3 × 20 mL) which was concentrated *in vacuo* to give crude **275** as a brown solid. The crude residue was purified by mass-directed preparative purification (20-minute run time; 5-95% water containing 0.1 M formic acid/MeCN; target *m/z* 205; product eluted at 17.1 minutes) to give the product as a clear colourless oil (391 mg, 59%). $\nu_{\max}/\text{cm}^{-1}$ (film) 3210, 3023, 2791 and 1610; δ_{H} (500 MHz, MeOD) 8.33 (1H, s, 2-H), 8.19 (1H, s, 8-H), 4.38 – 3.99 (5H, m, 1'-H, 4'-H and H-3'), 2.49 (1H, app. dq, J 14.7, 7.9, 2'-H₂), 2.29 – 2.16 (1H, m, 2'-H₃); δ_{C} (125 MHz MeOD) 150.2 (C-6), 148.3 (C-2), 146.4 (C-4), 141.8 (C-8), 120.1 (C-5), 52.2 (C-4'), 49.7 (C-3'), 46.4 (C-1'), 28.7 (C-2'); HRMS $[\text{M}+\text{H}]^+$ C₉H₁₃N₆⁺ calc. 205.1202, found 205.1198.

1-(9*H*-purin-6-yl)piperidin-3-amine (276)



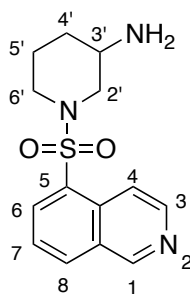
Following general procedure **4**, employing *tert*-butyl pyrrolidin-3-ylcarbamate (780 mg, 3.90 mmol) and heated at reflux for 2 h. Following this, the solid was isolated through filtration using a sintered funnel. The solid was dissolved in dichloromethane (50 mL) and TFA (25 mL) and stirred at room temperature for 1 h. Subsequently the reaction was concentrated *in vacuo* to give a crude residue. The residue was dissolved in dichloromethane (2 mL) and loaded onto a 1 g SCX cartridge, and the cartridge flushed with MeOH (3 × 20 mL). The product was eluted using ammonia (1 M solution in MeOH, 3 × 20 mL) which was concentrated *in vacuo* to give crude **276** as a yellow oil. The crude residue was purified by mass-directed preparative purification (20-minute run time; 5-95% water containing 0.1 M formic acid/MeCN; target *m/z* 219, 220; product eluted at 17.8 minutes) to give the *product* as a clear colourless oil (276 mg, 39%). $\nu_{\max}/\text{cm}^{-1}$ (film) 3153, 3000, 2843 and 1586; δ_{H} (500 MHz, MeOD) δ 8.21 (1H, s, 2-H), 8.02 (1H, s, 8-H), 4.90 (1H, m, 2'-H), 4.63 (1H, td, *J* 13.6, 4.6, 6'-H), 3.87 – 3.70 (2H, m, 2'-H), 3.34 (1H, tt, *J* 8.4, 3.9, 3'-H), 2.20 – 2.07 (1H, m, 4'-H), 1.88 – 1.60 (3H, m, 5'-H, 4'-H); δ_{C} (125 MHz MeOD) 153.6 (C-6), 150.3 (C-2), 149.9 (C-4), 138.8 (C-8), 118.7 (C-5), 47.8 (C-2'), 47.0 (C-3'), 45.4 (C-6'), 28.1 (C-4'), 22.2 (C-5'); HRMS $[\text{M}+\text{H}]^+$ C₁₀H₁₅N₆⁺ calc., 219.1358 found, 219.1354.

1-(isoquinolin-5-ylsulfonyl)pyrrolidin-3-amine (277)



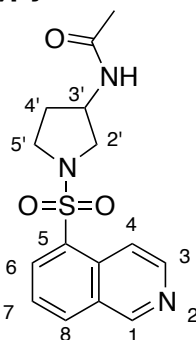
Compound 303 (274 mg, 0.73 mmol) was dissolved in CH₂Cl₂ (5 mL) and TFA (5 mL) was added and the reaction was stirred at room temperature for 2 h. The crude residue was dissolved in CH₂Cl₂ (2 mL) and loaded onto a 1 g SCX cartridge, and the cartridge flushed with MeOH (3 × 20 mL). The product was eluted using ammonia (1 M solution in MeOH, 3 × 20 mL) which was concentrated *in vacuo* to give crude **277** as an orange oil. The crude residue was purified by mass-directed preparative purification (20-minute run time; 5-95% water containing 0.1 M formic acid/MeCN; target m/z 278, 279; product eluted at 14.6 minutes) to give the product as a clear colourless oil (182 mg, 90%). $\nu_{\max}/\text{cm}^{-1}$ (film) 3270, 2893, 2812, 2376, 2040, 1672 and 1350; δ_{H} (500 MHz, DMSO-*d*₆) 9.49 (1H, dd, *J* 1.6, 0.9, 1-H), 8.70 (1H, dd, *J* 6.0, 1.6, 3-H), 8.53 – 8.37 (3H, m, 4-H, 6-H, 8-H), 7.86 (1H, td, *J* 7.7, 1.6, 7-H), 3.47 – 3.22 (4H, m, 2'-H, 5'-H), 2.95 (1H, dd, *J* 9.1, 4.0, 3'-H), 1.97 – 1.85 (1H, m, 4'-H_A), 1.61 – 1.51 (1H, m 4'-H_B). δ_{C} (125 MHz, DMSO-*d*₆) 153.9 (C-1), 145.3 (C-3), 134.2 (C-6), 133.3 (C-8), 133.1 (C-5), 131.7 (C-4a), 129.3 (C-8a), 127.1 (C-7), 117.7 (C-4), 55.5 (C-2'), 51.3 (C-5'), 46.6 (C-3'), 34.0 (C-4'). HRMS [M+H]⁺ C₁₃H₁₆N₃O₂S⁺ calc., 278.0969 found, 278.0959.

1-(isoquinolin-5-ylsulfonyl)piperidin-3-amine (278)



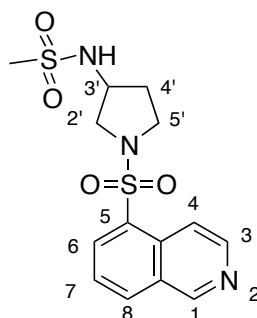
Following general procedure 5, employing *tert*-butyl piperidin-3-ylcarbamate (642 mg, 3.21 mmol) and stirred at room temperature for 18 h. The reaction mixture was concentrated *in vacuo* to give a crude solid. The solid was dissolved in dichloromethane (50 mL) and TFA (25 mL) and stirred at room temperature for 1 h. Subsequently the reaction was concentrated *in vacuo* to give a crude residue. The residue was dissolved in dichloromethane (2 mL) and loaded onto a 1 g SCX cartridge, and the cartridge flushed with MeOH (3 × 20 mL). The product was eluted using ammonia (1 M solution in MeOH, 3 × 20 mL) which was concentrated *in vacuo* to give crude **278** as a colourless oil. The crude residue was purified by mass-directed preparative purification (20-minute run time; 5-95% water containing 0.1 M formic acid/MeCN; target *m/z* 290, 291; product eluted at 14.4 minutes) to give the product as a clear colourless oil (204 mg, 32%). $\nu_{\max}/\text{cm}^{-1}$ (film) 3231, 2851, 2751, 1664 and 1349; δ_{H} (500 MHz, DMSO-*d*₆) 9.38 (1H, app. d, *J* 0.9, 1-H), 8.68 – 8.55 (2H, m, 3-H, 4-H), 8.49 – 8.37 (2H, m, 6-H, 8-H), 7.84 (1H, dd, *J* 8.3, 7.4, 7-H), 3.77 – 3.67 (1H, m, 2'-H_A), 3.59 (1H, m, 6'-H_A), 2.75 (1H, tt, *J* 9.7, 4.0, 3'-H), 2.71 – 2.61 (1H, m, 6'-H_B), 2.39 (1H, dd, *J* 11.6, 9.3, 2'-H_B), 1.90 – 1.70 (2H, m, 5'-H_A, 4'-H_A), 1.60 – 1.47 (1H, m, 4'-H_B), 1.21 – 1.05 (1H, m, 5'-H_B). δ_{C} (125 MHz DMSO-*d*₆) 162.9 (C-1), 153.7 (C-3), 144.5 (C-6, C-8), 144.3 (C-6, C-8), 140.9 (C-8a), 140.8 (C-5), 138.4 (C-4a), 136.2 (C-4), 127.0 (C-7), 57.1 (C-2'), 55.9 (C-6'), 54.9 (C-3'), 36.5 (C-5'), 31.6 (C-4'). HRMS [M+H]⁺ C₁₄H₁₈N₃O₂S⁺ calc. 292.1125 found, 292.1135.

***N*-(1-(isoquinolin-5-ylsulfonyl)pyrrolidin-3-yl)acetamide (279)**



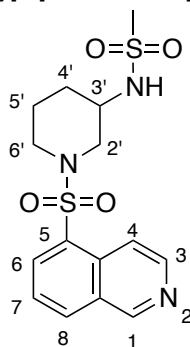
Following general procedure **5**, employing *N*-(pyrrolidin-3-yl)acetamide (410 mg, 3.21 mmol) and stirred at room temperature for 18 h. The solid dissolved in DMSO (1 mL) was purified by mass-directed preparative purification (20-minute run time; 5-95% water containing 0.1 M formic acid/MeCN; target *m/z* 319, 320; product eluted at 18.1 minutes) to give the product as a colourless solid (233 mg, 33%). *R_f* 0.18 (EtOAc). mp 210 °C (EtOH); $\nu_{\text{max}}/\text{cm}^{-1}$ (film) 3093, 3022, 2933, 2852, 2018, 1678 and 1367; δ_{H} (500 MHz, MeOD) 9.29 (1H, br, 1-H), 8.58 – 8.49 (2H, m, 3-H, 4-H), 8.39 – 8.28 (2H, m, 6-H, 8-H), 7.75 (1H, dd, *J* 7.8, 7.3, 7-H), 4.08 (1H, m, 3'-H_A), 3.47 – 3.34 (2H, m, 2'-H_A, 5'-H_A), 3.34 – 3.26 (1H, m, 2'-H_B), 3.19 – 3.14 (1H, m, 5'-H_B), 2.05 – 1.96 (1H, m, 4'-H), 1.73 – 1.62 (4H, m, 3'-H, CH₃); δ_{C} (125 MHz, MeOD) 171.9 (carbonyl C=O), 152.9 (C-1), 143.6 (C-3), 134.03 (C-6, C-8) 133.95 (C-6, C-8), 132.8 (C-5), 132.1 (C-4a), 129.4 (C-8a), 126.4 (C-7), 118.1 (C-4), 52.5 (C-5'), 49.4 (C-3'), 45.6 (C-2'), 30.3 (C-4'), 20.9 (CH₃); HRMS [M+H]⁺ C₁₅H₁₈N₃O₃S⁺ calc., 320.1074 found, 320.1075.

***N*-(1-(isoquinolin-5-ylsulfonyl)pyrrolidin-3-yl)methanesulfonamide (280)**



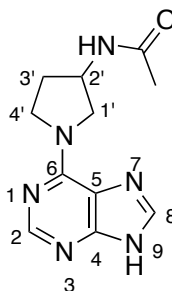
Following general procedure 5, employing *N*-(pyrrolidin-3-yl)methanesulfonamide (526 mg, 3.21 mmol) and stirred at room temperature for 18 h. The solid was dissolved in CH₂Cl₂ (5 mL), dry loaded onto silica and the crude residue was purified by mass-directed preparative purification (20-minute run time; 5-95% water containing 0.1 M formic acid/MeCN; target *m/z* 355, 356; product eluted at 15.0 minutes) to give the product as a clear colourless oil as a beige solid (306 mg, 39%). *R_f* 0.43 (10:90 MeOH–EtOAc). mp 210 °C (EtOH); $\nu_{\text{max}}/\text{cm}^{-1}$ (film) 3055, 2878 and 1371; δ_{H} (500 MHz, DMSO-*d*₆) 9.43 (1H, dd, *J* 1.1, 0.9, 1-H), 8.64 (1H, d, *J* 6.1, 3-H), 8.42 – 8.32 (2H, m, 4-H, 6-H), 8.23 (1H, app. dd, *J* 7.4, 1.2, 8-H), 7.73 (1H, dd, *J* 8.1, 7.4, 7-H), 4.88 (1H, dd, *J* 8.2, 4.7, 3'-H), 3.68 – 3.54 (2H, m, 5'-H), 3.42 (3H, s, mesyl CH₃), 2.20 – 2.08 (1H, m, 2'-H_A), 1.94 – 1.79 (1H, m, 4'-H_A), 1.77 – 1.65 (2H, m, 2'-H_B, 4'-H_B); δ_{C} (125 MHz, DMSO-*d*₆) 153.8 (C-1), 145.2 (C-3), 134.4 (C-6, C-8), 134.0 (C-6, C-8), 133.5 (C-5), 131.5 (C-4a), 129.1 (C-8a), 127.3 (C-7), 117.6 (C-4), 63.4 (C-3'), 49.50 (C-5', mesyl CH₃), 49.49 (C-5', mesyl CH₃), 36.5 (C-2'), 24.4 (C-4'); HRMS [M+H]⁺ C₁₄H₁₈N₃O₄S₂⁺ calc., 356.0742 found, 356.0742.

***N*-(1-(isoquinolin-5-ylsulfonyl)piperidin-3-yl)methanesulfonamide (282)**



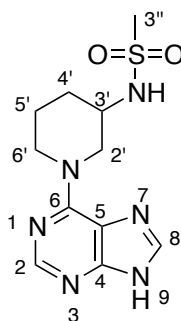
Following general procedure 5, employing *N*-(piperidin-3-yl)methanesulfonamide (48.2 mg, 3.21 mmol) and stirred at room temperature for 18 h. The solid was dissolved in CH₂Cl₂ (5 mL), dry loaded onto silica and purified by mass-directed preparative purification (20-minute run time; 5-95% water containing 0.1 M formic acid/MeCN; target *m/z* 369, 370; product eluted at 15.3 minutes) to give the product as a clear colourless oil (408 mg, 50%). $\nu_{\max}/\text{cm}^{-1}$ (film) 3009, 2349, 1370 and 1351; δ_{H} (500 MHz, DMSO-*d*₆) 9.51 (1H, br, 1-H), 8.72 (1H, d, *J* 6.1, 4-H), 8.52 (1H, br, 3-H), 8.40 (2H, m, 6-H, 8-H), 7.89 (1H, app. t, *J* 7.8, 7-H), 3.71 (1H, dd, *J* 11.5, 4.3, 2'-H_A), 3.50 (1H, dt, *J* 12.5, 4.3, 6'-H_A), 3.39 – 3.23 (2H, m, 3'-H, 6'-H_B), 3.16 – 3.07 (1H, m, 2'-H_B), 2.93 (3H, s, CH₃), 1.76 (2H, m, 5'-H_A), 1.27 – 1.14 (2H, m, 5'-H_B). δ_{C} (125 MHz, DMSO-*d*₆) 154.1 (C-1), 145.5 (C-3), 134.8 (C-6, C-8), 134.5 (C-6, C-8), 132.1 (C-8a), 131.4 (C-5), 129.2 (C-4a), 127.1 (C-4), 117.5 (C-7), 51.4 (C-2'), 49.5 (C-6'), 45.6 (C-3'), 41.1 (CH₃), 30.2 (C-4'), 23.6 (C-5'). HRMS [M+H]⁺ C₁₅H₂₀N₃O₄S₂⁺ calc. 370.0900 found, 370.0906.

***N*-(1-(9*H*-purin-6-yl)pyrrolidin-3-yl)acetamide (284)**



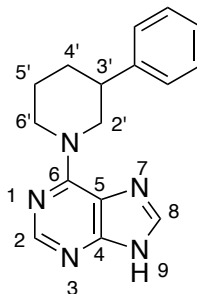
Following general procedure **4**, employing *N*-(pyrrolidin-3-yl)acetamide (499 mg, 3.90 mmol) and heated at reflux for 4 h. The solvent was removed *in vacuo* to give a crude oil and purified by flash column chromatography, eluting with 90:10 EtOAc–Hexane to give crude **284** as a colourless oil. The crude residue was purified by mass-directed preparative purification (20-minute run time; 5-95% water containing 0.1 M formic acid/MeCN; target *m/z* 246, 247; product eluted at 17.2 minutes) to give the product as a clear colourless oil (568 mg, 71%). $\nu_{\max}/\text{cm}^{-1}$ (film) 3588, 3360, 3032, 1709 and 1664; δ_{H} (500 MHz, DMSO-*d*₆) 12.94 (1H, br s, 9-H) 8.18 (1H, s, 8-H), 8.08 (1H, s, 2-H_A), 4.06 (3H, app. s, 1'-H, 2'-H_B), 3.86 (2H, m, 4'-H), 3.45 (3H, s, acetyl CH₃), 1.17 (2H, t, *J* 7.0, 3'-H); δ_{C} (125 MHz DMSO-*d*₆) 171.6 (acetyl C=O), 152.1 (C-6), 143.6 (C-2), 138.4 (C-4), 120.1 (C-5), 119.1 (C-8), 57.4 (C-3'), 31.7 (C-5'), 45.1 (C-2'), 29.1 (C-4'), 22.6 (acetyl CH₃); HRMS [M+H]⁺ C₁₁H₁₅N₆O⁺ calc. 247.1307, found 247.1302.

***N*-(1-(9*H*-purin-6-yl)piperidin-3-yl)methanesulfonamide (286)**



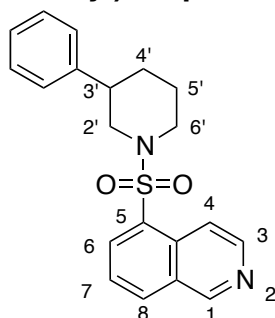
Following general procedure **4**, employing *N*-(piperidin-3-yl)methanesulfonamide (694 mg, 3.90 mmol) and heated at reflux for 6 h. The crude solid was purified by mass-directed preparative purification (20-minute run time; 5-95% water containing 0.1 M formic acid/MeCN; target *m/z* 296, 297; product eluted at 17.3 minutes) to give the product as a clear colourless oil (539 mg, 56%). $\nu_{\max}/\text{cm}^{-1}$ (film) 3284, 3069, 2944 and 1579; δ_{H} (500 MHz, DMSO-*d*₆) 8.01 (1H, s, 2-H), 7.80 (1H, s, 8-H), 5.10 (1H, d, *J* 11.3, 2'-H), 4.78 (1H, d, *J* 12.0, 6'-H), 3.31 – 3.07 (3H, m, 2'-H, 3'-H, 6'-H), 2.88 (3H, s, mesyl CH₃), 1.93 (1H, t, *J* 4.9, 4'-H or 5'-H), 1.75 – 1.59 (1H, m 4'-H or 5'-H), 1.53 – 1.37 (2H, m, 4'-H, 5'-H); δ_{C} (125 MHz DMSO-*d*₆) 153.8 (C-6), 151.7 (C-2), 138.3 (C-4), 137.7 (C-8), 119.1 (C-5), 50.8 (C-2'), 49.7 (C-3'), 45.1 (C-6'), 40.4 (mesyl CH₃), 32.0 (C-4' or C-5'), 23.7 (C-4' or C-5'); HRMS [M+H]⁺ C₁₁H₁₇N₆O₂S⁺ calc., 297.1134 found, 297.1141.

6-(3-phenylpiperidin-1-yl)-9H-purine (287)



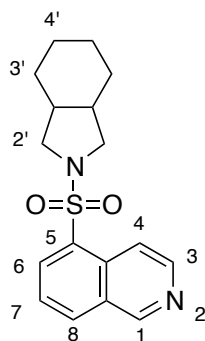
Following general procedure 4, employing 3-phenyl piperidine (237 mg, 3.90 mmol) and heated at reflux for 8 h. The solid was isolated through filtration using a sintered funnel. The crude solid was washed with MeOH (2 × 25 mL) and dichloromethane (2 × 25 mL) to give *purine 287* as a grey solid (907 mg, 85%). mp 247 °C (EtOH); $\nu_{\max}/\text{cm}^{-1}$ (film) 3123, 3012, 2882 and 1532; δ_{H} (500 MHz, DMSO- d_6) 8.21 (1H, s, 2-H), 8.10 (1H, s, 8-H), 7.38 – 7.32 (4H, m, phenyl), 7.27 – 7.22 (1H, m, phenyl 4-H), 2.76 (1H, tt, J 11.4, 3.8, 3'-H), 2.53 – 2.52 (2H, m, 2'-H), 2.02 – 1.95 (2H, m, 6'-H), 1.88 – 1.81 (2H, m, 4'-H), 1.60 (2H, app. qt, J 13.6, 4.0, 5'-H); δ_{C} (125 MHz, DMSO- d_6) 153.6 (C-6), 151.9 (C-2), 144.2 (phenyl C-1), 138.7 (C-4), 138.4 (C-8), 128.9 (phenyl C-2), 127.0 (phenyl C-3), 125.1 (phenyl C-4), 119.3 (C-5), 51.9 (C-2'), 45.6 (C-6'), 42.8 (C-3'), 31.2 (C-4'), 25.8 (C-5'); HRMS $[\text{M}+\text{H}]^+$ $\text{C}_{16}\text{H}_{18}\text{N}_5^+$ calc., 280.1562, found 280.1571.

5-((3-phenylpiperidin-1-yl)sulfonyl)isoquinoline (288)



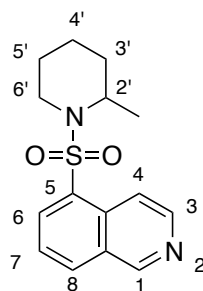
Following general procedure **5**, employing 3-phenylpiperidine (516 mg, 3.21 mmol) and stirred at room temperature for 18 h. The solid was dissolved in CH_2Cl_2 (5 mL), dry loaded onto silica and purified by flash column chromatography eluting with EtOAc, to give *fragment 288* was isolated as a colourless solid (475 mg, 61%). R_f 0.30 (EtOAc). mp 218 °C (EtOH); $\nu_{\text{max}}/\text{cm}^{-1}$ (film) 3028, 2671, 2063, 2043 and 1386; δ_{H} (500 MHz, $\text{DMSO-}d_6$) 9.51 (1H, app. d, J 1.0, 1-H), 8.70 (1H, d, J 6.1, 4-H), 8.50 (1H, dt, J 8.3, 1.1, 6-H), 8.45 (1H, dt, J 6.2, 1.0, 3-H), 8.38 (1H, ddd, J 7.4, 1.2, 1.0, 8-H), 7.87 (1H, dd, J 8.2, 7.4, 7-H), 7.33 – 7.25 (2H, m, phenyl), 7.21 (m, 3H, phenyl), 3.83 (1H, m, 2'-H_A), 3.79 – 3.72 (1H, m, 2'-H_B), 2.75 – 2.57 (3H, m, 3'-H, 6'-H), 1.84 – 1.70 (2H, m, 4'-H), 1.62 – 1.46 (2H, m, 5'-H); δ_{C} (125 MHz, $\text{DMSO-}d_6$) 154.1 (C-1), 145.4 (C-3), 143.2 (C-5), 134.7 (C-6, C-8), 134.4 (C-6, C-8), 132.5 (C-4a), 131.4 (C-8a), 129.3 (phenyl C-1), 129.0 (phenyl C-2), 127.6 (phenyl C-3), 127.2 (phenyl C-4, C-7), 127.1 (phenyl C-4, C-7), 117.6 (C-4), 51.7 (C-2'), 45.9 (C-6'), 42.3 (C-3'), 30.5 (C-4'), 25.3 (C-5'); HRMS $[\text{M}+\text{H}]^+$ $\text{C}_{20}\text{H}_{21}\text{N}_2\text{O}_2\text{S}^+$ calc., 353.1329 found, 353.1335.

5-((hexahydro-1*H*-isoindol-2(3*H*)-yl)sulfonyl)isoquinoline (289)



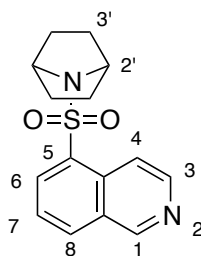
Following general procedure **5**, employing octahydro-1*H*-isoindole hydrochloride (516 mg, 3.21 mmol) and stirred at room temperature for 18 h. The solid was dissolved in CH₂Cl₂ (5 mL), dry loaded onto silica and purified by flash column chromatography eluting with EtOAc, to give *fragment 289* as a brown solid (335 mg, 48%. *R_f* 0.36 (EtOAc). mp 220 °C (EtOH); $\nu_{\text{max}}/\text{cm}^{-1}$ (film) 3282, 2952, 2801, 2389, 2103 and 1374; δ_{H} (500 MHz, MeOD) 9.25 (1H, dd, *J* 1.1, 0.9, 1-H), 8.54 (1H, dt, *J* 6.2, 1.0, 1H, 3-H), 8.50 (1H, d, *J* 6.2, 4-H), 8.31 (1H, dd, *J* 7.4, 1.2, 6-H), 8.27 (1H, app. dt, *J* 8.2, 1.1, 8-H), 7.71 (1H, dd, *J* 8.2, 7.4, 7-H), 3.22 (2H, dd, *J* 9.6, 6.8, 2'-H), 3.10 (2H, dd, *J* 9.5, 5.5, 2'-H), 1.29 – 0.95 (10H, m, 2a'-H, 3'-H, 4'-H); δ_{C} (125 MHz, DMSO-*d*₆) 152.9 (C-1), 143.5 (C-3), 133.6 (C-6, C-8), 133.6 (C-6, C-8), 133.6 (C-5), 132.0 (C-4a), 129.3 (C-8a), 126.4 (C-7), 118.2 (C-4), 51.0 (C-2'), 37.5 (C-2a'), 25.0 (C-3', C-4'), 22.2 (C-3', C-4'); HRMS [M+H]⁺ C₁₇H₂₁N₂O₂S₁⁺ calc., 317.1329 found, 317.1327.

5-((2-methylpiperidin-1-yl)sulfonyl)isoquinoline (290)



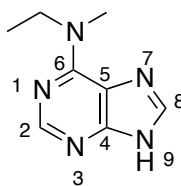
Following general procedure **5**, employing 2-methylpiperidine (318 mg, 3.21 mmol) and stirred at room temperature for 18 h. The solid was dissolved in CH₂Cl₂ (5 mL), dry loaded onto silica and purified by flash column chromatography eluting with EtOAc, to give *fragment 290* as a brown solid (346 mg, 54%). *R_f* 0.41 (EtOAc). mp 198 °C (EtOH); $\nu_{\max}/\text{cm}^{-1}$ (film) 2128, 1513 and 1358; δ_{H} (500 MHz, MeOD) 9.26 (1H, d, *J* 1.0, 1-H), 8.51 (1H, d, *J* 6.2, 4-H), 8.36 (1H, dd, *J* 7.4, 1.3, 6-H), 8.30 (1H, dt, *J* 6.2, 1.0, 3-H), 8.26 (1H, app. dt, *J* 8.3, 1.1, 8-H), 7.69 (1H, dd, *J* 8.2, 7.4, 7-H), 4.22 – 4.08 (1H, m, 2'-H), 3.57 – 3.47 (1H, m, 6'-H₂), 3.00 (1H, td, *J* 13.3, 2.7, 6'-H₃), 1.55 – 1.30 (5H, m, 3'-H, 4'-H, 5'-H), 1.13 – 1.02 (1H, m, 4'-H), 1.01 (3H, br, CH₃). δ_{C} (125 MHz, MeOD) 153.0 (C-1), 143.5 (C-3), 135.0 (C-5), 134.1 (C-6 or C-8), 133.6 (C-6 or C-8), 131.4 (C-4a), 129.3 (C-8a), 126.3 (C-7), 118.0 (C-4), 48.4 (C-2'), 39.7 (C-6'), 30.0 (C-3'), 25.2 (C-5'), 17.7 (C-4'), 14.8 (CH₃). HRMS [M+Na]⁺ C₁₅H₁₈N₂NaO₂S⁺ 313.0992 found, 313.0990.

5-(7-azabicyclo[2.2.1]heptan-7-ylsulfonyl)isoquinoline (291)



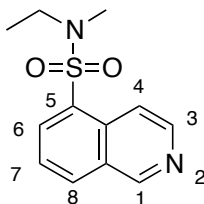
Following general procedure **5**, employing 7-azabicyclo[2.2.1]heptane hydrochloride (427 mg, 3.21 mmol) and stirred at room temperature for 18 h. The solid was dissolved in CH₂Cl₂ (5 mL), dry loaded onto silica and purified by flash column chromatography eluting with EtOAc, to give *fragment 291* was isolated as a white solid (91 mg, 18%). R_f 0.40 (EtOAc). mp 217 °C (EtOH); $\nu_{\max}/\text{cm}^{-1}$ (film) 2995, 2951, 2871 and 1368; δ_{H} (500 MHz, DMSO-*d*₆) 9.49 (1H, app. d, *J* 0.9, 1-H), 8.71 (1H, d, *J* 6.1, 4-H), 8.51 – 8.44 (2H, m, 3-H, 6-H or 8-H), 8.41 (1H, m, 6-H or 8-H), 7.90 – 7.83 (1H, m, 7-H), 4.22 (2H, td, *J* 2.9, 1.4, 2'-H), 1.65 (4H, m, 3'-H₂), 1.43 (4H, m, 3'-H₃); δ_{C} (125 MHz, DMSO-*d*₆) 154.0 (C-1), 145.3 (C-3), 135.0 (C-5), 134.6 (C-6, C-8), 133.6 (C6, C8), 131.2 (C4a), 129.1 (C8a), 127.0 (C7), 117.6 (C4), 59.7 (C2'), 30.3 (C3'). HRMS [M+H]⁺ C₁₅H₁₇N₂O₂S⁺ 289.1016 found, 289.1025.

***N*-ethyl-*N*-methyl-9*H*-purin-6-amine (292)**



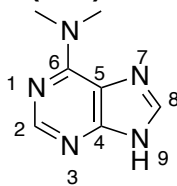
Following general procedure **4**, employing *N*-methylethanamine (230.1 mg, 3.90 mmol) and heated at reflux for 3.5 h. The crude solid was washed with MeOH (2 × 25 mL) and dichloromethane (2 × 25 mL) to give *purine* **292** as a yellow solid (126 mg, 22%). mp 287 °C (EtOH); $\nu_{\max}/\text{cm}^{-1}$ (film) 3066, 2965, 2788, 1984 and 1574; δ_{H} (500 MHz, DMSO- d_6) 12.94 (1H, br s, NH) 8.18 (1H, s, 8-H), 8.08 (1H, s, 2-H), 4.06 (2H, br, NCH₂CH₃), 3.45 (3H, br s, NCH₃) 1.17 (3H, t, J 7.0, NCH₂CH₃); δ_{C} (125 MHz DMSO- d_6) 154.1 (C-6), 152.4 (C-2), 151.5 (C-4), 138.4 (C-8), 119.2 (C-5), 44.9 (NCH₃), 35.7 (NCH₂CH₃), 13.2 (NCH₂CH₃); HRMS [M+H]⁺ C₇H₁₀N₅⁺ calc. 178.1093, found 178.1084.

***N*-ethyl-*N*-methylisoquinoline-5-sulfonamide (**293**)**



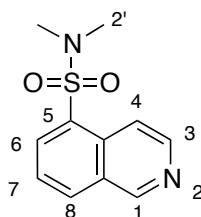
Following general procedure **5**, employing *N*-methylethanamine (195.8 mg, 3.32 mmol) and stirred at room temperature for 18 h. The solid was dissolved in CH₂Cl₂ (5 mL), dry loaded onto silica and purified by flash column chromatography eluting with EtOAc, to give fragment **293** as a white solid (309 mg, 56%). *R_f* 0.31 (EtOAc). mp 167 °C (EtOH); $\nu_{\max}/\text{cm}^{-1}$ (film) 3067, 2982, 2935, 1612 and 1351; δ_{H} (500 MHz, MeOD) 9.33 (1H, d, *J* 1.0, 1-H), 8.59 (1H, d, *J* 6.2, 4-H), 8.55- 8.51 (1H, m, 3-H), 8.39 – 8.27 (2H, m, 6-H, 8-H), 7.77 (1H, dd, *J* 8.2, 7.4, 7-H), 3.25 (2H, q, *J* 7.1, CH₂CH₃), 2.82 (3H, s, CH₃), 1.08 (3H, t, *J* 7.1, CH₂CH₃). δ_{C} (125 MHz, MeOD) 152.9 (C-1), 143.4 (C-3), 133.6 (C-5) 133.5 (C-6, C-8) 133.4 (C-6, C-8), 131.7 (C-4a), 129.2 (C-8a), 126.4 (C-7), 118.1 (C-4), 44.3 (CH₃), 32.7 (CH₂CH₃), 12.2 (CH₂CH₃). HRMS [M+H]⁺ C₁₂H₁₅N₂O₂S⁺ calc., 251.0859, found 251.0854.

***N,N*-dimethyl-9*H*-purin-6-amine (294)**



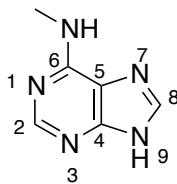
Following general procedure **4**, employing dimethylamine (2 M in ethanol, 2 mL) and heated at reflux for 3.5 h. The solid was isolated through filtration using a sintered funnel. The crude solid was washed with MeOH (2 × 25 mL) and dichloromethane (2 × 25 mL) to give purine **294** as a yellow solid (392 mg, 74%). mp 260 °C (EtOH) (lit²⁷⁶ 262°C); $\nu_{\max}/\text{cm}^{-1}$ (film) 3054, 2946, 2671 and 1587; δ_{H} (500 MHz, DMSO-*d*₆) 12.96 (1H, br s, 9-H) 8.18 (1H, s, NH), 8.09 (1H, s, 8-H), 3.40 (6H, br s, amine CH₃). δ_{C} (125 MHz DMSO-*d*₆) 154.7 (C-6), 152.3 (C-2), 151.5 (C-4), 138.2 (C-8), 119.4 (C-5), 38.3 (amine CH₃); HRMS [M+H]⁺ C₇H₁₀N₅⁺ calc. 164.0936, found 164.0930. Spectral data in accordance with literature.²⁷⁷

***N,N*-dimethylisoquinoline-5-sulfonamide (295)**



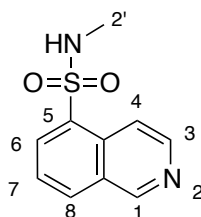
Following general procedure **5**, employing dimethylamine (2M in ethanol, 2 mL) and stirred at room temperature for 18 h. The solid was dissolved in CH₂Cl₂ (5 mL), dry loaded onto silica and purified by flash column chromatography eluting with EtOAc, to give fragment **295** as a yellow solid (396 mg, 76%). *R_f* 0.30 (EtOAc). mp 161 °C (EtOH); $\nu_{\max}/\text{cm}^{-1}$ (film) 3019, 2688, 2609, 1613 and 1353; δ_{H} (500 MHz, MeOD) 9.24 (1H, d, *J* 0.8, 1-H), 8.52 – 8.44 (2H, m, 3-H, 4-H), 8.26 (2H, d, *J* 7.7, 6-H, 8-H), 7.71 (1H, t, *J* 7.8, 7-H), 2.67 (6H, s, 2'-H). δ_{C} (125 MHz, MeOD) 152.9 (C-1), 143.5 (C-3), 134.3 (C-6, C-8), 133.9 (C-6, C-8), 132.1 (C-8a), 131.9 (C-5), 129.3 (C-4a), 126.3 (C-7), 118.2 (C-4), 36.4 (C-2'). HRMS [M+H]⁺ C₁₁H₁₃N₂O₂S⁺ calc., 237.0703, found 237.0703.

***N*-methyl-9*H*-purin-6-amine (296)**



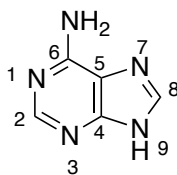
Following general procedure **4**, employing methylamine (2 M in methanol, 2 mL) and heated at reflux for 3.5 h. The solid was isolated through filtration using a sintered funnel. The crude solid was washed with MeOH (2 × 25 mL) and dichloromethane (2 × 25 mL) to give *purine* **296** as a beige solid (484.3 mg, 54%). mp 320 °C (EtOH); $\nu_{\text{max}}/\text{cm}^{-1}$ (film) 3312, 3025, 2898 and 1521; δ_{H} (500 MHz, DMSO- d_6) 12.90 (1H, br s, 9-H) 8.21 (1H, s, NH), 8.08 (1H, s, 8-H), 7.60 (1H, s, 2-H), 3.46 (br s, 2H, NH_2), 2.96 (3H, s, amine CH_3); δ_{C} (125 MHz DMSO- d_6) 155.4 (C-6), 152.9 (C-2), 149.7 (C-4), 139.0 (C-8), 119.4 (C-5), 27.4 (amine CH_3); HRMS $[\text{M}+\text{H}]^+$ $\text{C}_6\text{H}_8\text{N}_5^+$ calc. 150.0780, found 150.0769. ^1H and ^{13}C is consistent with the literature ²⁷⁷

***N*-methylisoquinoline-5-sulfonamide (297)**



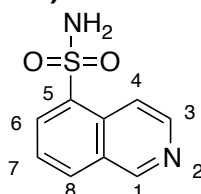
Following general procedure **5**, employing methylamine (1M in methanol, 2 mL) and stirred at room temperature for 18 h. The solid was dissolved in CH₂Cl₂ (5 mL), dry loaded onto silica and purified by flash column chromatography eluting with EtOAc, to give fragment **297** as a colourless solid (396 mg, 76%). *R_f* 0.30 (EtOAc). mp 153 °C (EtOH); $\nu_{\max}/\text{cm}^{-1}$ (film) 3068, 2811, 2232, 1618 and 1350; δ_{H} (500 MHz, MeOD) 9.27 (1H, t, *J* 1.2, 1-H), 8.54 – 8.38 (2H, m, 3-H, 4-H), 8.38 – 8.25 (2H, m, 6-H, 7-H), 7.71 (1H, ddd, *J* 8.5, 7.3, 1.3, 8-H), 4.76 (1H, s, NH), 2.50 – 2.39 (3H, m, 2'-H). δ_{C} (125 MHz, MeOD) 152.9 (C-1), 143.4 (C-3), 134.0 (C-5), 133.6 (C-6, C-8), 133.4 (C-6, C-8), 131.4 (C-8a), 129.3 (C-4a), 126.2 (C-7), 117.9 (C-4), 27.6 (C-2'). HRMS [M+H]⁺ C₁₀H₁₁N₂O₂S⁺ calc., 223.0547, found 223.0548.

9H-purin-6-amine (298)



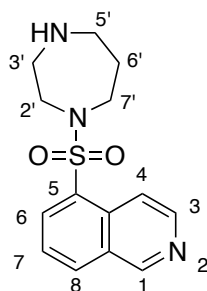
Following general procedure **4**, employing ammonia (1 M in methanol, 2.5 mL) and heated at reflux for 8 h. The solid was isolated through filtration using a sintered funnel. The crude solid was washed with MeOH (2 × 25 mL) and dichloromethane (2 × 25 mL) to give *purine* **298** as a colourless solid (171 mg, 39%). mp 360 °C (EtOH) (Lit ²⁷⁸ 360 °C) ; $\nu_{\max}/\text{cm}^{-1}$ (film) 3344, 3058, 2965, 2886 and 1574; δ_{H} (500 MHz, DMSO-*d*₆) 12.85 (1H, br s, 9-H), 8.13 (1H, s, 2-H), 7.16 (1H, s, 8-H), 3.45 (br s, 2H, NH₂); δ_{C} (125 MHz DMSO-*d*₆) 154.7 (C-6), 152.3 (C-2), 151.5 (C-4), 138.2 (C-8), 119.4 (C-5); HRMS [M+H]⁺ C₅H₆N₅⁺ calc. 136.0613, found 136.0608. Spectral data in accordance with literature.²⁷⁹

Isoquinoline-5-sulfonamide (299)



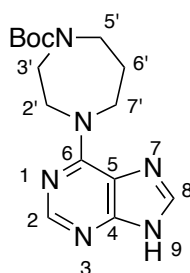
Following general procedure **5**, employing ammonia (1M in methanol, 2.5 mL) and stirred at room temperature for 18 h. The solid was dissolved in CH₂Cl₂ (5 mL), dry loaded onto silica and purified by flash column chromatography eluting with EtOAc, to give fragment **299** as an off-white solid (69.1 mg, 10%). R_f0.37 (10:90 MeOH–EtOAc). mp 155 °C (EtOH); $\nu_{\max}/\text{cm}^{-1}$ (film) 3291, 2973, 2880, 2462, 2043, 1620 and 1351; δ_{H} (500 MHz, MeOD) 9.27 (1H, dd, *J* 1.1 0.9, 1-H), 8.51 (1H, d, *J* 6.2, 4-H), 8.47 (1H, dt, *J* 6.2, 0.9, 3-H), 8.38 (1H, dd, *J* 7.4, 1.2, 6-H), 8.25 (1H, app. dt, *J* 8.3, 1.1, 8-H), 7.69 (1H, dd, *J* 8.2, 7.4, 7-H). δ_{C} (125 MHz, MeOD) 152.6 (C-1), 143.0 (C-3), 138.4 (C-5), 132.8 (C-8), 131.4 (C-6), 131.2 (C-4a), 129.2 (C-8a), 126.4 (C-7), 118.3 (C-4). HRMS [M+H]⁺ C₉H₉N₂O₂S⁺ calc., 209.03890, found 209.0389.

5-((1,4-diazepan-1-yl)sulfonyl)isoquinoline (300)



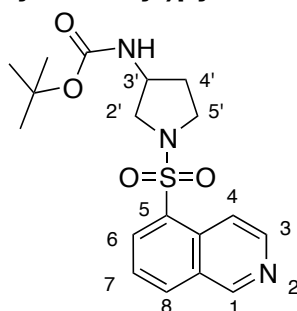
Following general procedure **5**, employing *tert*-butyl 1,4-diazepane-1-carboxylate (642 mg, 3.21 mmol) and stirred at room temperature for 18 h. The reaction mixture was concentrated *in vacuo* to give a crude solid. The solid was dissolved in dichloromethane (50 mL) and TFA (25 mL) and stirred at room temperature for 3 h. Subsequently the reaction was concentrated *in vacuo* to give a crude residue. The residue was dissolved in dichloromethane (2 mL) and loaded onto a 1 g SCX cartridge, and the cartridge flushed with MeOH (3 × 20 mL). The product was eluted using ammonia (1 M solution in MeOH, 3 × 20 mL) which was concentrated *in vacuo* to give **300** as a white solid (334 mg, 52%). mp 232 °C (EtOH); $\nu_{\max}/\text{cm}^{-1}$ (film) 3292, 3008, 2929, 2816 and 1378; δ_{H} (500 MHz, MeOD) 9.35 (1H, app. d, J 1.0, 1-H), 8.61 (1H, d, J 6.2, 4-H), 8.50 (1H, dt, J 6.2, 1.0, 3-H), 8.35 (2H, m, 6-H, 8-H), 7.79 (1H, dd, J 8.2, 7.4, 7-H), 3.56 – 3.44 (4H, m, 2'-H, 7'-H), 3.02 – 2.85 (4H, m, 3'-H, 5'-H), 1.85 (2H, tt, J 7.1, 4.9, 6'-H); δ_{C} (125 MHz, MeOD) 153.0 (C-1), 143.6 (C-3), 134.5 (C-5), 133.5 (C-6, C-8), 132.9 (C-6, C-8), 131.5 (C-4a), 129.4 (C-8a), 126.4 (C-7), 118.0 (C-4), 50.0 (C-7'), 49.3 (C-2'), 47.0 (C-3'), 46.7 (C-5'), 30.3 (C-6'). HRMS $[\text{M}+\text{H}]^+$ $\text{C}_{14}\text{H}_{18}\text{N}_3\text{O}_2\text{S}^+$ calc., 292.1125 found, 292.1136.

***tert*-butyl 4-(9*H*-purin-6-yl)-1,4-diazepane-1-carboxylate (301)**



Following general procedure **4**, employing *tert*-butyl 1,4-diazepane-1-carboxylate (780 mg, 3.90 mmol) and heated at reflux for 8 h. The solid was isolated through filtration using a sintered funnel. The crude solid was washed with MeOH (2 × 25 mL) and dichloromethane (2 × 25 mL) to give *purine* **301** as a colourless solid (1.03 g, 85%). mp 284 °C (EtOH); $\nu_{\max}/\text{cm}^{-1}$ (film) 3084, 2989, 2698 and 1692; δ_{H} (500 MHz, MeOD) 8.09 (1H, s, 2-H), 7.88 (1H, s, 8-H), 4.13 (4H, m, 2'-H, 7'-H), 3.02 – 2.92 (2H, m, 3'-H), 2.78 – 2.73 (2H, m, 5'-H), 1.96 – 1.86 (2H, m, 6'-H), 1.54 (9H, s, ^tBu); δ_{C} (125 MHz MeOD) 154.0 (C-6), 151.7 (C-2), 150.8 (Boc C=O), 138.9 (C-4) 138.1 (C-8), 118.6 (C-5), 70.8 (Boc C-O) 50.3 (C-7'), 48.7 (C-2'), 46.8 (C-3', C-5'), 30.3 (C-6'), 29.1 (Boc ^tBu); HRMS [M+H]⁺ C₁₅H₂₃N₆O₂⁺ calc., 319.1882, found 319.1898.

***tert*-butyl (1-(isoquinolin-5-ylsulfonyl)pyrrolidin-3-yl)carbamate (303)**



Following general procedure **5**, employing *N*-(pyrrolidin-3-yl)methanesulfonamide (597 mg, 3.21 mmol) and stirred at room temperature for 18 h. The solid was dissolved in CH₂Cl₂ (5 mL), dry loaded onto silica and purified by flash column chromatography eluting with EtOAc, to give the title *fragment* as a colourless solid (274 mg, 33%). *R_f* 0.32 (EtOAc). mp 209 °C (EtOH); $\nu_{\max}/\text{cm}^{-1}$ (film) 3229, 2977, 1601 and 1321; δ_{H} (500 MHz, DMSO-*d*₆) 9.37 (1H, dd, *J* 1.2, 0.9, 1-H), 8.58 (1H, d, *J* 6.1, 3-H), 8.45 – 8.32 (2H, m, 4-H, 6-H), 8.23 (1H, app. dd, *J* 7.4, 1.2, 8-H), 7.75 (1H, dd, *J* 8.1, 7.4, 7-H), 3.85 (1H, m, 3'-H) 3.31 – 3.28 (2H, m, 2'-H_A, 5'-H_A), 3.24 – 3.15 (1H, m, 5'-H_B), 2.95 (1H, dd, *J* 9.8, 4.9, 2'-H_B), 1.86 (1H, ddt, *J* 13.0, 7.9, 6.6, 4'-H_A), 1.59 (1H, dq, *J* 12.8, 6.5, 4'-H_B), 1.19 (s, 9H, ^tBu). δ_{C} (125 MHz, DMSO-*d*₆) 155.5 (Boc C=O), 153.9 (C-1), 145.4 (C-3), 134.5 (C-6, C-8), 133.7 (C-6, C-8), 132.6 (C-5), 131.7 (C-4a), 129.3 (C-8a), 127.0 (C-7), 117.7 (C-4), 78.5 (Boc C-O), 53.2 (C-2'), 50.4 (C-3'), 46.4 (C-5'), 30.8 (C-4'), 28.6 (Boc ^tBu); HRMS [M+H]⁺ C₁₈H₂₄N₃O₄S₁⁺ calc., 378.1493 found, 378.1498.

6.4 Biochemical Experimental

Aurora-A kinase assays were designed by Chris Arter.^{228,280}

6.4.1 Determination of Fragment IC₅₀

Each method used a Labchip EZ Reader II system (PerkinElmer) at room temperature using separation buffer (760367, PerkinElmer) containing Coating Reagent 8 (500 nM, 760278, PerkinElmer). The assays were performed in 384-well low-volume (30 μ l) plates (Corning). The kinase substrate was a fluorescein-labelled peptide [5-FAM-LRRASLG-CONH₂] dissolved in 20 mM Tris (pH 7.0), 200 mM NaCl, 5 mM MgCl₂, and 10% w/v glycerol. Measurements of substrate phosphorylation were made every two minutes for 30 cycles unless otherwise stated. Assays were carried out in duplicate using a 12-sipper chip (760404 PerkinElmer) with 2.5% final DMSO concentration. Fragments were evaluated by performing a 10-point, 5-fold serial dilution of fragment in DMSO (188 mM, 100% DMSO), followed by dilution with buffer (20 mM Tris (pH 7.0), 200 mM NaCl, 5 mM MgCl₂, and 10% w/v glycerol) to result in 4 \times fragment solutions, each concentration was repeated in triplicate. A solution containing both 4 \times substrate and 4 \times ATP (6 μ M and 320 μ M respectively) and a 2 \times enzyme solution (20 nM) were prepared in the same buffer. Each of the fragment solutions (20 μ l) was diluted two-fold with the solution containing both the substrate and ATP (20 μ l); and 14 μ l of the resulting solutions were added to the appropriate wells on a 384-well plate, followed by 14 μ l of the 2 \times enzyme solution, resulting in 10 final fragment concentrations (10 mM – 508 nM) and final substrate, ATP and enzyme concentrations of 1.5 μ M, 80 μ M, and 10 nM, respectively, in 10% final DMSO. The percentage conversion of substrate at each fragment concentration was generated by the EZ Reader software and plotted against time in GraphPad Prism 7 and includes error bars. The initial rate at each fragment concentration was plotted against the corresponding concentration to yield a dose-response curve, using a sigmoidal fit.

6.4.2 DMSO tolerance Studies²²⁸

The pseudo-WT Aurora-A DMSO tolerance values were determined by performing an 10-point, 2-fold serial dilution of 40% DMSO in Aurora-A buffer to result in 4 × stock solutions of DMSO. A 4 × substrate and ATP solution (6 μM and 320 μM, respectively) and a 2 × enzyme solution (100 and 62.5 nM for WT and pseudo-WT Aurora A, respectively) were prepared. Each of the 4 × DMSO stock solutions were diluted two-fold in the 4 × substrate and ATP solution and 14 μl of the produced solutions were added to the appropriate wells on the 384-well plate, followed by the 2 × enzyme solution, resulting in 12 final DMSO concentrations (10 – 0.02 % v/v) and final substrate, ATP and enzyme concentrations of 1.5 μM, 80 μM, 50 nM, and 31.25 nM, respectively. The percentage conversion of substrate at each DMSO concentration was generated by the EZ Reader software and plotted against time in GraphPad Prism 7. The initial rate at each DMSO concentration was plotted against the corresponding concentration. An ideal DMSO % for WT Aurora-A and pseudo-WT Aurora-A was determined as 2.5%.

6.4.3 Determination of ATP K_M ²²⁸

The pseudo-WT Aurora-A K_M ATP values were determined by performing a 12-point, 3- fold serial dilution of 12 mM ATP in Aurora-A buffer to result in 4 × stock solutions of ATP. A 4 × substrate solution (6 μM) and a 2 × enzyme solution (100 and 62.5 nM for WT and pseudo-WT Aurora A, respectively) were prepared. Each of the 4 × ATP stock solutions were diluted two-fold in the 4 × substrate solution and 14 μl of the produced solutions were added to the appropriate wells on the 384-well plate, followed by the 2 × enzyme solution, resulting in 12 final ATP concentrations (3 mM – 17 nM) and final substrate and enzyme concentrations of 1.5 μM, 50, and 31.25 nM concentrations, respectively. The percentage conversion of substrate at each ATP concentration was generated by the EZ Reader software and plotted against time in GraphPad Prism 7. The initial rate at each ATP concentration

was plotted against the corresponding ATP concentration to generate a Michaelis-Menten plot.

6.4.4 Thermal Shift Assay

This work was completed by Dr. Tilman-Berger of Prof. Stefan Knapp laboratory at the SGC Frankfurt.

The protein at 2 μ M in 10 mM HEPES, pH 7.5 and 250 mM NaCl was mixed with the fragments/ compounds at 200 mM concentration. The assays, data evaluation, and melting temperature (T_m) calculation were performed using a Real-Time PCR Mx3005p machine (Stratagene) with the protocols described previously.²⁵⁸

6.4.5 General Computational Procedures

General computational procedures All computational dockings were conducted on a LINUX computer using the CentOS 6.6 operating system. Parallel docking was conducted on the Milin6 cluster housed at the University of Leeds.

PBD pre-processing All PDBs were sourced from the RCSB PDB databank. Each PDB complex was first opened in Maestro Version 9.9.013 where they were visually inspected. If more than one protein molecule was present in the asymmetric unit, one was removed to generate a monomer and all water molecules were removed from the structure.

7 References

- 1 J. P. Garner, *Harv. Bus. Rev.*, 2008, **86**, 68–70.
- 2 I. Kola and J. Landis, *Nat. Rev. Drug Discov.*, 2004, **3**, 711.
- 3 S. Hoelder, P. A. Clarke and P. Workman, *Mol. Oncol.*, 2012, **6**, 155–176.
- 4 J. P. Hughes, S. S. Rees, S. B. Kalindjian and K. L. Philpott, *Br. J. Pharmacol.*, 2011, **162**, 1239–1249.
- 5 I. Gashaw, P. Ellinghaus, A. Sommer and K. Asadullah, *Drug Discov. Today*, 2012, **17**, 24-S30.
- 6 P. G. Wyatt, I. H. Gilbert, K. D. Read and A. H. Fairlamb, *Curr. Top. Med. Chem.*, 2011, **11**, 1275–1283.
- 7 R. MacArron, M. N. Banks, D. Bojanic, D. J. Burns, D. A. Cirovic, T. Garyantes, D. V. S. Green, R. P. Hertzberg, W. P. Janzen, J. W. Paslay, U. Schopfer and G. S. Sittampalam, *Nat. Rev. Drug Discov.*, 2011, **10**, 188–195.
- 8 P. B. Simpson and M. Reichman, *Nat. Rev. Drug Discov.*, 2014, **13**, 3–4.
- 9 T. Zhu, S. Cao, P.-C. Su, R. Patel, D. Shah, H. B. Chokshi, R. Szukala and M. E. Johnson, *J. Med. Chem.*, 2013, **56**, 6560–6572.
- 10 K. Moore and S. Rees, *J. Biomol. Screen.*, 2001, **6**, 69–74.
- 11 S. M. Paul, D. S. Mytelka, C. T. Dunwiddie, C. C. Persinger, B. H. Munos, S. R. Lindborg and A. L. Schacht, *Nat. Rev. Drug Discov.*, 2010, **9**, 203–214.
- 12 *Commissioner, Food and Drug Administration*, 2016.
- 13 J. R. Turner, *New Drug Development*, Springer International Publishing, 2nd edn., 2010.
- 14 A. L. Hopkins, *Nat. Chem. Biol.*, 2008, **4**, 682–690.
- 15 A. Mullard, *Nat. Rev. Drug Discov.*, 2014, **13**, 877–877.
- 16 M. N. Pangalos, L. E. Schechter and O. Hurko, *Nat. Rev. Drug Discov.*, 2007, **6**, 521–532.
- 17 M. J. Waring, J. Arrowsmith, A. R. Leach, P. D. Leeson, S. Mandrell, R. M. Owen, G. Pairaudeau, W. D. Pennie, S. D. Pickett, J. Wang, O. Wallace and A. Weir, *Nat. Rev. Drug Discov.*, 2015, **14**, 475–486.
- 18 G. M. Keserü and G. M. Makara, *Nat. Rev. Drug Discov.*, 2009, **8**, 203–212.
- 19 T. T. Ashburn and K. B. Thor, *Nat. Rev. Drug Discov.*, 2004, **3**, 673–683.
- 20 G. Vistoli, A. Pedretti and B. Testa, *Drug Discov. Today*, 2008, **13**, 285–294.
- 21 R. Testa, Bernard; Van DeWaterbeemd, H; Folkers, G; Guy, Wiley Online Library, 2nd editio., 2000, p. 25.
- 22 D. M. Coen and P. A. Schaffer, *Nat. Rev. Drug Discov.*, 2003, **2**, 278–288.
- 23 C. A. Lipinski, *J. Pharmacol. Toxicol. Methods*, 2000, **44**, 235–249.

- 24 P. Leeson, H. Oncology and C. Hospital, *Nature*, 1912, **481**, 455–456.
- 25 C. A. Lipinski, F. Lombardo, B. W. Dominy and P. J. Feeney, *Adv. Drug Deliv. Rev.*, 1997, **23**, 3–25.
- 26 C. A. Lipinski, *Drug Discov. Today Technol.*, 2004, **1**, 337–341.
- 27 Y. B. Choy and M. R. Prausnitz, *Pharmaceutical Res.*, 2011, **28**, 943.
- 28 T. M. Frimurer, R. Bywater, L. Nærum, L. N. Lauritsen and S. Brunak, *J. Chem. Inf. Comput. Sci.*, 2000, **40**, 1315–1324.
- 29 T. T. Wager, R. Y. Chandrasekaran, X. Hou, M. D. Troutman, P. R. Verhoest, A. Villalobos and Y. Will, *ACS Chem. Neurosci.*, 2010, **1**, 420–434.
- 30 A. Mullard, *Nat. Rev. Drug Discov.*, 2012, **11**, 173–175.
- 31 P. D. Leeson and B. Springthorpe, *Nat. Rev. Drug Discov.*, 2007, **6**, 881.
- 32 M. J. Waring and C. Johnstone, *Bioorganic Med. Chem. Lett.*, 2007, **17**, 1759–1764.
- 33 M. C. Wenlock, R. P. Austin, P. Barton, A. M. Davis and P. D. Leeson, *J. Med. Chem.*, 2003, **46**, 1250–1256.
- 34 M. M. Hann, *Multifaceted Roles Crystallogr. Mod. Drug Discov.*, 2015, **2**, 183–196.
- 35 M. Martignoni, G. M. M. Groothuis and R. de Kanter, *Expert Opin. Drug Metab. Toxicol.*, 2006, **2**, 875–894.
- 36 C. Pidgeon, S. Ong, H. Liu, X. Qiu, M. Pidgeon, A. H. Dantzig, J. Munroe, W. J. Homback, J. S. Kasher, L. Glunz and T. Szczerba, *J. Med. Chem.*, 1995, **38**, 590–594.
- 37 F. Lovering, J. Bikker and C. Humblet, *J. Med. Chem.*, 2009, **52**, 6752–6756.
- 38 H.-L. Wang, J. Katon, C. Balan, A. W. Bannon, C. Bernard, E. M. Doherty, C. Dominguez, N. R. Gavva, V. Gore, V. Ma, N. Nishimura, S. Surapaneni, P. Tang, R. Tamir, O. Thiel, J. J. S. Treanor and M. H. Norman, *J. Med. Chem.*, 2007, **50**, 3528–3539.
- 39 T. J. Ritchie and S. J. F. Macdonald, *Drug Discov. Today*, 2009, **14**, 1011–1020.
- 40 E. Zartler and M. Shapiro, *Fragment Based Drug Discovery*, 1st editio., 2008.
- 41 D. E. Scott, A. G. Coyne, S. A. Hudson and C. Abell, *Biochemistry*, 2012, **51**, 4990–5003.
- 42 M. I. Page and W. P. Jencks, *Proc. Natl. Acad. Sci.*, 1971, **68**, 1678–1683.
- 43 M. I. Page, *Chem. Soc. Rev.*, 1973, **2**, 295–323.
- 44 W. P. Jencks, *Proc. Natl. Acad. Sci.*, 1981, **78**, 4046 LP – 4050.
- 45 P. R. Andrews, D. J. Craik and J. L. Martin, *J. Med. Chem.*, 1984, **27**, 1648–1657.
- 46 C. E. Nakamura and R. H. Abeles, *Biochemistry*, 1985, **24**, 1364–1376.
- 47 C. L. M. J. Verlinde, G. Rudenko and W. G. J. Hol, *J. Comput. Aided. Mol. Des.*, 1992, **6**, 131–147.

- 48 S. B. Shuker, P. J. Hajduk, R. P. Meadows and S. W. Fesik, *Science* (80-.), 1996, **274**, 1531 LP – 1534.
- 49 C. W. Murray and T. L. Blundell, *Curr. Opin. Struct. Biol.*, 2010, **20**, 497–507.
- 50 M. Congreve, C. W. Murray and T. L. Blundell, *Drug Discov. Today*, 2005, **10**, 895–907.
- 51 M. Frederickson, O. Callaghan, G. Chessari, M. Congreve, S. R. Cowan, J. E. Matthews, R. McMenamin, D.-M. Smith, M. Vinković and N. G. Wallis, *J. Med. Chem.*, 2008, **51**, 183–186.
- 52 N. Abdel-Rahman, A. Martinez-Arias and T. L. Blundell, *Biochem. Soc. Trans.*, 2011, **39**, 1327 LP – 1333.
- 53 E. Valkov, T. Sharpe, M. Marsh, S. Greive and M. Hyvönen, *Targeting Protein–Protein Interactions and Fragment-Based Drug Discovery.*, Springer International Publishing, 1st edn., 2011.
- 54 N. Basse, J. L. Kaar, G. Settanni, A. C. Joerger, T. J. Rutherford and A. R. Fersht, *Chem. Biol.*, 2010, **17**, 46–56.
- 55 C. W. Murray, M. G. Carr, O. Callaghan, G. Chessari, M. Congreve, S. Cowan, J. E. Coyle, R. Downham, E. Figueroa, M. Frederickson, B. Graham, R. McMenamin, M. A. O'Brien, S. Patel, T. R. Phillips, G. Williams, A. J. Woodhead and A. J.-A. Woolford, *J. Med. Chem.*, 2010, **53**, 5942–5955.
- 56 A. J. Woodhead, H. Angove, M. G. Carr, G. Chessari, M. Congreve, J. E. Coyle, J. Cosme, B. Graham, P. J. Day, R. Downham, L. Fazal, R. Feltell, E. Figueroa, M. Frederickson, J. Lewis, R. McMenamin, C. W. Murray, M. A. O'Brien, L. Parra, S. Patel, T. Phillips, D. C. Rees, S. Rich, D.-M. Smith, G. Trewartha, M. Vinkovic, B. Williams and A. J.-A. Woolford, *J. Med. Chem.*, 2010, **53**, 5956–5969.
- 57 L. Chen, E. Cressina, F. J. Leeper, A. G. Smith and C. Abell, *ACS Chem. Biol.*, 2010, **5**, 355–358.
- 58 W. F. Lau, J. M. Withka, D. Hepworth, T. V Magee, Y. J. Du, G. A. Bakken, M. D. Miller, Z. S. Hendsch, V. Thanabal, S. A. Kolodziej, L. Xing, Q. Hu, L. S. Narasimhan, R. Love, M. E. Charlton, S. Hughes, W. P. van Hoorn and J. E. Mills, *J. Comput. Aided. Mol. Des.*, 2011, **25**, 621.
- 59 J. Tsai, J. T. Lee, W. Wang, J. Zhang, H. Cho, S. Mamo, R. Bremer, S. Gillette, J. Kong, N. K. Haass, K. Sproesser, L. Li, K. S. M. Smalley, D. Fong, Y.-L. Zhu, A. Marimuthu, H. Nguyen, B. Lam, J. Liu, I. Cheung, J. Rice, Y. Suzuki, C. Luu, C. Settachatgul, R. Shellooe, J. Cantwell, S.-H. Kim, J. Schlessinger, K. Y. J. Zhang, B. L. West, B. Powell, G. Habets, C. Zhang, P. N. Ibrahim, P. Hirth, D. R. Artis, M. Herlyn and G. Bollag, *Proc. Natl. Acad. Sci.*, 2008, **105**, 3041 LP – 3046.
- 60 M. M. Hann, A. R. Leach and G. Harper, *J. Chem. Inf. Comput. Sci.*, 2001, **41**, 856–864.
- 61 U. B. Ericsson, B. M. Hallberg, G. T. DeTitta, N. Dekker and P. Nordlund, *Anal. Biochem.*, 2006, **357**, 289–298.

- 62 F. H. Niesen, H. Berglund and M. Vedadi, *Nat. Protoc.*, 2007, **2**, 2212.
- 63 I. Navratilova and A. L. Hopkins, *ACS Med. Chem. Lett.*, 2010, **1**, 44–48.
- 64 A. Kuglstatler, M. Stahl, J.-U. Peters, W. Huber, M. Stihle, D. Schlatter, J. Benz, A. Ruf, D. Roth, T. Enderle and M. Hennig, *Bioorg. Med. Chem. Lett.*, 2008, **18**, 1304–1307.
- 65 H. Nordström, T. Gossas, M. Hämäläinen, P. Källblad, S. Nyström, H. Wallberg and U. H. Danielson, *J. Med. Chem.*, 2008, **51**, 3449–3459.
- 66 M. D. Hämäläinen, A. Zhukov, M. Ivarsson, T. Fex, J. Gottfries, R. Karlsson and M. Björnsne, *J. Biomol. Screen.*, 2008, **13**, 202–209.
- 67 S. Perspicace, D. Banner, J. Benz, F. Müller, D. Schlatter and W. Huber, *J. Biomol. Screen.*, 2009, **14**, 337–349.
- 68 S. A. Hofstadler and K. A. Sannes-Lowery, *Nat. Rev. Drug Discov.*, 2006, **5**, 585.
- 69 N. Drinkwater, H. Vu, K. M. Lovell, K. R. Criscione, B. M. Collins, T. E. Prisinzano, S.-A. Poulsen, M. J. McLeish, G. L. Grunewald and J. L. Martin, *Biochem. J.*, 2010, **431**, 51 LP – 61.
- 70 P. K. Chrysanthopoulos, P. Mujumdar, L. A. Woods, O. Dolezal, B. Ren, T. S. Peat and S.-A. Poulsen, *J. Med. Chem.*, 2017, **60**, 7333–7349.
- 71 S. Howard, V. Berdini, J. A. Boulstridge, M. G. Carr, D. M. Cross, J. Curry, L. A. Devine, T. R. Early, L. Fazal, A. L. Gill, M. Heathcote, S. Maman, J. E. Matthews, R. L. McMenamin, E. F. Navarro, M. A. O'Brien, M. O'Reilly, D. C. Rees, M. Reule, D. Tisi, G. Williams, M. Vinković and P. G. Wyatt, *J. Med. Chem.*, 2009, **52**, 379–388.
- 72 P. Bamborough, C. Chung, R. C. Furze, P. Grandi, A.-M. Michon, R. J. Sheppard, H. Barnett, H. Diallo, D. P. Dixon, C. Douault, E. J. Jones, B. Karamshi, D. J. Mitchell, R. K. Prinjha, C. Rau, R. J. Watson, T. Werner and E. H. Demont, *J. Med. Chem.*, 2015, **58**, 6151–6178.
- 73 C. A. Lepre, J. M. Moore and J. W. Peng, *Chem. Rev.*, 2004, **104**, 3641–3676.
- 74 D. Wyss and M. McCoy, *Curr. Opin. Drug Discov. Devel.*, 2002, **5**, 630–647.
- 75 B. Meyer and T. Peters, *Angew. Chemie Int. Ed.*, 2003, **42**, 864–890.
- 76 J. R. Huth, C. Park, A. M. Petros, A. R. Kunzer, M. D. Wendt, X. Wang, C. L. Lynch, J. C. Mack, K. M. Swift, R. A. Judge, J. Chen, P. L. Richardson, S. Jin, S. K. Tahir, E. D. Matayoshi, S. A. Dorwin, U. S. Lador, J. M. Severin, K. A. Walter, D. M. Bartley, S. W. Fesik, S. W. Elmore and P. J. Hajduk, *Chem. Biol. Drug Des.*, 2007, **70**, 1–12.
- 77 E. R. Zartler and M. J. Shapiro, *Curr. Opin. Chem. Biol.*, 2005, **9**, 366–370.
- 78 M. Congreve, R. Carr, C. Murray and H. Jhoti, *Drug Discov. Today*, 2003, **8**, 876–877.
- 79 N. Baurin, F. Aboul-Ela, X. Barril, B. Davis, M. Drysdale, B. Dymock, H. Finch, C. Fromont, C. Richardson, H. Simmonite and R. E. Hubbard, *J. Chem. Inf. Comput. Sci.*, 2004, **44**, 2157–2166.

- 80 A. Schuffenhauer, S. Ruedisser, M. Andreas, W. Jahnke, S. Paul and E. Jacoby, *Curr. Top. Med. Chem.*, 2005, **5**, 751–762.
- 81 A. C. Gibbs, M. C. Abad, X. Zhang, B. A. Tounge, F. A. Lewandowski, G. T. Struble, W. Sun, Z. Sui and L. C. Kuo, *J. Med. Chem.*, 2010, **53**, 7979–7991.
- 82 H. Köster, T. Craan, S. Brass, C. Herhaus, M. Zentgraf, L. Neumann, A. Heine and G. Klebe, *J. Med. Chem.*, 2011, **54**, 7784–7796.
- 83 C. W. Murray and D. C. Rees, *Angew. Chemie - Int. Ed.*, 2016, **55**, 488–492.
- 84 R. J. Hall, P. N. Mortenson and C. W. Murray, *Prog. Biophys. Mol. Biol.*, 2014, **116**, 82–91.
- 85 J. D. St. Denis, R. J. Hall, C. W. Murray, T. D. Heightman and D. C. Rees, *RSC Med. Chem.*, 2021, **12**, 321–329.
- 86 T. E. Nielsen and S. L. Schreiber, *Angew. Chemie Int. Ed.*, 2008, **47**, 48–56.
- 87 C. W. Murray and D. C. Rees, *Nat. Chem.*, 2009, **1**, 187.
- 88 A. L. Hopkins, G. M. Keserü, P. D. Leeson, D. C. Rees and C. H. Reynolds, *Nat. Rev. Drug Discov.*, 2014, **13**, 105–121.
- 89 M. L. Verdonk and D. C. Rees, *ChemMedChem*, 2008, **3**, 1179–1180.
- 90 N. Palmer, T. M. Peakman, D. Norton and D. C. Rees, *Org. Biomol. Chem.*, 2016, **14**, 1599–1610.
- 91 E. H. Demont, C. Chung, R. C. Furze, P. Grandi, A.-M. Michon, C. Wellaway, N. Barrett, A. M. Bridges, P. D. Craggs, H. Diallo, D. P. Dixon, C. Douault, A. J. Emmons, E. J. Jones, B. V Karamshi, K. Locke, D. J. Mitchell, B. H. Mouzon, R. K. Prinjha, A. D. Roberts, R. J. Sheppard, R. J. Watson and P. Bamborough, *J. Med. Chem.*, 2015, **58**, 5649–5673.
- 92 P. Cohen, *Nat. Rev. Drug Discov.*, 2002, **1**, 309.
- 93 M. Carmena and W. C. Earnshaw, *Nat. Rev. Mol. Cell Biol.*, 2003, **4**, 842.
- 94 J. M. Foran, F. Ravandi, S. M. O'Brien, G. Borthakur, M. Rios, P. Boone, J. Worrell, K. H. Mallett, M. Squires, L. H. Fazal and H. M. Kantarjian, *J. Clin. Oncol.*, 2008, **26**, 2518.
- 95 J. A. Apud and D. R. Weinberger, *CNS Drugs*, 2007, **21**, 535–557.
- 96 M. Lanier, G. Ambrus, D. C. Cole, R. Davenport, J. Ellery, R. Fosbeary, A. J. Jennings, A. Kadotani, Y. Kamada, R. Kamran, S.-I. Matsumoto, A. Mizukami, S. Okubo, K. Okada, K. Saikatendu, L. Walsh, H. Wu and M. S. Hixon, *J. Med. Chem.*, 2014, **57**, 5459–5463.
- 97 A.-M. C. Yvon, P. Wadsworth, M. A. Jordan and M. W. Kirschner, *Mol. Biol. Cell*, 1999, **10**, 947–959.
- 98 W. Margolin, *Nat. Rev. Mol. Cell Biol.*, 2005, **6**, 862.
- 99 K. A. Hurley, T. M. A. Santos, G. M. Nepomuceno, V. Huynh, J. T. Shaw and D. B. Weibel, *J. Med. Chem.*, 2016, **59**, 6975–6998.
- 100 Y. Ohashi, Y. Chijiwa, K. Suzuki, K. Takahashi, H. Nanamiya, T. Sato, Y. Hosoya, K. Ochi and F. Kawamura, *J. Bacteriol.*, 1999, **181**, 1348–1351.

- 101 N. R. Stokes, N. Baker, J. M. Bennett, J. Berry, I. Collins, L. G. Czaplewski, A. Logan, R. Macdonald, L. MacLeod, H. Peasley, J. P. Mitchell, N. Nayal, A. Yadav, A. Srivastava and D. J. Haydon, *Antimicrob. Agents Chemother.*, 2013, **57**, 317–325.
- 102 C. M. Tan, A. G. Therien, J. Lu, S. H. Lee, A. Caron, C. J. Gill, C. Lebeau-Jacob, L. Benton-Perdomo, J. M. Monteiro, P. M. Pereira, N. L. Elsen, J. Wu, K. Deschamps, M. Petcu, S. Wong, E. Daigneault, S. Kramer, L. Liang, E. Maxwell, D. Claveau, J. Vaillancourt, K. Skorey, J. Tam, H. Wang, T. C. Meredith, S. Sillaots, L. Wang-Jarantow, Y. Ramtohul, E. Langlois, F. Landry, J. C. Reid, G. Parthasarathy, S. Sharma, A. Baryshnikova, K. J. Lumb, M. G. Pinho, S. M. Soisson and T. Roemer, *Sci. Transl. Med.*, 2012, **4**, 126ra35--126ra35.
- 103 W. Jahnke, D. A. Erlanson, I. J. P. De Esch, C. N. Johnson, P. N. Mortenson, Y. Ochi and T. Urushima, *J. Med. Chem.*, 2020, **63**, 15494–15507.
- 104 A. F. Trindade, E. L. Faulkner, A. G. Leach, A. Nelson and S. P. Marsden, *Chem. Commun.*, 2020, **56**, 8802–8805.
- 105 D. Francis, A. Nelson and S. P. Marsden, *Chem. - A Eur. J.*, 2020, **26**, 14861–14865.
- 106 I. Colomer, C. J. Empson, P. Craven, Z. Owen, R. G. Doveston, I. Churcher, S. P. Marsden and A. Nelson, *Chem. Commun.*, 2016, **52**, 7209–7212.
- 107 A. M. Edwards, *Nat. Chem. Biol.*, 2011, **470**, 163–165.
- 108 D. G. Brown and J. Boström, *J. Med. Chem.*, 2016, **59**, 4443–4458.
- 109 A. W. Dombrowski, N. J. Gesmundo, A. L. Aguirre, K. A. Sarris, J. M. Young, A. R. Bogdan, M. C. Martin, S. Gedeon and Y. Wang, *ACS Med. Chem. Lett.*, 2020, **11**, 597–604.
- 110 M. H. Shaw, V. W. Shurtleff, J. A. Terrett, J. D. Cuthbertson and D. W. C. MacMillan, *Science (80-.)*, 2016, **352**, 1304–1308.
- 111 Z. Zuo, D. T. Ahneman, L. Chu, J. A. Terrett, A. G. Doyle and D. W. C. MacMillan, *Science (80-.)*, 2014, **345**, 437–440.
- 112 Chemicals Listed in Chemical Weapons Convention, <https://www.opcw.org>.
- 113 W. Chen, L. Ma, A. Paul and D. Seidel, *Nat. Chem.*, 2017, **10**, 165–169.
- 114 J. Dong, Q. Xia, X. Lv, C. Yan, H. Song, Y. Liu and Q. Wang, *Org. Lett.*, 2018, **20**, 5661–5665.
- 115 R. Grainger, T. D. Heightman, S. V. Ley, F. Lima and C. N. Johnson, *Chem. Sci.*, 2019, **10**, 2264–2271.
- 116 C. Bosset, H. Beucher, G. Bretel, E. Pasquier, L. Queguiner, C. Henry, A. Vos, J. P. Edwards, L. Meerpoel and D. Berthelot, *Org. Lett.*, 2018, **20**, 6003–6006.
- 117 A. Gomm, *Construction and identification of anti-trypanosomal hit compounds via a cross-dehydrogenative Minisci reaction*, 2020.
- 118 C. P. Johnston, R. T. Smith, S. Allmendinger and D. W. C. MacMillan, *Nature*, 2016, **536**, 322–325.

- 119 X. Zhang and D. W. C. MacMillan, *J. Am. Chem. Soc.*, 2017, **139**, 11353–11356.
- 120 J. A. Terrett, J. D. Cuthbertson, V. W. Shurtleff and D. W. C. MacMillan, *Nature*, 2015, **524**, 330–334.
- 121 O. Mitsunobu, *Synthesis (Stuttg.)*, 1981, **1**, 1–28.
- 122 T. D. Quach and R. A. Batey, *Org. Lett.*, 2003, **5**, 1381–1384.
- 123 J. C. Sheehan and R. W. Tulis, *J. Org. Chem.*, 1974, **39**, 2264–2267.
- 124 R. R. Dieter, R. K. ; Sharma, 1996, **3263**, 4180–4184.
- 125 D. F. Oliveira, P. C. M. L. Miranda and C. R. D. Correia, *J. Org. Chem.*, 1999, **64**, 6646–6652.
- 126 J. Yu, V. Truc, P. Riebel, E. Hierl and B. Mudryk, *Org. Synth. Database Online*, 2008, **85**, 64–71.
- 127 N. Holmberg-Douglas, Y. Choi, B. Aquila, H. Huynh and D. A. Nicewicz, *ACS Catal.*, 2021, **11**, 3153–3158.
- 128 P. Spieß, M. Berger, D. Kaiser and N. Maulide, *J. Am. Chem. Soc.*, 2021, **143**, 10524–10529.
- 129 K. Feng, R. E. Quevedo, J. T. Kohrt, M. S. Oderinde, U. Reilly and M. C. White, *Nature*, 2020, **580**, 621–627.
- 130 J. Cossy, M. Cases and D. G. Pardo, *Tetrahedron*, 1999, **55**, 6153–6166.
- 131 M. Yan, Y. Kawamata and P. S. Baran, *Chem. Rev.*, 2017, **117**, 13230–13319.
- 132 L. Eberson and K. Nyberg, *Tetrahedron*, 1976, **32**, 2185–2206.
- 133 L. Eberson, *J. Mol. Catal.*, 1983, **20**, 27–52.
- 134 T. Shono, H. Hamaguchi and Y. Matsumura, *J. Am. Chem. Soc.*, 1975, **97**, 4264–4268.
- 135 A. M. Jones and C. E. Banks, *Beilstein J. Org. Chem.*, 2014, **10**, 3056–3072.
- 136 T. Shono, Y. Matsumura and K. Tsubata, *J. Am. Chem. Soc.*, 1981, **103**, 1172–1176.
- 137 R. Nyberg, K. ; Servin, *Acta Chem. Scand.*, 1976, **30**, 640–642.
- 138 S. D. Ross, M. Finkelstein and R. C. Petersen, *J. Am. Chem. Soc.*, 1966, **88**, 4657–4660.
- 139 S. S. Libendi, Y. Demizu, Y. Matsumura and O. Onomura, *Tetrahedron*, 2008, **64**, 3935–3942.
- 140 P. D. Palasz, J. H. P. Utley and J. D. Hardstone, *J. Chem. Soc. Perkin Trans. 2*, 1984, **4**, 807–813.
- 141 T. Shono, *Tetrahedron*, 1984, **40**, 811–850.
- 142 P. Alfonso-Suárez, A. V Kolliopoulos, J. P. Smith, C. E. Banks and A. M. Jones, *Tetrahedron Lett.*, 2015, **56**, 6863–6867.
- 143 M. A. Kabeshov, B. Musio, P. R. D. Murray, D. L. Browne and S. V Ley, *Org. Lett.*, 2014, **16**, 4618–4621.
- 144 C. G. Zoski, *Handbook of Electrochemistry*, Elsevier Science, 1st edn., 2007.
- 145 T. Bach and H. Brummerhop, *J. Prakt. Chemie*, 1999, **341**, 312–315.
- 146 T. Shono, Y. Matsumura, K. Tsubata, K. Uchida, T. Kanazawa and K.

- Tsuda, *J. Org. Chem.*, 1984, **49**, 3711–3716.
- 147 J. B. McManus, N. P. R. Onuska, M. S. Jeffreys, N. C. Goodwin and D. A. Nicewicz, *Org. Lett.*, 2020, **22**, 679–683.
- 148 R. D. Taylor, M. MacCoss and A. D. G. Lawson, *J. Med. Chem.*, 2014, **57**, 5845–5859.
- 149 M. Aldeghe, S. Malhotra, D. L. Selwood and A. W. E. Chan, *Chem. Biol. Drug Des.*, 2014, **83**, 450–461.
- 150 T. Shono, Y. Matsumura, O. Onomura, M. Ogaki and T. Kanazawa, *J. Org. Chem.*, 1987, **52**, 536–541.
- 151 Y. Zhao and D. G. Truhlar, *Theor. Chem. Acc.*, 2008, **120**, 215–241.
- 152 Y. Zhao and D. G. Truhlar, *Acc. Chem. Res.*, 2008, **41**, 157–167.
- 153 P. C. Hariharan and J. A. Pople, *Theor. Chim. Acta*, 1973, **28**, 213–222.
- 154 J. Tomasi, B. Mennucci and R. Cammi, *Chem. Rev.*, 2005, **105**, 2999–3094.
- 155 M. J. Frisch, G. W. Trucks, H. B. Schlegel, G. E. Scuseria, M. a. Robb, J. R. Cheeseman, G. Scalmani, V. Barone, G. a. Petersson, H. Nakatsuji, X. Li, M. Caricato, a. V. Marenich, J. Bloino, B. G. Janesko, R. Gomperts, B. Mennucci, H. P. Hratchian, J. V. Ortiz, a. F. Izmaylov, J. L. Sonnenberg, Williams, F. Ding, F. Lipparini, F. Egidi, J. Goings, B. Peng, A. Petrone, T. Henderson, D. Ranasinghe, V. G. Zakrzewski, J. Gao, N. Rega, G. Zheng, W. Liang, M. Hada, M. Ehara, K. Toyota, R. Fukuda, J. Hasegawa, M. Ishida, T. Nakajima, Y. Honda, O. Kitao, H. Nakai, T. Vreven, K. Throssell, J. a. Montgomery Jr., J. E. Peralta, F. Ogliaro, M. J. Bearpark, J. J. Heyd, E. N. Brothers, K. N. Kudin, V. N. Staroverov, T. a. Keith, R. Kobayashi, J. Normand, K. Raghavachari, a. P. Rendell, J. C. Burant, S. S. Iyengar, J. Tomasi, M. Cossi, J. M. Millam, M. Klene, C. Adamo, R. Cammi, J. W. Ochterski, R. L. Martin, K. Morokuma, O. Farkas, J. B. Foresman and D. J. Fox, 2016, Gaussian 16, Revision C.01, Gaussian, Inc., Wallin.
- 156 I. Funes-Ardoiz and R. S. Paton, GoodVibes: version 2.0.3.
- 157 Accessible at fragalysis.diamond.ac.uk.
- 158 H. G. Thomas and A. Schmitz, *Synth. Commun.*, 1985, **19**, 31–33.
- 159 N. Farriol-Mathis, J. S. Garavelli, B. Boeckmann, S. Duvaud, E. Gasteiger, A. Gateau, A. L. Veuthey and A. Bairoch, *Proteomics*, 2004, **4**, 1537–1550.
- 160 P. Cohen, *Nat. Cell Biol.*, 2002, **4**, 127–130.
- 161 A. G. Manning, D. B. Whyte, R. Martinez, T. Hunter and S. Sudarsanam, *Science (80-.)*, 2011, **298**, 1912–1916.
- 162 A. Bononi, C. Agnoletto, E. De Marchi, S. Marchi, S. Patergnani, M. Bonora, C. Giorgi, S. Missiroli, F. Poletti, A. Rimessi and P. Pinton, *Enzyme Res.*, 2011, **1**, 1–26.
- 163 B. Nolen, S. Taylor and G. Ghosh, *Mol. Cell*, 2004, **15**, 661–675.
- 164 L. N. Johnson, M. E. M. Noble and D. J. Owen, *Cell*, 1996, **85**, 149–158.
- 165 M. Huse and J. Kuriyan, *Cell*, 2002, **109**, 275–282.

- 166 D. R. Knighton, J. Zheng, L. F. T. E. N. Eyck, V. A. Ashford, N. Xuong, S. S. Taylor and J. M. Sowadski, *Science (80-.)*, 1991, **253**, 407–414.
- 167 T. Schindler, W. Bornmann, P. Pellicena, W. T. Miller, B. Clarkson, J. Kuriyan, T. Schindler, W. Bornmann, P. Pellicena, W. T. Miller, B. Clarkson and J. Kuriyan, 2017, **289**, 1938–1942.
- 168 R. Bayliss, A. Fry, T. Haq and S. Yeoh, *Open Biol.* 2, 2012, **2**, 1–20.
- 169 A. P. Kornev, N. M. Haste, S. S. Taylor and L. F. Ten Eyck, *Proc. Natl. Acad. Sci. U. S. A.*, 2006, **103**, 17783–17788.
- 170 E. A. Nigg, *Nat. Rev. Mol. Cell Biol.*, 2001, **2**, 21–32.
- 171 L. Trinkle-Mulcahy and A. I. Lamond, *Curr. Opin. Cell Biol.*, 2006, **18**, 623–631.
- 172 L. S. Penna, J. A. P. Henriques and D. Bonatto, *Pharmacol. Ther.*, 2017, **173**, 67–82.
- 173 R. J. Van Vuuren, M. H. Visagie, A. E. Theron and A. M. Joubert, *Cancer Chemother. Pharmacol.*, 2015, **76**, 1101–1112.
- 174 D. M. Glover, M. H. Leibowitz, D. A. McLean and H. Parry, *Cell*, 1995, **81**, 95–105.
- 175 J. R. Bischoff, L. Anderson, Y. Zhu, K. Mossie, L. Ng, B. Souza, B. Schryver, P. Flanagan, F. Clairvoyant, C. Ginther, C. S. M. Chan, M. Novotny, D. J. Slamon and G. D. Plowman, *EMBO J.*, 1998, **17**, 3052–3065.
- 176 R. Giet and C. Prigent, *J. Cell Sci.*, 1999, **112**, 3591–3601.
- 177 J. Fu, M. Bian, Q. Jiang and C. Zhang, *Mol. Cancer Res.*, 2007, **5**, 1–10.
- 178 R. Bayliss, T. Sardon, I. Vernos and E. Conti, *Mol. Cell*, 2003, **12**, 851–862.
- 179 and T. K. K. Dhanasekaran Karthigeyan, Sallekoppal B. Benaka Prasad, Jayasha Shandilya, Shipra Agrawal, *Med. Res. Rev.*, 2011, **31**, 757–793.
- 180 G. Vader and S. M. A. Lens, *Biochim. Biophys. Acta*, 2008, **1786**, 60–72.
- 181 A. Yan, L. Wang, S. Xu and J. Xu, *Drug Discov. Today*, 2011, **16**, 260–269.
- 182 J. R. Brown, K. K. Koretke, M. L. Birkeland, P. Sanseau and D. R. Patrick, *BMC Evol. Biol.*, 2004, **4**, 1–10.
- 183 J. A. C. M. Goos, V. M. H. Coupe, B. Diosdado, P. M. Delis-Van Diemen, C. Karga, J. A. M. Beliën, B. Carvalho, M. P. Van Den Tol, H. M. W. Verheul, A. A. Geldof, G. A. Meijer, O. S. Hoekstra, R. J. A. Fijneman, N. C. T. Van Grieken, L. R. Perk, E. A. Te Velde, A. D. Windhorst, J. Baas, A. M. Rijken, M. W. Van Beek, H. J. Pijpers, H. Bril, H. B. A. C. Stockmann, A. Zwijnenburg, K. Bosscha, A. J. Van Den Brule, C. J. Hoekstra, J. C. Van Der Linden, I. H. Borel Rinkes, P. J. Van Diest, R. Van Hillegersberg, O. Kranenburg, M. G. Lam, N. Snoeren, I. H. Liem, R. M. Roumen and W. Vening, *Br. J. Cancer*, 2013, **109**, 2445–2452.
- 184 W. Siggelkow, D. Boehm, S. Gebhard, M. Battista, I. Sicking, A.

- Lebrecht, C. Solbach, B. Hellwig, J. Rahnenführer, H. Koelbl, M. Gehrman, R. Marchan, C. Cadenas, J. G. Hengstler and M. Schmidt, *BMC Cancer*, 2012, **12**, 1–11.
- 185 M. Lo Iacono, V. Monica, S. Saviozzi, P. Ceppi, E. Bracco, M. Papotti and G. V. Scagliotti, *J. Transl. Med.*, 2011, **9**, 1–6.
- 186 J. Den Hollander, S. Rimpi, J. R. Doherty, M. Rudelius, A. Buck, A. Hoellein, M. Kremer, N. Graf, M. Scheerer, M. A. Hall, A. Goga, N. Von Bubnoff, J. Duyster, C. Peschel, J. L. Cleveland, J. A. Nilsson and U. Keller, *Blood*, 2010, **116**, 1498–1505.
- 187 J. Zhu, J. L. Abbruzzese, J. Izzo, W. N. Hittelman and D. Li, *Cancer Genet. Cytogenet.*, 2005, **159**, 10–17.
- 188 P. Meraldi, R. Honda and E. A. Nigg, *EMBO J.*, 2002, **21**, 483–492.
- 189 Q. Liu, S. Kaneko, L. Yang, R. I. Feldman, S. V. Nicosia, J. Chen and J. Q. Cheng, *J. Biol. Chem.*, 2004, **279**, 52175–52182.
- 190 D. Zhang, T. Hirota, T. Marumoto, M. Shimizu, N. Kunitoku, T. Sasayama, Y. Arima, L. Feng, M. Suzuki, M. Takeya and H. Saya, *Oncogene*, 2004, **23**, 8720–8730.
- 191 M. Tatsuka, S. Sato, S. Kitajima, S. Suto, H. Kawai, M. Miyauchi, I. Ogawa, M. Maeda, T. Ota and T. Takata, *Oncogene*, 2005, **24**, 1122–1127.
- 192 Z. Z. Lin, Y. M. Jeng, F. C. Hu, H. W. Pan, H. W. Tsao, P. L. Lai, P. H. Lee, A. L. Cheng and H. C. Hsu, *BMC Cancer*, 2010, **10**, 1–14.
- 193 P. Yaish, A. Gazit, C. Gilon and A. Levitzki, *Science (80-.)*, 1988, **242**, 933–935.
- 194 R. S. K. Vijayan, P. He, V. Modi, K. C. Duong-Ly, H. Ma, J. R. Peterson, R. L. Dunbrack and R. M. Levy, *J. Med. Chem.*, 2015, **58**, 466–479.
- 195 D. J. M. Ratika Krishnamurty, *ACS Chem. Biol.*, 2010, **5**, 121–138.
- 196 V. Bavetsias and S. Linardopoulos, *Front. Oncol.*, 2015, **5**, 1–10.
- 197 D. Fancelli, J. Moll, M. Varasi, R. Bravo, R. Artico, D. Berta, S. Bindi, A. Cameron, I. Candiani, P. Cappella, P. Carpinelli, W. Croci, B. Forte, M. L. Giorgini, J. Klapwijk, A. Marsiglio, E. Pesenti, M. Rocchetti, F. Roletto, D. Severino, C. Soncini, P. Storici, R. Tonani, P. Zugnoni and P. Vianello, *J. Med. Chem.*, 2006, **49**, 7247–7251.
- 198 M. Payton, T. L. Bush, G. Chung, B. Ziegler, P. Eden, P. McElroy, S. Ross, V. J. Cee, H. L. Deak, B. L. Hodous, H. N. Nguyen, P. R. Olivieri, K. Romero, L. B. Schenkel, A. Bak, M. Stanton, I. Dussault, V. F. Patel, S. Geuns-Meyer, R. Radinsky and R. L. Kendall, *Cancer Res.*, 2010, **70**, 9846–9854.
- 199 B. Zhao, A. Smallwood, J. Yang, K. Koretke, K. Nurse, A. Calamari, R. B. Kirkpatrick and Z. Lai, *Protein Sci.*, 2008, **17**, 1791–1797.
- 200 P. Carpinelli, R. Ceruti, M. L. Giorgini, P. Cappella, L. Gianellini, V. Croci, A. Degrassi, G. Texido, M. Rocchetti, P. Vianello, L. Rusconi, P. Storici, P. Zugnoni, C. Arrigoni, C. Soncini, C. Alli, V. Patton, A. Marsiglio, D. Ballinari, E. Pesenti, D. Fancelli and J. Moll, *Mol. Cancer Ther.*, 2007, **6**, 3158–3168.

- 201 G. Borthakur, H. Dombret, P. Schafhausen, T. H. Brummendorf, N. Boisse, E. Jabbour, M. Mariani, L. Capolongo, P. Carpinelli, C. Davite, H. Kantarjian and J. E. Cortes, *Haematologica*, 2015, **100**, 898–904.
- 202 S. Geuns-Meyer, V. J. Cee, H. L. Deak, B. Du, B. L. Hodous, H. N. Nguyen, P. R. Olivieri, L. B. Schenkel, K. R. Vaida, P. Andrews, A. Bak, X. Be, P. J. Beltran, T. L. Bush, M. K. Chaves, G. Chung, Y. Dai, P. Eden, K. Hanestad, L. Huang, M. H. J. Lin, J. Tang, B. Ziegler, R. Radinsky, R. Kendall, V. F. Patel and M. Payton, *J. Med. Chem.*, 2015, **58**, 5189–5207.
- 203 T. L. Bush, M. Payton, S. Heller, G. Chung, K. Hanestad, J. B. Rottman, R. Loberg, G. Friberg, R. L. Kendall, D. Saffran and R. Radinsky, *Mol. Cancer Ther.*, 2013, **12**, 2356–2366.
- 204 J. S. Nair and G. K. Schwartz, *Oncotarget*, 2016, **7**, 12893–12903.
- 205 M. G. Manfredi, J. A. Ecsedy, A. Chakravarty, L. Silverman, M. Zhang, K. M. Hoar, S. G. Stroud, W. Chen, V. Shinde, J. J. Huck, D. R. Wysong, D. A. Janowick, M. L. Hyer, P. J. LeRoy, R. E. Gershman, M. D. Silva, M. S. Germanos, J. B. Bolen, C. F. Claiborne and T. B. Sells, *Clin. Cancer Res.*, 2011, **17**, 7614–7624.
- 206 T. B. Sells, R. Chau, J. A. Ecsedy, R. E. Gershman, K. Hoar, J. Huck, D. A. Janowick, V. J. Kadambi, P. J. Leroy, M. Stirling, S. G. Stroud, T. J. Vos, G. S. Weatherhead, D. R. Wysong, M. Zhang, S. K. Balani, J. B. Bolen, M. G. Manfredi and C. F. Claiborne, *ACS Med. Chem. Lett.*, 2015, **6**, 630–634.
- 207 D. Martin, S. Fallaha, M. Proctor, A. Stevenson, L. Perrin, N. McMillan and B. Gabrielli, *Mol. Cancer Ther.*, 2017, **16**, 1934–1941.
- 208 R. Tanaka, M. S. Squires, S. Kimura, A. Yokota, R. Nagao, T. Yamauchi, M. Takeuchi, H. Yao, M. Reule, T. Smyth, J. F. Lyons, N. T. Thompson, E. Ashihara, O. G. Ottmann and T. Maekawa, *Blood*, 2010, **116**, 2089–2095.
- 209 J. P. Jani, J. Arcari, V. Bernardo, S. K. Bhattacharya, D. Briere, B. D. Cohen, K. Coleman, J. G. Christensen, E. O. Emerson, A. Jakowski, K. Hook, G. Los, J. D. Moyer, I. Prumboom-Brees, L. Pustilnik, A. M. Rossi, S. J. Steyn, C. Su, K. Tsaparikos, D. Wishka, K. Yoon and J. L. Jakubczak, *Mol. Cancer Ther.*, 2010, **9**, 883–894.
- 210 P. Schöffski, S. F. Jones, H. Dumez, J. R. Infante, E. Van Mieghem, C. Fowst, P. Gerletti, H. Xu, J. L. Jakubczak, P. A. English, K. J. Pierce and H. A. Burris, *Eur. J. Cancer*, 2011, **47**, 2256–2264.
- 211 T. Force and K. L. Kolaja, *Nat. Rev. Drug Discov.*, 2011, **10**, 111–126.
- 212 A. Chowdhury, S. Chowdhury and M. Y. Tsai, *Leuk. Lymphoma*, 2012, **53**, 462–471.
- 213 T. Shimomura, S. Hasako, Y. Nakatsuru, T. Mita, K. Ichikawa, T. Kadera, T. Sakai, T. Nambu, M. Miyamoto, I. Takahashi, S. Miki, N. Kawanishi, M. Ohkubo, H. Kotani and Y. Iwasawa, *Mol. Cancer Ther.*, 2010, **9**, 157–166.
- 214 I. Aliagas-Martin, D. Burdick, L. Corson, J. Dotson, J. Drummond, C. Fields, O. W. Huang, T. Hunsaker, T. Kleinheinz, E. Krueger, J. Liang,

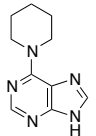
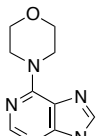
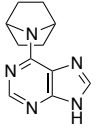
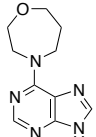
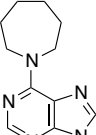
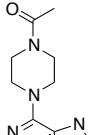
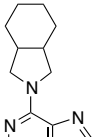
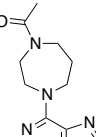
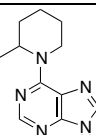
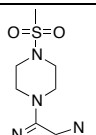
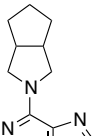
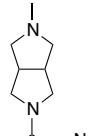
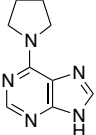
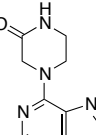
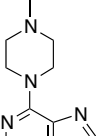
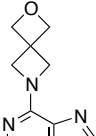
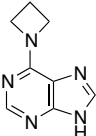
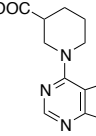
- J. Moffat, G. Phillips, R. Pulk, T. E. Rawson, M. Ultsch, L. Walker, C. Wiesmann, B. Zhang, B. Y. Zhu and A. G. Cochran, *J. Med. Chem.*, 2009, **52**, 3300–3307.
- 215 R. Ando, H. Ikegami, M. Sakiyama, S. Ooike, M. Hayashi, Y. Fujino, D. Abe, H. Nakamura, T. Mishina, H. Kato, Y. Iwase, H. Tomozane and M. Morioka, *Bioorganic Med. Chem. Lett.*, 2010, **20**, 4709–4711.
- 216 R. MacArron, M. N. Banks, D. Bojanic, D. J. Burns, D. A. Cirovic, T. Garyantes, D. V. S. Green, R. P. Hertzberg, W. P. Janzen, J. W. Paslay, U. Schopfer and G. S. Sittampalam, *Nat. Rev. Drug Discov.*, 2011, **10**, 188–195.
- 217 T. A. Halgren, R. B. Murphy, R. A. Friesner, H. S. Beard, L. L. Frye, W. T. Pollard and J. L. Banks, *J. Med. Chem.*, 2004, **47**, 1750–1759.
- 218 version 3.2.04, *ROCS (Rapid Overlay Chem. Struct., Inc*, Santa Fe.
- 219 J. Voller, L. Zahajská, L. Plíhalová, J. Jeřábková, D. Burget, A. C. Pataki, V. Kryštof, M. Zatloukal, J. Brábek, D. Rösel, V. Mik, M. Tkáč, T. Pospíšil, T. Gucký, K. Doležal and M. Strnad, *Bioorg. Chem.*, 2019, **90**, 103005.
- 220 Y. N. Wang, R. R. Y. Bheemanaboina, G. X. Cai and C. H. Zhou, *Bioorganic Med. Chem. Lett.*, 2018, **28**, 1621–1628.
- 221 T. Asano, I. Ikegaki, S. Satoh, M. Seto and Y. Sasaki, *Cardiovasc. Drug Rev.*, 1998, **16**, 76–87.
- 222 C. E. Allen, J. J. Caldwell, I. Collins, C. L. Chow, I. M. Westwood and R. L. M. Van Montfort, *Bioorganic Med. Chem.*, 2013, **21**, 5707–5724.
- 223 I. Colomer, C. J. Empson, P. Craven, Z. Owen, R. G. Doveston, I. Churcher, S. P. Marsden and A. Nelson, *Chem. Commun.*, 2016, **52**, 7209–7212.
- 224 J. A. H. Lainton, M. C. Allen, M. Burton, S. Cameron, T. R. G. Edwards, G. Harden, R. Hogg, W. Leung, S. Miller, J. J. Morrish, S. M. Rooke and B. Wendt, *J. Comb. Chem.*, 2003, **5**, 400–407.
- 225 S. H. Grimm, B. Gagestein, J. F. Keijzer, N. Liu, R. H. Wijdeven, E. B. Lenselink, A. W. Tuin, A. M. C. H. van den Nieuwendijk, G. J. P. van Westen, C. A. A. van Boeckel, H. S. Overkleeft, J. Neefjes and M. van der Stelt, *Bioorg. Med. Chem.*, 2019, **27**, 692–699.
- 226 A. Card, C. Caldwell, H. Min, B. Lokchander, H. Xi, S. Sciabola, A. V. Kamath, S. L. Clugston, W. R. Tschantz, L. Wang and D. J. Moshinsky, *J. Biomol. Screen.*, 2008, **14**, 31–42.
- 227 D. Perrin, C. Frémaux and A. Scheer, *J. Biomol. Screen.*, 2006, **11**, 359–368.
- 228 C. Arter, *Improving Modulation of the Aurora-A / TPX2 Interaction by Fragment Elaboration*, 2018.
- 229 F. C. Rowan, M. Richards, R. A. Bibby, A. Thompson, R. Bayliss and J. Blagg, *ACS Chem. Biol.*, 2013, **8**, 2184–2191.
- 230 M. Malumbres and I. P. de Castro, *Expert Opin. Ther. Targets*, 2014, **18**, 1377–1393.
- 231 K. Azzaoui, J. Hamon, B. Faller, S. Whitebread, E. Jacoby, A. Bender, J. L. Jenkins and L. Urban, *ChemMedChem*, 2007, **2**, 874–880.

- 232 H. van de Waterbeemd, D. A. Smith, K. Beaumont and D. K. Walker, *J. Med. Chem.*, 2001, **44**, 1313–1333.
- 233 D. E. Scott, A. G. Coyne, S. A. Hudson and C. Abell, *Biochemistry*, 2012, **51**, 4990–5003.
- 234 A. M. D'Alise, G. Amabile, M. Iovino, F. P. Di Giorgio, M. Bartiromo, F. Sessa, F. Villa, A. Musacchio and R. Cortese, *Mol. Cancer Ther.*, 2008, **7**, 1140–1149.
- 235 Y. Hiruma, A. Koch, S. Dharadhar, R. P. Joosten and A. Perrakis, *Proteins Struct. Funct. Bioinforma.*, 2016, **84**, 1761–1766.
- 236 M. Jacobs, K. Hayakawa, L. Swenson, S. Bellon, M. Fleming, P. Taslimi and J. Doran, *J. Biol. Chem.*, 2006, **281**, 260–268.
- 237 A. F. Trindade, E. L. Faulkner, A. G. Leach, A. Nelson and S. P. Marsden, *Chem. Commun.*, 2020, **56**, 8802–8805.
- 238 M. Harty, M. Nagar, L. Atkinson, C. M. Legay, D. J. Derksen and S. L. Bearne, *Bioorganic Med. Chem. Lett.*, 2014, **24**, 390–393.
- 239 M. J. Mulvihill, J. L. Gage and M. J. Miller, *J. Org. Chem.*, 1997, **3263**, 3357–3363.
- 240 WO2015/25197, 2015, 16.
- 241 L. W. Xu and C. G. Xia, *Tetrahedron Lett.*, 2004, **45**, 4507–4510.
- 242 L.-W. Xu, L. Li, C.-G. Xia, S.-L. Zhou, J.-W. Li and X.-X. Hu, *Synlett*, 2003, **23**, 2337–2340.
- 243 P. K. T. Lo, G. A. Oliver and M. C. Willis, *J. Org. Chem.*, 2020, **85**, 5753–5760.
- 244 I. B. Perry, T. F. Brewer, P. J. Sarver, D. M. Schultz, D. A. DiRocco and D. W. C. MacMillan, *Nature*, 2018, **560**, 70–75.
- 245 P. Beak, A. Basu, D. J. Gallagher, Y. S. Park and S. Thayumanavan, *Acc. Chem. Res.*, 1996, **29**, 552–560.
- 246 H. Xiong, W. Fietze, D. W. Andisik, G. E. Ernst, W. E. Palmer, L. Hinkley, J. G. Varnes, J. S. Albert and C. A. Veale, *Tetrahedron Lett.*, 2010, **51**, 6741–6744.
- 247 S. Bhattacharyya, *Tetrahedron Lett.*, 1994, **35**, 2401–2404.
- 248 R. M. de Figueiredo, J.-S. Suppo and J.-M. Campagne, *Chem. Rev.*, 2016, **116**, 12029–12122.
- 249 P. F. Thomson, P. Lagisetty, J. Balzarini, E. De Clercq and M. K. Lakshman, *Adv. Synth. Catal.*, 2010, **352**, 1728–1735.
- 250 M. González-Esguevillas, J. Miró, J. L. Jeffrey and D. W. C. MacMillan, *Tetrahedron*, 2019, **75**, 4222–4227.
- 251 P. J. Sarver, N. B. Bissonnette and D. W. C. Macmillan, *J. Am. Chem. Soc.*, 2021, **143**, 9737–9743.
- 252 K. A. Scott and J. T. Njardarson, ed. X. Jiang, Springer International Publishing, Cham, 2019, pp. 1–34.
- 253 S. Müller, A. Chaikuad, N. S. Gray and S. Knapp, *Nat. Chem. Biol.*, 2015, **11**, 818–821.
- 254 G. Manning, D. B. Whyte, R. Martinez, T. Hunter and S. Sudarsanam, *Science (80-.)*, 2002, **298**, 1912–1934.
- 255 P. Traxler and P. Furet, *Pharmacol. Ther.*, 1999, **82**, 195–206.

- 256 M. A. Fabian, W. H. Biggs, D. K. Treiber, C. E. Atteridge, M. D. Azimioara, M. G. Benedetti, T. A. Carter, P. Ciceri, P. T. Edeen, M. Floyd, J. M. Ford, M. Galvin, J. L. Gerlach, R. M. Grotzfeld, S. Herrgard, D. E. Insko, M. A. Insko, A. G. Lai, J. M. Lélías, S. A. Mehta, Z. V. Milanov, A. M. Velasco, L. M. Wodicka, H. K. Patel, P. P. Zarrinkar and D. J. Lockhart, *Nat. Biotechnol.*, 2005, **23**, 329–336.
- 257 S. P. Davies, H. Reddy, M. Caivano and P. Cohen, *Biochem. J.*, 2000, **351**, 95–105.
- 258 O. Fedorov, B. Marsden, V. Pogacic, P. Rellos, S. Müller, A. N. Bullock, J. Schwaller, M. Sundström and S. Knapp, *Proc. Natl. Acad. Sci. U. S. A.*, 2007, **104**, 20523–20528.
- 259 G. Saxty, S. J. Woodhead, V. Berdini, T. G. Davies, M. L. Verdonk, P. G. Wyatt, R. G. Boyle, D. Barford, R. Downham, M. D. Garrett and R. A. Carr, *J. Med. Chem.*, 2007, **50**, 2293–2296.
- 260 M. Chang, W. Li, G. Hou and X. Zhang, *Adv. Synth. Catal.*, 2010, **352**, 3121–3125.
- 261 S. Yamashita, N. Kurono, H. Senboku, M. Tokuda and K. Orito, *European J. Org. Chem.*, 2009, **8**, 1173–1180.
- 262 A. Sumita, Y. Otani and T. Ohwada, *Chem. Commun.*, 2017, **53**, 1482–1485.
- 263 C. Granchi, M. Lapillo, S. Glasmacher, G. Bononi, C. Licari, G. Poli, M. El Boustani, I. Caligiuri, F. Rizzolio, J. Gertsch, M. Macchia, F. Minutolo, T. Tuccinardi and A. Chicca, *J. Med. Chem.*, 2019, **62**, 1932–1958.
- 264 D. O. Kiesewetter and W. C. Eckelman, *J. Label. Compd. Radiopharm.*, 2004, **47**, 953–969.
- 265 F. De Simone, T. Saget, F. Benfatti, S. Almeida and J. Waser, *Chem. – A Eur. J.*, 2011, **17**, 14527–14538.
- 266 T. Shono, Y. Matsumura, K. Tsubata, Y. Sugihara, S. Yamane, T. Kanazawa and T. Aoki, *J. Am. Chem. Soc.*, 1982, **104**, 6697–6703.
- 267 P. Chuentragool, M. Parasram, Y. Shi and V. Gevorgyan, *J. Am. Chem. Soc.*, 2018, **140**, 2465–2468.
- 268 J. Wegner, S. V Ley, A. Kirschning, A.-L. Hansen, J. Montenegro Garcia and I. R. Baxendale, *Org. Lett.*, 2012, **14**, 696–699.
- 269 S. Gastaldi, S. Escoubet, N. Vanthuynne, G. Gil and M. P. Bertrand, *Org. Lett.*, 2007, **9**, 837–839.
- 270 G. W. Kirby, H. Mcguigan, J. W. M. Mackinnon and D. Mclean, *J. Chem. Soc. Perkin Trans. 1*, 1985, **9**, 1437–1442.
- 271 D. M. Hodgson, A. J. Thompson, S. Wadman and C. J. Keats, *Tetrahedron*, 1999, **55**, 10815–10834.
- 272 US5889178, 1999, 45–50.
- 273 J. E. T. Corrie, G. W. Kirby and J. W. M. Mackinnon, *J. Chem. Soc. Perkin Trans. 1*, 1985, **1**, 883–886.
- 274 C. Cesario, L. P. Tardibono and M. J. Miller, *J. Org. Chem.*, 2009, **74**, 448–451.
- 275 US2005/54658, 2005, 20–30.

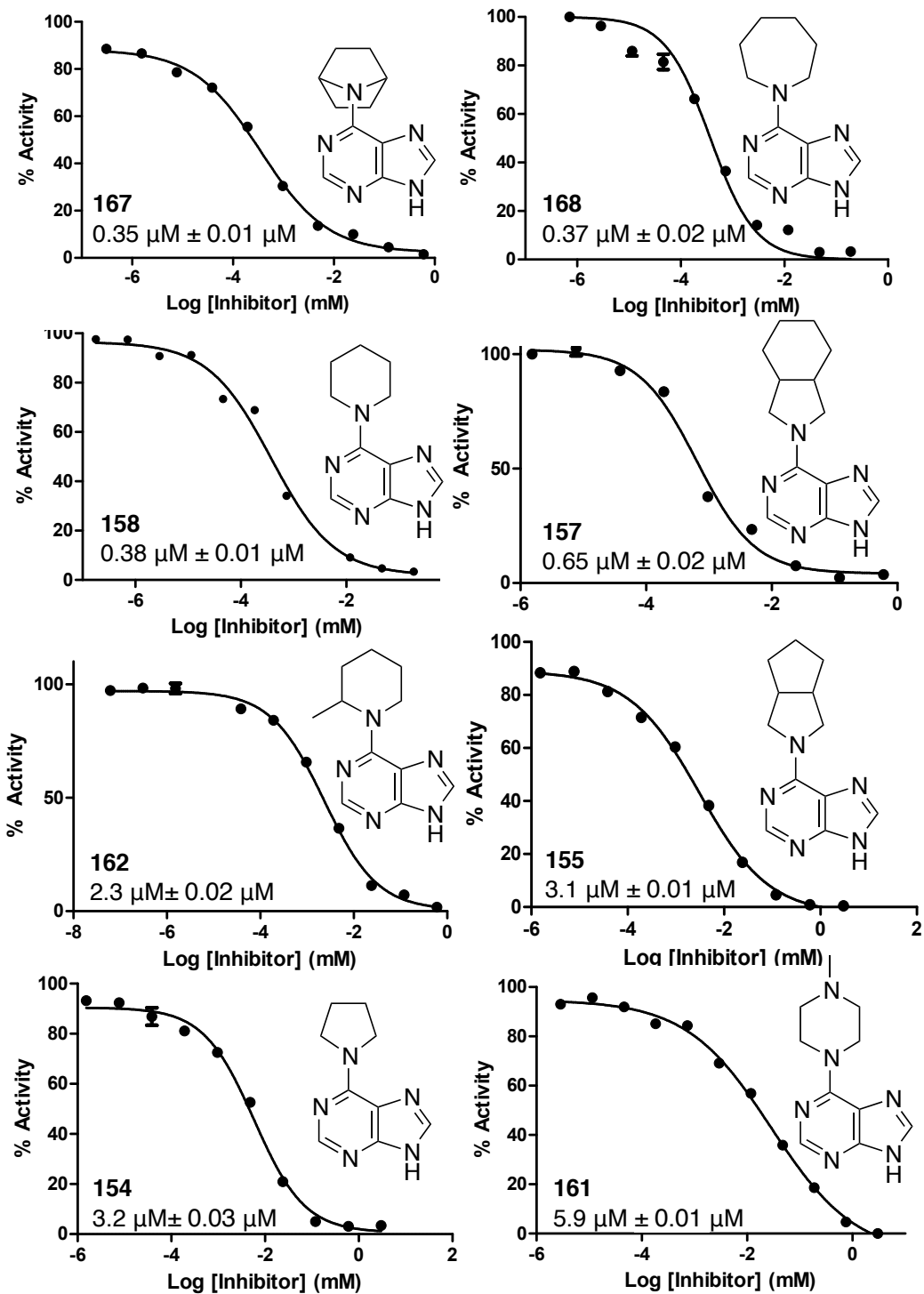
- 276 L. Čechová, P. Jansa, M. Šála, M. Dračínský, A. Holý and Z. Janeba, *Tetrahedron*, 2011, **67**, 866–871.
- 277 T. Itaya, H. Matsumoto and K. Ogawa, *Chem. Pharm. Bull.*, 1977, **57**, 364–370.
- 278 N. Singh, U. P. Singh, K. Nikhil, P. Roy and H. Singh, *J. Mol. Struct.*, 2017, **1146**, 703–712.
- 279 J. Kania and L. L. Gundersen, *European J. Org. Chem.*, 2013, **69**, 2008–2019.
- 280 R. Zhang, P. J. McIntyre, P. M. Collins, D. J. Foley, C. Arter, F. von Delft, R. Bayliss, S. Warriner and A. Nelson, *Chem. – A Eur. J.*, 2019, **25**, 6831–6839.

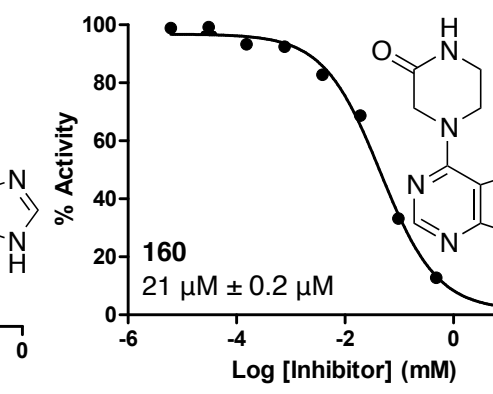
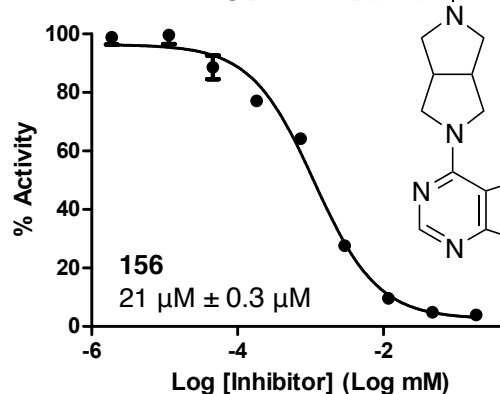
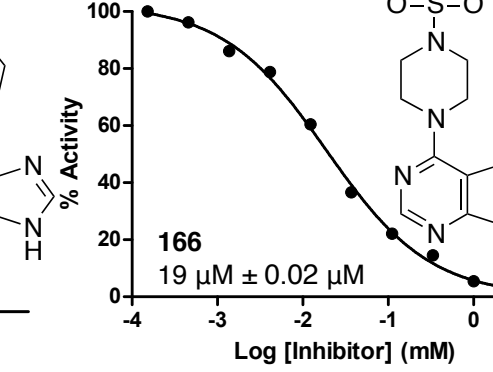
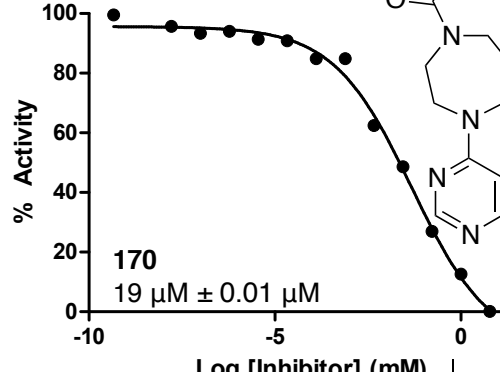
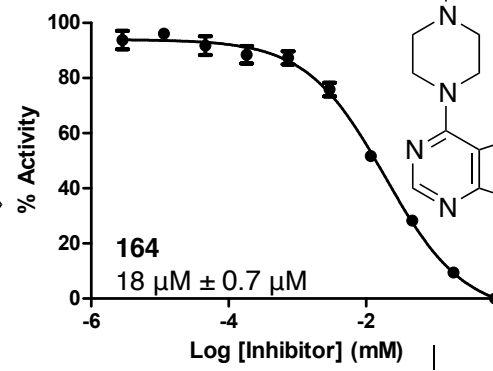
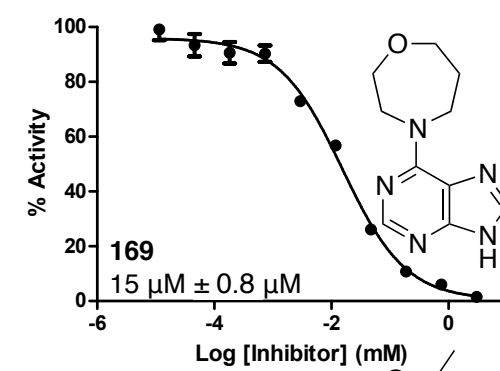
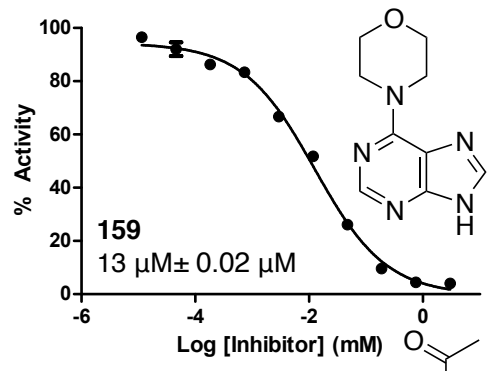
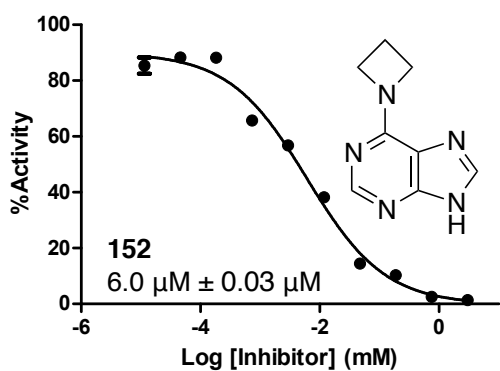
**Appendix 1: Synthesised Fragments and Their Potency
Against Aurora-A from Chapter 3**

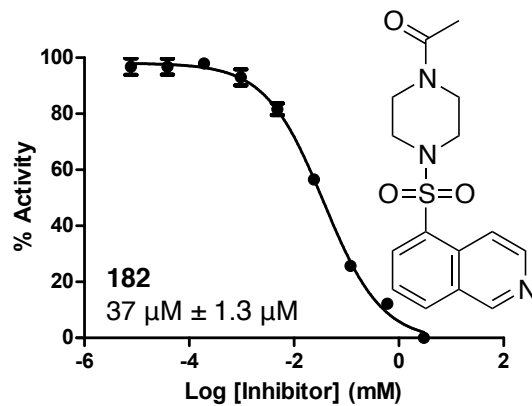
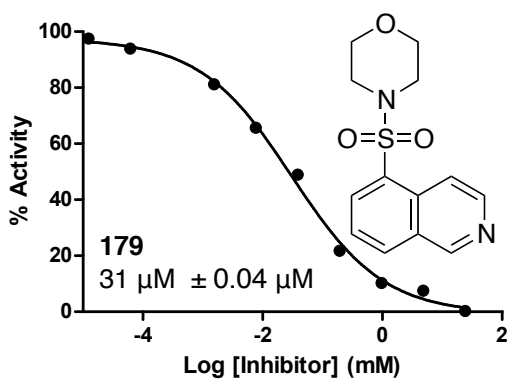
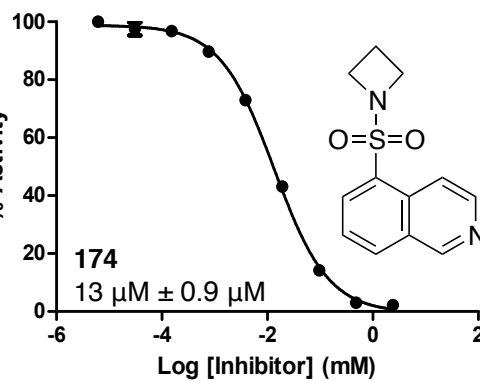
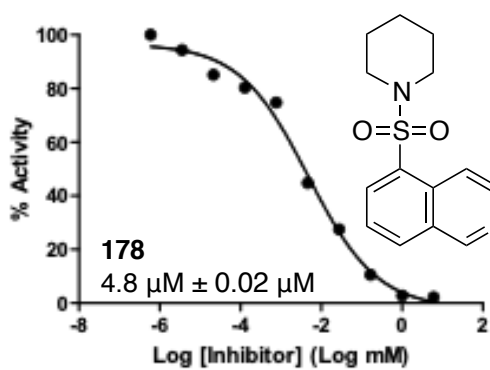
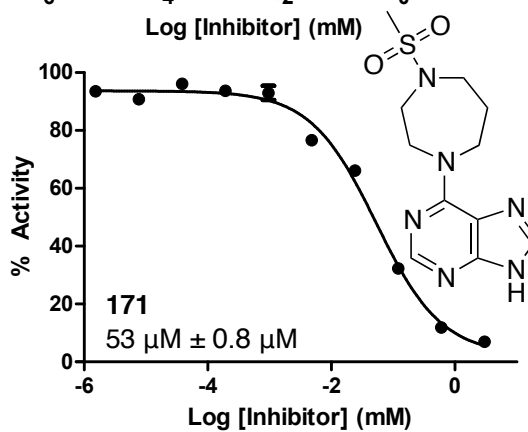
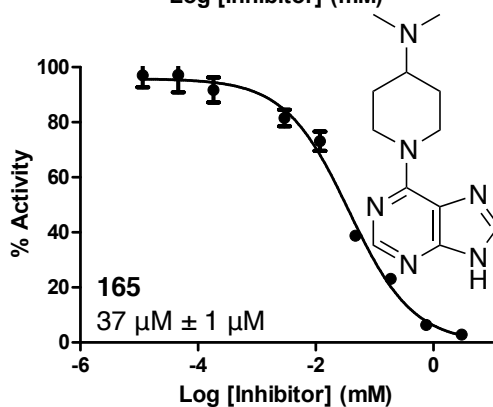
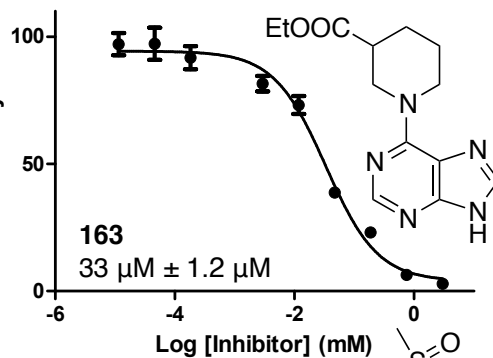
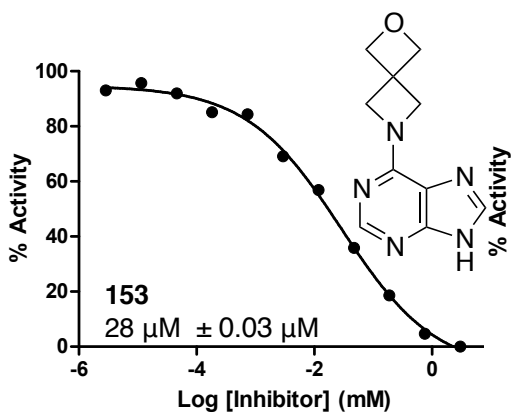
	Fragment	IC₅₀	pIC₅₀		Fragment	IC₅₀	pIC₅₀
158		370 nM	6.43	159		13 μM	4.9
167		350 nM	6.50	169		15 μM	4.8
168		367 nM	6.43	164		18.4 μM	4.74
157		650 nM	6.20	170		18.8 μM	4.73
162		2.3 μM	5.6	166		18.9 μM	4.72
155		3.1 μM	5.51	156		20.8 μM	4.68
154		3.20 μM	5.46	160		20.7 μM	4.68
161		5.86 μM	5.23	153		28.4 μM	4.5
152		6.0 μM	5.2	163		33.4 μM	4.48

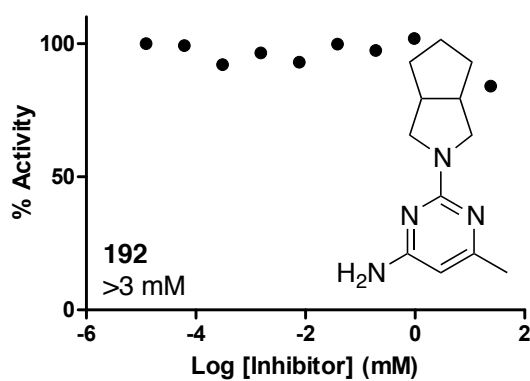
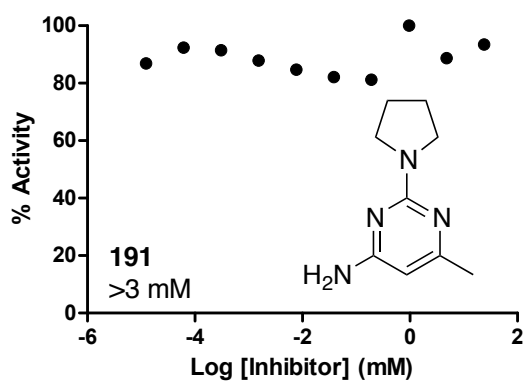
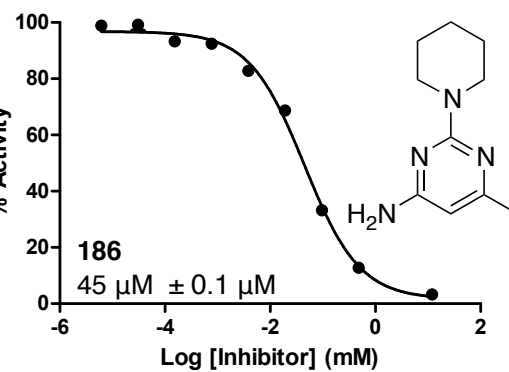
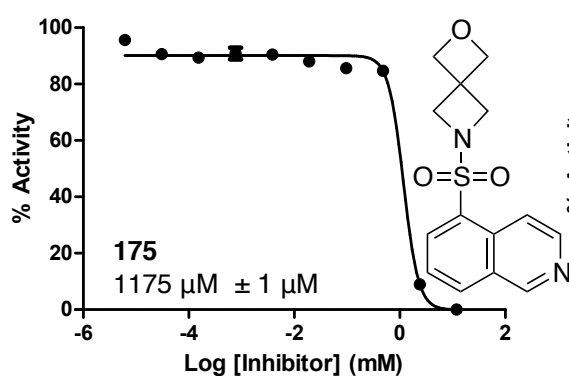
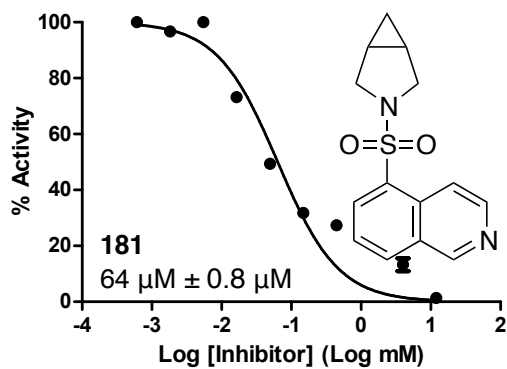
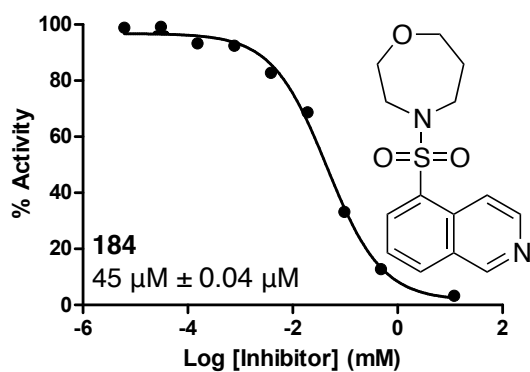
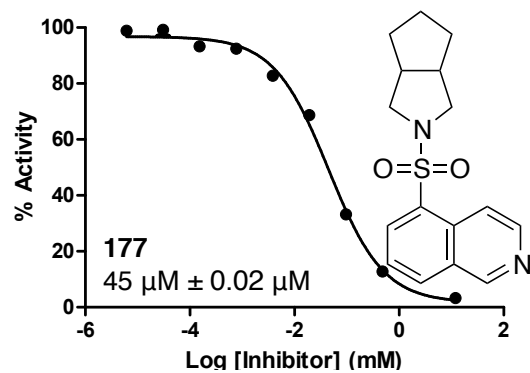
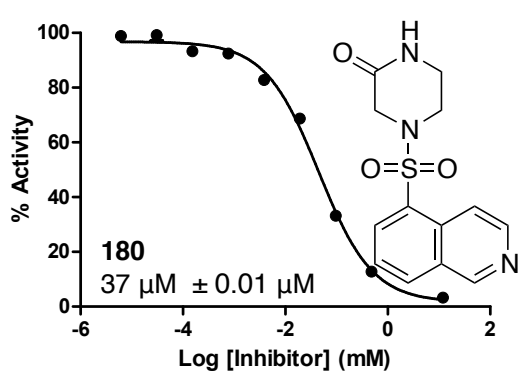
165		37 μM	4.4	184		44.9 μM	4.35
171		52.9 μM	4.28	181		63.7 μM	4.20
178		4.8 μM	5.32	175		1175 μM	2.94
174		13.4 μM	4.87	193		44.9 μM	4.35
179		30.6 μM	4.51	191		-	-
182		36.7 μM	4.43	192		-	-
180		36.8 μM	4.43	194		-	-
177		44.9 μM	4.35	195		-	-
				196		-	-

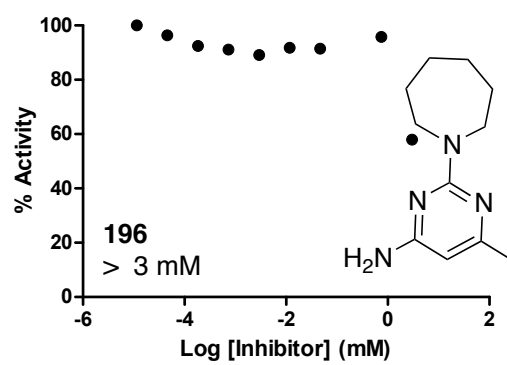
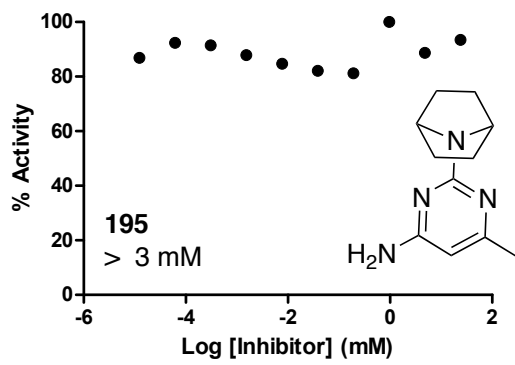
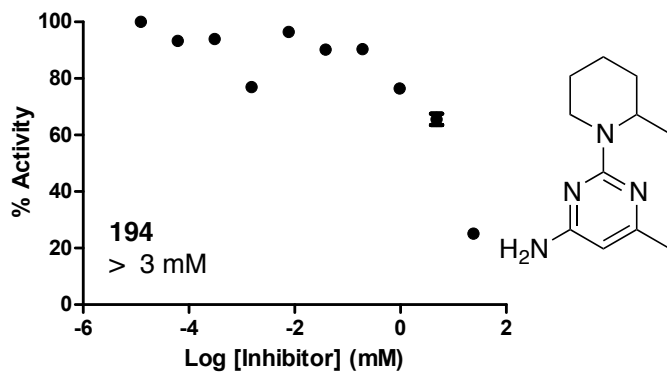
Appendix 2: IC₅₀ Curves of the Fragments Screened in Chapter 3



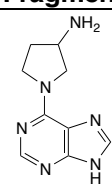
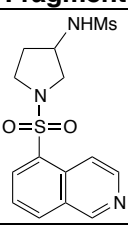
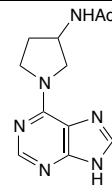
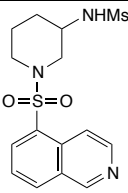
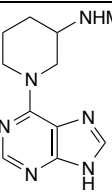
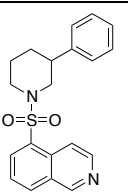
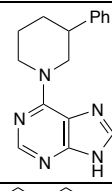
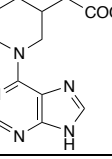
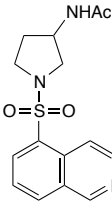




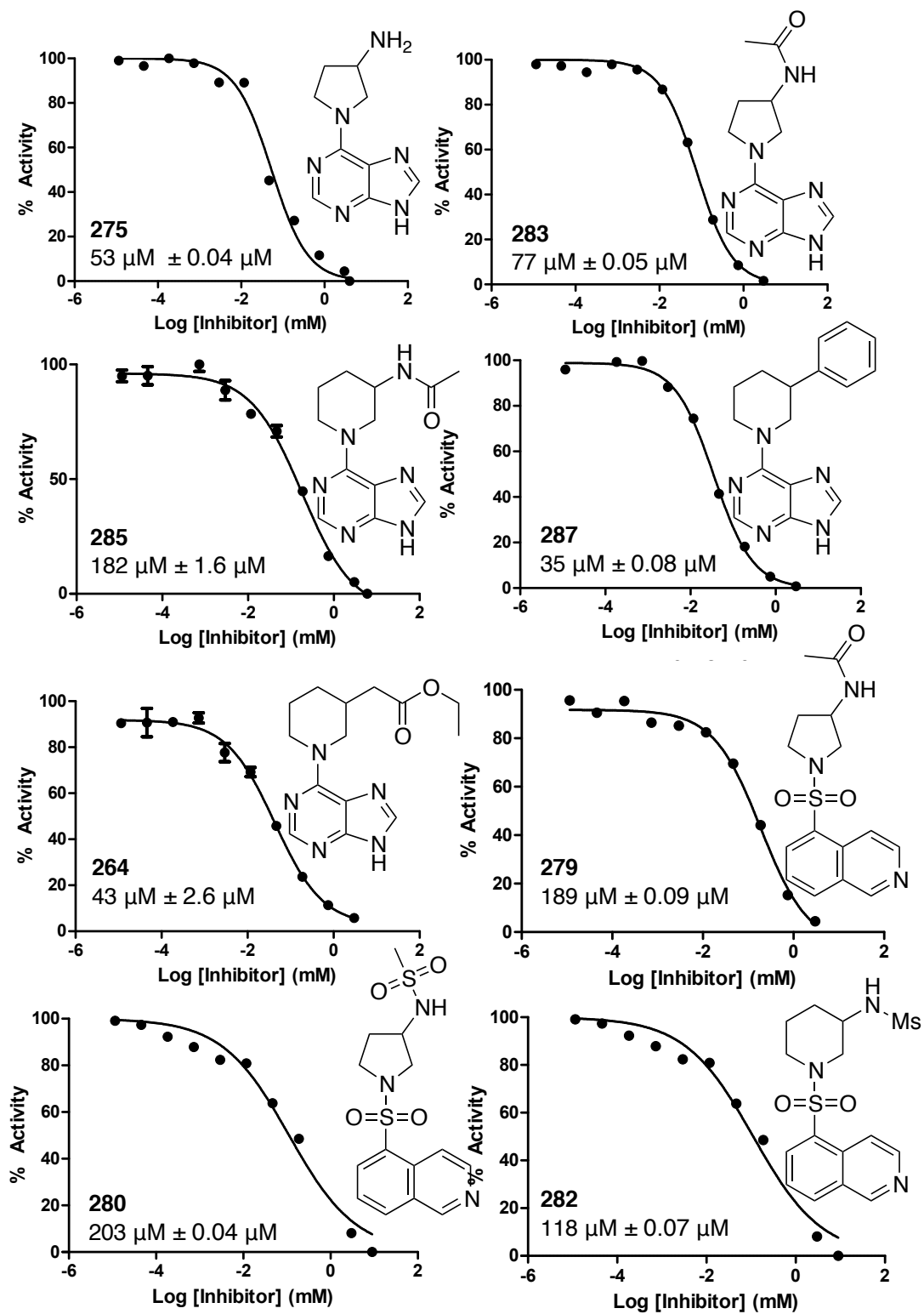


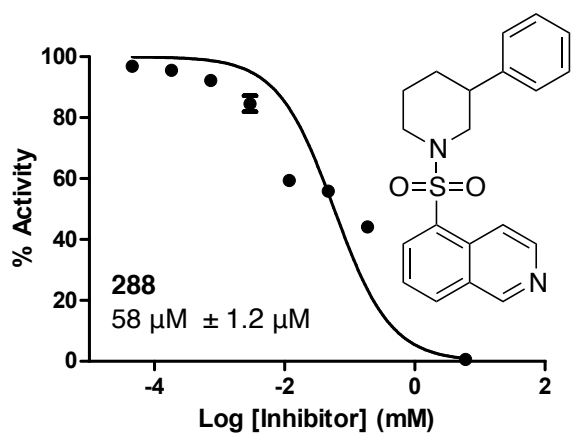


Appendix 3: Elaborated Fragments Screened in Chapter 3

	Fragment	IC ₅₀	pIC ₅₀		Fragment	IC ₅₀	pIC ₅₀
275		53 μ M	4.28	280		203 μ M	3.69
283		77 μ M	4.11	282		118 μ M	3.93
285		182 μ M	3.74	288		58 μ M	4.23
287		35 μ M	4.46				
264		43 μ M	4.37				
279		189 μ M	3.72				

Appendix 4: IC₅₀ Curves of the Elaborated Fragments Screened in Chapter 3





Appendix 5: Fragment Profiling Against 100-Kinases

Compound	Purine Compounds																								
	155	159	162	167	158	154	156	166	160	171	152	292	294	168	164	275	258	287	301	283	276	153	157	298	165
AURKBA	0		1	0	1	0	2	0	-1	-1	1	2	1	1	0	-1	-1	-1	-1	-1	0	-1	2	-1	-2
BMXA	1	-1	2	1	2	0	1	1	0	0	0	1	0	2	0	0	0	0	0	0	0	0	4	0	0
BRAFA	0	-1	1	0	0	0	1	0	-1	0	0	1	1	0	0	-1	-1	-1	-1	0	0	-1	2	0	-1
AAK1A	1	0	2	1	2	1	2	1	-1	0	1	2	1	2	0	-1	0	0	-2	0	0	0	2	-1	-1
ABL1A	1	-1	2	1	3	0	1	0	-1	0	0	2	1	2	0	-1	-1	-1	-1	0	0	-1	3	0	0
CAMKK2B	0	-1	1	1	1	0	1	-1	-1	-1	0	1	1	0	0	-1	-1	0	-1	-1	1	-1	2	-1	-1
CASKA	0	0	0	0	0	-1	0	1	1	0	0	-1	-2	-2	1	-1	0	0	0	1	1	-1	0	-2	-2
CSNK1DA	-1	-1	1	1	0	-1	1	1	0	0	1	3	2	1	0	0	-1	-1	-1	1	0	0	2	2	0
CSNK2A1A	1	-1	1	0	0	0	2	1	0	-1	1	2	2	0	1	-1	-1	-1	-1	0	0	0	3	1	0
CSNK2A2A	1	-1	0	0	0	0	2	1	0	-1	1	2	2	0	1	-1	-1	-1	-1	0	0	0	3	0	-1
DAPK3A	-1	-1	-1	0	-1	0	1	0	-1	-1	1	1	0	-1	0	0	-1	-1	0	0	0	-1	0	-1	0
DYRK1AA	-1	-2	0	-1	-1	-2	0	-1	-1	-1	1	3	2	0	1	-1	0	-1	-1	-1	0	0	1	0	-1
FESA	1	-1	1	1	0	-1	2	0	-1	-1	1	3	1	1	0	-1	-1	-1	0	0	0	0	2	0	0
GSG2A	-1	-1	0	0	0	0	1	0	-1	-1	1	1	1	0	0	0	-1	-1	-1	0	1	-1	1	0	-1
TTKA	1	-1	1	2	1	-1	2	1	-1	-1	0	2	0	1	0	-1	0	0	-1	0	0	-1	3	-1	-1
EPHA2A	1	-1	0	0	0	-1	2	-1	-1	-1	1	3	1	1	0	-1	-2	-1	-1	0	0	0	2	0	0
MAPK1A	1	1	0	0	0	0	2	1	0	0	1	3	1	-1	1	1	-1	0	2	2	0	1	1	0	-1
MERTKA	-1	-1	-1	-1	-1	-1	0	1	0	0	1	2	1	-1	0	0	-1	-1	0	0	2	0	0	0	0
MST3A	-1	-1	0	0	0	0	3	0	-1	-1	1	2	2	0	2	1	-1	-1	1	0	-1	1	2	0	0
MST4A	1	0	0	0	0	0	2	0	0	0	0	2	1	0	2	1	0	0	1	0	-3	1	2	1	0
PAK4A	2	0	1	0	1	0	3	-1	0	0	1	2	1	-1	1	1	0	-1	0	1	-1	1	3	0	0
PHKG2A	0	-1	-1	-1	-1	-1	0	-1	-1	-1	0	1	0	-1	0	0	-1	-1	0	0	0	-1	0	0	-1
PIM1A	0	-1	0	0	0	0	2	-1	-1	-1	-1	1	0	-1	0	0	0	0	0	-1	-1	-1	1	-1	-1
RPS6KA1A	1	-1	0	-1	1	-1	2	0	-1	-1	0	2	1	-2	0	0	-1	-1	-1	0	0	0	2	0	-1
STK10A	-2	-1	0	1	0	0	2	-1	-1	-1	1	3	1	0	0	1	-1	-1	0	0	0	0	2	-1	0
AKT3A	-1	0	-1	-1	-1	-1	1	1	1	0	0	1	0	0	0	0	0	0	1	1	1	0	0	0	0
BMP2KA	2	0	1	1	1	1	2	-1	-1	-1	1	2	1	1	1	0	-1	-1	-1	-1	-1	0	1	-1	-1
CDC42BPAA	-1	0	0	0	0	0	-3	1	1	1	0	-3	-1	-1	0	-1	1	1	0	1	1	1	0	1	1
CLK3A	0	-1	0	-1	0	-1	0	-1	0	-1	0	2	0	0	3	-1	-1	-1	-1	-1	0	-1	0	0	-1
DYRK2A	0	-1	0	-1	-1	0	2	-1	1	-1	2	2	2	0	0	-1	-1	-1	-1	0	0	-1	0	1	-1
CAMK1DA	0	1	1	-1	-1	-1	1	-1	-1	-1	0	2	1	1	0	3	0	1	1	-1	-1	0	0	0	0
CAMK1GA	0	-1	-1	0	0	0	3	-1	-1	-1	1	2	1	0	0	1	-1	-1	1	0	-1	1	2	0	-1
CAMK2BA	0	-1	-1	-4	0	-1	1	-1	-1	0	0	1	0	0	0	0	0	0	0	-1	0	0	0	0	0
CAMK2DA	0	0	0	-1	-1	-2	1	1	-1	-1	1	2	1	0	0	0	0	-1	-1	1	-1	0	1	0	0
CAMK4A	1	-1	0	0	0	-1	3	0	-1	-1	1	5	2	0	0	0	-1	-1	0	0	0	0	2	0	-1
BMPR2A	2	-1	0	0	0	1	3	0	0	-1	1	2	1	0	2	1	0	-1	-1	0	-1	1	2	0	-1
CDK2A	1	-1	0	0	0	-1	3	0	-1	-1	0	3	1	0	0	0	-1	-1	0	0	0	0	2	0	-1
CDKL1A	0	0	-1	0	3	0	0	1	1	1	0	0	0	0	1	-1	0	0	0	0	1	0	0	0	0
CHEK2A	0	0	0	0	0	0	3	-1	0	-1	0	4	3	0	0	1	-1	-1	0	0	-1	0	0	1	-1
CLK1A	0	-1	0	-1	0	0	2	-1	-1	-1	0	2	1	0	1	-1	-1	-1	-1	0	-1	0	1	0	-1
DAPK1A	-1	-1	-1	-1	-1	0	2	0	0	-1	0	1	1	-1	0	0	-1	-1	0	0	0	0	0	0	0
DMPK1A	1	-1	0	1	1	0	2	-1	-1	0	0	3	2	1	0	1	-1	-1	1	0	-1	1	2	0	0
EPHA5A	0	-1	-1	-1	-1	-1	2	0	0	0	0	3	1	0	0	0	-1	-1	0	1	0	0	1	1	0
EPHA7A	0	-1	-1	-1	1	1	4	0	0	0	1	2	0	-1	0	1	-1	-1	0	0	0	0	1	0	0
EPHB3A	0	-3	-1	-1	0	-1	2	0	-1	0	-1	2	1	-3	0	-1	-1	0	0	0	0	0	1	0	0

Compound	Purine Compounds																								
	155	159	162	167	158	154	156	166	160	171	152	292	294	168	164	275	258	287	301	283	276	153	157	298	165
FGFR1B	0	-1	0	1	1	0	4	-1	0	-1	0	3	2	0	1	0	-1	-1	0	0	-1	0	1	0	0
FGFR2A	0	-1	0	1	0	0	4	-1	0	-1	1	3	2	0	1	0	-1	-1	0	1	-1	1	2	0	0
FGFR3A	0	-1	0	1	1	0	4	-1	0	-1	1	3	2	1	1	0	-1	-1	0	0	-1	0	2	0	0
GAKA	-1	-1	0	-1	0	0	4	0	0	-1	0	4	2	0	0	-1	0	-1	0	0	0	0	1	0	-1
GPRK5A	0	-1	0	0	0	0	3	-1	-3	0	0	2	1	0	0	0	-1	-1	0	-1	-1	0	0	0	0
GSK3BB	0	-1	0	0	0	-1	2	-1	0	-1	0	2	1	0	3	0	-1	-1	0	0	-1	1	1	-1	-1
MAP2K1A	0	-1	-1	0	-1	0	4	0	0	0	0	3	2	0	1	1	-1	-1	0	0	0	1	1	0	0
MAP2K4A	1	-1	0	0	0	0	3	0	0	-1	1	4	2	1	1	1	-1	-1	-1	0	-1	-1	2	1	-1
MAP2K6A	0	0	0	0	0	0	3	0	0	0	0	4	2	0	1	0	0	-1	0	0	-1	1	1	1	0
MAP3K5A	0	0	1	0	1	1	3	-1	0	-1	1	3	3	1	0	0	-1	-1	-1	0	-1	0	1	0	-1
MAPK10A	-1	-1	-1	0	0	-1	2	0	-1	0	1	1	1	0	0	-1	-1	-1	-2	0	-1	0	0	0	-1
MAPK8B	1	-1	0	1	0	0	3	-1	-1	-1	0	2	2	0	1	0	-1	-1	-1	-1	-1	-1	1	0	-1
MAPK13A	-1	-1	-1	0	0	0	1	-1	-1	-1	-1	0	0	-1	0	-1	-1	0	0	-1	-1	0	-1	-1	-1
MAPK14A	0	0	-1	-1	-1	-2	1	1	1	1	2	1	0	0	0	0	0	0	-2	1	1	0	0	1	0
MARK3A	0	-1	0	1	1	0	2	-1	-1	0	0	2	2	1	0	1	-1	-1	0	0	-1	0	0	-1	0
MARK4A	-1	-1	0	0	1	0	2	-1	-1	-1	0	3	2	0	1	1	-1	-1	0	0	-1	0	0	0	-1
MELKA	0	-1	-1	0	0	0	1	-1	-1	-1	0	2	1	0	0	0	-1	-1	0	0	0	0	0	0	0
PIM3A	-1	-1	-1	-1	-1	-1	0	0	0	-1	1	1	1	0	0	0	0	-1	-1	1	0	1	0	0	0
NEK1A	0	0	0	-1	0	0	2	0	0	0	1	3	3	0	1	1	0	0	-1	0	-1	0	1	2	0
NEK2A	-1	0	-1	-1	-1	0	2	1	0	1	1	2	3	-1	0	0	-1	-1	-1	0	-1	0	0	2	0
NEK7A	2	0	-1	-2	-2	-1	1	0	-1	0	1	1	-1	1	0	1	0	-1	1	0	0	1	1	-1	1
OSR1A	0	-1	0	0	0	0	3	-1	0	-1	2	4	2	0	0	0	-1	-1	0	0	0	2	0	1	0
PAK1A	-1	-1	0	0	0	0	0	1	1	1	1	1	0	0	0	0	0	0	-1	1	1	1	0	0	0
PCTK1A	-1	-1	-1	-1	-1	-1	0	0	0	0	0	1	0	0	0	0	-1	-1	0	0	0	0	0	-1	-1
PKMYT1A	-1	-1	-1	-1	0	0	1	1	0	0	0	0	0	-2	0	0	0	0	-1	1	0	0	0	1	0
PLK4A	0	-1	0	1	0	0	3	-1	-1	-1	1	3	1	1	0	0	-1	-1	-1	0	-1	0	1	-1	-1
RPS6kA5A	0	-1	-1	-1	-1	1	2	0	0	-1	2	2	2	-1	0	2	-1	-1	0	1	-1	1	0	2	0
SLKA	1	-1	0	0	0	0	3	-1	-1	-1	0	2	1	1	0	1	-1	-1	1	0	0	1	1	0	0
SRCA	0	0	0	0	0	0	3	0	0	0	0	2	2	1	0	0	0	0	-1	0	0	0	2	3	0
SRPK1A	-1	-1	-1	-1	0	-1	1	1	1	0	0	4	1	0	0	-1	0	-1	-2	1	0	-2	0	0	0
STK17AA	-1	-1	-1	-1	-1	0	1	-1	-1	0	0	2	2	-1	0	0	0	-1	-1	0	-1	-1	0	-1	-1
STK17BA	0	-1	-1	-1	-1	-1	3	0	0	0	0	3	1	0	0	-1	-1	-1	-2	-1	0	0	0	0	-1
EPHB1A	-1	-2	-1	-1	0	-1	2	0	0	-1	-1	2	0	-1	0	-1	-1	-1	0	0	0	1	0	-1	0
HIPK2	0	0	0	0	0	-1	1	1	0	0	1	3	1	1	1	1	0	-1	-1	0	1	1	1	1	1
MAP2K7A	2	1	-1	0	-1	0	-1	0	0	1	0	2	1	1	0	0	0	-1	-1	1	-1	0	-1	1	0
STK3A	1	-1	1	1	1	0	3	-1	-1	-1	1	3	2	1	0	1	-1	-1	0	0	-1	1	2	0	-1
STK38LA	1	-1	0	0	1	-1	1	-1	-1	-1	0	4	1	0	0	0	-1	-1	-1	0	0	0	2	0	-1
STK39A	0	-1	0	0	0	0	3	-1	0	-1	1	4	2	0	1	1	-1	-1	0	0	-1	1	1	1	0
STK4A	1	0	1	1	1	0	3	0	0	-1	1	3	2	1	1	1	-1	-1	-1	0	-1	1	2	0	-1
STK6A	0	-1	0	0	0	0	2	-1	-1	-1	0	2	1	0	0	0	-1	-1	-1	-1	0	0	0	-1	-1
TAF1A	-2	0	-1	-1	-1	-1	-1	1	2	2	0	0	-1	-1	0	0	-1	0	0	0	1	3	1	1	1
TOPKA	0	0	0	0	0	1	1	0	0	0	0	2	1	0	0	0	0	0	0	0	0	0	0	1	0
ULK1A	0	-1	-1	0	0	0	2	-1	-1	-1	1	3	2	0	0	1	-1	-1	0	0	-1	0	0	0	-1
ULK3A	1	-1	0	0	0	0	3	-1	-1	-1	1	3	2	0	1	1	-1	-1	-1	0	-1	1	2	1	-1
VRK1A	0	0	0	0	0	0	2	-1	-1	-1	1	4	2	1	1	1	0	0	-1	0	-1	0	1	-1	1
BRD4	-1	0	0	0	0	0	1	0	0	0	0	0	0	0	0	0	0	1	-1	0	0	0	0	0	-4

Compound	Purine Compounds																								
	155	159	162	167	158	154	156	166	160	171	152	292	294	168	164	275	258	287	301	283	276	153	157	298	165
BRPF1B	-1	-2	-1	-1	-1	-1	1	0	0	0	1	1	1	0	1	1	0	-1	-1	1	0	1	0	0	0
DCAMKL1A	-1	-1	-1	-1	-1	-1	1	-1	-1	-1	0	1	1	-1	0	1	-1	-1	0	0	0	0	0	-1	0
EPHA4A	0	0	0	0	0	0	1	1	0	0	0	1	0	0	0	0	0	0	0	1	0	1	1	0	0
FLT1A	1	-1	0	0	0	0	3	-1	0	-1	1	3	2	0	1	0	-1	-1	0	0	-1	0	1	0	0
MAPK15A	-1	-1	-1	-1	0	-1	0	-1	0	-1	-1	0	0	-1	1	0	-1	-1	0	-1	0	0	-1	-1	-1
MAPKAPK2	0	-1	-1	0	0	0	2	0	0	0	1	1	2	0	0	3	0	0	0	0	0	0	0	1	0
PDK4A	-1	1	-5	0	0	1	-3	1	0	0	0	-2	-1	1	-2	1	1	1	0	1	0	0	0	1	1
TIF1A	0	0	-1	-1	-1	-1	-1	1	-1	1	1	1	1	1	1	0	-1	-1	0	1	-1	1	1	0	0
TLK1A	0	0	0	0	-1	-1	2	0	0	0	0	3	1	0	1	2	-1	-1	0	0	-1	0	0	0	0
WNK1A	-1	0	-1	0	-1	0	1	2	2	0	1	1	0	0	-1	-1	-1	0	1	0	1	2	1	0	0
BRPF1A	1	0	1	1	1	3	1	-1	-1	0	0	0	0	0	0	1	1	1	0	-1	-2	0	0	0	0
NQO2A	0	-1	0	-1	-1	-1	-1	0	0	0	0	0	0	0	0	-1	-1	-1	-1	0	-1	0	0	0	0
FECH	0	0	0	0	-1	-1	0	0	-1	0	0	-3	-1	0	0	0	0	-1	-1	0	1	-1	0	-1	-1

Compound	Isoquinoline-5-sulfonyl Compounds																					
	177	179	290	183	293	178	297	176	174	182	295	280	277	261	291	288	270	300	270	299	272	302
AURKBA	-1	1	-1	0	0	-1	0	0	0	0	0	0	2	0	0	-2	0	2	1	1	-1	-1
BMXA	-2	-1	-1	-1	0	-1	0	0	0	-1	0	-1	0	-1	-1	-1	-1	-1	0	-1	-1	0
BRAFA	2	0	1	1	0	2	-1	1	0	3	0	-1	-1	1	1	-1	-1	-1	-1	-1	-1	-1
AAK1A	0	-1	0	0	0	0	-1	0	-1	0	0	0	0	0	-1	0	-1	0	0	-1	-2	0
ABL1A	-1	-1	0	0	0	0	0	0	0	0	-1	-1	0	0	-1	-1	-1	0	0	-1	-1	-1
CAMKK2B	-1	0	0	1	1	1	0	1	1	0	1	0	1	0	0	-1	0	2	1	1	-1	-1
CASKA	-2	1	0	0	0	1	0	0	0	2	1	1	0	2	0	0	0	1	0	0	0	1
CSNK1DA	-1	0	-1	-1	0	-1	0	-1	0	0	0	-1	1	-1	-1	-2	-1	0	0	0	-1	0
CSNK2A1A	-1	0	0	0	0	0	0	0	0	0	0	0	0	-1	-1	-1	-1	0	0	0	-1	-1
CSNK2A2A	-2	1	0	0	0	0	0	1	0	-1	0	0	-1	-1	0	-1	0	0	0	0	-1	-1
DAPK3A	0	0	0	0	0	0	0	1	1	1	1	1	3	0	0	-1	1	3	2	0	-1	-1
DYRK1AA	-1	0	0	1	1	0	1	0	1	-1	0	-1	1	0	0	-1	0	2	0	1	-1	1
FESA	-1	-1	-1	-1	0	0	0	0	0	-1	0	-1	1	-1	0	-1	0	1	1	0	-1	0
GSG2A	-1	1	-1	-1	0	-1	1	0	0	-1	1	1	3	0	0	-1	1	2	2	2	-1	-1
TTKA	-1	-1	0	1	0	0	0	0	0	0	0	0	0	2	1	0	-1	0	-1	0	-1	0
EPHA2A	-1	-1	0	0	1	0	1	0	1	0	2	0	1	0	0	-1	0	1	1	0	-1	-1
MAPK1A	-2	-1	-1	-1	-1	-1	0	-1	-1	0	0	0	1	0	-1	-1	-1	2	0	-1	-1	0
MERTKA	-3	-1	-1	-1	1	0	0	1	1	0	2	1	3	-1	-1	-1	0	2	1	0	-1	0
MST3A	-2	-1	-1	-1	0	-1	0	-1	0	-1	0	-1	0	-1	-1	-1	0	1	1	1	0	-1
MST4A	-3	0	-1	-1	0	0	0	0	0	-1	0	0	0	-1	-1	0	0	1	1	1	0	0
PAK4A	-1	-1	-1	-1	-1	-1	-1	-1	-1	-1	0	-1	1	-1	-1	-1	0	1	0	0	-1	0
PHKG2A	-1	-1	0	0	1	0	1	0	0	0	1	0	3	0	0	-1	3	3	2	1	-1	-1
PIM1A	-1	0	0	0	0	0	1	1	1	-1	0	-1	3	0	0	0	1	3	3	1	0	-1
RPS6KA1A	-1	-1	1	2	1	0	1	0	0	0	1	0	1	0	0	-1	0	1	0	0	-1	-1
STK10A	-1	-1	0	0	0	0	0	0	0	0	1	-1	2	-1	0	-1	0	1	1	-1	-2	0
AKT3A	-2	-1	-1	-1	0	0	0	0	0	0	2	0	2	-1	0	-1	0	2	0	0	0	0
BMP2KA	0	-1	1	1	1	1	0	0	-2	1	0	0	1	-2	0	-1	-1	1	0	0	-1	0
CDC42BPAA	-1	1	0	-1	0	0	0	0	1	0	1	1	-1	1	0	1	1	-1	-1	0	1	0
CLK3A	0	-1	1	3	3	1	0	0	0	0	1	0	1	-1	0	-1	0	1	0	0	-1	-1
DYRK2A	0	0	0	1	0	0	1	0	0	0	0	-1	0	0	0	-1	0	0	0	3	-1	-1
CAMK1DA	-2	-1	-1	-1	0	0	0	0	0	-2	0	-1	1	-2	0	0	0	2	2	0	0	0
CAMK1GA	-2	-1	-1	-1	0	-1	0	0	1	-1	0	-1	1	-1	0	-1	0	1	1	0	-1	0
CAMK2BA	0	-1	2	1	1	1	0	0	0	1	0	0	2	2	0	-1	1	2	1	-1	-1	-1
CAMK2DA	-1	-1	2	1	0	0	-2	-1	-1	2	0	0	0	3	0	0	1	0	0	-1	-1	0
CAMK4A	-1	-1	0	1	0	-1	0	-1	-1	0	1	-1	0	-1	0	-1	-1	1	0	0	-1	0
BMPR2A	0	-1	0	1	0	0	0	-1	-1	0	0	-1	-1	1	0	-1	-1	-1	-1	0	-1	0
CDK2A	-2	-1	0	0	1	0	2	0	0	-1	1	-1	0	-1	0	-1	0	0	2	0	-1	0
CDKL1A	-3	0	-2	-2	0	-1	0	0	0	1	0	0	-1	-1	0	0	0	1	1	0	0	0
CHEK2A	-1	-1	-1	-1	0	-1	0	-1	-1	-1	0	-1	2	0	0	-1	0	1	0	1	-1	0
CLK1A	0	-1	1	1	1	1	1	0	-1	1	1	0	1	0	0	-1	0	2	1	2	-1	1
DAPK1A	1	-1	0	1	0	1	0	-1	0	1	0	-1	3	-3	0	-1	0	3	1	1	-2	0
DMPK1A	-1	-1	-1	-1	0	-1	0	-1	-1	-1	0	-1	1	-1	0	-1	-1	1	0	0	-1	1
EPHA5A	-1	-1	-1	-2	0	-1	1	-1	0	0	2	0	2	-2	0	-1	1	2	1	1	0	1
EPHA7A	-1	-1	-1	-1	0	0	0	0	0	-1	1	-1	1	-2	0	-1	0	2	2	0	-1	0
EPHB3A	-1	0	0	0	1	0	1	0	0	0	2	0	2	0	0	0	1	1	1	0	-1	0

Compound	Isoquinoline-5-sulfonyl Compounds																						
	177	179	290	183	293	178	297	176	174	182	295	280	277	261	291	288	270	300	270	299	272	302	
FGFR1B	-1	-1	-1	0	0	0	0	-1	-1	0	1	-1	0	-1	0	-1	1	1	1	0	-1	0	
FGFR2A	-1	-1	0	0	0	0	0	-1	-1	0	1	-1	0	-1	0	-1	0	0	0	0	0	-1	0
FGFR3A	-1	-1	0	0	0	0	0	-1	-1	0	0	-1	0	-1	0	-1	0	0	0	0	0	-1	0
GAKA	-1	-1	0	0	0	0	1	0	0	0	0	0	-1	0	0	-1	-1	0	-1	0	0	0	
GPRK5A	-1	0	0	1	1	0	1	0	-1	-1	1	-1	1	0	0	0	1	2	2	1	-2	-2	
GSK3BB	-1	-1	0	1	1	0	0	-1	-1	0	1	-1	1	2	0	-1	0	1	1	0	-1	0	
MAP2K1A	-1	-1	-2	0	-1	-1	0	0	0	0	1	0	1	-1	0	0	-1	0	0	1	-1	0	
MAP2K4A	-1	-1	0	0	0	0	0	-1	-1	-1	0	-1	0	0	0	-1	-1	0	-1	0	-1	0	
MAP2K6A	-1	0	-1	-1	0	-1	0	-1	-1	-1	0	-1	1	-1	0	-1	-1	0	0	0	-1	0	
MAP3K5A	-1	-1	0	0	0	0	0	-1	-1	0	0	-1	1	-1	0	-1	-1	0	0	0	-1	0	
MAPK10A	-1	-1	1	2	1	1	1	0	-1	1	1	-1	1	3	0	-1	-1	1	0	1	-1	-1	
MAPK8B	-1	-1	1	1	1	0	1	-1	-1	0	1	-1	0	2	0	-1	-1	0	-1	0	0	0	
MAPK13A	0	-1	2	2	2	1	1	0	0	1	0	-1	2	2	0	-1	0	2	2	0	0	-1	
MAPK14A	-1	0	-1	-2	0	-1	1	0	-1	-1	1	0	1	-3	0	-1	1	1	1	0	-1	1	
MARK3A	-1	-1	1	1	1	1	1	0	-1	0	0	-2	1	0	0	-1	1	1	1	1	-1	-1	
MARK4A	-1	-1	0	1	1	0	1	0	0	0	0	-1	1	0	0	-1	1	1	1	1	-1	-1	
MELKA	-1	-1	1	1	1	1	1	-1	0	1	1	-1	2	1	0	-1	1	2	2	1	-1	-1	
PIM3A	0	0	0	0	0	-5	0	0	-1	1	1	0	3	-1	0	-1	0	1	2	0	-1	1	
NEK1A	-1	0	-1	-1	-1	-1	0	-1	-1	-1	-1	0	1	-1	0	-1	0	1	0	0	-1	0	
NEK2A	-1	-1	0	0	-1	-1	-1	-1	-1	1	-1	1	2	1	0	-1	-1	-1	-1	0	-1	0	
NEK7A	1	-1	-2	0	0	-1	-1	-1	1	-1	0	1	-1	0	0	1	0	0	1	0	2	0	
OSR1A	-1	-1	-1	-1	0	-1	0	-1	0	-1	0	0	0	-1	0	-1	-1	0	0	1	-1	0	
PAK1A	-1	0	-2	-2	-1	-1	0	0	0	0	1	0	2	-3	0	0	1	1	1	0	0	2	
PCTK1A	-1	-1	0	0	1	0	1	-1	-1	0	1	0	1	0	0	-1	1	2	5	0	-1	0	
PKMYT1A	-1	1	-1	-2	-1	-1	3	1	1	-1	1	0	-1	-3	0	1	0	0	1	1	1	2	
PLK4A	-1	-1	1	1	1	1	0	-1	-1	1	1	-1	0	1	0	-1	-1	1	0	0	-1	0	
RPS6kA5A	-1	-1	0	0	0	0	0	-1	-1	1	0	-1	1	-1	0	-1	0	1	1	1	-1	0	
SLKA	0	-1	0	0	0	-1	1	0	0	-1	0	-1	2	-1	0	-1	0	1	1	0	-1	0	
SRCA	0	0	-1	-1	0	-1	0	0	-1	-2	0	-1	0	-1	0	0	-1	0	0	0	-1	-2	
SRPK1A	0	1	0	-1	2	0	1	0	-1	-1	2	-1	0	0	0	-1	0	1	0	0	0	0	
STK17AA	0	-1	1	1	0	1	0	-1	-1	1	0	-1	3	-1	0	0	0	3	2	1	-1	0	
STK17BA	-1	-1	1	2	1	1	0	-1	-1	1	1	-1	1	1	0	-1	-1	0	0	1	-1	1	
EPHB1A	0	0	0	2	0	1	1	-1	0	0	2	-2	2	0	0	-1	0	2	2	0	-1	0	
HIPK2	1	1	-1	-2	0	-1	0	-1	-2	-2	0	0	0	-1	0	1	0	-1	0	0	-2	-1	
MAP2K7A	0	-2	-1	1	1	0	-1	-2	-1	1	-1	1	1	-3	0	0	2	1	1	1	-1	1	
STK3A	-1	-1	0	0	0	0	0	-1	-1	-1	0	-1	1	-1	0	-1	-1	0	0	0	-1	0	
STK38LA	-1	-1	-1	0	1	-1	2	-1	-1	-1	1	-1	0	-1	0	-1	0	1	2	1	-1	0	
STK39A	-1	-1	-1	-1	0	-1	0	-1	-1	-1	0	-1	1	-1	0	-1	0	0	0	1	-1	0	
STK4A	-1	-1	0	0	0	0	0	-1	-1	-1	0	-1	1	-1	0	-1	-1	0	0	0	-1	0	
STK6A	-1	-1	2	2	2	1	1	0	0	2	1	-1	0	1	0	-1	0	1	0	0	-1	-1	
TAF1A	1	0	0	0	0	0	-1	0	-1	-1	1	0	1	1	0	0	0	1	0	0	-1	0	
TOPKA	0	0	0	-1	1	0	0	0	0	0	0	0	0	-6	0	0	0	0	0	1	0	0	
ULK1A	-1	-1	0	1	0	0	0	-1	-1	0	0	-1	2	-1	0	-1	1	2	2	1	-1	-1	
ULK3A	-1	-1	0	0	0	0	0	-1	-1	0	0	-1	-1	0	0	-1	-1	0	0	1	-1	0	
VRK1A	0	0	-1	-1	0	-1	0	0	-1	-1	0	0	0	0	0	1	0	1	0	0	-1	-1	
BRD4	-1	0	-1	-1	0	0	1	1	0	0	0	0	-1	-4	0	1	0	0	1	1	1	1	

Compound	Isoquinoline-5-sulfonyl Compounds																					
	177	179	290	183	293	178	297	176	174	182	295	280	277	261	291	288	270	300	270	299	272	302
BRPF1B	-1	0	-2	-2	0	-1	0	0	0	0	1	0	1	-3	0	0	1	1	1	1	0	1
DCAMKL1A	0	-1	0	1	1	1	1	0	0	1	1	0	3	0	0	-1	1	3	2	1	-1	-1
EPHA4A	0	-4	0	-5	0	0	0	0	0	0	1	0	1	0	0	0	0	1	1	0	0	0
FLT1A	-1	-1	0	0	0	0	0	-1	-1	0	0	-1	1	-1	0	-1	0	1	1	0	-1	0
MAPK15A	-1	-1	0	1	1	1	1	0	0	0	1	-1	2	1	0	-1	1	3	2	1	0	-1
MAPKAPK2	-1	0	-1	-1	0	-1	0	0	0	-1	0	0	2	-3	0	-1	0	3	1	1	0	0
PDK4A	0	0	-1	-1	0	0	1	1	0	0	0	0	1	0	0	0	0	0	1	1	1	0
TIF1A	0	-1	-2	-2	-1	-1	0	0	0	1	-1	2	2	-1	0	-1	1	0	0	0	0	2
TLK1A	-1	-1	-1	-1	-1	-1	1	-1	-1	0	0	-1	2	-1	0	-1	-1	3	2	0	-1	0
WNK1A	1	-1	0	-2	-1	-1	-1	-1	-1	-1	1	-1	2	3	0	0	0	1	-1	-1	-1	0
BRPF1A	0	0	-2	-2	0	-1	2	1	0	-1	-1	-1	0	-3	0	0	1	1	1	1	0	0
NQO2A	-1	2	-1	-1	-1	-1	2	-1	-1	-1	2	1	2	-1	0	0	0	1	2	1	3	0
FECH	-1	-1	1	2	0	0	0	0	1	2	0	-1	2	1	0	1	0	3	1	1	1	2